Theoretical and Laboratory Experimental Studies of Vehicle-Excited Bridge Vibration

Thesis submitted in accordance with the requirements of the University of Liverpool for the degree of Doctor in Philosophy

by

Jing Yang

This work is sponsored by University of Liverpool and China Scholarship Council

September 2017

Contents

Abstract

Theoretical studies of vehicle-bridge interactions have been conducted extensively, but a relatively much smaller amount of work concerns experimental studies of this problem. Full-scale tests of vehicle-bridge vibrations can be done to estimate the performance of the vehicle-bridge system or validate theoretical models, but are expensive compared with small-scale experiments in a lab. In addition, continuous bridges are paid relatively much less attention compared with simply supported bridges in the literature. This thesis is dedicated to the theoretical and the laboratory experimental studies of a four-span continuous plate structure subjected to moving cars.

Firstly, the mode shapes of a multi-span continuous beam are approximated by using a number of sinusoidal functions which are the mode shapes of the beam with simply supported boundaries. The analytical solution of the continuous beam subjected to a moving force can be derived as one simple expression for the whole length of the beam based on the approximated modes, and the contributions of bridge frequencies to the modal responses of the beam would be clearly shown in the analytical solution, which can provide guidance for identifying the modal properties of the beam. This idea is illustrated by a two-span beam. The response of a simple beam subjected to a moving force is compared with that of a two-span continuous beam. The second part of this thesis is about the vehicle-bridge interaction and separation, which are investigated by using the moving sprung mass model.

After that, a general approach of simulating vehicle-bridge interactions is applied to a four-span plate structure traversed by one or two moving cars at different speeds. There are two types of situations for two cars: the two cars are either separated or connected together with pitching rotation allowed for each car. The adjacent loads of two-connected-cars are almost equal distance away from each other, which is like a series of moving equidistant loads. A Laser Vibrometer is used to measure the car speeds, and four laser displacement transducers at each span are utilized to capture the structural responses. The theoretical model of the rig is updated and validated with experimental results. A frequency spectrum analysis of measured structural displacements and an in-depth parametric analysis based on the validated theoretical model are carried out.

Acknowledgements

I would like to thank University of Liverpool (UOL) and China Scholarship Council who support my four years' PhD study financially and spiritually. I wish to express my sincere gratitude to my excellent supervisor, Prof. Huajiang Ouyang who guides me into the area of structural vibration with great patience and encourages me to explore the edge of this area. He always gives me inspirations when I got stuck in research and modifies my writing work again and again with great caution, which has influenced me significantly. I would like also to thank my co-supervisor, Dr. Dan Stăncioiu from Liverpool John Moores University, who teaches me much about experiments and gave me inspirations from time to time for my PhD work. I also like to express my gratitude to my second supervisor, Dr. Steve Jones for his concern and encouragement for my work.

I feel very grateful for studying in the Dynamic & Control research group in UOL, where everyone helps each other as a big family. I still remember that Dr. Xiaojun Wei and Dr. Amir Nobari helped me a lot to get used to the new research life at UOL at the beginning of my PhD study. I gained much knowledge by discussing problems with my colleagues, Dr. Xiaojun Wei, Dr. Amir Nobari, Shancheng Cao, Yanlong Xie and other group members. My experimental work cannot be finished without the big help from Mr. Raymond Edun, Mr. Derek Neary, Mr. Daniel Potts, Shancheng Cao and a number of other good people. The names are too many to list, but I remember them all.

Finally, I wish to dedicate this thesis to my parents, Qixin Yang and Changlan Wang, and my grandparents, Dajin Yang and Yunying Wang for their great care and love, as well as my sister, Ying Yang for her constant support and encouragement.

Symbols

A	Section area
c	Damping coefficient of beam
C	Damping matrix
E	Young's modulus of material
f	External force
f_c	Contact force between vehicle and bridge
f_{d}	Driving frequency related to a moving vehicle in the unit of Hz
f_{t}	Travelling frequency related to a series of moving axle loads
g	Gravity acceleration
I	Second moment of area of a structural cross section
I_{v}	Second moment of area of a vehicle
k_{v}	Contact stiffness between the wheel and rail or bridge
K	Stiffness matrix
l	Length of beam one-span of a beam with equal spans
m_{v}	Mass of a vehicle
M	Mass matrix
q_i	Modal coordinate of bridge in ith mode
q_{v}	Vehicle vertical displacement
q	Vector of modal coordinates of a bridge
s	Wheelbase of a car
S_i	Ratio of driving frequency to structural natural frequency in ith mode
S_i'	Ratio of the frequency of the input harmonic force ω_0 to the ith natural frequency of the beam ω_i
t	Time instant
T	Kinetic energy
u	Longitudinal deflection of one point of a beam
v	Travelling speed of a force or vehicle
V	Potential energy
w	Vertical deflection of a beam, plate or structure
W_e	Work done by external and damping forces

W_{si}	Static deflection caused by a moving force in the ith mode
x	Distance of a beam section centre point from left origin
z	Upward vertical distance of section points away from neutral axis of structural section
δ	Dirac function
δ_{ij}	Kronecker delta function
θ	Vehicle rotation angle along y axis
λ_i	Dimensionless parameter in ith mode related to the boundary conditions of a beam
φ_i	ith mode of a structure
$\boldsymbol{\varphi}$	Vector of modes of a structure
ω_{d}	Driving frequency related to a moving vehicle in the unit of rad/s
ω_i	ith natural frequency of a bridge
ω_{v}	Vibration frequency of a sprung mass
ω_0	Frequency of an external harmonic force

Abbreviations

AASHTO	American Association of State Highway and Transportation Officials
AVR	Automatic Video Recorder
CMS	Component Mode Synthesis
DAF	Dynamic Amplification Factor
DOF	Degree of Freedom
DQE	Differential Quadrature Element
EMD	Empirical Mode Decomposition
FE	Finite Element
FRF	Frequency Response Function
HHT	Hilbert Huang Transform
HT	Hilbert Transform
MS	Modal Superposition
PSD	Power Spectral Density
PEM	Pseudo Excitation Method
PIM	Precise Integration Method
STFDD	Short Time Frequency Domain Decomposition
STFT	Short Time Fourier Transform
WIM	Weight-In-Motion

1. Introduction

Moving load problems are a kind of dynamic problems in which the load on an object changes its location in time at a high enough speed. Examples are many, like trains crossing a bridge, bullets being shot out from a gun, a working crane and so on. A brief overview of moving load problems can be found in (Ouyang, 2011). In this thesis, the vibration of a railway bridge crossed by travelling trains is the concern. The vibration of a highway bridge travelled by vehicles is also introduced in the literature review as a reference.

1.1. Train-Bridge Dynamics

With growing globalization and tourism, the communication between different cities, areas and countries is booming, leading to strong demand for fast transportation. As a safe, fast and comfortable means of transportation with high loading capacity and low energy consumption, high-speed rail has been expanding across Japan, European Union, US, China and many other places across the globe (UIC, 2017a). According to the International Union of Railways (UIC) (UIC, 2017a), high speed rail is a whole 'system' constituted by many elements: infrastructure (new built tracks especially for high speeds above 250 km/h or existing tracks especially upgraded for high speeds up to 200 km/h or even 220 km/h in some cases), rolling stock (specially designed train sets), operating conditions and equipment, etc. Japan opened the world's first high speed railway line from Tokyo to Osaka with a designed operational speed of 210 km/h (later increased) in 1964. France is thought to be the first country in Europe who started the operation of a high speed line between Paris and Lyons in 1981, at a speed up to 260 km/h. China has experienced a rapid development of high-speed railway in recent decades, ranking first in the world currently in terms of the mileage in operation with 23,914 km and construction scale of high-speed railway with 10,730 km by 1st March 2017 (He et al., 2017; UIC, 2017b). The distribution of high-speed railways in Europe and China by 1 March 2017 can be seen in Figure 1.1 and Figure 1.2, respectively. According to the report by UIC (UIC, 2017b), there are 37,343 km long high speed lines in operation and 15,981 km long high speed lines under construction by 1st March 2017.

Bridges are widely built in high-speed railways to provide high enough stiffness for the railway infrastructure and save arable lands. For example, the averaged ratio of the bridge length to the whole length of railway lines for the major high-speed railway operational lines in China is over 50% and the maximum ratio is as high as 94.2% on the Guangzhou-Zhuhai intercity railway (Sun, 2011; He et al., 2017). Short-span bridges are the main bridges constructed in the high-speed railway lines. Among them, simply supported bridges make up the largest portion and continuous bridges are used for larger spans than the simply supported bridges (Yan et al., 2015).

Figure 1.1. Distribution of high-speed railway in Europe by 1 March 2017 (from http://www.uic.org, accessed 04/04/2017)

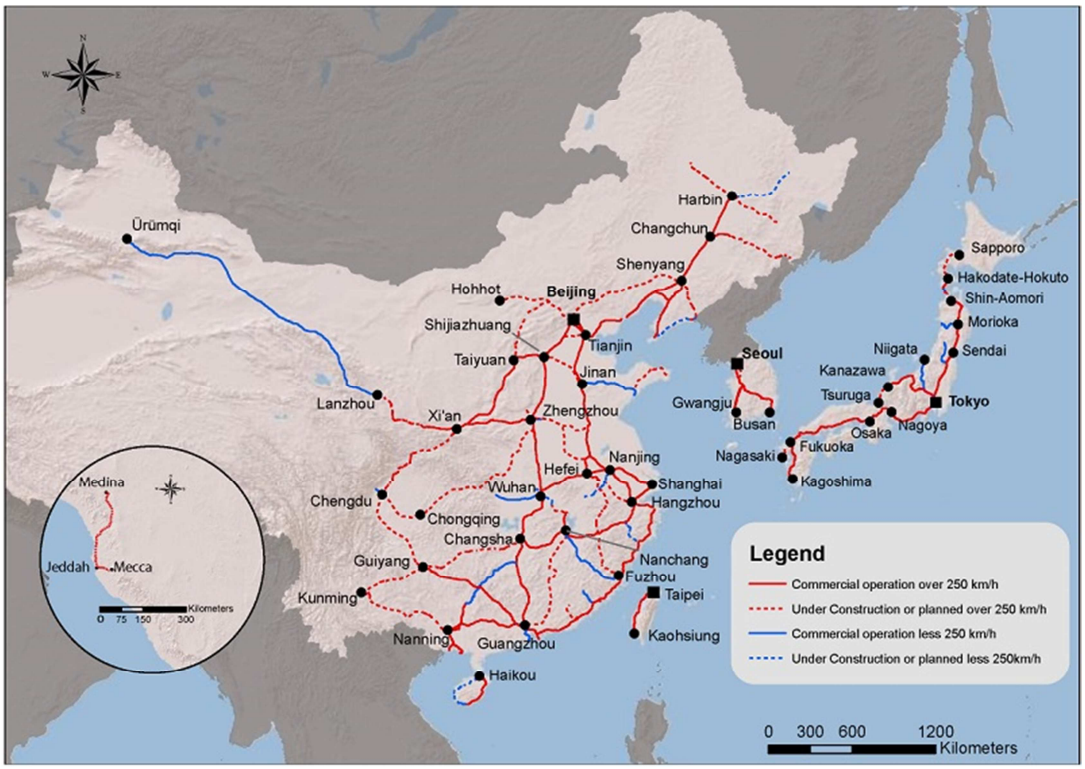

Figure 1.2. Distribution of high-speed railway in Asia by 1 March 2017 (from http://www.uic.org, accessed 04/04/2017)

If a vehicle's mass is not negligible compared with a bridge's mass, the inertial force generated from the transverse vibration of the vehicle must be taken into account in calculating the transverse vibrations of the vehicle and the bridge, making the calculation complicated. The dynamic response of a bridge subjected to a moving load can be much higher than that excited by the corresponding static load (Kou and DeWolf, 1997; Baeza and Ouyang, 2008), especially with the presence of bridge surface irregularities (Kou and DeWolf, 1997; Pesterev et al., 2004), which causes the fatigue of the bridge and reduces the service life of the bridge. Due to the high traffic density of high speed rails, this situation for high-speed rails could be worse than that in normal rails. Furthermore, repeated high-speed wheel loads may force the bridge into *resonance* (Yang et al., 2004) which amplifies the dynamic response of the bridge with time and, therefore, should be avoided in the design stage of the bridge. The safety and riding comfort of the high-speed train are also big concerns, which raise the research interest in the vibration of the trains (He et al., 2017). A better understanding of the train-bridge dynamic system is necessary in order to build better bridges to resist vibrations, and to make better trains to reduce the vibration of bridges along with enough safety and riding comfort.

1.2. Research Motivations

The vibration of a bridge crossed by moving trains has been studied for more than one and a half centuries since the collapse of Stephenson's bridge at Chester in England in 1847 (Iwnicki, 2006). Numerous researchers have dedicated themselves to the development of the theoretical models of this problem, initially from the moving force model to the moving mass model, the moving oscillator model (Frýba, 1999) and the moving vehicle model. With the rapid development of computers and the Finite Element (FE) method, the structural analysis of complicated and large structures has been feasible since the 1940s (Yang et al., 2004), making the numerical simulation for a real bridge subjected to travelling trains more sophisticated and accurate.

On the other hand, experimental techniques, like modal testing (Ewins, 2000) and ambient vibration testing (Au, 2011) make the identification of structural frequencies not hard to achieve. In addition, various sensors, like accelerometers, strain gauges, laser vibrometers and so on provide convenient means of measuring the dynamic response of real structures. Some wireless sensors, like wireless strain gauges and accelerometers (Sekiya et al., 2016) become cheap compared with wired sensors and enable the data processing centre to be far away from the sensors. A large number of wireless sensors can be placed on a bridge to obtain its mode shapes (Whelan et al., 2010) or monitor the bridge for a long time (Moreu et al., 2017) at a reasonable cost.

Theoretical study of the train-bridge dynamics contributes to a better railway design and maintenance, but theoretical models need to be updated and validated by experimental results. On the other hand, modal testing on a real bridge demands placing many sensors on the bridge to identify its mode shapes. In this case, theoretical models can be used to predict the mode shapes of the bridge, although the accuracy of the predicted mode shapes depends on a variety of factors of the theoretical model.

Full-scale tests on railways are usually conducted to identify the modal properties of bridges, validate the theoretical models of a train-bridge dynamic system and so on, but demand a close collaboration with railway staff, which may be one of the reasons why full-scale experiments of the train-bridge dynamic system are rarely seen in the

literature (Green and Cebon, 1994; Xia et al., 2003a; Liu et al., 2009; Zhai et al., 2013). On the other hand, *small-scale experiments* in a lab can avoid these drawbacks (Stăncioiu et al., 2011; Yang et al., 2017). Advantages of doing small-scale experiments in a lab are many. For example, many new sensors and new modelling or identification methods are tested in a lab firstly and then applied to real scenarios (Li et al., 2015). Furthermore, theoretical models of vehicle-bridge systems could be verified by small-scale experimental results. However, reports on small-scale experiments on the train-bridge dynamic system are few in the literature. This thesis is devoted to the theoretical and laboratory experimental studies of the train-bridge dynamic systems.

Apart from the above motivations, another motivation of this thesis is about the type of bridge to study. Simply supported bridges have been widely studied, but relatively much less attention is paid to the study of continuous bridges in the literature. Numerical results in section 3.1 of this thesis show that the Dynamic Amplification Factor (DAF, which is defined as the ratio between the maximum dynamic displacement of a structure at its mid-span and its static deflection at the same place) of a two-span continuous beam traversed by a moving force can be as large as 3.21 at the second mid-span when the speed ratio of the moving force to the critical speed of the beam is 0.85, which is much larger than the maximum DAF of a simply supported beam (about 1.75). Normally, only using the first mode of a simply supported bridge is good enough to obtain accurate dynamic displacement of the beam subjected to moving loads (Yang et al., 2004). However, more modes are needed in the calculation for a continuous bridge, as the first few frequencies may be close to each other, which can be seen from the values of the dimensionless parameter λ (the product of wavenumber and span length) for a multi-span beam (Blevins, 1979). Therefore, the dynamic effect of a continuous bridge should be investigated carefully for designing a safe and long-life high-speed railway.

The analytical solution of a simple bridge subjected to a moving force can help researchers quantify the contributions of different frequency components in the dynamic response of the bridge, which can provide guidance for identifying modal properties of the bridge, for example, bridge natural frequencies from the structural response (Yang and Lin, 2005). However, the analytical solution of a continuous beam subjected to a moving force cannot be described by one expression for the

whole length of the beam due to the different expressions for the mode shapes of different spans of the beam, and the complexity of the solution for a span increases with the number of the span. It is worth studying to describe the mode shapes of a continuous beam by using one expression for the whole length of the beam and to derive the analytical solution of the continuous beam subjected to a moving force.

1.3. Aim and Objectives

The aim of this thesis is to study the dynamic interaction between moving cars and a four-span continuous plate structure in a lab by theories and experiments in order to gain further understanding of vehicle-bridge dynamic interaction. To this end, there are several interesting aspects that are worth investigating.

(1) To describe the mode shapes of a continuous beam approximately by one equation for the whole length of the beam and to derive the analytical solution of the equation of motion of the continuous beam subjected to a moving load in one equation.

(2) To assess the vibration behaviour of a beam/plate structure excited by a moving force model, a moving sprung mass model and a moving rigid body model.

(3) To implement the Mode Superposition (MS) method and an iterative algorithm for analysing moving-load problems.

(4) To develop a contact loss model for the moving sprung mass model.

(5) To build a proper theoretical model for an experimental vehicle-bridge dynamic system (a four-span continuous plate structure traversed by moving cars) and determine its dynamic responses efficiently.

(6) To identify the material and geometric properties of the experimental system and to update and verify the theoretical model with experimental results.

(7) To study the influences of vehicle speed, vehicle mass, vehicle length, wheel/rail contact stiffness and the number of moving vehicles on the dynamic responses of the plate structure theoretically and experimentally in the lab.

1.4. Outline of the Thesis

Firstly, a review of more than 200 publications in the area of vehicle-bridge dynamics is conducted in Chapter 2, including theoretical work and experimental work. After that, a simply supported and a two-span continuous Euler-Bernoulli beam traversed by a moving constant force or a moving harmonic force are studied analytically in Chapter 3. The mode shapes of a two-span continuous beam are described approximately by one equation for the whole length of the beam and used in the analytical solution of the beam subjected to a moving force (constant or harmonic).

A beam traversed by a moving sprung mass considering separation between the mass and the beam is presented in Chapter 4. The equation of motion of the beam is transformed into modal coordinates by using the MS method and coupled with that of the mass during the no-separation period. The coupled equation is solved by using the Newmark-Beta method. Free vibration occurs for the beam and the mass during separation period. The vibrations of a simple beam and a two-span continuous beam subjected to a sprung mass are compared with those of the beams traversed by a moving force.

A four-span plate structure traversed by a moving car is studied theoretically and experimentally in a lab in Chapter 5. The equation of motion of the plate structure and that of the car are solved separately by an iterative method. The Euler-Bernoulli beam model is compared with an FE model for the plate structure in terms of the modal shapes of the structures. The car is treated as a two degrees-of-freedom (DOFs) rigid body with heave and pitch motions. An offset ratio is chosen as an updated parameter to make the numerical frequencies of the plate structure closer to the experimental counterparts. The theoretical model of the car-plate dynamic system is validated by measured displacements of the structure subjected to a moving car at different speeds. The spectra of the measured structural displacement responses with and without the moving car (free vibration) are also investigated. Then, a parametric analysis based on the validated theoretical model is carried out to study the influences of car model, point damping (provided by additional supporting actuators), car speed, car mass, car length and contact stiffness on the vibration of the system.

Two cars are utilized to excite the plate structure in Chapter 6. The two cars are either separated or connected by a connector which allows the rotation of each car. A number of tests with different car speeds are conducted in the lab. The dynamic displacements of the plate structure and time-varying car speeds are acquired. Spectra of the structural dynamic displacements are also presented. The influences of the number of cars, loads of two-connected cars and car accelerations on the dynamic response of the structure are investigated numerically in the last section of this chapter.

Conclusions of this thesis and discussions about future work are made in Chapter 7, which is followed by references.

2. Literature Review

Theoretical models of the train-bridge system have been developed from a moving force on a beam to complicated vehicles travelling on realistic FE-modelled bridges (Yang et al., 2004; Thompson, 2008). The solutions of theoretical models range from analytical solutions to numerical solutions. However, there is a trade-off between the complexity of the system model and the computational time. It is of significant importance to establish a theoretical model of the vehicle-bridge system with acceptable computational efficiency based on the desired accuracy for the results and the complexity of the system.

To predict accurately the dynamic responses of a specific real vehicle-bridge system, accurate information about the parameters, like the geometry, material properties, boundary conditions and modal properties of the system is necessary. Such information may be obtained from the design company of the bridge and the train manufacturer. However, the physical values of these parameters are different from the design values because of the errors caused by the structural construction, the manufacturing process and the aging effect. In this case, obtaining actual values of the system parameters becomes important for predicting accurate results and detecting damage of the system. In engineering, modal testing is usually carried out to obtain the modal properties (frequencies, damping and mode shapes) of the bridge and the train. These obtained modal properties are often used to update the theoretical model (Aktan et al., 1998; Sehgal and Kumar, 2016; Yang et al., 2017) or assess the state of the system (Zhu and Law, 2015). Impact hammer testing and shaker testing are two common methods to excite small structures for modal testing in the lab, but they are expensive and sometimes hard to implement for bridges in reality.

On the other hand, moving vehicles can excite bridges to vibrations with high signal-to-noise ratios, which is very helpful for modal analysis of the bridges. Normally, sensors can be placed on a bridge to obtain the modal properties of the bridge. However, it was found that the modal properties, including frequencies and mode shapes could also be extracted from the responses of vehicles passing over the bridge (Yang and Lin, 2005; Yang et al., 2014; Zhu and Law, 2015). Actually, the responses

of the bridge or the vehicles contain the information of the whole train-bridge system because of the interaction between the trains and the bridge, which is a characteristic of the interaction system and could provide different means of identification for the interaction system. Similarly, the properties of the vehicles can be extracted from the responses of the vehicles (Yang and Lin, 2005) or the bridge (Karoumi et al., 2005; Deng and Cai, 2009). The contact forces between the vehicles and the bridge can be identified either from the instrumented bridge (Chan and Ashebo, 2006; Yu and Chan, 2007; Deng and Cai, 2010b) or from the instrumented vehicles (OBrien et al., 2014).

The theoretical and experimental work in the field of vehicle-bridge interaction is reviewed in this chapter. Firstly, various theoretical models are classified into four main categories based on vehicle models, namely the moving force model, the moving mass model, the moving oscillator model and the moving vehicle model. The applications of moving load in the identification of vehicle or bridge properties are discussed in the following section. There are two main types of identification parameters: bridge parameters, including bridge material properties, bridge modal properties, bridge damage like cracks etc.; and vehicle parameters, including axle loads and distance, vehicle speed and so on. Another important approach for studying the train-bridge dynamic system is experiments, including field tests and laboratory tests, which are all overviewed in the last two sections.

2.1. Theoretical Work

While a moving train-wheel load can be treated as a *moving force*, a *moving mass*, a *moving oscillator* or a more complicated *moving vehicle* consisting of springs, dashpot and rigid-bodies in theoretical models, a bridge can be modelled as a beam, a plate or an FE model (Au et al., 2001; Nguyen et al., 2009; Xia and Zhang, 2005; Zhai et al., 2013). If the moving load was treated as a *moving force*, it would not be hard to solve the problem. Taking a constant force moving at a constant velocity on a simply supported beam for example, the equation of motion of the beam after applying *MS method* has the same form as a single DOF system excited by a harmonic force, which can be solved analytically (Frýba, 1999). On the other hand, if the mass of the moving vehicle is considered, the contact force between the vehicle and the bridge would change with time, as the contact force includes an inertial force

of the vehicle. The inertial force is dependent on the motion of the vehicle, which is influenced by the motion of the bridge, so the contact force actually is an interaction force varying with time. In this case, the equation of motion of the bridge cannot be solved analytically.

In order to determine the dynamic response of the bridge under moving vehicles, *MS method* can be used to separate the space component from the time component in the whole solution. The whole solution is equal to the sum of different modes multiplied by their corresponding modal coordinates. Another way is the *direct method* (Song et al., 2003; Lou, 2007; Neves et al., 2012). By using the *FE method*, the whole solution is discretized into a number of elements in space and nodal coordinates in time. The solution of a point within an element is given by the product of the nodal coordinates of the system and the shape function of the system. As for the dynamic response of large structures, the number of structural modes needed for computation is much smaller than the number of DOFs of the structures' FE models, thus the *MS method* is generally thought to be highly efficient in this case, compared with the *direct method.*

After applying the *MS* or *FE method*, only the generalised or modal coordinates in the time domain are the remaining unknowns in the equation of motion of bridges. The next question is to solve the equations of motion of the bridges and vehicles. There are generally two methods: the *coupled method* (Yang et al., 2000; Sun and Dhanasekar, 2002; Zhai et al., 2009; Lou et al., 2012) and the *iterative method* (Lei and Noda, 2002; Nguyen et al., 2009; Liu et al., 2009; Feriani et al., 2010; Zhang and Xia, 2013). The *coupled method* eliminates the contact forces from the equations of motion of the bridge and vehicles. Then the equations of motion of bridges and vehicles are actually combined to one equation with time varying mass, damping and stiffness matrices, which can be solved by a numerical integration method. The *Component Mode Synthesis (CMS) method* (De Salvo et al., 2010; Salcher and Adam, 2015) is one example of the coupled method. It combines the DOFs of the bridge in modal coordinates with the DOFs of the vehicle into one equation of motion for the whole system. On the other hand, the *iterative method* solves the equations of motion of the bridge and vehicles separately by imposing the displacement compatibility and force equilibrium at the contact interface. A numerical integration method is still needed but the equations do not have time-varying coefficient matrices. Some other

methods to solve the vehicle-bridge interaction problem are exemplified in the following. Neves *et al.* (2012) combined the equations of vehicles and a bridge with additional compatibility equations, leaving displacements and contact forces as unknowns. The combined equation was then solved directly by a block factorization algorithm. However, the wheel/rail contact loss was not allowed. This drawback was then resolved in (Neves et al., 2014). Liu *et al.* (2014) proposed a non-iterative method to solve the motion of the vehicle and that of the bridge separately by estimating the forces acting on the vehicle at every time step from the displacements and velocities of the wheel sets at the previous time step under the condition of small enough time steps.

For the integration methods, Zhai (1996) proposed a predictor-corrector integration method to analyse large-scale linear algebraic equations with diagonal mass matrixes. This method combined a new explicit method and the Newmark method and avoided solving the linear algebraic equations. Hence the integration efficiency was improved compared with implicit integration methods. Due to the usage of the predictor, the accuracy of the method was higher than explicit integration methods.

Basically, a real bridge vibrates in three directions. These three vibrations influence each other through the wheel/rail contact, but the influence is sometimes small and could be ignored depending on the situation and the purpose of the study. The vertical vibration of a bridge is one of the major concerns in design. The lateral vibration of the train-bridge system is important in studying train derailment (Xiao et al., 2010). The longitudinal vibration of the rail is a big factor affecting the wheel and rail wear. In this thesis, the vertical vibration of the bridge is the only concern. The influences of the lateral vibration and longitudinal vibration on the vertical vibration of the bridge are small for the experimental rig in the lab and thus ignored. However, the lateral vibration and the longitudinal vibration of the train-bridge system are also mentioned at appropriate places in this chapter.

2.1.1. Moving force model

Many researchers' interests have been attracted to the vibration of a bridge subjected to moving trains since Stephenson's Bridge collapsed in 1847 in England (Iwnicki, 2006). If the *mass ratio* of a vehicle to a bridge is small, the vehicle-bridge dynamic system can be modelled as the *moving force model* (Figure 2.1).

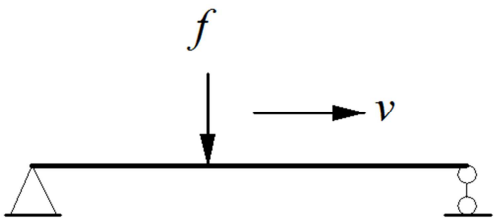

Figure 2.1. Moving force model

(a) Theoretical model

Stokes is believed to be the first researcher who treated the train-bridge dynamic system as a moving load problem (Timoshenko, 1953). Olsson (1991) solved the moving force problem by both an analytical method and the FE method. Assumptions inherent in the problem were also discussed. Fryba (1999) gave the derivation process for the closed-form solutions of the vibration of an Euler-Bernoulli beam crossed by a moving constant force in different scenarios and validated the theoretical results by comparing with experimental results in his monograph. The moving harmonic force problem was also discussed and validated by experimental results of the vibration of a bridge excited by a moving locomotive. Fryba also considered the scenario of a strip of distributed force moving on a beam to simulate the dynamic response of a large-span railway bridge subjected to a number of train carriages. Savin (2001) derived the analytical solution for the vibration of beams passed over by successive moving forces. A simplified method of calculating maximum dynamic deflection of the beam under successive forces was given. Pesterev *et al.* (2003b) determined the function of the maximum deflection of a beam with respect to the velocity of a moving force based on the first beam mode. Garinei and Risitano (2008) firstly analysed the dynamic responses of small and medium bridges travelled by a combined force including a constant component and alternating components in the range of 0-6 Hz. Then several equidistant combined forces were studied. The results showed that alternating forces, even with much lower amplitudes than that of the constant force, could lead to unacceptably large deflections and thus should be reduced. Dimitrovová and Varandas (2009) analysed the effect of the sudden change of the foundation stiffness of a beam on the critical speed of the moving load at which the first mode of the beam is excited into resonance.

Wu *et al.* (1987) studied the vibration of a *multi-span plate* subjected to one or a series of forces moving at variable speeds by the *FE* and *MS* methods. Wang and Lin (1998) firstly carried out the modal analysis of a multi-span Timoshenko frame structure, taking account of the effects of axial inertia, rotatory inertia and shear deformation of each frame. The vibration of the frame structure excited by a moving concentrated force or a moving distributed force was studied by the MS method next. Yau (2001) studied the impact factor of continuous beams subjected to a series of moving forces. It was found that the number of spans reduces the impact factor of the beams. Martinez-Castro *et al.* (2006) tackled the vibrations of non-uniform multi-span beams traversed by moving forces by using a semi-analytic method. The numerical mode shapes of the beams were firstly obtained by the FE method. Then the resulting equations of motion of the beams after applying the MS method were solved analytically.

Belotserkovskiy (1996) studied the vibration of *an infinite beam* resting on identical periodic simple elastic supports subjected to a harmonic concentrated force by using the Fourier Transformation. Jin (2004) studied the vibration of an infinite beam on a poroelastic half space passed over by a harmonic force by using Fourier Transformation. Kargarnovin and Younesian (2004) were concerned with the dynamic response of an infinite Timoshenko beam resting on a generalized Pasternak-type viscoelastic foundation subjected to an arbitrary-distributed moving force.

Eftekhari and Khani (2010) firstly used the FE method to discretize the spatial domain of the equation of motion of the moving force-beam system. Then the Differential Quadrature Element (DQE) method was employed in each time step to solve the resulting time domain equation. Hu *et al.* (2013) adopted a generalized multi-symplectic integrator method to deal with the moving force problem.

(b) Resonance and cancellation

The free vibrations of a bridge passed by train loads may cancel to null, which is known as the phenomenon of *cancellation*, or on the other hand appear to be in *resonance* because of the accumulation of the free vibrations. Yang *et al.* (2004) used a series of forces to simulate a number of train carriages. The closed-form solution of the dynamic response of a simply supported beam traversed by a sequence of moving

forces was derived. The phenomenon of resonance and cancellation were identified and the optimal design criteria were proposed for bridges. Museros et al. (2013) analysed the free vibrations of a simply supported beam and an elastically supported beam after the exit of a moving force. The scenarios of cancellation and maximum response were discussed. Xia *et al.* (2014) derived the analytical solutions for a simply supported beam subjected to a moving force or a series of moving forces. For each scenario, the conditions for the cancellation and resonance were discussed. Then a numerical study for the dynamic response of a bridge under high-speed trains was carried out to verify the analytical solutions. Sha *et al.* (2016) investigated the resonance and cancellation phenomenon in a periodic viaduct under a series of equidistance moving forces.

(c) Train-track vibration

The vibration of the railway track system resting on the ground subjected to train loads is another interesting research topic which has drawn much attention. A few examples can be found in (Steenbergen and Metrikine, 2007; Koziol et al., 2008; Sheng, 2015). Steenbergen and Metrikine (2007) studied the beam resting on the half-space to a moving harmonic force by using three different approaches. Hoang *et al.* (2017) studied analytically the vibration of a periodically supported beam subjected to moving forces and applied to a non-ballasted railway track. Zhao *et al.* (2017) studied the nonstationary random vibration of an infinite beam resting on a Kelvin foundation subjected to moving random forces by using the Pseudo Excitation Method (PEM) and the Fourier Transform.

2.1.2. Moving Mass Model

When the inertial effect of moving vehicles cannot be ignored, it is essential to use more complicated models for the vehicles. The *moving mass model* (Figure 2.2) is the simplest model including the inertial effect of a moving vehicle. If the contact stiffness and contact damping are also considered, the *moving sprung mass model* (Figure 2.3) is needed.

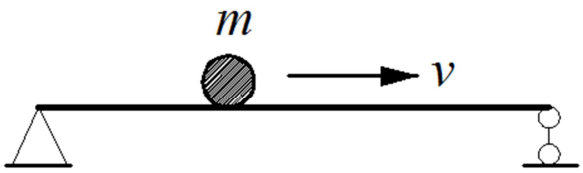

Figure 2.2. Moving mass model

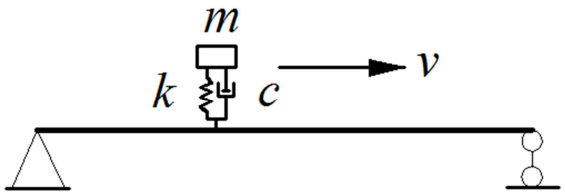

Figure 2.3. Moving sprung mass model

(a) Traditional approach

Ting *et al.* (1974) derived the integration form of the equation of motion of the mass-beam dynamic system by using a Green function. A backward difference method and a numerical integration method were applied for the time domain and the spatial domain, respectively. Humar and Kashif (1995) studied the vibration of a plate travelled by a sprung mass by using the FE method. Pesterev and Bergman (2000) improved the solution for the shear force and bending moment of a beam subjected to a sprung mass with an arbitrarily varying speed. Pesterev *et al.* (2003a) compared the moving sprung mass model with the moving mass model and found that the dynamic stress of the beam varies with the model even when the contact spring stiffness of the sprung mass becomes infinite. The reason was thought to be the high frequency components in the contact force for the moving sprung mass model, which did not vanish with the increase of the contact spring stiffness. Bowe and Mullarkey (2008) derived the final forms for a beam subjected to a moving mass by both the direct method and the MS method, and compared the results by these two methods with those in the literature. Feriani *et al.* (2010) compared the performance of two iterative schemes which act on the whole time history (WTH) and in the single time step (STS), respectively.

Akin and Mofid (1989) determined the vibration of a beam with various boundary conditions subjected to a moving mass by using an analytical-numerical method and

compared the result with that obtained by the FE method. Chatterjee *et al.* (1994a) investigated the vibrations of continuous bridges with surface irregularities subjected to a moving mass or a moving sprung mass. The MS method and the iterative method were utilized to solve the problem. Yang *et al.* (1995) performed a parametric study for various simple and continuous beams traversed by one or two bidirectional five-axle trucks. Each truck was modelled as three lumped masses resting on the beam with three sets of springs and dashpots. The effects of a defined speed parameter, the vehicle/bridge frequency ratio, the bridge damping and the bridge surface roughness on defined impact factors (the increase between the dynamic response and the static response divided by the static response) were studied. De Salvo *et al.* (2010) found the mode shapes of continuous beams with non-uniform cross sections and solved the moving mass-beam problem by using the CMS method.

Mamandi and Kargarnovin (2010) carried out a parametric sensitivity analysis of the dynamic response of an inclined Timoshenko beam travelled by successive (mainly one or two) moving masses/forces. The mass of the moving mass or equivalent moving concentrated force, the speed of the moving mass/force, the beam's inclination angle, length of the beam, height of the beam and spacing between successive moving masses/forces were taken into account. Nikkhoo *et al.* (2014) tackled the vibration of an undamped Kirchhoff plate excited by two streams of successive moving masses with opposite travelling directions representing traffic in two lanes on a bridge. Yamchelou and Nouri (2016) did a parametric study for the vibration of a beam excited by a moving mass with different accelerations and mass ratios between the mass and the beam.

(b) Contact loss

Lee (1995) is thought to be the first researcher who took into account of the effect of *separation* between the moving mass and the beam. He found that the application of suitable tensile axial forces on the beam could help avoid the separation between the travelling mass and the beam. Lee (1996) also showed that there was a higher chance for *separation* between the mass and the beam to occur when the *mass ratio* of the mass to the beam increased, especially at high velocity of the mass, and the effect of *separation* on dynamic response of the beam could be significant. Pesterev and Bergman (1998) proved theoretically that the time-varying mass matrix of the mass-

beam system was invertible.

(c) Other approaches

Apart from the traditional methods to solve the train-bridge dynamic problem, there are some other methods. Cifuentes (1989) determined the vibration of a beam excited by a moving mass by using a *combined FE/Finite Difference* (*FD*) method. Rao (2000) studied the *internal and external resonances* of an Euler-Bernoulli beam subjected to one or a series of moving masses by using a *perturbation approach* based on the method of multiple scales. Verichev and Metrikine (2000) investigated the dynamic rigidity of a Timoshenko beam resting on an elastoviscous base in a moving contact with a mass by using the Fourier Transformation. DeFaria and Oguamanam (2004) studied the vibration of a plate under a moving mass by using adaptive Mindlin elements and the perturbation method. Bajer and Dyniewicz (2009) used the space-time FE method to solve the moving mass problem. Kumar and Saleeb (2009) modelled the interaction between masses/oscillators and a beam/plate in ABAQUS by using the 'hard' contact and contact loss was allowed. Chen *et al.* (2014) studied the interaction between an accelerating mass and a Timoshenko beam by using the Spectral Element Method in Time Domain (TSEM).

2.1.3. Moving Oscillator Model

A more realistic model for a train is the *moving oscillator model* (Figure 2.4) which is made of an unsprung mass, a sprung mass and a spring or a dashpot connecting the two masses.

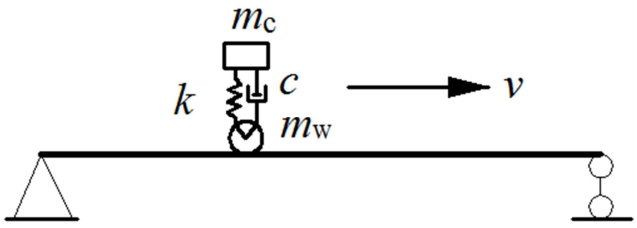

Figure 2.4. Moving oscillator model

(a) Theoretical model

Olsson (1985) proposed a general vehicle-bridge element to model the vehicle-bridge interaction phenomenon with the MS method. Klasztorny and Langer (1990) studied the dynamic stability and the steady-state response of a single-span beam subjected to a stream of moving oscillators. Yang and Lin (1995) defined an interaction element comprised of a bridge element and the suspension units of a vehicle (modelled as an oscillator) resting on the bridge element. The DOFs of the vehicle body were eliminated on the interaction element level by using the dynamic condensation method. However, the accuracy of the vehicle response was not good enough. Such a drawback was overcome by modelling vehicles as oscillators (Yang and Yau, 1997; Yang and Wu, 2001). Cheung *et al.* (1999) studied the vibration of a multi-span non-uniform beam travelled by one or a series of moving oscillators by using the MS method with assumed beam modes. Cheng *et al.* (2001) presented a vehicle-track-bridge element to consider the effect of track structure on the dynamic response of the vehicle-track-bridge system. While the vehicle was treated as a moving oscillator, the track was modelled as a Bernoulli-Euler beam supported by springs and dampers connecting the track with the bridge deck. Biondi *et al.* (2005) studied the dynamics of the train-track-bridge system by using the CMS method to couple the continuous media (rails and bridge) and the oscillators (train loads). Muscolino *et al.* (2009) revealed theoretically that the influence of impulse on the dynamic response of oscillators was significant when the oscillators entered and left a bridge. Wang *et al.* (2010) studied the resonance of a two-span continuous beam under a series of moving oscillators. It was found that the continuous beam could have two critical speeds corresponding to two resonance responses under a certain range of the span length at the train speed of 500 km/h.

(b) Contact loss

Cheng *et al.* (1999) studied the *separation* between moving oscillators and a *multi-span continuous beam* by using numerical modal shapes obtained by means of the FE method. The impact at the moment of reattachment was implemented through a proposed algorithm. Stăncioiu *et al.* (2008b) studied the *separation* between an oscillator and a beam and the *reattachment* effect afterwards. The scenario of a moving oscillator moving on a truss structure considering the *separation* and

reattachment between the oscillator and the truss structure was studied by Baeza and Ouyang (2008). The *MS method* and the FE method were utilized to solve the oscillator-structure dynamic problem. Michaltsos (2010) studied the oscillator-beam interaction considering irregularities of the beam and *separation* between the oscillator and the beam. Ebrahimi *et al.* (2015) studied the vibration of a simply supported Euler-Bernoulli beam with different numbers (zero to three) of intermediate supports subjected to a moving oscillator.

2.1.4. Moving Vehicle Model

With the development of high-performance computers, it becomes possible for researchers to establish and calculate the *moving vehicle model* (Figure 2.5) with more details about the train. Whereas the bridge model is usually built in a commercial FE software, the vehicle model is normally established analytically by treating it as a rigid-body structure with connecting springs and dashpots (Au et al., 2001). Using the FE method to establish both the vehicle model and the bridge model was also studied in (Li et al., 2010; Neves et al., 2012).

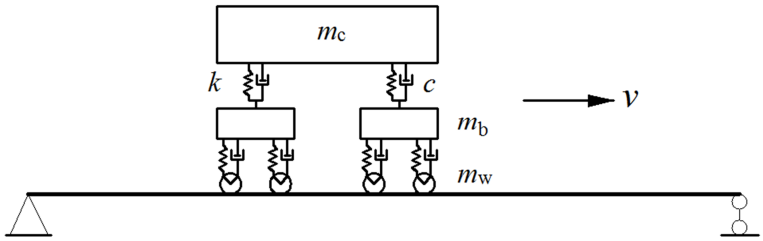

Figure 2.5. An example of moving vehicle model

(a) Vehicle and bridge model

Fryba (1968) studied the vibration of a simply supported beam subjected to a travelling two-axle system considering beam surface irregularities. Hwang and Nowak (1991) conducted the parametric analysis of the dynamic loads exerted on a bridge with surface roughness subjected to trucks. Truck type, total weight, axle distances, and speed were treated as random variables and simulated by the Monte Carlo method. The bridge surface roughness was simulated by a Power Spectral Density (PSD) function. Composite steel girder bridges and prestressed concrete girder bridges were studied. Chatterjee *et al.* (1994b) investigated suspension bridges

with different boundary conditions traversed by a moving vehicle. The vehicle models in 1D, 2D and 3D were compared. Marchesiello *et al.* (1999) studied the dynamic response of a three-span plate interacting with a seven-DOF moving vehicle by using the analytical modes of the plate. Lou and Zeng (2005) derived the equation of motion of a vehicle-bridge dynamic system based on the stationary value of the total potential energy of the dynamic system with the assumption of no separation between wheels and rails, which was solved by a numerical integration method. Ouyang and Mottershead (2007) studied the vibration of a beam excited by a moving flexible body with conformal contact by using a combined numerical-analytical method. Xia and Zhang (2005) combined the MS method with the FE method to simulate the dynamic interaction between the China-Star high-speed train and a bridge with 24 m-span prestressed concrete box girders on the Qin-Shen Special Passenger Railway in China. Zhai *et al.* (2013) established a train model with 35 DOFs for every carriage and illustrated in detail that strong dynamic interactions existed within the system of the train, track and bridge and it was necessary to investigate train-track-bridge dynamic interaction. Yang and Yau (2015) studied the resonance caused by the pitch motion of a vehicle passing over a number of simple bridges.

Lou (2005) introduced a bridge-track-vehicle element to take into account the pitching effect of the vehicle. The vehicle was modelled as a four DOFs multi-body with one car-body, two wheels and springs and dashpots connecting the car-body and the wheels. Lei and Noda (2002) studied the interaction between a vehicle and a track system with random vertical track profile by the FE method. The equations of motion of the vehicle and the track system were established separately and solved by an iterative method. Pesterev *et al.* (2004) derived the analytical solution for the contact force between a moving vehicle and road surface with irregularities by using the MS method. Xu *et al.* (2009) studied the random vibration between a moving vehicle and a Kirchhoff plate on a Kelvin foundation by using a 2D moving element method and the Pseudo Excitation Method (PEM). Lou *et al.* (2012) proposed a rail-track-bridge element with the length of the bridge element longer than that of the rail element.

Li and Su (1999) simulated the resonant vibration of a girder bridge traversed by a number of train carriages using the moving force model and the moving vehicle

model, respectively. It was found that the resonance of a small or medium-span girder bridge subjected to a high-speed train with many vehicles may be caused by the free vibration of the bridge. Zhu and Law (2002) investigated the vibration of a multi-lane continuous bridge deck travelled by a number of vehicles. Each vehicle was modelled as a seven-DOF system. Xia *et al.* (2003b) analysed the dynamics of a high-speed railway bridge under articulated trains. Nguyen *et al.* (2009) simulated a real train consisting 15 vehicles passing over a slab simply supported bridge. Each vehicle was modelled as a 27 DOFs system and the bridge was discretized into different elements. An iterative method was implemented to solve the train motion and the bridge motion through a linear contact model. Guo *et al.* (2012) established a three-dimensional (3D) model for a train-track-bridge dynamic system, where several identical vehicles were included (each vehicle treated as a 27 DOFs rigid-body structure) and a rail-ballast-beam FE model was built for a bridge. The MS method was applied for the equation of motion of the bridge and the coupled equation of motion of the train-bridge system was derived based on the wheel/rail rigid contact. The simulated results had good agreement with field measured results.

Huang and Wang (1998) analysed the effect of the longitudinal grade on the vibration of highway bridges passed over by different vehicles. The eleven-DOF vehicle model was established to represent the HS20-44 truck in America. Three multi-span girder bridges with rough bridge decks were considered. Cojocaru *et al.* (2004) studied the vibration of a beam traversed by a moving second elastic beam which was represented as a train and connected with the beam by means of a rigid interface. Xu *et al.* (2011) did a sensitivity analysis for a vehicle-bridge system with random surface roughness by using PEM and the Precise Integration Method (PIM). Then the sensitivities were used in the optimization at the design stage with the riding comfort of the vehicle as an objective function. Zhang and Xia (2013) compared the time-step iteration (TSI) method with the inter-system iteration (ISI) method applied in the vehicle-bridge interaction system. Lou and Au (2013) derived the formulae for calculating accurate bending moments and shear forces of Bernoulli-Euler beams under moving vehicles by using the FE method. Doménech et al. (2014) did a comprehensive sensitivity analysis for the vehicle-bridge interaction parameters by using different vehicle models.

(b) Wheel/rail contact

Stăncioiu *et al.* (2008a) considered the *separation* and *reattachment* of a two-axle system moving on a beam. The wheel/rail contact was assumed to be at a point. There are four possible contact scenarios for the two-axle system travelling on the beam: only the front wheel, only the rear wheel, no wheels or both wheels separated from the beam. In each scenario, the equation of motion for the whole system is different and the contact scenario at every time step needs to be judged. The vibration of a continuous beam with multiple elastic supports travelled by a two-axle system considering separation and reattachment was also studied by them (Stăncioiu et al., 2009). Zhu *et al.* (2015) used a linear complementarity method to study a vehicle-bridge dynamic system considering separation and random roughness and the conventional trial-and-error iterative process in numerical simulation was avoided.

Liu *et al.* (2008) studied the dynamic response of a simply supported bridge traversed by vehicles (each vehicle modelled as a ten-DOF system) with Hertz contact springs considering separation. Dinh *et al.* (2009) investigated the scenario of a ten-car train passing over a two-span continuous beam at different speeds and rail irregularity wavelengths. While each car was modelled as a 31 DOFs rigid-body structure composed of one car body, two bogies and four wheel-sets with connecting springs and dashpots, the bridge FE model was built by using 3D beam elements. A 3D wheel/rail rolling contact model was established based on Hertz and Kalker contact theories and separation was allowed at the wheel/rail interface. Ju (2013) studied the influence of the displacement difference between two adjacent simply supported girders caused by foundation settlements or rotations on train derailment coefficients. The wheel/rail separation was considered in a nonlinear moving wheel element. Salcher and Adam (2015) included Kalker's linear creep theory in the train-bridge interaction model by using a modified CMS method. An example of a ballasted single-span steel bridge traversed by a Railjet train with seven passenger cars was studied. It was concluded that a sophisticated model of the train-bridge system was essential for quantifying the effect of rail irregularities on the system dynamic response.

It should be noticed that the point wheel/rail contact assumption is acceptable for calculating the vertical dynamic responses (displacement and acceleration) of the

vehicle and the bridge (Ju and Liao, 2010; Guo et al., 2012; Antolín et al., 2013). However, if the accurate contact force or the contact stress/strain is the concern, e.g. in studying the train safety or rail wear, more sophisticated wheel/rail contact models are needed (Antolín et al., 2013). For sophisticated wheel/rail contact theories, one may refer to the detailed overview by Kalker (1991). As the dynamic responses of the vehicle and the bridge are the main concerns in this thesis, the point wheel/rail contact assumption is adopted.

(c) Vehicle-track vibration

Sheng *et al.* (2004) developed a theoretical model incorporating vehicles, a track with irregularities and a layered ground to predict the dynamic wheel-rail forces and the displacement power spectra of the track and the ground surface. Ma and Liu (2016) proposed a theoretical model based on the periodic-Fourier-modal method for studying the vibration of a floating slab track with random irregularities subjected to a number of vehicles.

2.1.5. Identification of a Vehicle-Bridge System

Apart from using the aforementioned various theoretical models of the vehicle-bridge dynamic system to predict the dynamic responses of the system, identifying the system properties from vehicular or bridge responses is another important research topic and reviewed in this section. Please note that identifications for the vehicle-bridge system are discussed theoretically only here. The applications in reality are described in section 2.2 (experimental work).

(a) Identification of modal properties of bridges

Unlike traditional methods of identifying the modal properties of bridges by using sensors to measure the dynamic responses, extracting modal properties from vehicle responses does not need the installation of sensors on bridges and could scan the modal properties of a number of bridges with high efficiency. Hence this approach has drawn much research interest in recent years.

To identify bridge frequencies from vehicle responses, Yang and Lin (2005) derived the analytical solution for the dynamic responses of both the moving sprung mass

and an Euler-Bernoulli beam based on the assumption that the mass ratio of mass to beam is small and the inertial effect of the mass can be ignored. The spectrum analysis of the mass response and the beam response revealed some useful information associated with the moving speed of the mass, sprung mass frequency and the beam frequencies. The possibility of identifying the bridge frequencies from the vehicular response was discussed. Yang and Chang (2009b) demonstrated the feasibility of using Empirical Mode Decomposition (EMD) technique to extract higher beam frequencies from a moving mass response. Yang and Chang (2009a) investigated the influences of the key dynamic parameters of the sprung mass-beam system on the vertical dynamic response of the moving mass. It was found that the smaller the initial mass/beam acceleration amplitude ratio in each mode is, the greater the possibility of identifying the bridge frequency in that mode from the mass response is. However, the bridge surface roughness was not considered in the above works. To overcome this drawback, Yang *et al.* (2012) proposed to use two connected vehicles to remove or reduce the blurring effect of road surface roughness. To enhance the visibility of bridge frequencies from the vehicular response, Yang *et al.* (2013b) used the singular spectrum analysis with a band-pass filter to filter out the vehicle frequency for identifying bridge frequencies.

While the above works focused on extracting bridge frequencies from the passing vehicles, some researchers recently began to study the feasibility of constructing the bridge mode shapes from the passing vehicles' responses. Zhang *et al.* (2012) extracted the structural mode shape squares from the acceleration response of a tapping vehicle by using the Short Time Fourier Transform (STFT). Yang *et al.* (2014) constructed the mode shapes of a simply supported bridge from the passing vehicular responses by using Hilbert Transform (HT). Malekjafarian and OBrien (2014) identified the bridge modes from vehicular responses by using the Short Time Frequency Domain Decomposition (STFDD). The signals from the axles of two successive trailers towed by a tractor were used and external excitations were also applied to the bridge to reduce the effect of road roughness on the accuracy of identification results. Malekjafarian and OBrien (2017) believed that it was a good idea to excite a bridge by using a travelling tractor connected by two trailers and an external excitation with a frequency close to one of the bridge frequencies. The two axle responses of the second trailer were measured and a subtraction was done

between the two responses to reduce the effect of road surface roughness. The bridge mode shapes could be estimated from the measured axle responses by Hilbert Huang Transform (HHT).

(b) Damage detection of bridges

Damage identification of the bridge under traffic load is another interesting and important research topic and has been studied extensively. There are normally two approaches known as the *indirect method* (OBrien and Malekjafarian, 2016) and the *direct method* (Sun et al., 2016) based on measured signals from the vehicle or the bridge, respectively. A recent overview in this topic could be found in (Zhu and Law, 2015). Malekjafarian *et al.* (2015) presented another critical review on the indirect bridge monitoring using vehicular responses passing over the bridge. A very recent good discussion about the merits and limitations of using the indirect method to detect the bridge damage was given in (Hester and González, 2017). Zhang *et al.* (2012) proposed a damage index based on the mode shape square extracted from an instrumented tapping vehicle, which was found robust to noise. Feng and Feng (2016) proposed to use a video-based sensor to record the time history vibration of a beam traversed by moving vehicles. The first mode shape of the beam was constructed from the measured data and the curvature of the mode was then used to identify the damage of the beam.

(c) Identification of vehicle axle loads

Apart from the above large amount of work dedicated to the identification of bridge parameters, there are also some researchers identifying vehicle parameters. Karoumi *et al.* (2005) studied the identification of vehicular axle loads from the measured strain data embedded in a bridge by minimizing the difference between the measured strain and the evaluated strain which was obtained with the usage of a determined influence line. The axle positions, axle loads, speed and acceleration were evaluated. OBrien *et al.* (2014) identified the contact force between a moving vehicle and a bridge by using the vehicle response. The applications of this method to the identifications of the bridge's bending stiffness and road pavements were also discussed.

The bridge-weight-in-motion is a significant application for identifying the vehicle axle loads from bridge responses and has attracted wide research interests. Chan and Ashebo (2006) identified the vehicle axle forces acting on a continuous beam by mounting eleven strain sensors on the beam. MS method and impulse function were used to inversely calculate the axle forces. Ding *et al.* (2009) evaluated the contact forces between a vehicle and a bridge with surface irregularities by using an evolutionary spectral method. The dynamic response of the vehicle-bridge system was separated into two parts: vehicle induced response and bridge surface irregularities induced response. Each part was calculated separately and then added together. Deng and Cai (2010b) used the influence surface concept to identify the vehicle axle loads travelling on a concrete slab bridge which was modelled as a 3D FE model in ANSYS program. The dynamic response of the bridge was separated into an inertial part and an interaction part. It was found that the inertial part has a significant effect on the identified results and should be excluded from the bridge response if the influence surface concept is used. As the acceleration of the bridge cannot be measured at every point in reality, the inertial part needed to be obtained from the vehicle-bridge interaction simulation.

2.1.6. Vibration Control of a Vehicle-Bridge System

As the vehicle-bridge dynamic system is a time-varying system, it is quite different from linear time-invariant systems to control the vibration of such a system. Tomás-Rodríguez and Banks (2010) gave a good introduction about the time-varying system and the control methods for such a system in their book. The optimal control and sliding mode control methods were discussed in detail in the book. Passive control methods have been developed for a long time and studied widely for supressing the vibration of bridges excited by moving vehicles (Papadimitriou et al., 1997; Yau and Yang, 2004; Samani and Pellicano, 2012; Pisal and Jangid, 2016). For example, Samani and Pellicano (2012) studied the performances of different absorbers for supressing the vibration of a simply supported beam traversed by equidistance moving forces.

On the other hand, semi-active or active control methods have drawn much attention recently because of the smartness of these methods. Patten *et al.* (1999) implemented an adjustable semi-active hydraulic actuation system to a real bridge in service.

Giraldo and Dyke (2007) compared passive control, semi-active control and active control for the oscillator-beam dynamic system and proposed to use semi-active or active control methods for the system. Nikkhoo *et al.* (2007) used a linear optimal control algorithm with time-varying gains to control the vibration of a beam subjected to a moving mass. The displacement and velocity of the beam were used as feedbacks. Stăncioiu and Ouyang (2014) studied the optimal control and discussed the implementation of the control method for the mass-beam dynamic system. Nikkhoo (2014) utilized piezoelectric patches mounted on the top and bottom surfaces of an Euler-Bernoulli beam as actuators and the classic linear optimal algorithm was used to control the vibrations of the beam with various boundary conditions subjected to a simple rectangular impulse force, a moving force and a moving mass.

2.2. Experimental Work

Experimental work is important for validating theoretical models and assessing the condition of real systems. Experimental results are often different from predicted results by theoretical models. Model updating is usually adopted to tackle this problem (Mottershead and Friswell, 1993). The material properties and modal properties of a vehicle-bridge dynamic system are significant values to be determined by experiments in many cases. It is ideal to have the complete information of the whole system. However, this is hard to achieve in reality. In most cases, only partial information about a bridge or vehicles is available or can be measured. Therefore, it is necessary to study the identification problem from partial information of the whole system.

To assess the real structural or vehicular properties, field tests are to be carried out. However, field tests are expensive in terms of labour and equipment, and traffic control is often needed. These drawbacks can be overcome by doing laboratory experiments. It is ideal to do laboratory experiments especially when the main purpose of the experiments is to verify modelling or identification methods. In addition, the experimental conditions can be adjusted or controlled by experimental staff depending on the experimental purposes. The experimental work in the area of vehicle-bridge interaction is reviewed based on field tests and laboratory experiments in the following two sections.

2.2.1. Field Experiments

To predict accurately dynamic responses of a real vehicle-bridge system, it is of great significance to determine the actual geometric and material parameters of the system and to validate the theoretical models by experiments. In spite of the large amount of work dedicated to the theoretical study of the vehicle-bridge dynamic problem, much less experimental work has been reported in the literature.

(a) Model updating and validation

Green and Cebon (1994) identified the modal properties of a three-span highway bridge by impact tests on the bridge with an instrumented hammer. The wheel loads of a vehicle and the dynamic response of the bridge were measured simultaneously when the vehicle was travelling on the bridge (Green, 1990). The identified modal properties of the bridge and measured wheel loads were used in a convolution integral to predict the dynamic response of the bridge. The predicted dynamic response of the bridge was compared with the measured response. Kwark *et al.* (2004) compared simulation results with experimental results of the dynamic response of a bridge crossed by a Korean high-speed train. Xia *et al.* (2003a) measured the free vibration response and the dynamic response of the Antoing Bridge on the railway line between Paris and Brussels excited by one and two high-speed Thalys trains. Lee and Yhim (2005) adopted the FE method to analyse the dynamic response of a two-span continuous box girder bridge subjected to moving forces. Shell elements with six DOFs per node were utilized and field experiments were conducted to verify the numerical results. Zhai *et al.* (2009) established a 3D vehicle-track model and validated it with full-scale field experiments. Kim and Kim (2010) fabricated a 25 m prestressed concrete girder as a test specimen and modal testing was performed on the specimen at every prestressed stage. Then the identified modal properties were used to predict the dynamic response of a girder railway bridge passed by a moving train.

Cai *et al.* (2007) studied the influence of approach-span conditions on a bridge's dynamic response subjected to moving vehicles by using a experimentally validated theoretical model. Zhang *et al.* (2008) simulated a high-speed railway bridge consisting of 28-span 24 m simple box girders traversed by the Pioneer Train. The

simulated results were compared with measured results. Liu *et al.* (2009) measured the ambient vibration and high-speed train-induced vibration of a composite railway bridge with seven spans to validate their train-bridge interaction model. Arvidsson and Karoumi (2014) reviewed the theoretical models and experiments in the field of train-bridge interaction and discussed key modelling parameters. Feng and Feng (2015) updated the theoretical model of a short-span plate girder railway bridge by using the measured response of the bridge subjected to freight trainloads in the time domain with a low-cost remote vision sensor. Koziol (2016) experimentally validated the wavelet-based approach of solving the infinite Euler-Bernoulli beam resting on a nonlinear foundation subjected to a set of moving forces for the train-track interaction problem.

(b) Identification of bridge or vehicle parameters

To assess the bridge or the vehicle condition, various works have been done for identifying the bridge or vehicle parameters by using different signal processing techniques or algorithms. Paultre *et al.* (1995) evaluated the Dynamic Amplitude Factor (DAF) of three highway bridges in Canada by measuring the forced vibrations of the bridges excited by one or two trucks. The free vibrations of the bridges were also measured to evaluate the modal properties of the bridges and calibrate the FE model of the bridges. Huang *et al.* (1999) identified the modal properties of a three-span continuous bridge by *impulse testing* with impulsive forces generated from a loaded truck. The recorded data was processed by applying the Ibrahim time-domain identification technique. The identified results were compared with those by ambient test. Brownjohn *et al.* (2003) assessed the upgrading works of a highway bridge by doing dynamic tests on the bridge combined with the updating of the bridge FE model. Gonzalez *et al.* (2010) used the moving force model to estimate the critical speed and the DAF of the bridge by doing the field experiment of a truck passing over a simply supported bridge. Kim and Kim (2010) identified the material properties, natural frequencies and modal damping ratios of a 25-meter concrete girder specimen by full scale tests and estimated the dynamic performance of a prestressed concrete girder railway bridge under the passage of a moving train. Deng and Cai (2010a) identified vehicular axle loads travelling at different speeds on an instrumented bridge with bumps on the bridge deck by using a proposed

methodology (Deng and Cai, 2010b). Yang *et al.* (2013a) carried out field tests to measure various bridges' natural frequencies by using a hand-drawn cart. The reliability of this approach was verified by comparing with an ambient test and a free vibration test. The influence of the elastic properties of the cart wheels was examined as well. Han *et al.* (2015) monitored the truck traffic across a bridge in China by using Weight-In-Motion (WIM), Automatic Video Recorder (AVR) and image processing techniques. The DAFs of the bridge under different recorded trucks were calculated and compared with Chinese codes and the American Association of State Highway and Transportation Officials (AASHTO) specification. Nagayama et al. (2015) identified a bridge's frequencies from the responses of two cars passing over the bridge by using the cross power spectrum of the two cars' responses. Lee *et al.* (2016) developed a moving cart system instrumented with an accelerometer, a microphone and an impact hammer to indirectly measure the Frequency Response Function (FRF) of structures. The cart system moves at a speed of 0.4 m/s and stops to measure the FRF of a foot bridge with the impact hammer as excitation in a field test. Modal analysis was done by using Power Spectral Density Estimate (PSE) and Proper Orthogonal Mode (POM). Kong *et al.* (2017) extracted the frequencies and mode shapes from responses of a bridge excited by two passing vehicles. The first vehicle response with a time shift was subtracted from the second vehicle response to reduce the effect of the road surface roughness and a residual response could be obtained. Then the modal properties of the bridge were extracted from the residual response by FFT and STFT.

2.2.2. Laboratory Experiments

The above-mentioned field experiments usually require a close collaboration with the railway or highway operation administration office, which means that the field tests could only be done under certain time and other conditions. Another way to study the train-bridge dynamics experimentally is conducting laboratory tests, which avoid the above drawback of field experiments and allow researchers a greater control of experimental conditions.

(a) Model updating and validation

Bilello *et al.* (2004) validated the theoretical model of a beam subjected to a moving mass by experimental results. Stăncioiu *et al.* (2011) investigated the vibration of a four-span continuous beam subjected to one or two rolling balls travelling at various speeds experimentally and theoretically (as a one-dimensional moving mass-beam model). Yang *et al.* (2017) built a 3D FE model for a four-span continuous plate with two rails on top of the plate which guide the movement of a model car. Shell and 3D beam elements were used for the plate and the rails, respectively. The offset ratio between the shell element and the beam element was updated based on measured frequencies of the plate structure (plate and rails). Good agreement was found between the measured vibration data and the predicted values.

Bian *et al.* (2014) developed a computer-controlled sequential loading system to generate equivalent vertical loading on a ballastless high-speed railway sample by using actuators for simulating the dynamic excitation due to moving trains. One advantage of this method is that high train speeds, like a 360 km/s train speed, can be modelled in the lab.

(b) Identification of vehicle or bridge parameters

Zhu and Law (1999) identified the moving loads exerted on a multi-span continuous Timoshenko beam with non-uniform cross-section by using different combinations of measured responses. Chan and Ashebo (2006) identified the moving force between a travelling vehicle and a multi-span continuous beam by using the measured bending moment of the beam. Cerda *et al.* (2012) compared an indirect approach of identifying the bridge damage (using the measured vehicular response) with a direct approach (using the measured bridge response) based on laboratory tests. Zhang *et al.* (2012) validated a proposed damage identification method by using the response of a tapping vehicle passing over a damaged plate in the lab. Chang *et al.* (2013) carried out a laboratory study on identifying a beam damage by using the pseudo-static method derived from a vehicle-bridge interaction system. McGetrick et al. (2015) experimentally investigated the feasibility of identifying the global stiffness of a beam by using a passing vehicular response. Kim *et al.* (2016) utilized the subtracted responses of two connected travelling vehicles on a simply supported beam to reduce the effect of the surface roughness of the beam on

identifying the beam's frequencies. A laboratory experiment was conducted to verify this approach and examine its feasibility.

2.3. Concluding Remarks

More than two hundred publications are reviewed in this chapter. Among them, several papers influence my research significantly. Baeza and Ouyang (2008) solved the vibration of a truss structure excited by a moving oscillator considering the separation and impact at the moment of reattachment between the two systems by using the MS method with structural FE modes. Yang and Fonder (1996) gave a good demonstration for using iterative methods to solve vehicle-bridge interaction problems. Nguyen *et al.* (2009) established a sophisticated vehicle model with 27 DOFs, a bridge FE model and a 3D contact model for a real vehicle-structure system. Stăncioiu *et al.* (2011) conducted experiments of a four-span beam subjected to one or two moving balls and compared experimental results with theoretical results.

Although various theoretical models and identification methods for vehicle-bridge systems have been developed in the literature, the work of applying these theories into real systems with experimental validation is relatively sparse. In addition, choosing appropriate modelling and solving techniques for a real vehicle-bridge system depends on the complexity and scenario of the system and thus a case study of the system with experimental validation is essential. Furthermore, publications about identification of bridge properties are mostly limited to simply supported bridges. To the author's best knowledge, very little work concerns about continuous bridges. One characteristic of a continuous bridge is that the product of a wavenumber for one mode and the span length of the bridge is often close to that for a neighbour mode (Blevins, 1979), which means their adjacent natural frequencies may be close to each other. This characteristic increases the difficulty of identifying the modal properties of continuous bridges in reality. The theoretical and experimental studies of a four-span continuous plate structure traversed by one and two moving train-vehicles will be illustrated in the following chapters of this thesis.

3. Moving Force Problem

The vehicle-bridge dynamic problem was first treated as a moving force problem in the literature (Timoshenko, 1953). A moving force model is often used to calculate the vibration of a bridge subjected to one or a number of vehicles when the mass ratio of every vehicle to the bridge is small (Frýba, 1999; Yang and Lin, 2005). The analytical solutions of a simply supported beam traversed by constant or harmonic forces are available, which allow researchers to have an insight into the frequency components of the beam vibrations. This can provide guidance for identifying the modal properties of a bridge when moving vehicles are adopted as excitations for the bridge. However, the vibration of a continuous beam passed by moving forces is very difficult to derive analytically because the analytical mode shapes of a continuous beam cannot be described by a single expression for the whole length of the beam. In this chapter, to tackle this problem, the mode shapes of a continuous beam are approximated by a number of modal functions of the beam when the intermediate supports are removed. A single expression is used to describe the approximate modes of a multi-span continuous beam and the analytical solution of a continuous beam subjected to a moving force is then also derived in one equation. The modal components are clearly shown in the analytical solution, which is beneficial for identifying the modal properties of the continuous beam. A two-span continuous beam is adopted as an example to demonstrate and verify this method.

3.1. A Beam Traversed by a Moving Force

A uniform beam subjected to a moving constant force is considered in this section. We assume that the beam's cross-section stays plane after deflection. An example is shown in Figure 3.1. Hamilton's principle is adopted to derive the equation of motion for this model.

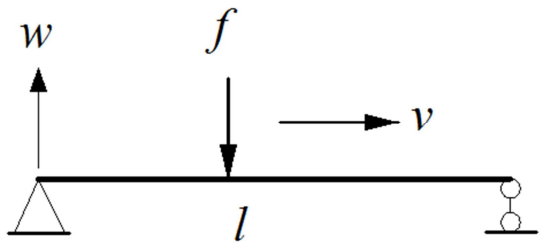

Figure 3.1. Simply supported beam subjected to a moving force

The potential energy of the beam is written as

$$V = \frac{1}{2}\int_0^l \int_A Ez^2 \left(\frac{\partial^2 w}{\partial x^2}\right)^2 \mathrm{d}A\mathrm{d}x = \frac{1}{2}\int_0^l EI \left(\frac{\partial^2 w}{\partial x^2}\right)^2 \mathrm{d}x \tag{3.1}$$

Where

E is the Young's modulus of the beam

$I = \int_A z^2 \mathrm{d}A$ is the second moment of area of the cross section,

A the cross-sectional area of the beam,

w the upward vertical deflection of the beam,

x the horizontal coordinate of a point on the neutral axis measured from the left end of the beam

z the vertical coordinate of a point on the cross-section measured from the neutral axis of the beam

l the length of one-span beam.

The kinetic energy is given by

$$T = \frac{1}{2}\int_0^l \int_A \rho(\dot{u}^2 + \dot{w}^2)\mathrm{d}A\mathrm{d}x = \frac{1}{2}\int_0^l \int_A \rho((z\dot{w}')^2 + \dot{w}^2)\mathrm{d}A\mathrm{d}x = \frac{1}{2}\int_0^l \rho I(\dot{w}')^2 \mathrm{d}x +$$

$$\frac{1}{2}\int_0^l \rho A\dot{w}^2 \mathrm{d}x \tag{3.2}$$

where u is the longitudinal deflection of one point of the beam. The dot over a symbol and the prime up beside a symbol denote the derivative with respect to time t and the derivative with respect to space x, respectively.

The work done by external and damping forces is written as

$$\delta W_e = \int_0^l [-f\delta(x - vt)\delta w - c\frac{\partial w}{\partial t}\delta w]\mathrm{d}x \tag{3.3}$$

where

δ Dirac delta function,

f external force,

c damping coefficient of the beam,

v the travelling speed of force.

Substituting Eq. (3.2) and Eq. (3.3) into Hamilton's principle below

$$\int_{t_1}^{t_2}(\delta(T-V)+\delta W_e)\mathrm{d}t=0 \tag{3.4}$$

where t_1 and t_2 are two time instants, gives the equation of motion of a beam subjected to a moving force as

$$\rho A\frac{\partial^2 w}{\partial t^2}+EI\frac{\partial^4 w}{\partial x^4}-\rho I\frac{\partial^4 w}{\partial t^2\partial x^2}+c\frac{\partial w}{\partial t}=-f\delta(x-vt) \tag{3.5}$$

Eq. (3.5) includes effects of rotation and damping. It should be noted that Eq. (3.5) does not consider shear effects. In fact, only when the ratio between the beam height and length is large enough, the shear effect and rotation effect become obvious. Damping is not significant for most engineering materials and its effect is also small except near resonance. Hence for undamped thin beams, Eq. (3.5) can be reduced to

$$\rho A\frac{\partial^2 w}{\partial t^2}+EI\frac{\partial^4 w}{\partial x^4}=-f\delta(x-vt) \tag{3.6}$$

MS method is used to solve Eq. (3.6). The solution can be expressed as a form of modal expansion

$$w(x,t)=\sum_{i=1}^{\infty}\varphi_i(x)q_i(t) \tag{3.7}$$

The mode shape satisfies

$$-\omega^2\rho A\varphi+EI\frac{\partial^4\varphi}{\partial x^4}=0 \tag{3.8}$$

Eq. (3.8) is an eigenvalue problem whose solution is

$$\varphi=C_1\sin\left(\frac{\lambda}{l}x\right)+C_2\cos\left(\frac{\lambda}{l}x\right)+C_3\sinh\left(\frac{\lambda}{l}x\right)+C_4\cosh(\frac{\lambda}{l}x) \tag{3.9}$$

where $\lambda = \sqrt[4]{\frac{\omega^2 \rho A l^4}{EI}}$ is a dimensionless parameter related to the boundary condition of the beam; C_1, C_2, C_3, and C_4 are coefficients. λ, C_1, C_2, C_3, and C_4 are to be determined by the boundary conditions of the beam.

Eq. (3.9) satisfies

$$\int_0^l \rho A \varphi_i \varphi_j \mathrm{d}x = M_{ii}\,\delta_{ij}, \quad \int_0^l EI \varphi_i \frac{\partial^4 \varphi_j}{\partial x^4} \mathrm{d}x = \omega_i^2 M_{ii} \delta_{ij}, \quad i,j = 1,2,3 \ldots \quad (3.10)$$

where $\delta_{ij}$is the Kronecker delta function, which equals 1 when $i = j$ and 0 otherwise; M_{ii} is the coefficient to be determined when $i = j$.

Substituting Eq. (3.7) into Eq. (3.6), multiplying the resultant equation by φ_i and integrating it over the beam length, one can get

$$\ddot{q}_i + \omega_i^2 q_i = -\frac{f}{M_{ii}} \varphi_i(vt) \quad (3.11)$$

3.1.1. A Simply Supported Beam Subjected to a Moving Constant Force

For a simply supported beam, Eq. (3.9) becomes

$$\varphi_i = \sin\left(\frac{i\pi x}{l}\right), i = 1,2,3 \ldots \quad (3.12)$$

M_{ii} is calculated from Eq. (3.10) to be $\frac{1}{2}\rho AL$ in this case.

The natural frequencies of a simply supported beam are $\omega_i = \sqrt{\frac{EI}{\rho A}}\left(\frac{i\pi}{l}\right)^2, i = 1,2,3 \ldots$ and $\lambda_i = i\pi$.

Thus for a simply supported beam, Eq. (3.11) becomes

$$\ddot{q}_i + \omega_i^2 q_i = -\frac{2f}{\rho AL} \sin(\frac{i\pi v}{l} t) \quad (3.13)$$

Applying the initial conditions of $q_i(0) = 0, \dot{q}_i(0) = 0$, the solution of Eq. (3.13) can be derived as

$$q_i(t) = -\frac{1}{\omega_i^2 - \left(\frac{i\pi v}{l}\right)^2} \frac{2f}{\rho AL} \sin\left(\frac{i\pi v}{l} t\right) + \frac{\frac{i\pi v}{l\omega_i}}{\omega_i^2 - \left(\frac{i\pi v}{l}\right)^2} \frac{2f}{\rho AL} \sin(\omega_i t) \quad (3.14)$$

where $\frac{i\pi v}{l}$ is defined as the driving frequency in the ith mode and represented by ω_{d}^{i} (unit: rad/s) in this thesis. The driving frequency can also be expressed as $f_{\mathrm{d}}^{i} = \frac{\omega_{\mathrm{d}}^{i}}{2\pi} = \frac{iv}{2l}$ in the unit of Hz.

Now introduce the static deflection caused by the moving force in the ith mode

$$W_{si} = -\frac{f}{M_{ii}\omega_i^2} \tag{3.15}$$

and the frequency ratio of driving frequency to structural natural frequency in the ith mode

$$S_i = \frac{\omega_{\mathrm{d}}^{i}}{\omega_i} = \frac{i\pi v}{l\omega_i} \tag{3.16}$$

For a simply supported beam, $W_{si} = -\frac{2f}{\rho AL\omega_i^2}$.

Then, Eq. (3.14) could be expressed as

$$q_i(t) = \frac{W_{si}}{1-S_i^2}\left[\sin\left(\frac{i\pi v}{l}t\right) - S_i \sin(\omega_i t)\right] \tag{3.17}$$

Substituting Eq. (3.12) and Eq. (3.17) into Eq. (3.7), one can obtain the deflection of a simply supported beam as

$$w(x,t) = \sum_{i=1}^{\infty} \frac{W_{si}}{1-S_i^2}\left[\sin\left(\frac{i\pi x}{l}\right)\left(\sin\left(\frac{i\pi v}{l}t\right) - S_i\ \sin(\omega_i t)\right)\right] \tag{3.18}$$

It can be seen from Eq. (3.18) that two types of frequencies exist in the dynamic displacement of the beam, namely driving frequencies $\frac{i\pi v}{l}$ which is related to the speed of the moving force and natural frequencies of the beam ω_i. Their contributions to the corresponding modal displacements of the simple beam can be found from Eq. (3.18) to be $\left|\frac{W_{si}}{1-S_i^2}\sin\left(\frac{i\pi x}{l}\right)\right|$ and $\left|\frac{S_i W_{si}}{1-S_i^2}\sin\left(\frac{i\pi x}{l}\right)\right|$, respectively.

3.1.2. Approximate Modes of a Continuous Beam

It can be seen from Eq. (3.11) that if $\varphi(x)$ is available in analytical form, Eq. (3.11) could be solved analytically for a beam subjected to a moving force. Although the analytical mode is available for continuous beams, the mode expression varies with span. This makes the analytical solution for each span different and needs to be

calculated separately. Moreover, the initial conditions for the next span depend on previous spans. The analytical solution for the last span would be very complicated, especially when the number of spans is large. Therefore, the analytical solution for continuous beams is rarely seen in the literature.

To obtain the analytical solution for continuous beams in a simple form, approximate modes of continuous beams with one expression for the whole beam length are derived first. Then, the equation of motion is solved analytically for continuous beams.

The supports of a beam can be modelled as elastic springs with large enough stiffness. A beam with n extra spring supports at arbitrary locations is shown as Figure 3.2. These elastic springs can be seen as external forces imposed on a free-free beam (Wu and Lin, 1990).

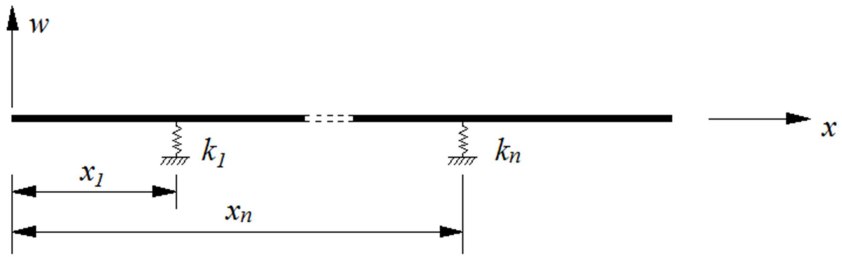

Figure 3.2. Model of a free-free beam with extra spring supports

The beam is assumed as an Euler-Bernoulli beam whose equation of motion can be described as

$$EI\frac{\partial^4 w(x,t)}{\partial x^4}+\rho A\frac{\partial^2 w(x,t)}{\partial t^2}=-\sum_{i=1}^{n}k_i w(x_i,t)\delta(x-x_i) \tag{3.19}$$

where k_i is the elastic stiffness of the ith spring.

Assume

$$w(x,t)=\sum_{j=1}^{m}\bar{\varphi}_j(x)q_j(t) \tag{3.20}$$

where $\bar{\varphi}_j(x)$ is the jth mode of the free-free beam without springs, m the number of modes used and $q_j(t)$ is the corresponding generalized coordinate.

Substituting Eq. (3.20) into Eq. (3.19), multiplying the resultant equation by $\bar{\varphi}_j(x)$ and integrating the whole equation over the beam length, the following equation can be derived

$$\ddot{q}_j(t) + \bar{\omega}_j^2 q_j(t) = -\sum_{i=1}^{n} k_i \bar{\varphi}_j(x_i) \bar{\boldsymbol{\varphi}}(x_i)^{\mathrm{T}} \mathbf{q}(t) \tag{3.21}$$

where $\bar{\omega}_j$ is the jth natural frequency of the free-free beam without springs; $\bar{\boldsymbol{\varphi}}(\mathrm{x_i})$ is the $m \times 1$ vector of modes of the free-free beam without springs; $\mathbf{q}(t)$ is the $m \times 1$ vector of generalized coordinates. One can obtain m different equations from Eq. (3.21) for different j which is an integer between 1 and m. Putting these equations together, the vector form of Eq. (3.21) is obtained as

$$\ddot{\mathbf{q}}(t) + \mathrm{diag}(\bar{\omega}_j^2)\mathbf{q}(t) = -\sum_{i=1}^{n} k_i \bar{\boldsymbol{\varphi}}(x_i) \bar{\boldsymbol{\varphi}}(x_i)^{\mathrm{T}} \mathbf{q}(t) \tag{3.22}$$

By introducing the relationship

$$\mathbf{q}(t) = \mathbf{p}\mathrm{e}^{\mathrm{i}\omega t} \tag{3.23}$$

where $\mathbf{p}$ is a coefficient vector and ω denotes the natural frequency of the free-free beam with springs, Eq. (3.22) can be transformed as

$$\left[\mathrm{diag}\left(\bar{\omega}_j^2\right) + \sum_{i=1}^{n} k_i \bar{\boldsymbol{\varphi}}(x_i) \bar{\boldsymbol{\varphi}}(x_i)^{\mathrm{T}} - \mathrm{diag}(\omega^2)\right]\mathbf{p} = \mathbf{0} \tag{3.24}$$

where $\mathbf{p}$ is the $m \times 1$ vector containing the m coefficients p_j. Eq. (3.24) is an eigenvalue problem wherein the unknowns are ω and $\mathbf{p}$. After solving Eq. (3.24), one can obtain the modes of free-free beam with springs as

$$\varphi_j(x) = \sum_{k=1}^{m} \bar{\varphi}_k(x) p_k^{(j)} \tag{3.25}$$

where $p_k^{(j)}$ is the element of $\mathbf{p}^{(j)}$ which is the corresponding eigenvector of eigenvalue ω_j^2.

Please note that Eq. (3.24) and Eq. (3.25) can be applied to a beam with arbitrary end supports and extra spring supports. $\bar{\varphi}_k$ would become the kth mode shape for the corresponding end supports, although the free-free beam is demonstrated above.

To verify this method and see the accuracy of approximate modes, a simply supported beam with one extra equidistance elastic support shown in Figure 3.3 is taken here as an example. The geometric and material properties are adopted from (Stăncioiu et al., 2008b): $EI = 63000\ \mathrm{Nm}^2$, $\rho A = 20.245\ \mathrm{kg/m}$ and one span length

of $l = 2.25$ m. The approximate modes obtained by this method will be compared with the numerical modes by the FE method and analytical modes.

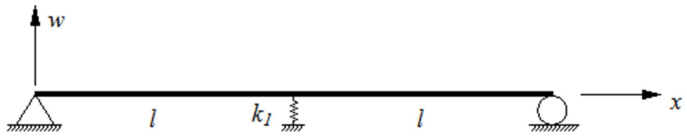

Figure 3.3. Simply supported beam with one spring support

(a) Modal properties of simply supported beam

The analytical frequencies with a simply supported beam with no elastic supports can be written as

$$f_i = \frac{1}{2\pi}\sqrt{\frac{EI}{\rho A}}\left(\frac{j\pi}{2l}\right)^2 \quad (j = 1,2,3,\dots) \quad (\text{unit: Hz}) \tag{3.26}$$

The first 8 analytical frequencies of the simply supported beam can be calculated from Eq. (3.26). The FE model for the simply supported beam is established in ABAQUS and then its numerical modes are obtained by modal analysis. The frequencies of the beam obtained from ABAQUS are compared with the analytical ones. It is found that using 20 B23 elements is enough to reach a good accuracy. The error between the two types of frequencies is shown in Table 3.1. The first eight numerical frequencies obtained by the FE method are very close to the analytical ones. Figure 3.4 shows that the 5th to 8th numerical mode shapes by the FE method are very smooth.

Table 3.1 The comparison between analytical and numerical frequencies (unit: Hz)

Mode	1	2	3	4	5	6	7	8
Ana. fre.	4.3272	17.309	38.945	69.235	108.18	155.78	212.03	276.94
FE fre.	4.3272	17.309	38.946	69.242	108.21	155.86	212.24	277.40
Error	0.00%	0.00%	0.00%	0.01%	0.03%	0.05%	0.10%	0.17%

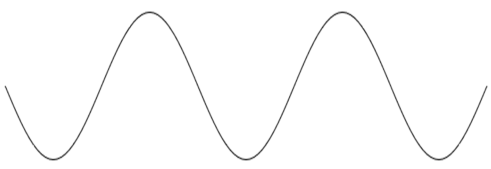

(a)

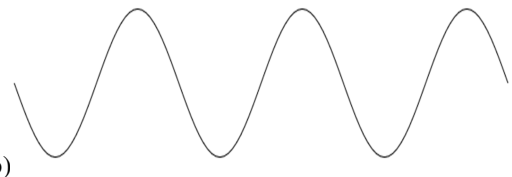

(b)

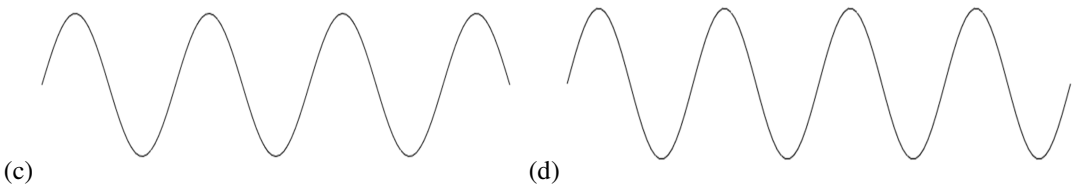

(c) (d)

Figure 3.4. Numerical modes by FE: (a) 5th mode, (b) 6th mode, (c) 7th mode, (d) 8th mode

(b) Modal properties of a two-span continuous beam

If a middle pinned support is added to the simply supported beam, the beam's boundary condition becomes two-span continuous supported. The material and geometric properties are the same as those for Figure 3.3. Three different methods are used to obtain the frequencies and mode shapes of the continuous beam. 20 B23 elements are used to obtain the FE frequencies. The analytical frequencies of the continuous beam are calculated by treating each span of the continuous beam as one individual beam and applying appropriate boundary conditions to the two individual beams (Rao, 2007), which have the form

$$f_i = \frac{1}{2\pi}\sqrt{\frac{EI}{\rho A}}\left(\frac{\lambda_i}{l}\right)^2 \text{ (unit: Hz)} \tag{3.27}$$

where λ_i is determined by the boundary conditions applied to the ith mode shape of the continuous beam and the derivation process is shown below.

The analytical modal shapes can be expressed as (Rao, 2007)

$$\varphi_{li}(x) = \sin\left(\frac{\lambda_i}{l}x\right) - \frac{\sin(\lambda_i)}{\sinh(\lambda_i)}\sinh\left(\frac{\lambda_i}{l}x\right), x \in [0, l], i = 1, 2, 3 \ldots \tag{3.28}$$

$$\varphi_{ri}(x) = \mathrm{A}_2 \sin\left(\frac{\lambda_i}{l}x'\right) + B_2\left[\cos\left(\frac{\lambda_i}{l}x'\right) - \cosh\left(\frac{\lambda_i}{l}x'\right)\right] + C_2 \sinh\left(\frac{\lambda_i}{l}x'\right),$$

$$x' = (x - \frac{L}{2}) \in [0, l] \tag{3.29}$$

where φ_{li} and φ_{ri} are the mode shapes of the first span and the second span, respectively, and

$$A_{2i} = \frac{\sinh(\lambda_i)\cos(\lambda_i) - 2\sin(\lambda_i)\cosh(\lambda_i) + \sin(\lambda_i)\cos(\lambda_i)}{\sinh(\lambda_i) - \sin(\lambda_i)}$$

$$B_{2i} = \sin(\lambda_i)$$

$$C_{2i} = \cos(\lambda_i) - \frac{\sin(\lambda_i)}{\sinh(\lambda_i)}\cosh(\lambda_i) - A_{2i}$$

The non-dimensional parameters λ for the first eight modes of the continuous beam with two equal span lengths are shown in Table 3.2. They are calculated by applying the boundary conditions of the continuous beam to Eq. (3.28) and Eq. (3.29).

Table 3.2 Non-dimensional parameters for two equal span continuous beams

Mode	1	2	3	4	5	6	7	8
λ	3.1416	3.9266	6.2832	7.0686	9.4248	10.2102	12.5664	13.3518

An elastic spring of stiffness 1×10^{12} N/m is added at the middle point of the previous simply supported beam and the present method introduced in this section is adopted to calculate the 'present frequencies' (frequencies procured by the present method) in Table 3.3. Fourteen modal shapes of the simply supported beam are used in the calculation for the present frequencies. The FE model of the two-span continuous beam is built and the numerical frequencies are obtained by the modal analysis in ABAQUS. It can be seen from the table that the accuracy of the present frequencies is very high with errors for first eight frequencies being less than 1%.

Table 3.3 Frequencies of the two-span continuous beam by three different methods (unit: Hz)

Mode	1	2	3	4	5	6	7	8
Analytical fre.	17.309	27.04	69.235	87.626	155.78	182.82	276.94	312.64
Present fre.	17.309	27.06	69.235	87.799	155.78	183.58	276.94	314.89
Error1	0.00%	0.06%	0.00%	0.20%	0.00%	0.42%	0.00%	0.72%
FE fre.	17.309	27.04	69.243	87.641	155.86	182.96	277.40	313.31
Error2	0.00%	0.00%	0.01%	0.02%	0.05%	0.08%	0.17%	0.21%

Note: Present fre. - the frequencies obtained by the present method,
Error1 - error between present frequencies and analytical frequencies,
Error2 - error between FE frequencies and analytical frequencies.

It was found that using 14 analytical modes of the simply supported beam to approximate the continuous beam can produce very accurate mode shapes of the continuous beam, as shown in Figure 3.5 for the comparison between analytical

mode shapes, FE mode shapes and the mode shapes by the present method in the first 8 modes.

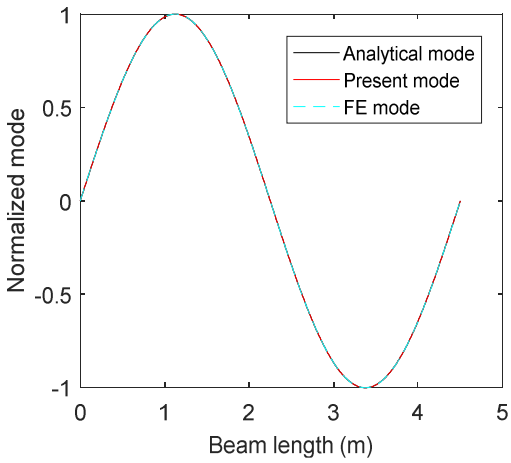

(1)

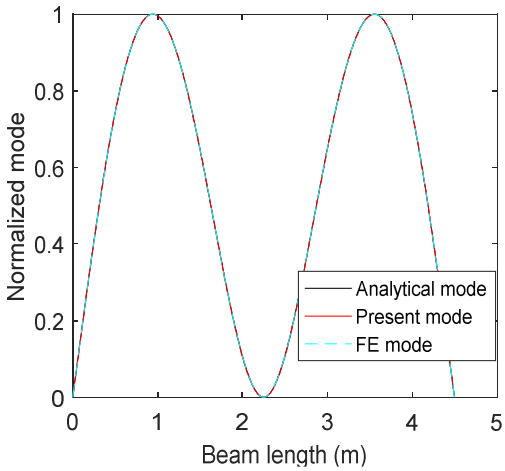

(2)

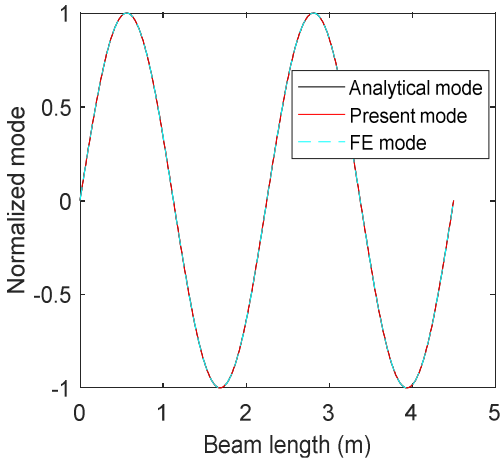

(3)

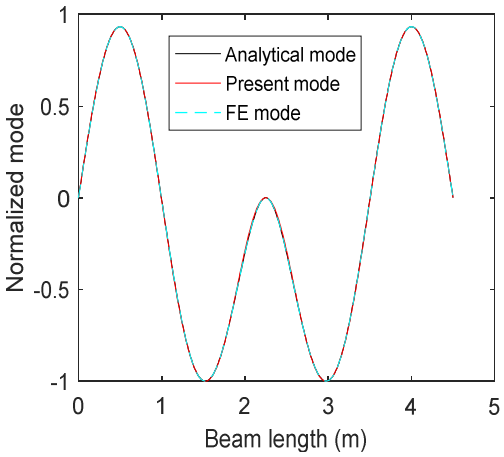

(4)

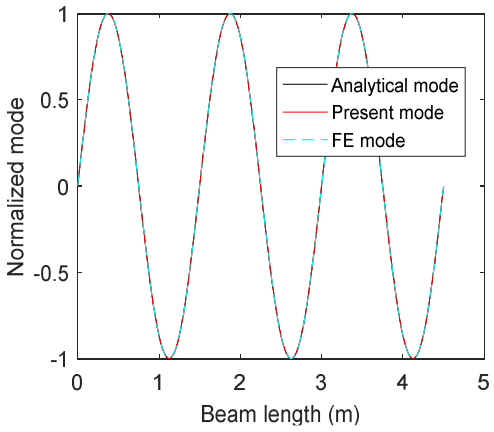

(5)

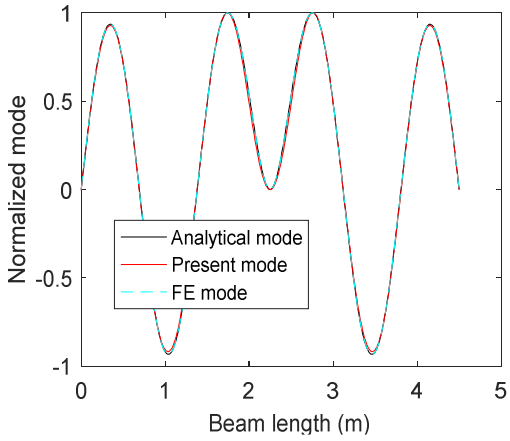

(6)

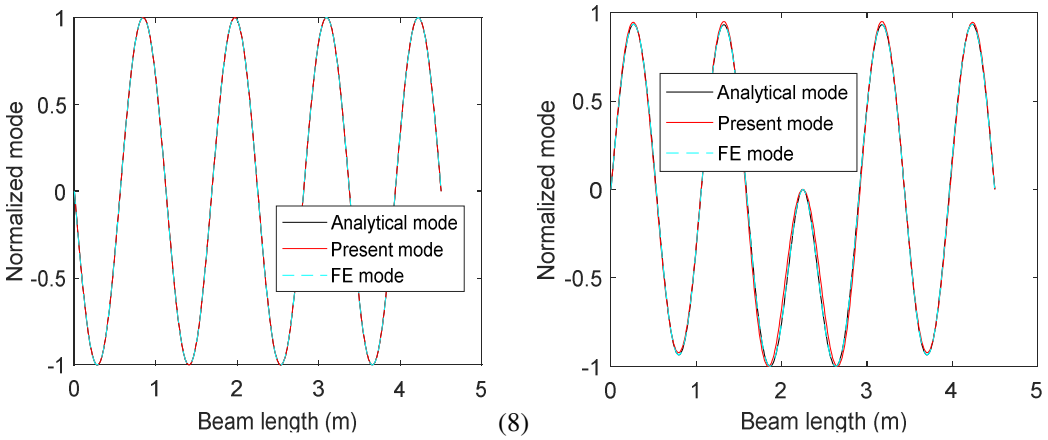

Figure 3.5. Comparison between the first 8 analytical modes, present modes and FE modes of the two-span continuous beam

The expressions for the first eight approximate mode shapes of the two-span continuous beam can be written as the following:

$$\varphi_1(x) = \sin(\frac{2\pi}{L}x) \tag{3.30}$$

$$\varphi_2(x) = -\sin\left(\frac{\pi}{L}x\right) - 0.909067\sin\left(\frac{3\pi}{L}x\right) + 0.0650185\sin\left(\frac{5\pi}{L}x\right) -$$

$$0.0161288\sin\left(\frac{7\pi}{L}x\right) + 0.005841\sin\left(\frac{9\pi}{L}x\right) -$$

$$0.0026089\sin\left(\frac{11\pi}{L}x\right) + 0.0013356\sin(\frac{13\pi}{L}x) \tag{3.31}$$

$$\varphi_3(x) = -\sin(\frac{4\pi}{L}x) \tag{3.32}$$

$$\varphi_4(x) = -0.5194158\sin\left(\frac{\pi}{L}x\right) +$$

$$0.6450743\sin\left(\frac{3\pi}{L}x\right) + \sin\left(\frac{5\pi}{L}x\right) - 0.1072308\sin\left(\frac{7\pi}{L}x\right) + 0.0346894\sin\left(\frac{9\pi}{L}x\right) -$$

$$0.0149913\sin\left(\frac{11\pi}{L}x\right) + 0.007578\sin(\frac{13\pi}{L}x) \tag{3.33}$$

$$\varphi_5(x) = \sin(\frac{6\pi}{L}x) \tag{3.34}$$

$$\varphi_6(x) = 0.3341662\sin\left(\frac{\pi}{L}x\right) - 0.349719\sin\left(\frac{3\pi}{L}x\right) + 0.5116485\sin\left(\frac{5\pi}{L}x\right) +$$

$$\sin\left(\frac{7\pi}{L}x\right) - 0.1262567\sin\left(\frac{9\pi}{L}x\right) + 0.0468124\sin(\frac{11\pi}{L}x) - 0.0224626\sin(\frac{13\pi}{L}x) \tag{3.35}$$

$$\varphi_7(x) = -\sin(\frac{8\pi}{L}x) \tag{3.36}$$

$$\varphi_8(x) = -0.2390081\sin\left(\frac{\pi}{L}x\right) + 0.2426749\sin\left(\frac{3\pi}{L}x\right) - 0.2709403\sin\left(\frac{5\pi}{L}x\right) +$$

$$0.43718\sin\left(\frac{7\pi}{L}x\right) + \sin\left(\frac{9\pi}{L}x\right) - 0.1354074\sin\left(\frac{11\pi}{L}x\right) + 0.0543915\sin(\frac{13\pi}{L}x) \quad (3.37)$$

where $L = 2l$ is the whole length of the continuous beam.

Please note that the above expressions for the mode shapes of a two-span continuous beam with equal span lengths are valid for this type of beam with any geometric and material properties and any length of the beam, although these expressions are derived from a particular case. In addition, Eq. (3.30) to Eq. (3.37) are just one of many sets of approximate solutions. The general form of the mode shapes of the two-span continuous beam can be written as

$$\varphi_i = \sum_{n=1}^{14} C_i^{\mathrm{n}}\sin(\frac{n\pi}{L}x) \quad (3.38)$$

where C_i^n is the coefficient of the term of $\sin\left(\frac{n\pi}{L}x\right)$ in the ith mode.

3.1.3. A Two-Span Continuous Beam Subjected to a Moving Constant Force

(a) Analytical solution

Substituting the approximate mode shapes of the continuous beam Eq. (3.38) into the equation of motion of a beam subjected to a moving constant force in modal coordinates Eq. (3.11), one can obtain

$$\ddot{q}_i + \omega_i^2 q_i = -\frac{f}{M_{ii}}\sum_{n=1}^{14} C_i^{\mathrm{n}}\sin(\frac{n\pi v}{L}t) \quad (3.39)$$

where ω_i is the ith natural frequency of the two-span continuous beam.

Similarly to Eq. (3.17), the solution of Eq. (3.39) can be written as

$$q_i(t) = \sum_{n=1}^{14} \frac{W_{si}}{1-(S_i^n)^2} C_i^n \left[\sin\left(\frac{n\pi v}{L}t\right) - S_i^n \sin(\omega_i t)\right] \quad (3.40)$$

where $S_i^n = \frac{n\pi v}{L\omega_i}$, $W_{si} = -\frac{f}{M_{ii}\omega_i^2}$, $M_{ii} = \int_0^L \rho A\varphi_i(x)\varphi_i(x)\mathrm{d}x$ and $\varphi_i(x)$ is the ith mode shape of the continuous beam.

By using the expressions for $\varphi_i(x)$ in Eq. (3.30) to Eq. (3.37), M_{ii} is calculated as following:

$$M_{11} = \frac{\pi}{2}\rho AL,\ M_{22} = \frac{29}{100}\pi\rho AL,\ M_{33} = \frac{\pi}{2}\rho AL,\ M_{44} = \frac{27}{100}\pi\rho AL$$

$$M_{55} = \frac{\pi}{2}\rho AL,\ M_{66} = \frac{6}{25}\pi\rho AL,\ M_{77} = \frac{\pi}{2}\rho AL,\ M_{88} = \frac{11}{50}\pi\rho AL \quad (3.41)$$

The displacement of the continuous beam is the sum of mode shapes of the beam times corresponding modal coordinates

$$w(x,t) = \sum_{i=1}^{\infty} \varphi_i(x) q_i(t) \quad (3.42)$$

It can be seen from Eq. (3.42) that the contribution of the ith frequency to the modal displacement of the continuous beam response is $|\sum_{j=1}^{14} C_i^{\mathrm{j}} \sin(\frac{j\pi}{L}x) \sum_{n=1}^{14} \frac{W_{si}}{1-(S_i^n)^2} C_i^n S_i^n|$.

The acceleration of the continuous beam can be written as

$$a(x,t) = \sum_{i=1}^{\infty} \varphi_i(x) \ddot{q}_i(t) \quad (3.43)$$

where $\ddot{q}_i$ is the second derivative of q_i with respect to time t, which is

$$\ddot{q}_i(t) = \sum_{n=1}^{14} \frac{W_{si}}{1-(S_i^n)^2} C_i^n \left[-\left(\frac{n\pi v}{L}\right)^2 \sin\left(\frac{n\pi v}{L}t\right) + S_i^n \omega_{\mathrm{i}}^2 \sin(\omega_i t)\right] \quad (3.44)$$

It can be seen from Eq. (3.43) and Eq. (3.44) that the contribution of the ith frequency to the modal acceleration of the continuous beam response is

$$A_i = |\sum_{j=1}^{14} C_i^{\mathrm{j}} \sin(\frac{j\pi}{L}x) \sum_{n=1}^{14} \frac{W_{si}\omega_i^2}{1-(S_i^n)^2} C_i^n S_i^n| \quad (3.45)$$

(b) Validation

To verify the above analytical solutions for the two-span continuous beam subjected to a moving force by using the approximate mode shapes of the beam, a numerical example is given here for comparing the analytical solutions with numerical solutions. The material and geometric properties of a two-span continuous beam are from (Nguyen et al., 2009): $\rho = 5400\ \mathrm{kg/m^3}$, $A = 7.73\ \mathrm{m^2}$, $E = 28.25\ \mathrm{GPa}$, $I = 7.84\ \mathrm{m^4}$ and $m_{\mathrm{v}} = 4.255 \times 10^4\ \mathrm{kg}$. The example bridge is a simply supported bridge with the length of $l = 30\ \mathrm{m}$ (Nguyen et al., 2009). The length of the continuous beam is assumed to be $L = 2l = 60\ \mathrm{m}$. The vehicle loading is treated as a constant force of $f = m_{\mathrm{v}}g$ moving at a speed of 360 km/h. The above properties are different from the properties used in section 3.1.2 for deriving the approximate mode

shapes of the continuous beam, which is to verify the universality of the mode shapes derived in section 3.1.2. The numerical method of solving this problem is described below.

The equation of motion of the continuous beam after applying MS method can be described in modal coordinates as

$$\ddot{q}_i(t) + \omega_i^2 q_i(t) = -\frac{f\varphi_i(vt)}{M_{ii}} \tag{3.46}$$

The first eight analytical frequencies and mode shapes of the continuous beam, which are given in Eq. (3.27) to Eq. (3.29), respectively, are adopted in the Newmark integration which can give directly the acceleration of the beam (Yang et al., 2004). Eight beam modes are used in the calculations.

To study the influence of the vehicle speed on the structural dynamic response, a notion of critical speed is introduced here (Ouyang, 2011)

$$v_{cr} = \frac{l\omega_1}{\pi} \tag{3.47}$$

where ω_1 is the first natural frequency of the beam in the unit of rad/s. $v_{cr} = 868.388$ km/h is calculated in this example.

A speed ratio of the vehicle speed to the critical speed is introduced here

$$\frac{v}{v_{cr}} = \frac{\pi v}{l\omega_1} \tag{3.48}$$

which matches the frequency ratio S_1 defined in Eq. (3.16), and $S_1 = 0.415$ is calculated in this example.

It can be seen from Figure 3.6 that the present results of the continuous beam at first mid-span agree well with corresponding numerical results, which validates the approximate mode shapes of the two-span continuous beam and the analytical solutions of the beam by using the approximate mode shapes. The dynamic displacement ratio is defined as the ratio between the dynamic displacement at first mid-span and the static deflection at the same point. The maximum dynamic displacement ratio is the Dynamic Amplification Factor (DAF) which is 1.425 in this example.

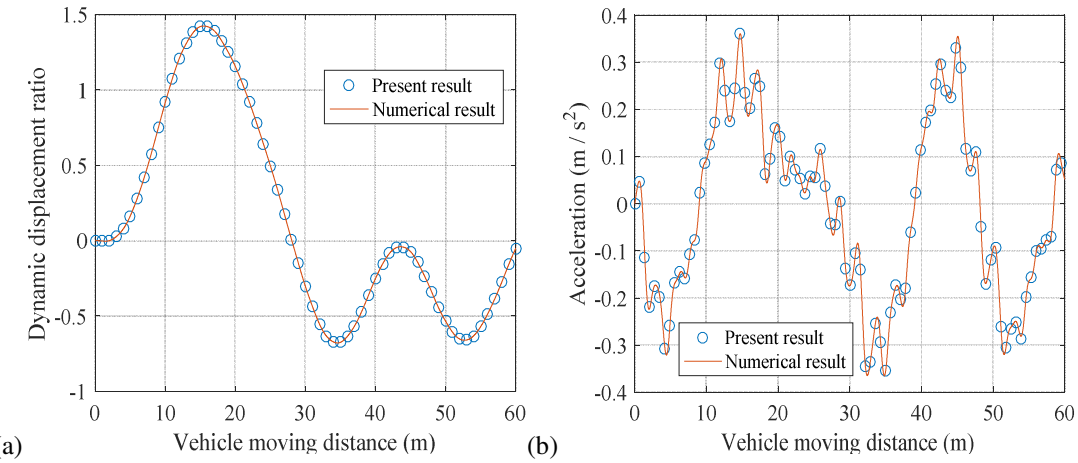

Figure 3.6. Comparison between present results and numerical results at first mid-span for the vibration of a two-span beam subjected to a moving force: (a) displacement, (b) acceleration

The acceleration spectrum of the bridge vibrating freely at location 3*L*/16 after the passage of the moving force by FFT of the data calculated analytically using approximated modes is shown in Figure 3.7. The first two bridge frequencies are excited into large amplitudes, which is different from that for a simply supported bridge whose first mode is largely excited only (Yang et al., 2004).

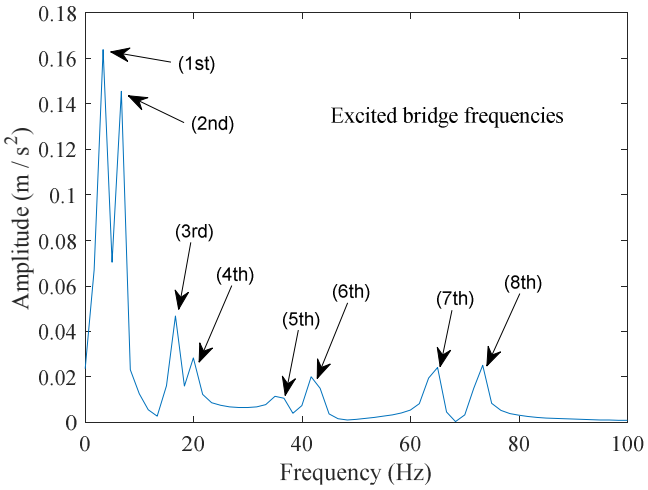

Figure 3.7. Excited bridge frequencies of the bridge acceleration response at 3*L*/16

(c) DAF of simply supported beam and two-span continuous beam

Yang *et al.* (2004) defined the Impact Factor for a simply supported beam bridge as

$$I = \frac{R_d\left(\frac{L}{2}\right) - R_s\left(\frac{L}{2}\right)}{R_s\left(\frac{L}{2}\right)} \tag{3.49}$$

where $R_d\left(\frac{L}{2}\right)$ and $R_s\left(\frac{L}{2}\right)$ denote the maximum dynamic and static response of the bridge at the beam mid-span subjected to a moving load. Comparing the definition for the DAF in this thesis and the Impact Factor *I* by Yang *et al.* (2004), it is found that DAF=*I*+1. Yang *et al.* (2004) proposed a formula to estimate *I* for the displacement of a simply supported bridge traversed by a vehicle with a speed ratio of S_1 as follows

$$I_u = \begin{cases} 1.54S_1 & \text{for } S_1 < 0.5 \\ 0.77 & \text{for } S_1 \geq 0.5 \end{cases} \tag{3.50}$$

Therefore, $I_u = 1.54 \times 0.415 = 0.639$ for a simply supported bridge with the same properties and span length as the two-span continuous bridge in this example. DAF would be 1.639 for the simple bridge, which is larger than the DAF for the two-span continuous bridge (1.425).

It is found that the impact factor I_u basically only changes with the speed ratio S_1 (Yang et al., 2004). The DAF of the simply supported beam and DAF of the two-span continuous beam with the same span length against the speed ratio are shown in Figure 3.8. It can be seen in the figure that the DAF at the first mid-span of the two-span continuous beam is smaller than that of the simply supported beam in the whole speed ratio range from 0.05 to 1. However, the DAF at the second mid-span of the continuous beam increases from 1 at speed ratio of 0.45 to about 3.25 at speed ratio of 0.85. The reason of the trend of DAF at the second mid-span is discussed below.

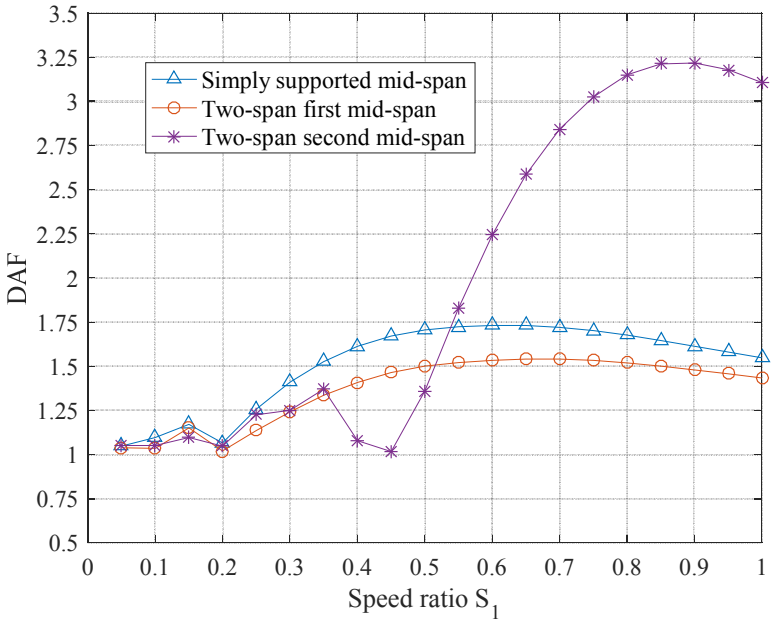

Figure 3.8. Comparison between DAF of simply supported beam and DAF of two-span continuous beam against speed ratio

The first two mode shapes of the two-span continuous beam are depicted in Figure 3.9. There is one cycle of the first mode in the whole length of the beam, whereas there exists two cycles of the second mode in the whole length of the beam. The critical speed where the beam is excited into resonance at the first frequency is $v_{\mathrm{cr}} = f_1 L = \frac{\omega_1 L}{2\pi} = \frac{\omega_1 l}{\pi}$ which is same as Eq. (3.47). The vehicle speed where the beam is excited into resonance at the second frequency is

$$v_{\mathrm{cr2}} = \frac{f_2 L}{2} = \frac{\omega_2 l}{2\pi} \tag{3.51}$$

The ratio between v_{cr2} and v_{cr} is

$$\frac{v_{\mathrm{cr2}}}{v_{\mathrm{cr}}} = \frac{\omega_2}{2\omega_1} = \frac{\lambda_2^2}{2\lambda_1^2} = \frac{3.9266^2}{2\times 3.1416^2} = 0.7811 \tag{3.52}$$

which is a constant number. The reason why the DAF of the two-span beam at the second mid-span is maximum and very high (DAF=3.21) at the speed ratio of around 0.85 is that the first and second modes of the beam are both almost excited into high amplitudes at this speed ratio, which is also found in Figure 3.7. The reason why DAF is not maximum at resonance speed ratio of 1 is that the beam displacement amplitude increases with time and there is not enough time for the beam response excited into largest amplitude (the period of the moving force on the beam is limited).

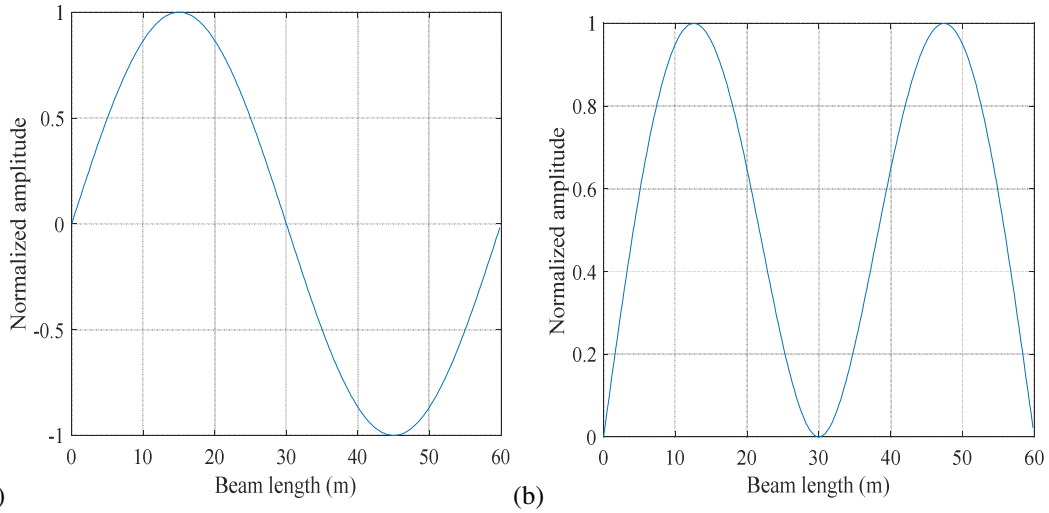

Figure 3.9. (a) First, (b) second normalized mode shapes of a two-span continuous beam

3.2. A Beam Traversed by a Moving Harmonic Force

The vibration of a bridge excited by moving harmonic forces is an important research topic, which has the application of identifying the modal properties of a bridge by using a moving vehicle with harmonic forces as excitation for the bridge (Zhang et al., 2012). If the analytical solution of such a problem can be derived, the frequency components would be shown in the solution expression and this could provide guidance for identifying the bridge modal properties. We consider a sinusoidal force moving at a constant speed on an Euler-Bernoulli uniform beam. An example is shown as Figure 3.10.

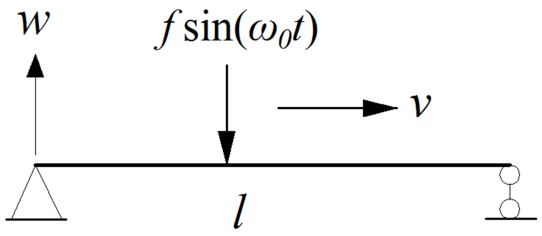

Figure 3.10. Simply supported beam subjected to a moving harmonic force

Replacing f in Eq. (3.11) with $f\sin(\omega_0 t)$, one can obtain the equation of motion for a beam subjected to a moving harmonic force as follows

$$\ddot{q}_i + \omega_i^2 q_i = -\frac{f}{M_{ii}} \sin(\omega_0 t)\, \varphi_i(vt) \tag{3.53}$$

where ω_0 is the frequency of the external force.

3.2.1. A Simply Supported Beam Subjected to a Moving Harmonic Force

The ith mode shape of a simply supported beam is known as Eq. (3.12), which is $\varphi_i(x) = \sin(\frac{i\pi}{l}x)$ and $M_{ii} = \frac{1}{2}\rho Al$. Substituting Eq. (3.12) into Eq. (3.53) leads to

$$\ddot{q}_i + \omega_i^2 q_i = -\frac{2f}{\rho Al}\sin(\omega_0 t)\sin(\frac{i\pi v}{l}t) \tag{3.54}$$

Applying the trigonometric function relationship, Eq. (3.54) can be transformed to

$$\ddot{q}_i + \omega_i^2 q_i = -\frac{f}{\rho Al}[\cos(\omega_0 - \frac{i\pi v}{l})t - \cos(\omega_0 + \frac{i\pi v}{l})t] \tag{3.55}$$

The particular solution of Eq. (3.55) can be expressed as

$$q_{\mathrm{p}i}(t) = A_i \cos\left(\omega_0 - \frac{i\pi v}{l}\right)t + B_i\cos\left(\omega_0 + \frac{i\pi v}{l}\right)t \tag{3.56}$$

where ω_i is the natural frequency of the simply supported beam, given by $\omega_i = \sqrt{\frac{EI}{\rho A}}\left(\frac{i\pi}{l}\right)^2$ and the coefficients A_i and B_i can be found by substituting Eq. (3.56) into Eq. (3.55) as

$$A_i = -\frac{f}{\rho Al}\frac{1}{\omega_i^2 - \left(\omega_0 - \frac{i\pi v}{l}\right)^2} \tag{3.57}$$

$$B_i = \frac{f}{\rho Al}\frac{1}{\omega_i^2 - \left(\omega_0 + \frac{i\pi v}{l}\right)^2} \tag{3.58}$$

The homogeneous solution of Eq. (3.55) can be expressed as

$$q_{\mathrm{h}i}(t) = C_i \sin(\omega_i t) + D_i\cos(\omega_i t) \tag{3.59}$$

where the coefficients C_i and D_i are to be determined by the initial conditions.

The total solution of Eq. (3.55) is given by the sum of its homogeneous solution and particular solution as

$$q_i(t) = A_i \cos\left(\omega_0 - \frac{i\pi v}{l}\right)t + B_i\cos\left(\omega_0 + \frac{i\pi v}{l}\right)t + C_i \sin(\omega_i t) + D_i \cos(\omega_i t) \tag{3.60}$$

Substituting Eq. (3.60) into the initial conditions of $q_i(0) = 0$ and $\dot{q}_i(t) = 0$, one can obtain

$$D_i = -(A_i + B_i) \tag{3.61}$$

$$C_i = 0 \tag{3.62}$$

Thus, the total solution of Eq. (3.55) is given

$$q_i(t) = -\frac{f}{\rho Al}\frac{1}{\omega_i^2 - \left(\omega_0 - \frac{i\pi v}{l}\right)^2}\cos\left(\omega_0 - \frac{i\pi v}{l}\right)t + \frac{f}{\rho Al}\frac{1}{\omega_i^2 - \left(\omega_0 + \frac{i\pi v}{l}\right)^2}\cos\left(\omega_0 + \frac{i\pi v}{l}\right)t$$

$$-\frac{f}{\rho Al}\frac{4\omega_0\frac{i\pi v}{l}}{[\omega_i^2-\left(\omega_0-\frac{i\pi v}{l}\right)^2][\omega_i^2-\left(\omega_0+\frac{i\pi v}{l}\right)^2]}\cos(\omega_i t) \tag{3.63}$$

A frequency ratio of the frequency of the input force ω_0 to the ith natural frequency of the beam ω_i is defined as below

$$S_i' = \frac{\omega_0}{\omega_i} \tag{3.64}$$

Substituting the static deflection parameter of $W_{si} = -\frac{f}{M_{ii}\omega_i^2} = -\frac{2f}{\rho AL\omega_i^2}$ defined in Eq. (3.15), the frequency ratio of $S_i = \frac{i\pi v}{l\omega_i}$ defined in Eq. (3.16) and the frequency ratio of $S_i' = \frac{\omega_0}{\omega_i}$ in Eq. (3.64) into Eq. (3.63), one can get

$$q_i(t) = \frac{W_{si}}{2}\frac{1}{1-(S_i'-S_i)^2}\cos\left(\omega_0 - \frac{i\pi v}{l}\right)t - \frac{W_{si}}{2}\frac{1}{1-(S_i'+S_i)^2}\cos\left(\omega_0 + \frac{i\pi v}{l}\right)t$$

$$+\frac{2W_{si}S_iS_i'}{[1-\left(S_i'-S_i\right)^2][1-\left(S_i'+S_i\right)^2]}\cos(\omega_i t) \tag{3.65}$$

The deflection of the simply supported beam can be given as

$$w(x,t) = \sum_{i=1}^{\infty}\sin(\frac{i\pi}{l}x)\,[\frac{W_{si}}{2}\frac{1}{1-(S_i'-S_i)^2}\cos\left(\omega_0 - \frac{i\pi v}{l}\right)t - \frac{W_{si}}{2}\frac{1}{1-(S_i'+S_i)^2}\cos\left(\omega_0 + \frac{i\pi v}{l}\right)t$$

$$+\frac{2W_{si}S_iS_i'}{[1-\left(S_i'-S_i\right)^2][1-\left(S_i'+S_i\right)^2]}\cos(\omega_i t)] \tag{3.66}$$

It can be seen from Eq. (3.66) that three types of frequencies exist in the dynamic displacement of the beam, namely natural frequencies of the beam ω_i, left shift frequencies to the input frequency $\omega_0 - \frac{i\pi v}{l}$, and right shift frequencies to the input frequency $\omega_0 + \frac{i\pi v}{l}$. Their contributions to the corresponding modal displacements of the simple beam response are $\left|\sin(\frac{i\pi}{l}x)\frac{2W_{si}S_iS_i'}{\left[1-(S_i'-S_i)^2\right]\left[1-(S_i'+S_i)^2\right]}\right|$,

$\left|\sin(\frac{i\pi}{l}x)\frac{W_{si}}{2}\frac{1}{1-(S_i'-S_i)^2}\right|$, and $\left|\sin(\frac{i\pi}{l}x)\frac{W_{si}}{2}\frac{1}{1-(S_i'+S_i)^2}\right|$, respectively.

3.2.2. A Two-Span Continuous Beam Subjected to a Moving Harmonic Force

Substituting the approximate mode shapes of the continuous beam Eq. (3.38) into the equation of motion of a beam subjected to a moving harmonic force in modal coordinates which is Eq. (3.53), one can obtain

$$\ddot{q}_i + \omega_i^2 q_i = -\frac{f}{M_{ii}}\sin(\omega_0 t)\sum_{n=1}^{14} C_i^n \sin(\frac{n\pi v}{L}t) \tag{3.67}$$

where M_{ii} and A_i^n are available in Eq. (3.41) and Eq. (3.38), respectively.

Similarly to Eq. (3.65), the solution of Eq. (3.67) can be described as

$$q_i(t) = \sum_{n=1}^{14} C_i^n [\frac{W_{si}}{2}\frac{1}{1-\left(S_i'-S_i^n\right)^2}\cos\left(\omega_0 - \frac{n\pi v}{L}\right)t - \frac{W_{si}}{2}\frac{1}{1-\left(S_i'+S_i^n\right)^2}\cos\left(\omega_0 + \frac{n\pi v}{L}\right)t$$

$$+\frac{2W_{si}S_i^nS_i'}{[1-(S_i'-S_i^n)^2][1-(S_i'+S_i^n)^2]}\cos(\omega_i t)] \tag{3.68}$$

where $W_{si} = -\frac{f}{M_{ii}\omega_i^2}$, $S_i^n = \frac{n\pi v}{L\omega_i}$ and $S_i' = \frac{\omega_0}{\omega_i}$. Please note that the ω_i in Eq. (3.68) is the ith natural frequency of the continuous beam.

The displacement of the continuous beam is as follows

$$w(x,t) = \sum_{i=1}^{\infty}\varphi_i(x)q_i(t) \tag{3.69}$$

where $\varphi_i(x) = \sum_{j=1}^{14} C_i^j \sin(\frac{j\pi}{L}x)$ and $q_i(t)$ is shown in Eq. (3.68).

It can be seen from Eq. (3.68) and Eq. (3.69) that the contribution of the ith frequency to the modal displacement of the continuous beam response is

$$D_i = |\sum_{j=1}^{14} A_i^j \sin\left(\frac{j\pi}{L}x\right) \sum_{n=1}^{14} \frac{2A_i^n W_{si} S_i^n S_i'}{\left[1-\left(S_i'-S_i^n\right)^2\right]\left[1-\left(S_i'+S_i^n\right)^2\right]}| \tag{3.70}$$

The acceleration of the continuous beam can be expressed as

$$a(x,t) = \sum_{i=1}^{\infty} \varphi_i(x)\ddot{q}_i(t) \tag{3.71}$$

where $\ddot{q}_i(t)$ is the second derivative of $q_i(t)$ with respect to time t and it can be derived from Eq. (3.68) as below

$$\ddot{q}_i(t) = \sum_{n=1}^{14} C_i^n [-\frac{W_{si}}{2}\frac{\left(\omega_0 - \frac{n\pi v}{L}\right)^2}{1-\left(S_i'-S_i^n\right)^2}\cos\left(\omega_0 - \frac{n\pi v}{L}\right)t + \frac{W_{si}}{2}\frac{\left(\omega_0 + \frac{n\pi v}{L}\right)^2}{1-\left(S_i'+S_i^n\right)^2}\cos\left(\omega_0 + \frac{n\pi v}{L}\right)t$$

$$-\frac{2W_{si}S_i^n S_i'\omega_i^2}{[1-\left(S_i'-S_i^n\right)^2][1-\left(S_i'+S_i^n\right)^2]}\cos(\omega_i t)] \tag{3.72}$$

The contribution of the ith frequency to the modal acceleration of the continuous beam response can be seen from Eq. (3.71) and Eq. (3.72) to be

$$A_i = |\sum_{j=1}^{14} C_i^j \sin\left(\frac{j\pi}{L}x\right) \sum_{n=1}^{14} \frac{2C_i^n W_{si} S_i^n S_i' \omega_i^2}{\left[1-\left(S_i'-S_i^n\right)^2\right]\left[1-\left(S_i'+S_i^n\right)^2\right]}| \tag{3.73}$$

Similarly to the numerical example in section 3.1.3, the vibration of the same bridge subjected to a moving harmonic force with the same amplitude as that in the example is shown in Figure 3.11. The input frequency of the moving force is supposed to be the same as the third frequency of the bridge. The results obtained by the present method are very close to those by the numerical method. Compared with the vibration of the bridge excited by a moving constant force in Figure 3.6, the displacement response of the bridge subjected to the moving harmonic force is much smaller, but the acceleration response of the bridge is much bigger. The spectrum of the acceleration response is shown in Figure 3.12. Compared with the spectrum of the acceleration response of the bridge subjected to a moving constant force in Figure 3.7, the amplitudes of the 3rd and 4th bridge frequencies of the vibration of the beam subjected to the harmonic force increase significantly. It is noted that the 3rd and 4th bridge frequencies are close to each other (16.1 Hz and 20.4 Hz).

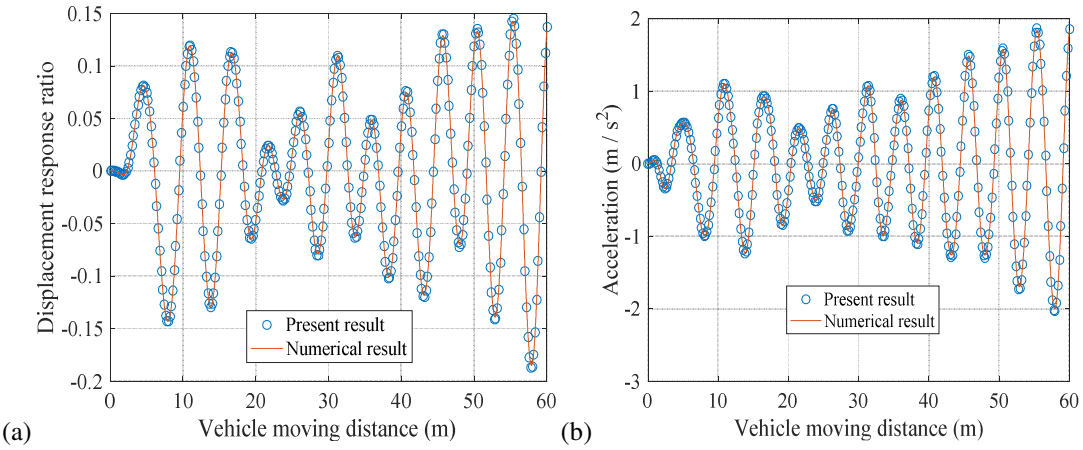

Figure 3.11. Comparison between present results and numerical results at first mid-span for the vibration of a two-span beam subjected to a moving harmonic force with input frequency $\boldsymbol{\omega_0 = \omega_3}$: (a) displacement, (b) acceleration

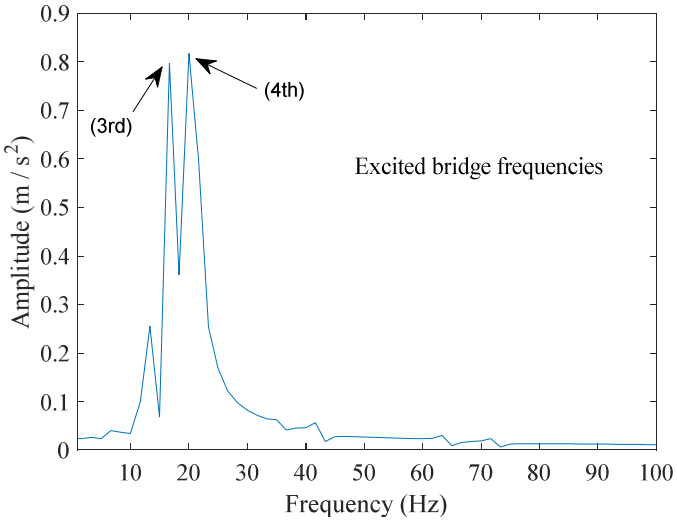

Figure 3.12. Excited bridge frequencies of the bridge acceleration response at 3*L*/16 by using a moving harmonic force with input frequency $\boldsymbol{\omega_0 = \omega_3}$

3.3. Concluding Remarks

In order to obtain the approximate mode shapes of a continuous beam valid on the whole length of the beam, the equation of motion of the free vibration of the continuous beam is established first by treating the middle supports as elastic forces acting on the same beam but with simple supports. Then the free vibration problem is transformed to an eigenvalue problem where frequencies of the continuous beam and the corresponding coefficient vectors are the eigenvalues and eigenvectors to be

solved, respectively. The mode shapes of the continuous beam can be expressed as the sum of those coefficients times the corresponding sinusoidal functions which are the modes of the beam with simple supports as the boundary. Although a specific numerical example for a continuous beam is used to obtain those coefficients, the approximate modes are valid for any length, any geometric and material properties of the beam. It should be mentioned that the solution of those coefficients depends on the properties of the beam and the length of the beam and they are not unique, which means many approximate modes are available.

A two-span continuous Euler-Bernoulli beam is used as an example to verify this method. It is found that the first eight modes of the two-span continuous beam can be approximated accurately by fourteen simple beam modes. The analytical solutions of a two-span continuous beam subjected to a moving constant force or a moving harmonic force are derived by using the approximated modes obtained, and these analytical results are very close to the results by using the numerical method.

It is found from the results that the DAF of a two-span continuous beam at the first mid-span is smaller than that of a simply supported beam. However, the DAF at the second mid-span of the continuous beam can reach 3.21 at the speed ratio of 0.85, which means that the dynamic effect can be very strong for continuous bridges at high vehicle speeds. The moving harmonic force can significantly amplify the bridge vibration at the input frequencies which are close to any natural frequencies. This is very helpful for identifying the bridge modal properties accurately at low vehicle speeds.

4. Moving Sprung Mass Problem

The interaction between a vehicle modelled as a sprung mass and a bridge modelled as a beam is solved in this chapter and compared with the moving force model. The influence of the mass ratio between the vehicle and the bridge and the speed ratio between the vehicle speed and the critical speed on the bridge response are discussed. The separation between the vehicle and the bridge is studied as well. The dynamic response of a two-span continuous beam is compared with that of a simply supported beam. It should be mentioned that the initial conditions of a bridge and the bridge irregularities are not considered in this chapter, although they may have a significant influence on the vehicle-bridge vibration. It is the future work after this thesis.

4.1. A Beam Subjected to a Moving Sprung Mass

Figure 4.1 shows an example model of a simply supported beam subjected to a sprung mass which represents a vehicle. The vehicle mass is m_{v} and the contact stiffness between the vehicle and the beam is k_{v}. The contact damping is small and ignored in the study of this thesis.

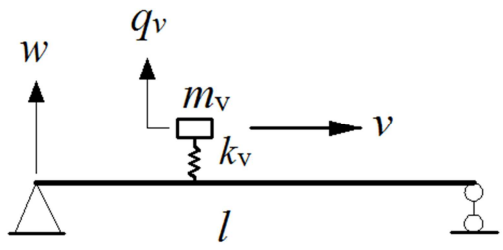

Figure 4.1. Sprung mass moving on a simply supported beam

The equation of motion of the beam and the vehicle in the vertical direction can be described as

$$\rho A\ddot{w} + EIw'''' = -f\delta(x - x_{\mathrm{v}}) \tag{4.1}$$

$$m_{\mathrm{v}}\ddot{q}_{\mathrm{v}} + k_{\mathrm{v}}q_{\mathrm{v}} = k_{\mathrm{v}}w(x_{\mathrm{v}}, t) \tag{4.2}$$

where x_{v} is the location of the beam point having contact with the vehicle in time. Please note that the zero position of the vehicle defined in Eq. (4.2) is the equilibrium position of the vehicle under its gravity force. The contact force f in Eq. (4.1) is

$$f = m_{\mathrm{v}} g + k_{\mathrm{v}}(w(x_{\mathrm{v}}, t) - q_{\mathrm{v}}) \tag{4.3}$$

It should be mentioned that Eq. (4.1) to Eq. (4.3) are valid for a beam with any types of boundary conditions subjected to a travelling sprung mass, although a simply supported beam model is shown in Figure 4.1.

4.2. Vehicle-Bridge Interaction

The interaction between the vehicle modelled as a sprung mass and a beam bridge is coupled into a total equation of motion and solved by using the Newmark-Beta method in this section. The moving force model is compared with moving sprung mass model at different mass ratios and speed ratios for a simply supported bridge and a two-span continuous beam.

4.2.1. A Beam Traversed by a Sprung Mass without Separation

Supposing that a vehicle (a sprung mass) moves along a beam at a speed without separation between the vehicle and the beam, substituting Eq. (4.3) into Eq. (4.1) and applying the MS method to the resultant equation yields

$$M_{ii}\ddot{q}_i + M_{ii}\omega_i^2 q_i + k_{\mathrm{v}}\varphi_i(x_{\mathrm{v}}) \sum_{j=1}^{\infty} \varphi_j(x_{\mathrm{v}}) q_j - k_{\mathrm{v}} q_{\mathrm{v}} \varphi_i(x_{\mathrm{v}}) = -m_{\mathrm{v}} g \varphi_i(x_{\mathrm{v}})$$

$$i = (1, 2, \dots \dots) \tag{4.4}$$

where $M_{ii} = \int_0^l \rho A \varphi_i(x) \varphi_i(x) \mathrm{d}x$ which was defined in Eq. (3.10).

Applying MS method to Eq. (4.2) leads to

$$\ddot{q}_{\mathrm{v}} + \omega_{\mathrm{v}}^2 q_{\mathrm{v}} = \omega_{\mathrm{v}}^2 \sum_{j=1}^{\infty} \varphi_j(x_{\mathrm{v}}) q_j \tag{4.5}$$

where ω_{v} is the vibration frequency of the vehicle

$$\omega_{\mathrm{v}} = \sqrt{\frac{k_{\mathrm{v}}}{m_{\mathrm{v}}}} \tag{4.6}$$

When n modes are included in Eq. (4.4), n coupled equations can be obtained. These equations together with Eq. (4.5) can be rewritten in the matrix form of

$$\mathbf{M}\ddot{\mathbf{q}} + \mathbf{K}\mathbf{q} = \mathbf{F} \tag{4.7}$$

where

$$\mathbf{M} = \begin{bmatrix} \mathrm{diag}(M_{ii}) & 0 \\ 0 & m_v \end{bmatrix},$$

$$\mathbf{K} = \begin{bmatrix} k_\mathrm{v}\boldsymbol{\varphi}(x_\mathrm{v})\boldsymbol{\varphi}^\mathrm{T}(x_\mathrm{v}) + \mathrm{diag}(\omega_i^2) & -k_\mathrm{v}\boldsymbol{\varphi}(x_\mathrm{v}) \\ -k_\mathrm{v}\boldsymbol{\varphi}^\mathrm{T}(x_\mathrm{v}) & k_\mathrm{v} \end{bmatrix},$$

$$\mathbf{F} = \begin{bmatrix} -m_\mathrm{v}\mathrm{g}\boldsymbol{\varphi}(x_\mathrm{v}) \\ 0 \end{bmatrix},$$

$$\mathbf{q} = [q_1\ q_2 \dots q_n\ q_\mathrm{v}]^\mathrm{T},$$

$$\boldsymbol{\varphi}(x_\mathrm{v}) = [\varphi_1(x_\mathrm{v})\ \varphi_2(x_\mathrm{v}) \dots \varphi_n(x_\mathrm{v})]^\mathrm{T},$$

$\boldsymbol{\varphi}^\mathrm{T}(x_\mathrm{v})$ is the transpose of the vector $\boldsymbol{\varphi}(x_\mathrm{v})$, and $\mathrm{diag}(\omega_i^2)$ is a diagonal matrix with ω_i^2 as its $i \times i$ element, and $\mathrm{diag}(\frac{k_\mathrm{v}}{M_{ii}})$ and $\mathrm{diag}(\frac{m_\mathrm{v}g}{M_{ii}})$ are diagonal matrices with $\frac{k_\mathrm{v}}{M_{ii}}$ and $\frac{m_\mathrm{v}g}{M_{ii}}$ as their $i \times i$ elements, respectively.

Eq. (4.7) can be solved by a number of numerical integration methods, like Runge-Kutta method, Newmark-Beta method and so on. Newmark-Beta method is utilized in this thesis.

The contact force between the vehicle and the bridge can be expressed as

$$f(t) = m_\mathrm{v}g + k_\mathrm{v}(\textstyle\sum_{i=1}^{n} \varphi_i(x_\mathrm{v})q_i(t) - q_\mathrm{v}) \tag{4.8}$$

If the vehicle moves at a constant speed v, then $x_\mathrm{v} = vt$. If the vehicle speed varies at a constant acceleration a (when a is negative, the speed decelerates) and the initial speed of the vehicle is v_0, the location x_v of the vehicle after time t would be $x_\mathrm{v} = v_0 t + \frac{1}{2}at^2$.

4.2.2. A Simply Supported Bridge

A comparison between the moving force model and the moving sprung mass model is conducted in this section. Two numerical examples are adopted to study the influence of the mass ratio of a vehicle to a bridge and the speed ratio of the vehicle speed to the critical speed on the vehicle-bridge vibration. The effect of contact stiffness between the vehicle and the bridge is also discussed.

(a) Example 1 – simply supported beam

An example of one uniform Bernoulli-Euler beam with simply supported boundary conditions subjected to a moving sprung mass is studied in this section. The parameters in this example are: beam length 4.5 m, flexural rigidity 63,000 Nm^2, mass per unit length of the beam 20.245 kg/m, which are from the reference (Stăncioiu et al., 2008b). The contact stiffness k_v is assumed to be big enough to model a rigid point contact between the vehicle and the beam. In this section, $k_\mathrm{v} = 1 \times 10^7$ N/m is found to be large enough to model the rigid contact between the sprung mass and the beam in simulations, as the beam displacement does not change with contact stiffness larger than 10^7 N/m. The vehicle moves over the beam at a constant speed. A time step is chosen to be smaller than a quarter of the moving mass's vibrating period $\frac{\mathrm{T}}{4} = \frac{\pi}{2\omega_\mathrm{v}} = \frac{\pi}{2\sqrt{\frac{k_\mathrm{v}}{m_\mathrm{v}}}} = 1.1 \times 10^{-3}$ s (for mass ratio 0.05) to capture the vibration of the mass. A small time step of $\Delta t = 1 \times 10^{-4}$ s is used in the Newmark-Beta integration method.

It can be observed from Figure 4.2 and Figure 4.3 that the difference between the moving mass result and the moving force result is small for a small mass ratio, but this difference becomes bigger for a larger mass ratio, which indicates that the interaction between the vehicle and the bridge increases with the mass ratio. The same trend is also found for the relationship between the interaction and the speed ratio. In addition, moving mass results lag behind moving force results, and this phenomenon is more obvious with a larger mass and speed ratio.

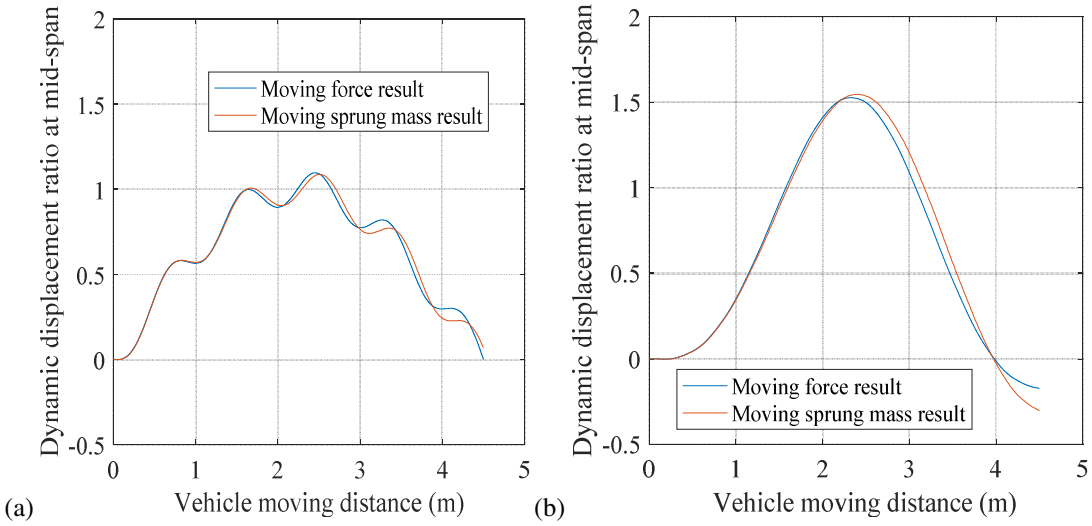

Figure 4.2. Dynamic displacement ratio history at mid-span with mass ratio of 0.05 at speed ratio of: (a) 0.1, (b) 0.35

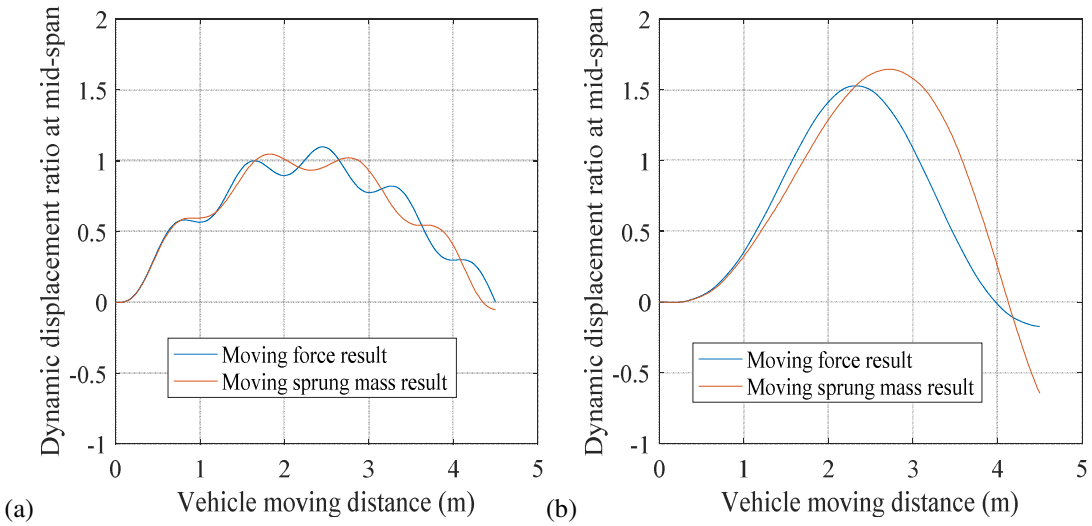

Figure 4.3. Dynamic displacement ratio history at mid-span with mass ratio of 0.3 at speed ratio of: (a) 0.1, (b) 0.35

The contact force ratio histories between the contact force and the gravity force of the vehicle are shown in Figure 4.4 and Figure 4.5. The contact force ratio varies more obviously in terms of amplitudes with a bigger mass ratio and a bigger speed ratio, which validates the above finding that the vehicle-bridge interaction increases with the mass ratio and the speed ratio. Another interesting phenomenon is that the contact force ratio at the speed ratio of 0.35 becomes bigger when the vehicle is at the middle area of the beam. This phenomenon may explain the fact that the dynamic displacement ratio excited by a moving mass is bigger than that by a moving

constant force at the speed ratio of 0.35 when the vehicle or force are at the middle area of the beam in Figure 4.2 and Figure 4.3.

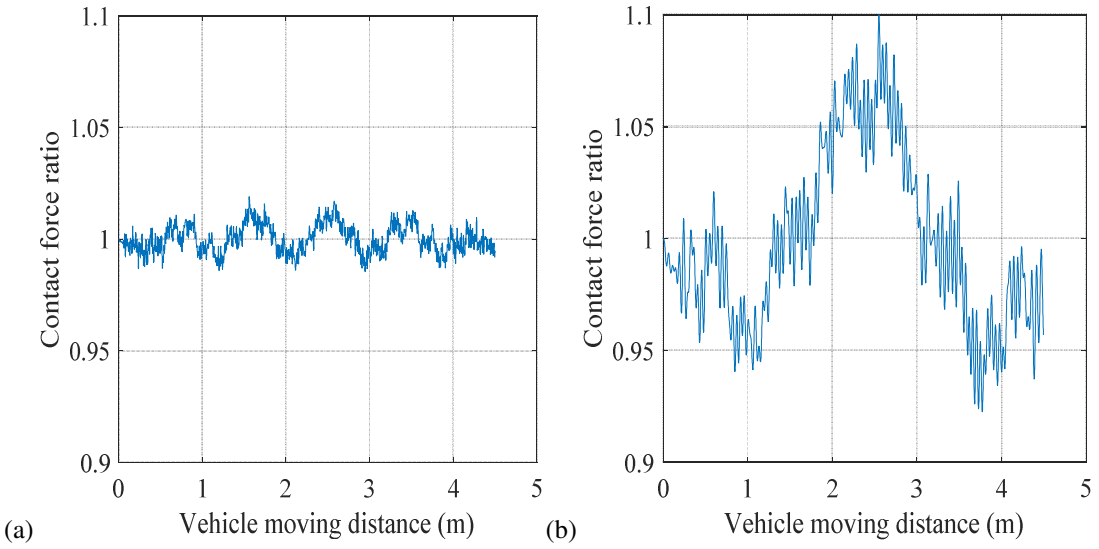

Figure 4.4. Contact force ratio history with mass ratio of 0.05 at speed ratio of: (a) 0.1, (b) 0.35 by moving sprung mass model

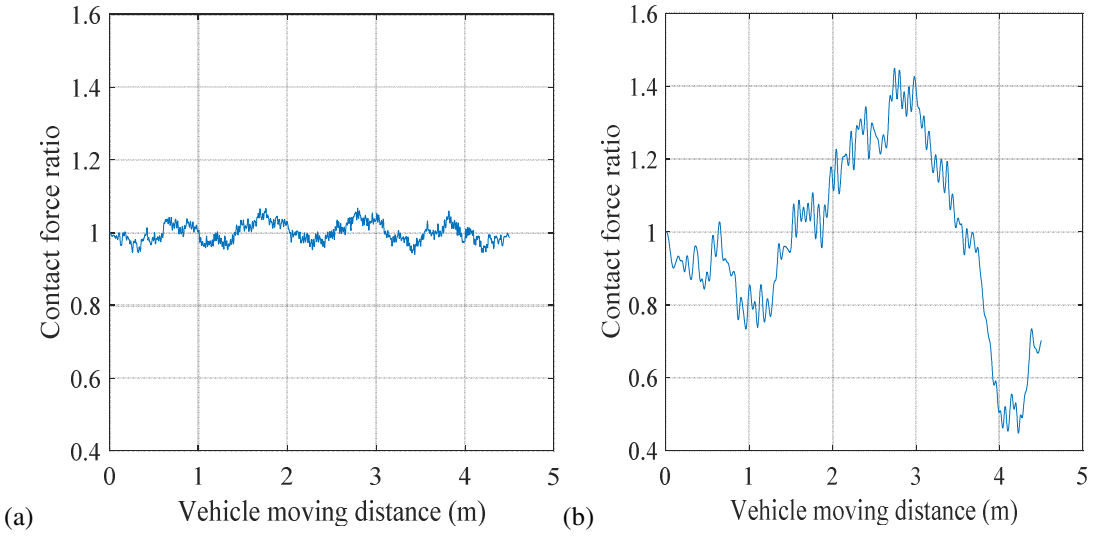

Figure 4.5. Contact force ratio history with mass ratio of 0.3 at speed ratio of: (a) 0.1, (b) 0.35 by moving sprung mass model

The displacement history of the beam at mid-span is compared with that at the contact point with the mass in Figure 4.6 and Figure 4.7. It can be seen from the figures that the response at the contact point is generally smaller than that at mid-span when the vehicle is away from the middle of the beam, but the difference becomes small when the vehicle is at the middle part of the beam. One reason for this

phenomenon may be that the first mode of the beam is largest at the beam mid-span and the first mode makes the largest contribution to the displacement of the beam.

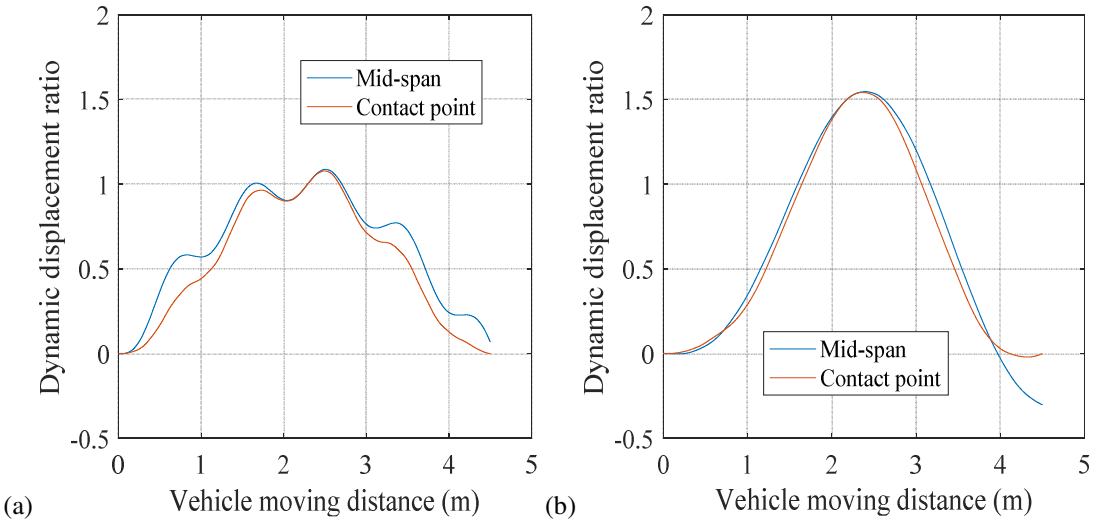

Figure 4.6. Dynamic displacement ratio history at mid-span and contact point with mass ratio of 0.05 at speed ratio of: (a) 0.1, (b) 0.35 by moving sprung mass model

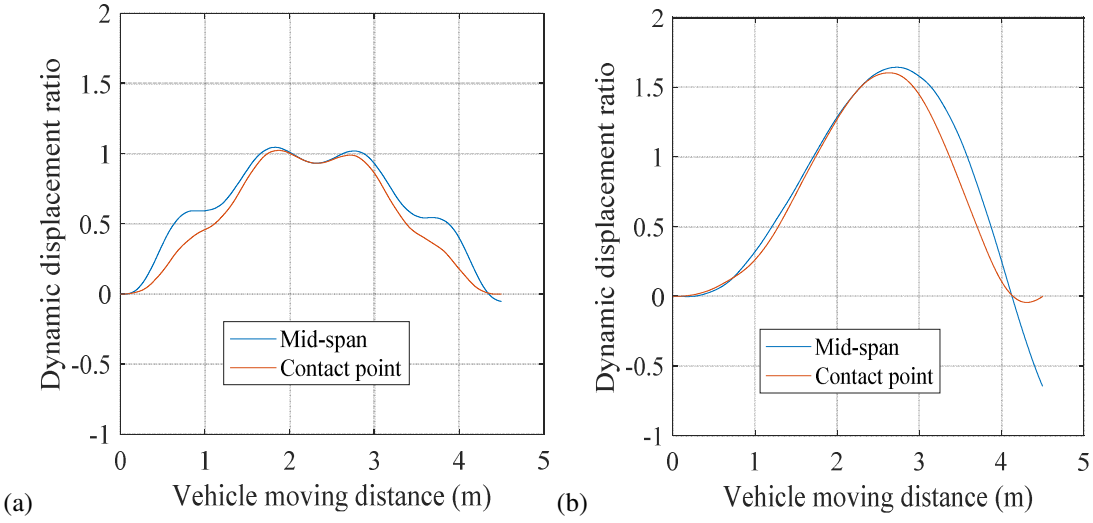

Figure 4.7. Dynamic displacement ratio histories of bridge at mid-span and at contact point for mass ratio of 0.3 at speed ratio of: (a) 0.1, (b) 0.35 by moving sprung mass model

(b) Example 2 – simply supported bridge

The material and geometric properties of a real simply supported bridge are from (Nguyen et al., 2009): $\rho = 5400\ \text{kg/m}^3$, $A = 7.73\ \text{m}^2$, $E = 28.25\ \text{Gpa}$, $I = 7.84\ \text{m}^4$ and the span length $l = 30\ \text{m}$. The total vehicle mass is 42.55 t and the contact stiffness is 1060 kN/m in (Nguyen et al., 2009).

Only the first mode is used in Nguyen's paper. A comparison between the results obtained by the sprung mass model in this chapter and the results in Nguyen's paper are compared in Figure 4.8. Good agreement can be seen in the figure, which verifies the theoretical and coding work for the sprung mass model by the author of this thesis. Different vehicle mass and contact stiffness are studied in the following.

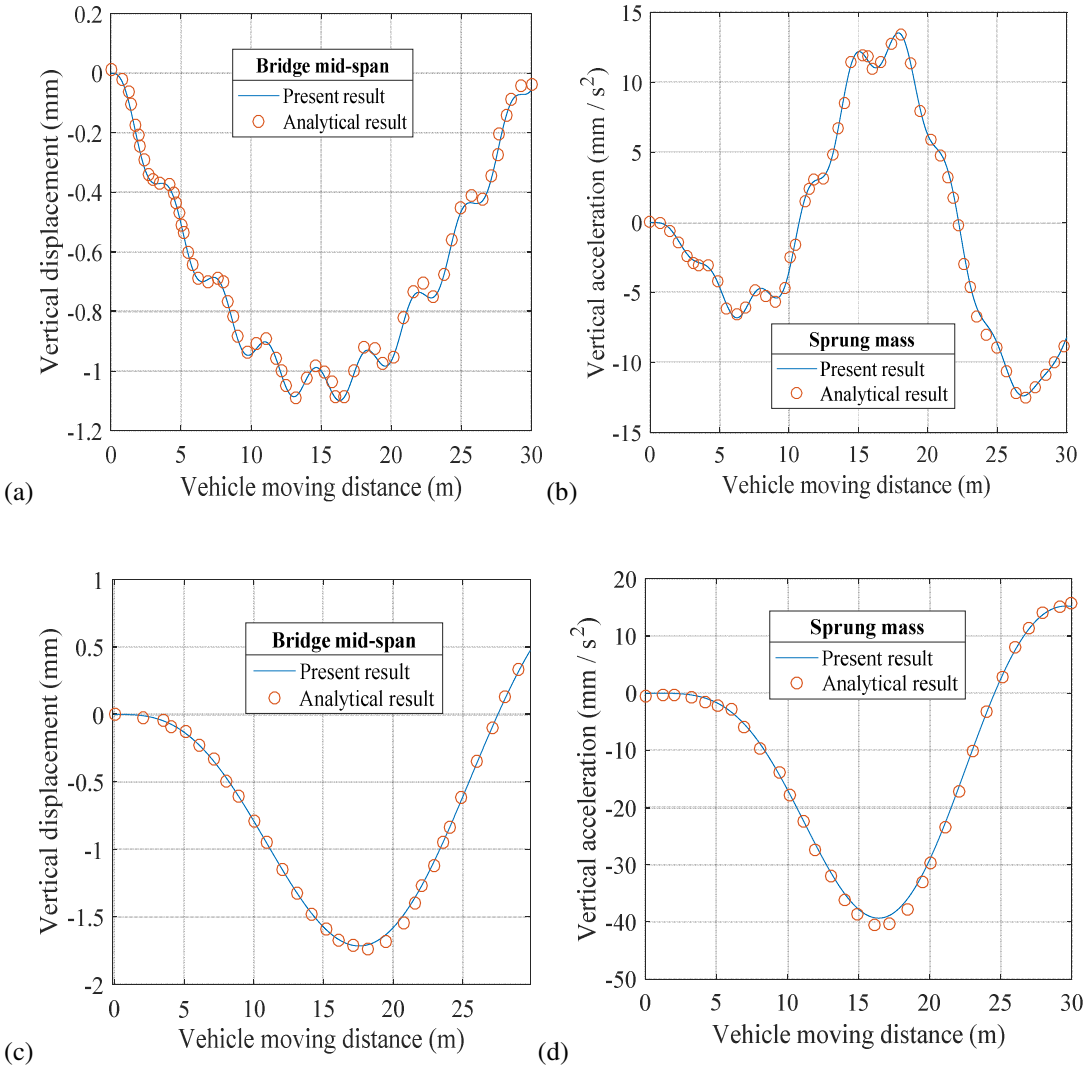

Figure 4.8. Comparison between the present results by the sprung mass model and the analytical results in Figure 9 of (Nguyen et al., 2009) at vehicle speed of 50 km/h (a, b) and 360 km/h (c, d)

Another contact stiffness $k_v = 10^{11}$ is used to model the rigid contact between the sprung mass and the beam. A small time step of $\Delta t = 1 \times 10^{-4}$ s is used in the Newmark-Beta integration method, which is smaller than $\frac{T}{4} = \frac{\pi}{2\sqrt{\frac{k_v}{m_v}}} = 10^{-3}$ s. Figure 4.9 and Figure 4.10 for this example are basically same as Figure 4.3 and Figure 4.5

for example 1, respectively, which indicates that the dynamic response ratio is only related to the speed ratio and the mass ratio. The vibration of a beam subjected to a moving force is only related to the speed ratio, which can be seen from its analytical solution (Yang et al., 2004). The mass ratio is another factor needed to be considered for the moving sprung mass model. Please note that the contact stiffness in this example (1×10^{11} N/m) is much higher than that in example 1 (1×10^{7} N/m). The influence of contact stiffness on the vehicle-bridge vibration is discussed in the next section.

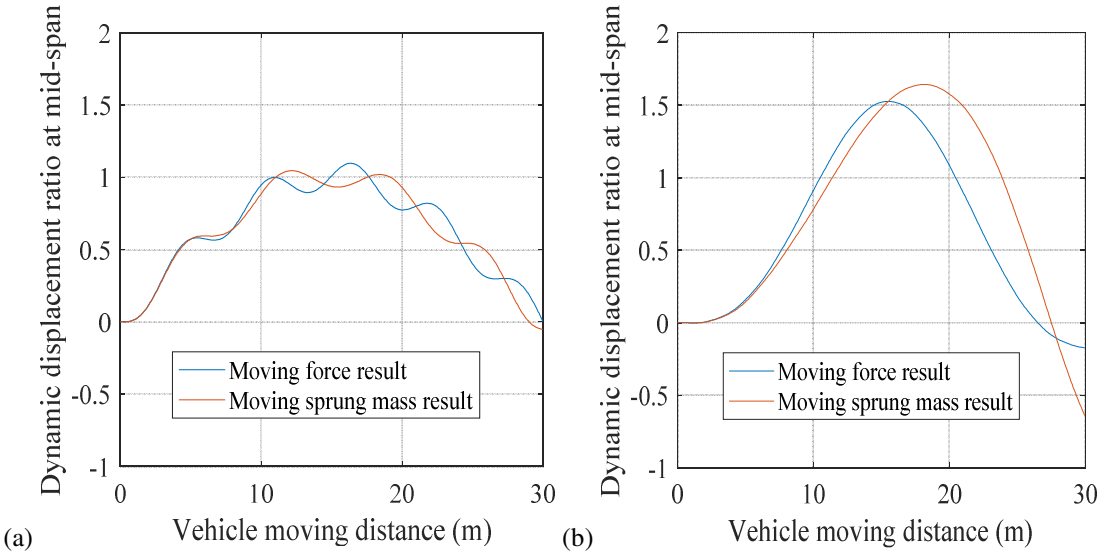

Figure 4.9. Dynamic displacement ratio history at mid-span with mass ratio of 0.3 at speed ratio of: (a) 0.1, (b) 0.35

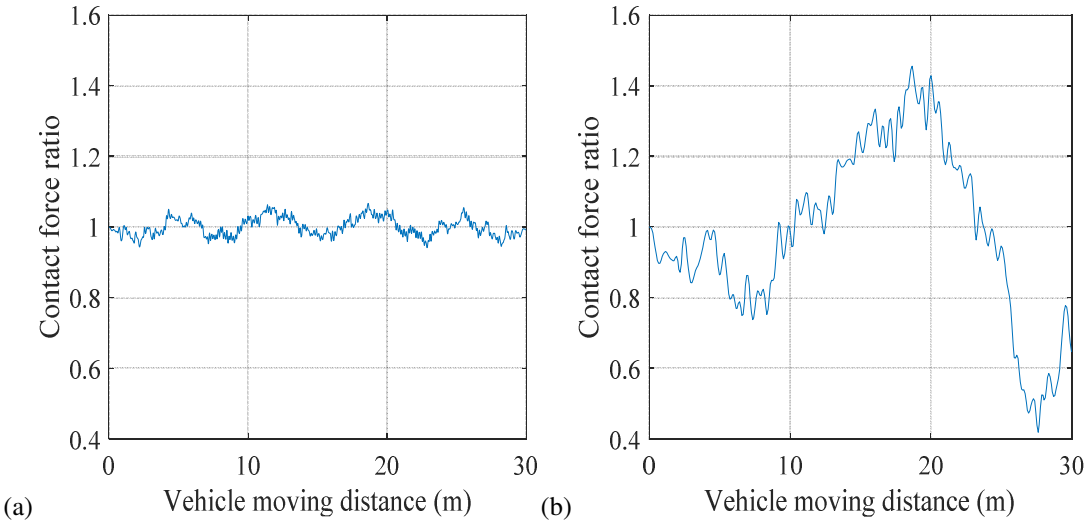

Figure 4.10. Contact force ratio history with mass ratio of 0.3 at speed ratio of: (a) 0.1, (b) 0.35

(c) Contact stiffness

Figure 4.11 shows the displacement and contact force responses with different contact stiffness for example 2. A big difference can be found between the results by using $k_v = 10^7$ N/m and the results by using $k_v = 10^{11}$ N/m.

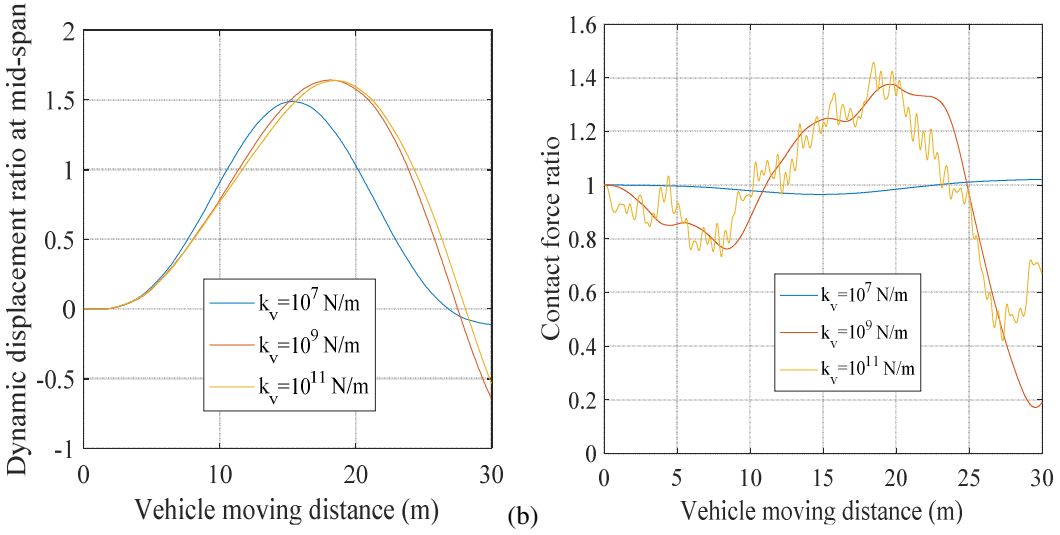

Figure 4.11. Comparison of moving sprung mass results with different contact stiffness: (a) displacement ratio at mid-span, (b) contact force ratio, for mass ratio of 0.3 and speed ratio of 0.35 in example 2

The moving mass model as Figure 2.2 can be used to model the rigid contact between the vehicle and the bridge (Ouyang, 2011). The moving mass model is adopted here and its results are compared with the results by the moving sprung mass model with different contact stiffness, which are shown in Figure 4.12. It is seen in the figure that the results when using $k_v = 10^{11}$N/m agree well with the results by the moving mass model. In addition, high frequency oscillation occurs in the contact force when using the moving sprung mass model with $k_v = 10^{11}$N/m, whereas this phenomenon does not occur in the result when using the moving mass model. It is found in simulations that the bridge displacement responses by using contact stiffness higher than $k_v = 10^{11}$N/m do not change any more, and the contact forces change slightly with contact stiffness between 10^{11}N/m and 10^{13}N/m, but do not change with contact stiffness higher than 10^{13}N/m.

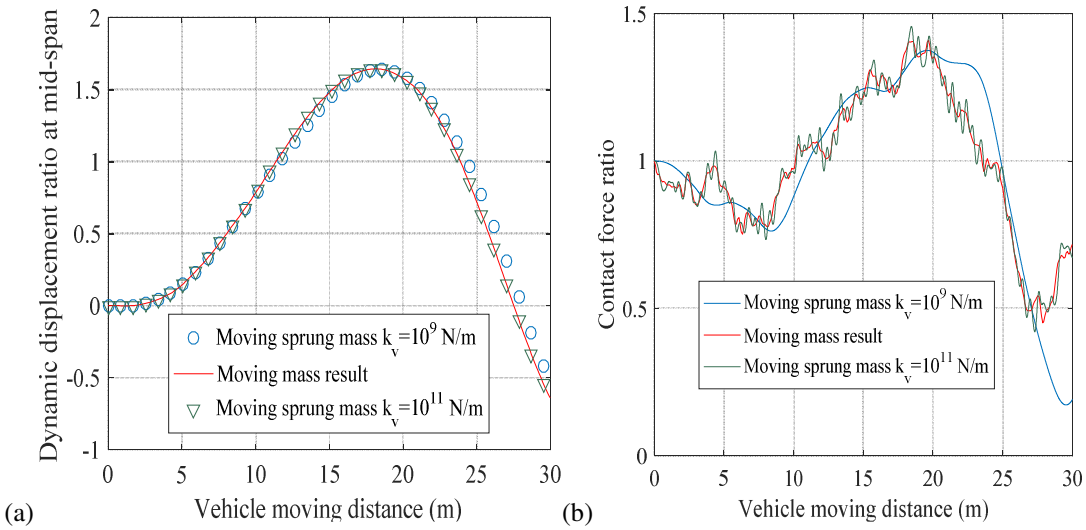

Figure 4.12. Comparison between moving sprung mass results with different contact stiffness and moving mass result: (a) displacement response ratio at mid-span, (b) contact force ratio, for mass ratio of 0.3 and speed ratio of 0.35 in example 2

4.2.3. A Two-Span Continuous Beam

The same numerical example as section 3.1.3 is adopted here. The contact stiffness of $k_{\mathrm{v}} = 1 \times 10^{13}$ N/m is used in this example to model the rigid contact. A small time step of $\Delta t = 1 \times 10^{-4}$ s is used in the Newmark-Beta integration method, which is smaller than $\frac{\mathrm{T}}{4} = \frac{\pi}{2\sqrt{\frac{k_{\mathrm{V}}}{m_{\mathrm{V}}}}} = 1.8 \times 10^{-4}$ s (for mass ratio 0.05).

Figure 4.13 shows the comparison between moving force results and moving sprung mass results. When the speed ratio is small, the two types of results are basically the same, but the difference becomes obvious with a bigger speed ratio. The maximum displacement response at bridge mid-span (DAF) obtained by the moving sprung mass model is bigger than that by the moving force model, which may be due to the increase of contact force in the mid-span area as shown in Figure 4.14. These findings are the same as those for the simply supported bridge.

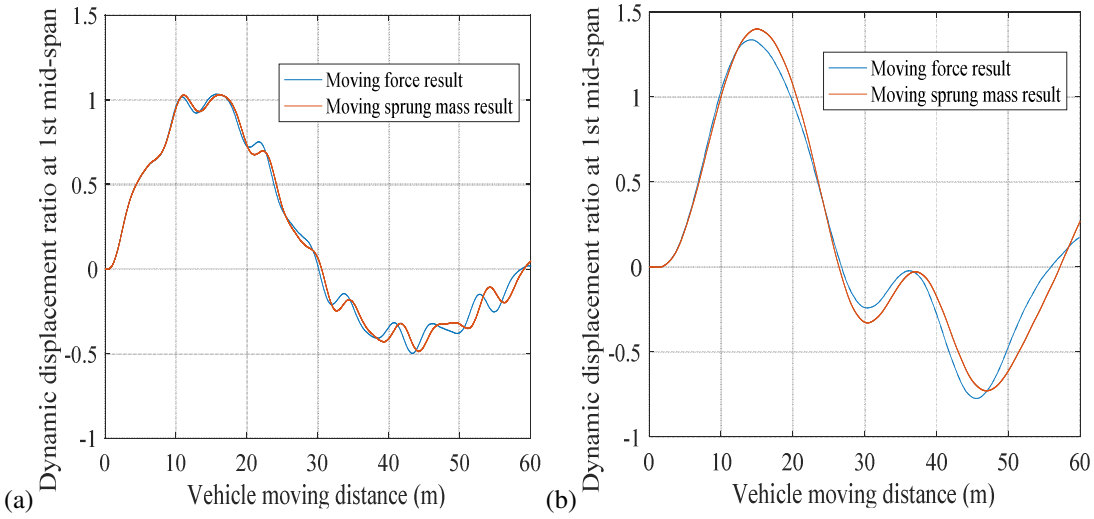

Figure 4.13. Dynamic displacement ratio history at first mid-span with mass ratio of 0.05 at speed ratio of: (a) 0.1, (b) 0.35

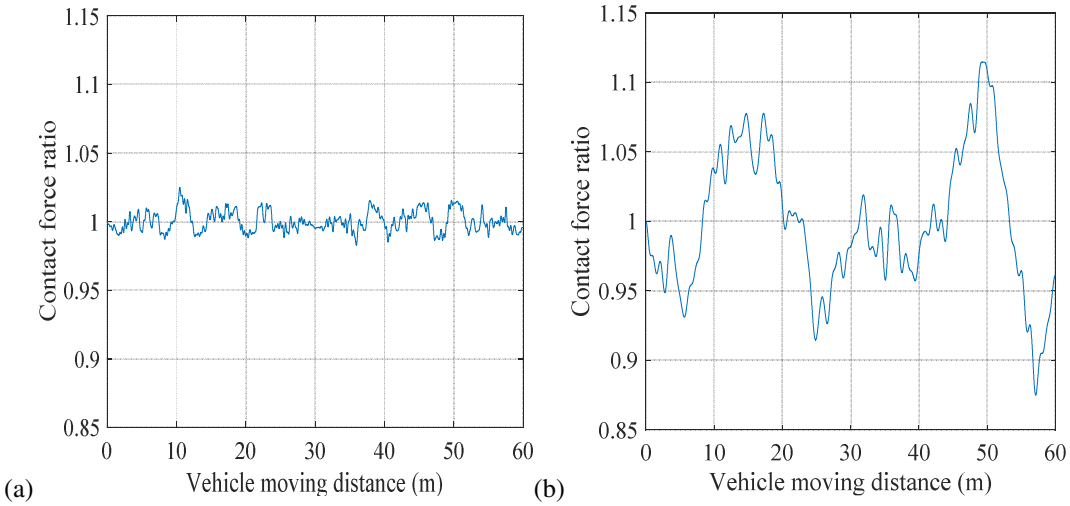

Figure 4.14. Contact force ratio history for mass ratio of 0.05 at speed ratio of: (a) 0.1, (b) 0.35 by moving sprung mass model

The maximum displacement response ratio of bridge at contact point or moving coordinate is smaller than that at corresponding mid-span, as shown in Figure 4.15. It is noticed that the maximum displacement ratio (DAF) at second mid-span is 3.454 which is larger than that obtained by the moving force model (3.213) in Figure 3.8. Figure 4.16 shows that first two frequencies of the continuous beam are excited to high amplitudes, which verifies the explanation for the DAF of the continuous beam at the second mid-span for Figure 3.8 in section 3.1.3.

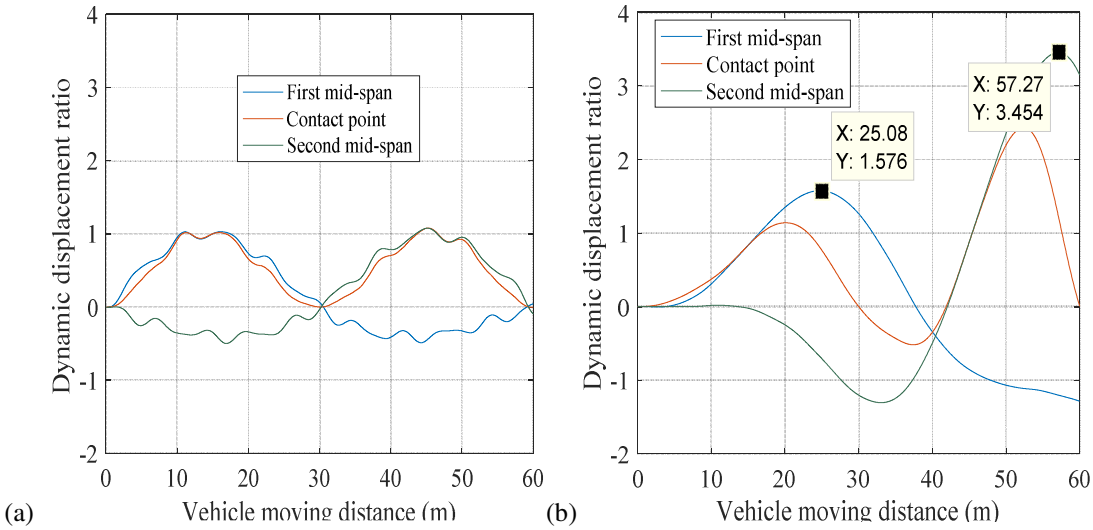

Figure 4.15. Comparison of bridge displacement response ratio at first and second mid-span and at moving contact point for mass ratio of 0.05 and speed ratio of (a) 0.1, (b) 0.85 by the moving sprung mass model

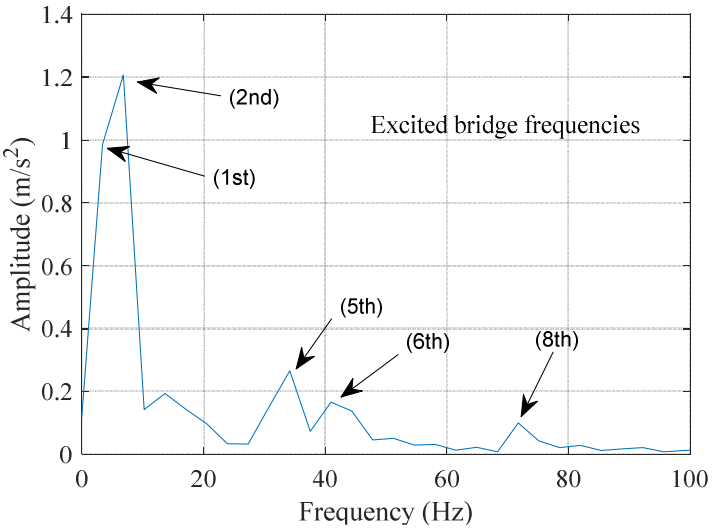

Figure 4.16. Acceleration spectrum of bridge at first mid-span for mass ratio of 0.05 and speed ratio of 0.85

4.3. Vehicle-Bridge Separation

It is found in simulations that the contact force between vehicle wheels and a bridge could become negative when the vehicle speed is high enough and this phenomenon is more likely to happen for a higher mass ratio of the vehicle to the bridge (Lee, 1998; Cheng et al., 1999; Stăncioiu et al., 2008b). As the contact force is always non-negative in reality, the negative contact force in simulations actually indicates that

the vehicle is separated from the rail or bridge and the contact force should be changed to zero from this moment of separation in this case in simulations. After separation, the vehicle wheel usually gets reattached with the rail or bridge again. Separation and reattachment are discussed in this section by using a moving sprung mass model.

4.3.1. Vehicle-Bridge Vibration during Separation

(a) Free vibration during separation

When separation between the moving vehicle and the supported beam occurs, Eq. (4.7) is not valid any more. Obviously, the contact force between the two subsystems is zero and the moving vehicle and the beam undergo free vibrations during the separation period. The separation condition can be derived from Eq. (4.3) for contact force no bigger than zero and is expressed as follows:

$$q_{\mathrm{v}} - w(x_{\mathrm{v}}, t) \geq \frac{m_{\mathrm{v}} g}{k_{\mathrm{v}}} \tag{4.9}$$

The equation of motion of a beam vibrating freely during separation can be expressed as

$$\rho A\ddot{w} + EIw'''' = 0 \tag{4.10}$$

Substituting the ith beam mode shape into Eq. (4.9), multiplying the mode shape with it and integrating the resultant equation over the whole beam length, one can derive

$$\ddot{q}_i(t) + \omega_i^2 q_i(t) = 0 \tag{4.11}$$

The analytical solution of Eq. (4.11) is given as

$$q_i = q_i(0)\cos(\omega_i t) + \frac{\dot{q}_\iota(0)}{\omega_i}\sin(\omega_i t) \tag{4.12}$$

where $q_i(0)$ and $\dot{q}_\iota(0)$ are the initial conditions of beam.

The deflection of the beam during separation is written as

$$w(x,t) = \sum_{i=1}^{\infty} \varphi_i(x)\left(q_i(0)\cos(\omega_i t) + \frac{\dot{q}_\iota(0)}{\omega_i}\sin(\omega_i t)\right) \tag{4.13}$$

The free vibration of the vehicle during separation can be described as

$$\frac{\mathrm{d}^2 q_\mathrm{v}}{\mathrm{d}t^2} = -g \tag{4.14}$$

where g is the gravity acceleration.

Integrating Eq. (4.14) over any time period within the separation period, the vertical displacement of vehicle can be derived as

$$q_\mathrm{v} = q_\mathrm{v}(0) + \dot{q}_\mathrm{v}(0)t - \frac{1}{2}gt^2 \tag{4.15}$$

where $q_\mathrm{v}(0)$ and $\dot{q}_\mathrm{v}(0)$ are the displacement and speed of the vehicle, respectively, at the instant of separation.

(b) Reattachment

When the vehicle wheel reattaches the bridge and the vehicle-bridge interaction takes place again, the contact force changes from non-positive to positive. The reattachment condition can be expressed as follows:

$$q_\mathrm{v} - w(x_\mathrm{v}, t) < \frac{m_\mathrm{v} g}{k_\mathrm{v}} \tag{4.16}$$

Eq. (4.7) is applied again to describe the vehicle-bridge interaction if Eq. (4.16) is satisfied. A small time step is needed to capture the reattachement time moment.

(c) Determining the time instant for separation and reattachment

The difference between the vertial displacement of the vehicle wheel and corresponding beam deflection is adopted as the indicator for separation and reattachment. The time instant when the displacement difference increases to $\frac{m_\mathrm{v} g}{k_\mathrm{v}}$ is the moment when separation begines, as shown in Eq. (4.9). When the difference between the vertial displacement of the vehicle wheel and the corresponding beam deflection becomes less than $\frac{m_\mathrm{v} g}{k_\mathrm{v}}$ after separation reattachment takes place, which is shown in Eq. (4.16). However, it is difficult to find the exact time instants for separation and reattachment in the numerical simulation. A small time step is used in the simulation to reduce the error of finding these time instants. In addition, the displacement difference between any two adjacent time instants is assumed to be linear when the interval between the two time instants is small. This linear assumption is used to find the moment when the displacement difference is equal to

$\frac{m_v g}{k_v}$ for separation when the difference changes from less than $\frac{m_v g}{k_v}$ at one time instant to larger than $\frac{m_v g}{k_v}$ at the next time instant in the numerical simulation.

4.3.2. Separation for a Simply Supported Bridge

The same bridge properties as the example 2 in section 4.2.2 from (Nguyen et al., 2009) are used here. The contact stiffness of $k_v = 1 \times 10^{11}$ N/m is utilized in this example. A small time step of $\Delta t = 1 \times 10^{-5}$ s is adopted in the numerical integration of the vehicle-bridge equation of motion.

A numerical example of separation can be seen in Figure 4.17 and Figure 4.18 for displacement response and contact force, respectively. It is shown in the figures that the simulated results considering separation are quite different from those without considering separation. When no separation happens, the bridge displacement and the vehicle displacment are basically the same at the moving coordinate. However, the bridge displacement becomes obviously larger (in absolute value) than that of the vehicle when separation takes place, and the difference between the bridge displacement and the vehicle displacement considering separation is bigger than that without considering separation. It also can be seen from the figures that the displacement difference becomes more obvious after separation when the contact force goes up dramatically with the vehicle approaching the end of the bridge.

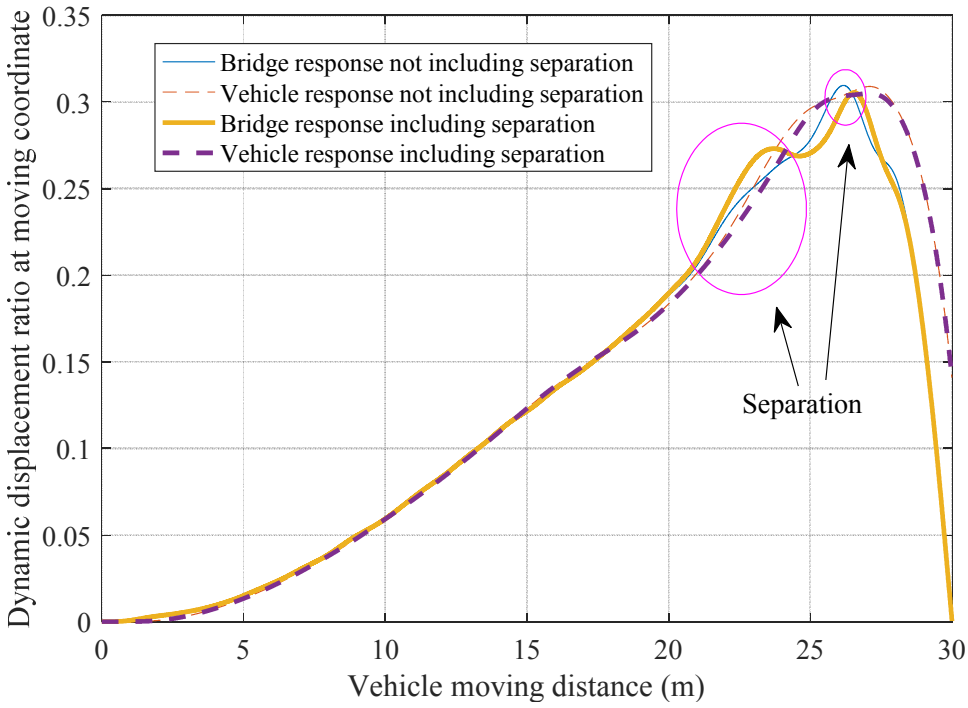

Figure 4.17. Displacement response ratio histories of bridge and vehicle at moving coordinate for mass ratio of 0.5 and speed ratio of 1.9 by using $k_{\mathrm{v}} = 10^{11}$ N/m

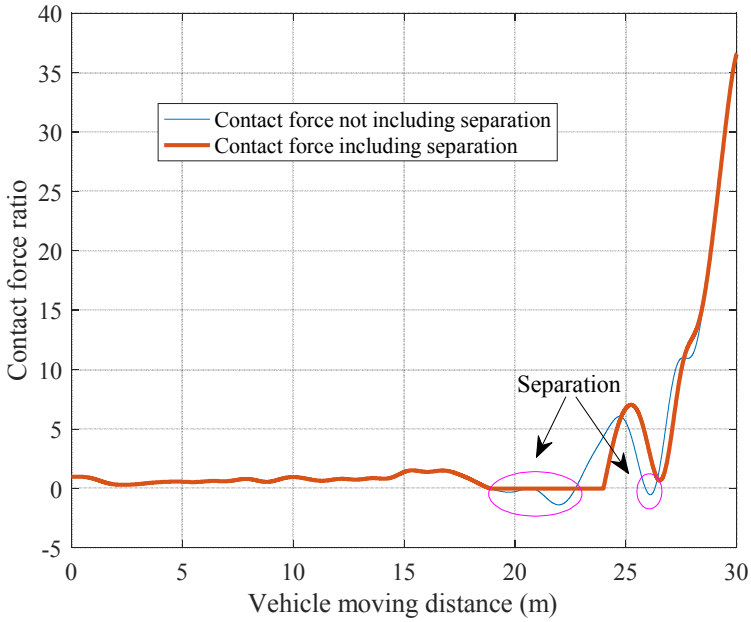

Figure 4.18. Contact force ratio histories for mass ratio of 0.5 and speed ratio of 1.9 by using $k_{\mathrm{v}} = 10^{11}$ N/m

(a) Influence of contact stiffness

The influence of contact stiffness on the displacement response ratio histories of the bridge and the vehicle at moving coordinate and the contact force ratio history can be seen in Figure 4.19, Figure 4.17, Figure 4.18 and Figure 4.20. When the contact stiffness is 10^{10} N/m, the bridge response and vehicle response are quite different even during the no-separation period as shown in Figure 4.19. When the contact stiffness is 10^{11} N/m, the difference between the bridge displacement response at moving coordinate and the vehicle displacement response is small during the no-separation period, but becomes big during separation and after separation as shown in Figure 4.17. This trend is more obvious for contact force ratio when the contact stiffness is 10^{12} N/m as shown in Figure 4.20. The bridge response is almost the same as the vehicle response and the contact loss and reattachment happens more times. It is like an elastic body bouncing on another body.

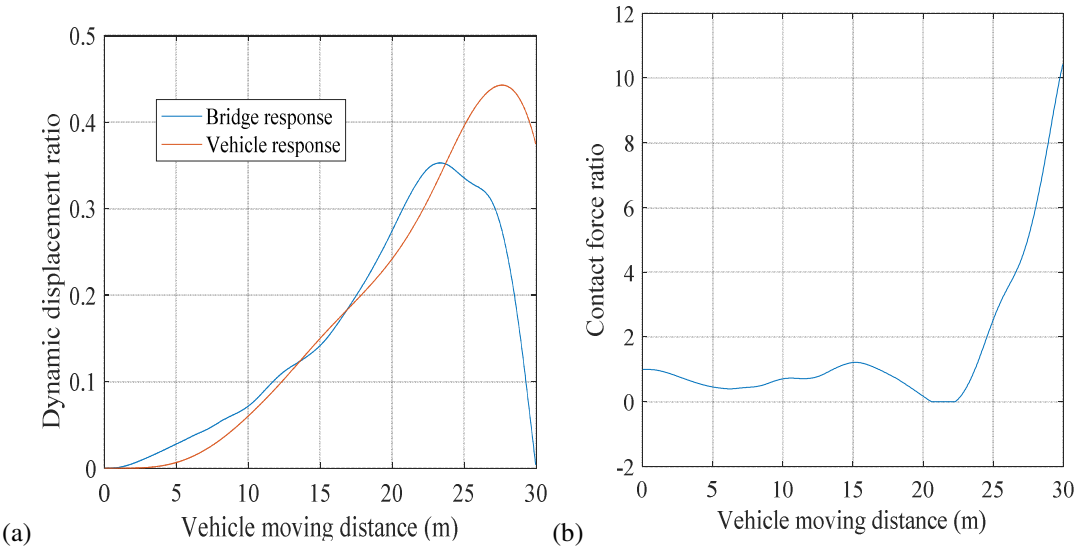

Figure 4.19. (a) Displacement displacement ratio histories of bridge and vehicle at moving coordinate, (b) contact force ratio history for mass ratio of 0.5 and speed ratio of 1.6 by using $k_{\mathrm{v}} = 10^{10}$ N/m

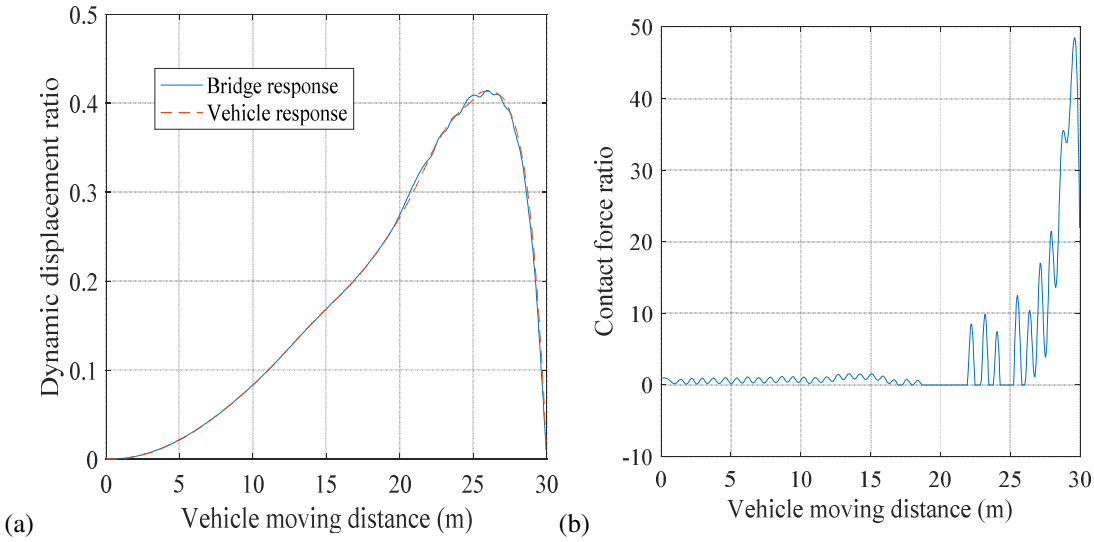

Figure 4.20. (a) Displacement ratio histories of bridge and vehicle at moving coordinate, (b) contact force ratio history for mass ratio of 0.5 and speed ratio of 1.6 by using $k_{\mathrm{v}} = 10^{12}$ N/m

(b) Influence of mass ratio

The contact stiffness of $k_{\mathrm{v}} = 10^{11}$ N/m is used in this section to study the influence of mass ratio on vehicle-bridge separation. It is found from simulations that separation begins to take place only when the vehicle speed is high enough and this vehicle speed changes for different mass ratios. Figure 4.21 gives the trend between the speed ratio from which separation begins to happen and the mass ratio between the vehicle and the bridge. It is shown in the figure that the speed ratio decreases dramatically with the mass ratio first and approaches about 1.3 when the mass ratio is bigger than 0.4. In reality, the speed ratio even for high-speed railways cannot reach such big value of 1.3. For example, the critical speed for this example of a real girder bridge is $v_{\mathrm{cr}} = \frac{l\omega_1}{\pi} = \sqrt{\frac{EI}{\rho A}}\frac{\pi^2}{l} = 868.38$ km/h. Supposing the highest train speed can reach 600 km/h, the highest speed ratio in this case is 0.69. This indicates that separation is unlikely to happen for high-speed trains running on simply supported bridges. It should be mentioned that bridge irregularities are not included in this example, which may be an important factor for vehicle-bridge separation. It should be noticed that Figure 4.21 is valid for any simply supported beams, although it is obtained from a particular beam, as speed and mass ratios are the only factors

affecting the structural response ratio when the contact stiffness is large enough, which has been discussed in section 4.2.2 (b).

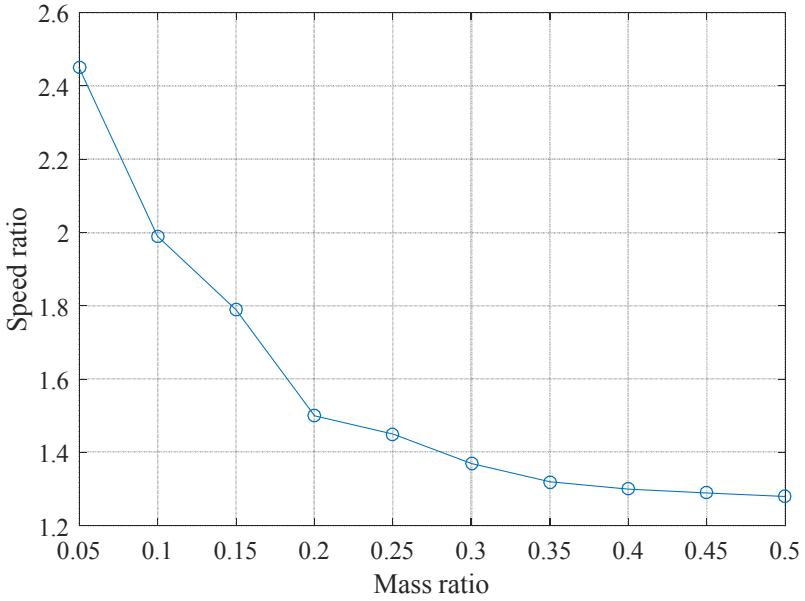

Figure 4.21. The speed ratios from which separation begins to happen for different mass ratios for a simply supported beam

4.3.3. Separation for a Two-Span Continuous Beam

The same numerical example of section 4.2.3 from (Nguyen et al., 2009) is used here. The same contact stiffness of $k_{\mathrm{v}} = 2 \times 10^{10}$ N/ is adopted in this example. A small time step of $\Delta t = 1 \times 10^{-5}$ s is adopted in the numerical integration of the vehicle-bridge equation of motion.

An example of separation for the two-span continuous beam is depicted in Figure 4.22 and Figure 4.23. It can be seen in the figure that the vehicle displacement ratio and the bridge displacement ratio at moving coordinate are almost identical during the no-separation period, but quite different during separation. A much bigger difference between the bridge displacement at the moving coordinate and the vehicle displacement can be observed in Figure 4.22 in the results including separation compared with that in the results without including separation.

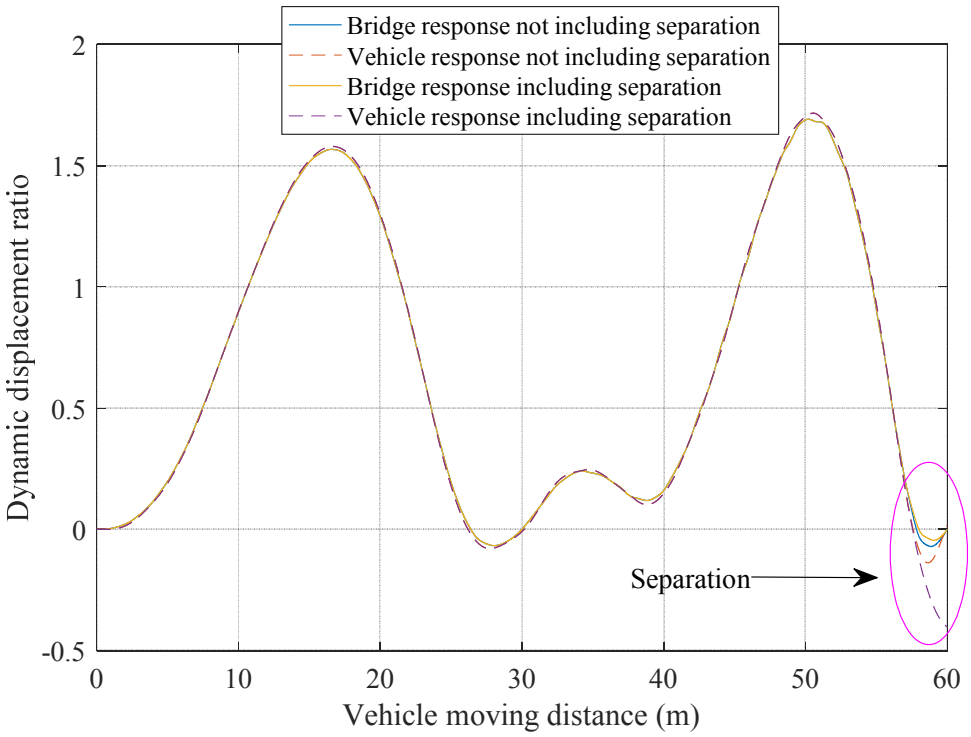

Figure 4.22. Displacement response ratio histories of bridge and vehicle at moving coordinate for mass ratio of 0.4 and speed ratio of 0.3 by using $k_{\mathrm{v}} = 2 \times 10^{10}$ N/m

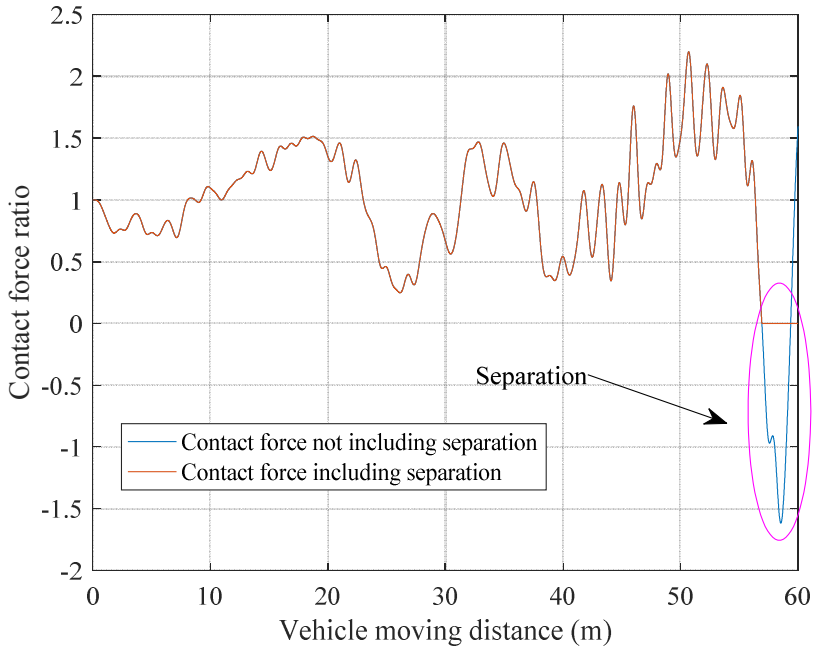

Figure 4.23. Contact force ratio histories for mass ratio of 0.4 and speed ratio of 0.3 by using $k_{\mathrm{v}} = 2 \times 10^{10}$ N/m

Figure 4.24 gives the speed ratio from which separation begins to take place for different mass ratios for a two-span continuous beam. The speed ratio decreases with the speed ratio, and approaches about 0.25 when the mass ratio is bigger than 0.3.

This means separation is very likely to happen for a continuous bridge with big mass ratios in reality.

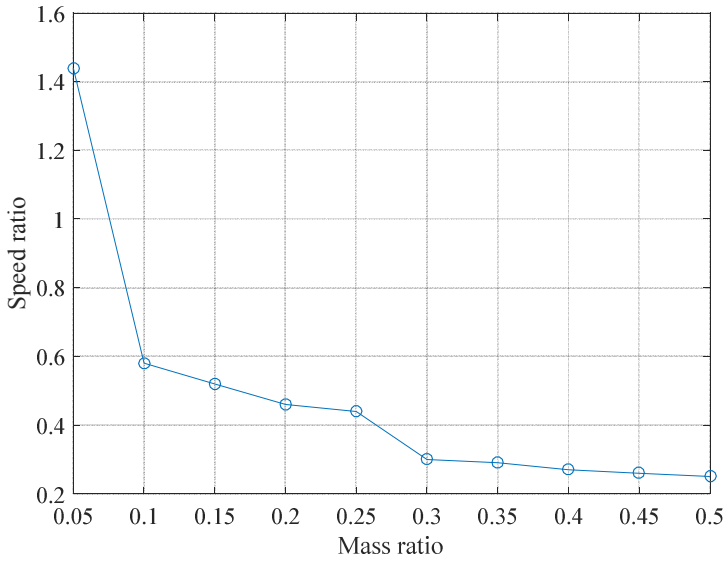

Figure 4.24. The speed ratios from which separation begins to happen for different mass ratios for a two-span continuous beam

4.4. Concluding Remarks

A moving sprung mass model can simulate the interaction between a vehicle and a bridge effectively. Vehicle-bridge separation and reattachment can also be included into this model by just changing the vehicle and bridge motions to free vibrations during the separation period. Impact is not needed to be taken into consideration at the moment of reattachment. The vehicle-bridge coupled equation can be directly applied again to the motions of the vehicle and the bridge at the moment of reattachment. It is found in simulations that separation can have a significant effect on the vibration of the vehicle and the bridge.

The moving force model is compared with the moving sprung mass model. It is found that the vehicle-bridge interaction is stronger at bigger mass ratios of the vehicle to the bridge and higher speed ratios of the vehicle speed to the critical speed. In this case, the bridge response excited by a moving sprung mass is larger than that by a moving force. When the vehicle-bridge interaction is weak, the moving sprung mass model can be replaced by the moving force model. It should be noticed that using smaller contact stiffness can yield a smaller bridge response. Large enough

contact stiffness should be used to model the rigid contact between a rail vehicle and a bridge.

Vehicle-bridge separation is more likely to happen for a bigger mass ratio and at a higher speed ratio. For a bigger mass ratio, a lower speed ratio can lead to separation. The simply supported beam and the two-span continuous beam are compared. It is found from simulations that the vehicle-bridge separation is unlikely to happen for a simply supported bridge with span length of 30 m and zero initial conditions (no vibrations) under current high-speed train speeds if the bridge irregularities can be ignored. However, separation is likely to happen for a two-span continuous beam with a mass ratio bigger than 0.3. It should be mentioned that the contact stiffness has a big influence on separation. The above conclusion is made by using the contact stiffness of 1×10^{11} N/m and 2×10^{10} N/m for a simply supported beam and a two-span continuous beam, respectively.

5. Vibration of a Four-Span Continuous Plate Structure Subjected to One Moving Car

For the vibration of a girder bridge excited by a moving train in reality, it was found that a small number of bridge modes were excited (Xia et al., 2003a). This indicates that using the MS method with few modes would be good enough to obtain acceptably accurate results for a real girder bridge. In this case, the computation efficiency by using the MS method is much higher than that by using the direct integration method, as the number of bridge modes used is much smaller than the DOFs of the bridge FE model.

Beam theories and plate theories are commonly used to model simple bridges or rails (Marchesiello et al., 1999; Cheung et al., 1999), but they are not good enough to model complicated bridges with complex internal structures and boundary conditions. Generally, the analytical modes of complicated structures are not available. In this case, the FE method must be adopted to capture their numerical modes. A good way of using the MS method for complicated structures is that the real modes of complicated structures are approximated by their numerical counterparts in the MS method (Baeza and Ouyang, 2008; Xia and Zhang, 2005). The accuracy of this method depends on the accuracy of the structural FE models and model updating is normally needed to obtain more accurate structure models.

The dynamic response of a single span beam subjected to moving vehicles has drawn much research attention, but a relatively smaller amount of research work has been done for the interaction between multi-span beams and moving vehicles (Marchesiello et al., 1999; Cheung et al., 1999; Henchi and Fafard, 1997; Martinez-Castro et al., 2006; Pu and Liu, 2010; De Salvo et al., 2010; Wang et al., 2013) and the experimental study of the vibration of multi-span beams excited by moving vehicles is even less frequent (Stăncioiu et al., 2011; Chan and Ashebo, 2006).

The travelling speeds of the moving masses or the cars in the laboratory studies of moving load problems are often treated as constant in the literature, but in some tests the speed is variable due to the rolling friction at the masses/beam or the wheels/rails

and the car axle/bearing interfaces. The influence of car speed variations on the dynamic response of a four-span continuous plate with two rails on top is investigated experimentally and theoretically in this chapter.

The work in this chapter is a further development of the work by Stăncioiu *et al.* (2011). Based on the experiments reported by Stăncioiu *et al.*, a more complicated rig is developed. Two rails and four actuators are attached on top of the plate and on the bottom surface of the plate, respectively, and the moving masses are now replaced by a moving car. The presence of four actuators imposes four time-varying forces at four locations of the plate structure (one location at each span individually) based on an active control algorithm according to the feedback signals which are the displacements measured by four laser displacement transducers, for the purpose of controlling the vibration of the plate structure. It should be noted here that vibration control is not the work in this thesis, but is studied by a colleague in the student's research group, and as the experimental rig is shared the actuators are kept. In the experiments of this thesis, the four actuators are not switched on and thus do not produce any active forces. However, their presence even without actuation presents a small amount of (passive) stiffness, masses and damping that should be accounted for in order to make an accurate model. The moving car is the only excitation source, but the properties of the whole structure are changed locally where actuators are attached, so the stiffness, point masses and damping of the actuators should be considered in the model of the whole structure. The model by Stăncioiu *et al.* (2011) is two dimensional. It is necessary to develop a 3-dimensional model to capture accurate modes of the more complicated structure, including its torsional modes, and to examine the influence of four contact points between the moving car and the rails on the dynamic response of the car-plate system.

This chapter first presents the details of the MS method and an iterative method based on the model of a sprung mass moving on a simply supported beam. Numerical modes of the beam are obtained by the FE method and applied in the MS method. This approach can be extended to be a general way of solving moving load problems, which is to use ABAQUS to obtain numerical modes of a structure and to implement the MS method using the structural numerical modes obtained from ABAQUS and an iterative method in MATLAB. This approach is verified firstly

against the results of an example in (Nguyen et al., 2009). Then the vibration of a four-span continuous plate with two rails and four actuators excited by a moving model car is studied by simulations and experiments. Experimental results and numerical ones are found to agree very well. Then an in-depth parametric analysis is done using the experimentally validated numerical model.

5.1. MS Method by Numerical Modes and Iterative Method

The iterative method applied in this thesis is referred to as the iteration scheme which is performed in every single time step. The Newmark integration method is combined with the iterative method in every time step. The moving sprung mass model is adopted to demonstrate the combined MS method and the iterative method in this section.

5.1.1. Iterative Procedures for the Moving Sprung Mass Model

For the moving sprung mass problem shown in Figure 5.1, the equation of motion for the beam and the mass can be written as

$$\rho A \frac{\partial^2 w(x,t)}{\partial t^2} + EI \frac{\partial^4 w(x,t)}{\partial x^4} = k_{\mathrm{v}}(q_{\mathrm{v}} - w(x_{\mathrm{v}},t)) \cdot \delta(x - vt) \tag{5.1}$$

$$-m_{\mathrm{v}}g - k_{\mathrm{v}}\big(q_{\mathrm{v}} - w(x_{\mathrm{v}},t)\big) = m_{\mathrm{v}} \frac{\mathrm{d}^2 q_{\mathrm{v}}(t)}{\mathrm{d}t^2} \tag{5.2}$$

where ρ and E are the density and Young's modulus of the beam, respectively; A and I are the area and second moment of area of the beam's cross section; k_{v} is the stiffness of the spring between the mass and the beam; m_{v} is the mass of the moving mass; w and q_{v} are the deflection of the beam and the displacement of the mass, respectively. Please note that the initial displacement of the sprung mass is $-\frac{m_{\mathrm{v}}g}{k_{\mathrm{v}}}$ here, which is different from that in section 4.1. The mass is assumed to travel at a constant speed of v, so the location of mass can be described as

$$x_{\mathrm{v}} = vt \tag{5.3}$$

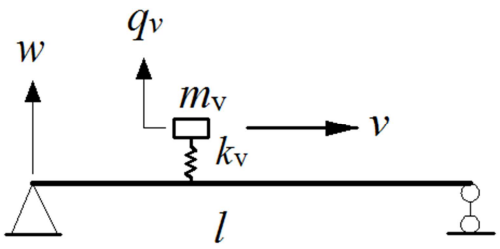

Figure 5.1. Moving sprung mass model

Eq.(5.2) can be rewritten as

$$m_{\mathrm{v}}\ddot{q}_{\mathrm{v}}(t) + k_{\mathrm{v}}q_{\mathrm{v}}(t) = -m_{\mathrm{v}}g + k_{\mathrm{v}}w(x_{\mathrm{v}}, t) \tag{5.4}$$

Applying the MS method to Eq.(5.1), it can be changed to

$$\ddot{q}_i + \omega_i^2 q_i = k_{\mathrm{v}}\left[q_{\mathrm{v}}(t) - \sum_{j=1}^{n} \varphi_j(vt) \cdot q_j(t)\right] \cdot \varphi_i(vt) \tag{5.5}$$

where q_i is the modal coordinate and n is the number of modes used. i is an integer between 1 and n. Combining n equations for different i together, Eq. (5.4) and Eq.(5.5) can be written in matrix form as

$$m_{\mathrm{v}}\frac{\mathrm{d}^2 q_{\mathrm{v}}(t)}{\mathrm{d}t^2} + k_{\mathrm{v}}q_{\mathrm{v}}(t) = -m_{\mathrm{v}}g + k_{\mathrm{v}}\boldsymbol{\varphi}^{\mathrm{T}}\mathbf{q} \tag{5.6}$$

$$\mathbf{M}\ddot{\mathbf{q}} + \mathbf{K}\mathbf{q} = k_{\mathrm{v}}(q_{\mathrm{v}}(t) - \boldsymbol{\varphi}^T\mathbf{q})\boldsymbol{\varphi} \tag{5.7}$$

where $M_{ij} = \delta_{ij}$, $K_{ij} = \omega_i^2\delta_{ij}$, $\mathbf{q} = [q_1, q_2, \dots, q_n]^{\mathrm{T}}$, $\omega_i^2 = \frac{EI}{\rho A}\left(\frac{i\pi}{l}\right)^4$, and $\boldsymbol{\varphi} = [\varphi_1(vt),\ \varphi_2(vt), \dots, \varphi_n(vt)]^T$.

From time t_0 to time $t_0 + \Delta t$, the iterative procedure is as follows

Step 1. Calculate ${}^0\mathbf{S}_b = \mathbf{M}(a_1\,{}^0\mathbf{q} + a_3\,{}^0\dot{\mathbf{q}} + a_4\,{}^0\ddot{\mathbf{q}})$ and ${}^0s_v = m_{\mathrm{v}}(a_1\,{}^0u + a_3\,{}^0\dot{u} + a_4\,{}^0\ddot{u})$,where ${}^0\mathbf{S}_b$ and ${}^0s_v$ are the results at time t_0, $a_1 = \frac{1}{\alpha\Delta t^2}, a_3 = \frac{1}{\alpha\Delta t}, a_4 = \frac{1}{2\alpha} - 1$ and α is a Newmark integration parameter;

Step 2. Assume the initial $\mathbf{q}$ before any iterations at time $t_0 + \Delta t$ as ${}^{\Delta t}\mathbf{q}^{(0)} = {}^0\mathbf{q}$;

Step 3. Calculate ${}^{\Delta t}\dot{\mathbf{q}}^0 = a_2\left({}^{\Delta t}\mathbf{q}^0 - {}^0\mathbf{q}\right) - a_5\,{}^0\dot{\mathbf{q}} - a_6\,{}^0\ddot{\mathbf{q}}$, and ${}^{\Delta t}\ddot{\mathbf{q}}^0 = a_1\left({}^{\Delta t}\mathbf{q}^0 - {}^0\mathbf{q}\right) - a_3\,{}^0\dot{\mathbf{q}} - a_4\,{}^0\ddot{\mathbf{q}}$, where $a_2 = \frac{\beta}{2\Delta t}, a_5 = \frac{\beta}{\alpha} - 1, a_6 = \left(\frac{\beta}{2\alpha} - 1\right)\Delta t$, α and β are Newmark integration parameters;

Step 4. Calculate ${}^{\Delta t}p_{\mathrm{v}}^0 = -m_{\mathrm{v}}g + k_{\mathrm{v}}\,{}^{\Delta t}\boldsymbol{\varphi}^{T\,\Delta t}\mathbf{q}^0$;

Step 5. The equation of motion of the mass after doing Newmark integration can be obtained as $(k_{\mathrm{v}} + a_1 m_{\mathrm{v}})\,{}^{\Delta t}q_{\mathrm{v}}^0 = {}^{\Delta t}p_{\mathrm{v}}^0 + {}^0s_{\mathrm{v}}$, so ${}^{\Delta t}q_{\mathrm{v}}^0 = \frac{{}^{\Delta t}p_{\mathrm{v}}^0 + {}^0s_{\mathrm{v}}}{k_{\mathrm{v}} + a_1 m_{\mathrm{v}}}$;

Step 6. Calculate ${}^{\Delta t}\dot{q}_{\mathrm{v}}^0 = a_2\left({}^{\Delta t}q_{\mathrm{v}}^0 - {}^0q_{\mathrm{v}}\right) - a_5\,{}^0\dot{q}_{\mathrm{v}} - a_6\,{}^0\ddot{q}_{\mathrm{v}}$ and ${}^{\Delta t}\ddot{q}_{\mathrm{v}}^0 = a_1\left({}^{\Delta t}q_{\mathrm{v}}^0 - {}^0q_{\mathrm{v}}\right) - a_3\,{}^0\dot{q}_{\mathrm{v}} - a_4\,{}^0\ddot{q}_{\mathrm{v}}$;

Step 7. Calculate ${}^{\Delta t}\mathbf{P}_b^0 = k_{\mathrm{v}}\left({}^{\Delta t}q_{\mathrm{v}}^0 - {}^{\Delta t}\boldsymbol{\varphi}^{T\,\Delta t}\mathbf{q}^0\right){}^{\Delta t}\boldsymbol{\varphi}$;

Step 8. The equation of motion of the beam after doing Newmark integration can be obtained as $(\mathbf{K} + a_1\mathbf{M})\,{}^{\Delta t}\mathbf{q}' = {}^{\Delta t}\mathbf{P}_b^0 + {}^0\mathbf{S}_b$, so ${}^{\Delta t}\mathbf{q}' = (\mathbf{K} + a_1\mathbf{M})^{-1} \cdot ({}^{\Delta t}\mathbf{P}_b^0 + {}^0\mathbf{S}_b)$;

Step 9. Check if the following convergent criteria is satisfied

$$\frac{L^2\,\mathrm{norm}\left({}^{\Delta t}\mathbf{q}' - {}^{\Delta t}\mathbf{q}^k\right)}{L^2\,\mathrm{norm}({}^{\Delta t}\mathbf{q}' - {}^0\mathbf{q})} \leq \epsilon \tag{5.8}$$

where k is the iterative number which is 0 here and ϵ (tolerance) is suggested to be between 1.0×10^{-5} and 1.0×10^{-8} by Yang and Fonder (1996).

If Eq. (5.8) is satisfied, the iterative scheme from time t to $t + \Delta t$ is ended and go back to step 1 for next time step, otherwise ${}^{\Delta t}\mathbf{q}^1$ is updated by ${}^{\Delta t}q^1 = {}^{\Delta t}q^0 + \eta({}^{\Delta t}q' - {}^{\Delta t}q^0)$, where η is a relaxation coefficient which is between 0 and 1. The iterative scheme ends when the mass exits the beam. Although the moving sprung mass model is used here to demonstrate the MS method and iterative method, they can be applied to other more complicated models.

5.1.2. *Numerical Verification*

The parameters of a real simply supported bridge in (Nguyen et al., 2009) are taken as a numerical example here: beam length $l = 30$ m, Young's modulus of the beam $E = 2.825 \times 10^{10}\ \mathrm{N/m^2}$, cross-sectional area of the beam $A = 7.73\ \mathrm{m^2}$, second moment of area of the beam $I = 7.84\ \mathrm{m^4}$, the density of the beam $\rho = 5.4 \times 10^3\ \mathrm{kg/m^3}$, the stiffness of the contact spring $k_\mathrm{v} = 1.06 \times 10^6\ \mathrm{N/m}$, and the moving mass $m_\mathrm{v} = 4.255 \times 10^4$ kg.

The critical speed (defined as the speed of a moving constant force at which the structure is excited into resonance in its first mode) of the bridge is calculated as $v_\mathrm{cr} = \frac{l\omega_1}{\pi} = 868.384\ \mathrm{km/h}$. The dynamic responses of the moving sprung-bridge system given in Figure 5.2 are very close to the analytic results in Figure 9 in Nguyen *et al.* (2009), which indicates that the approach presented in this chapter works well. Please note that only the first mode is used in the computation for comparison in the figure, as such is the case for the 'analytic' results in (Nguyen et al., 2009).

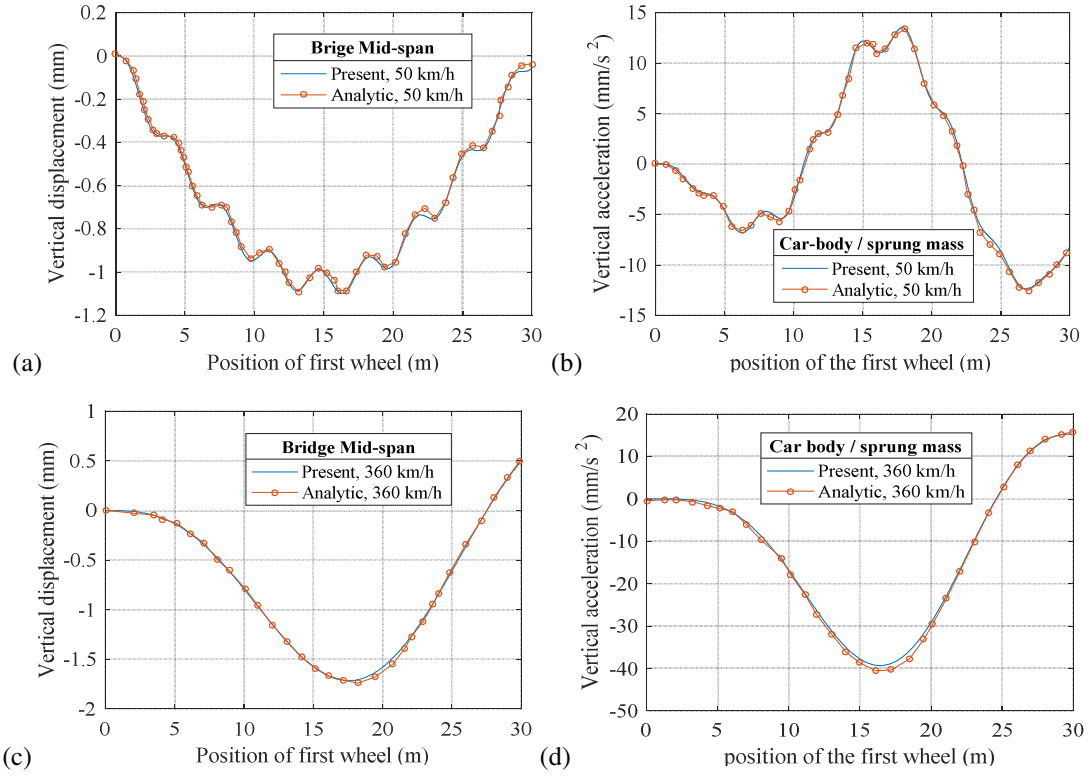

Figure 5.2. Comparison of vertical displacements of bridge mid-span and accelerations of car body/sprung mass at speeds of 50 km/h (a, b) and 360 km/h (c, d) ('Analytic' refers to the 'Analytic' curve in Figure 9 in (Nguyen et al., 2009))

5.2. Theoretical Study of a Moving Car-Bridge Rig

The experimental rig is introduced first, and then the geometric and material properties of the rig are measured or identified. The theoretical models of the car and the infrastructure are described in the following sections. Three different tests are carried out finally. The experimental results are compared with the simulated results and the spectra of the experimental results are also discussed.

5.2.1. Experimental Setup

A four-span continuous plate with four grounded elastic springs (representing four actuators) and a moving car on top is shown in Figure 5.3. The whole length of the plate is 3.6 m with four equal spans. There are front and rear extra spans used to help decelerate and accelerate the movement of cars. The time history of the car speed is measured by using a laser vibrometer (Polytec PSV-500) shown in the figure. Figure 5.4 shows the first two spans and the first span in more detail. The actuators are attached to the plate via thin rods functioning as elastic springs, point masses and damping. They are used in vibration control by another colleague. Their average stiffness is measured to be around 8548 N/m. The mass of each thin rod is 50 g. A 4.335 kg model car can travel along the two rails glued on top of the plate. The width of the plate is 101.67 mm and the thickness of the plate is 3.16 mm. The two rails are the same and the width and height of each rail are 6.85 mm and 8.52 mm, respectively. An optoNCDT1401 laser-displacement transducer is mounted below each span of the plate structure individually to measure dynamic response of the plate (without contact) shown in Figure 5.5. The dSPACE acquisition system is used to obtain real-time data. It should be pointed that vibration experiments of a 4-span continuous structure of this degree of complexity subjected to a moving car have not been reported in the literature.

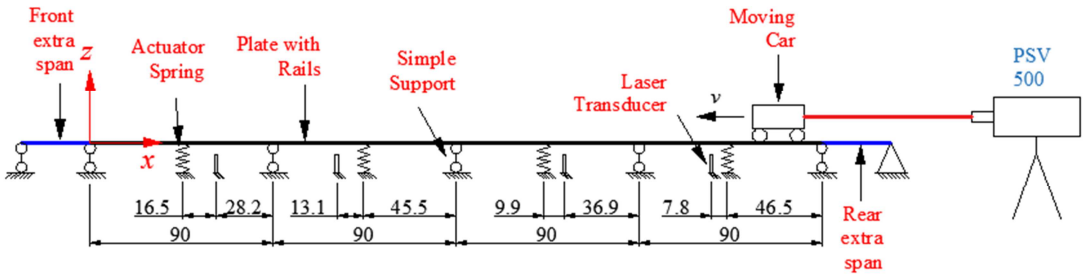

Figure 5.3. Lateral view of the whole experimental setup (unit: cm)

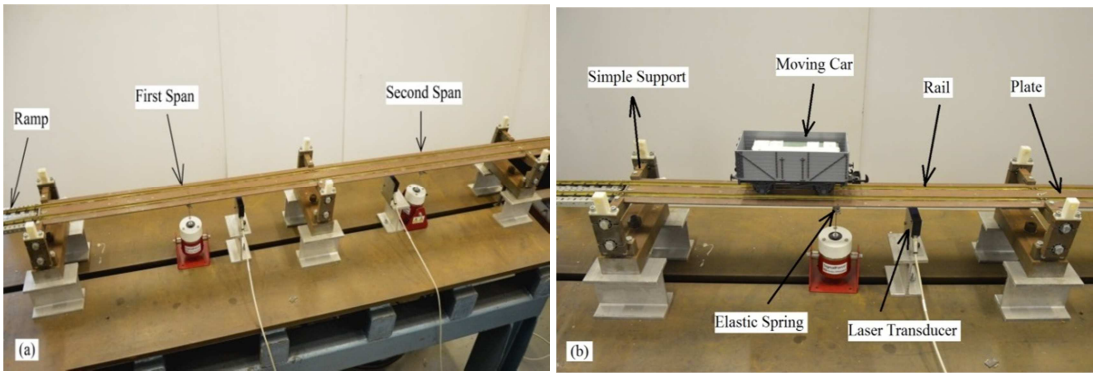

Figure 5.4. Pictures of experimental setup: (a) first two spans, (b) first span

Figure 5.5. Laser transducer used to measure displacement

5.2.2. Parameter Identification for Structural Model

(a) Identification of material and geometric properties of plate and rail

To know the area and second moment of area of the rail section, a clear picture of the rail section was taken and its profile was then detected by using image processing and saved in a CAD drawing. Figure 5.6 shows the picture of the rail section and the CAD drawing of its profile. The two figures look similar but not the same, which

could be caused by the error of edge detection for the picture. The area and second moment of area of the rail section are calculated from its CAD drawing to be around $A_{\mathrm{r}} = 28.0\ \mathrm{mm}^2$ and $I_{\mathrm{r}} = 207.0\ \mathrm{mm}^4$ respectively. The cross section of the plate is rectangular. The area and second moment of area of the plate are calculated to be $A_{\mathrm{p}} = bh = 321.3\ \mathrm{mm}^2$ and $I_{\mathrm{p}} = \frac{bh^3}{12} = 267.3\ \mathrm{mm}^4$ respectively, where b is the width of the plate and h is the height of the plate. The density of the rail and the plate are identified to be around 8356.5 $\mathrm{kg/m}^3$ and 7699.8 $\mathrm{kg/m}^3$ respectively.

The Young's modulus of an Euler-Bernoulli beam can be identified from measured natural frequencies of their theoretical formula below

$$f_k = \frac{\lambda_k^2}{2\pi l^2}\sqrt{\frac{EI}{\rho A}} \tag{5.9}$$

where f_k is the kth frequency of the beam and can be obtained by modal testing; λ_k is the product of the kth wavenumber of the beam and the span length of the beam which can be calculated by using beam theory according to its boundary conditions; l is the length of one span of the beam. l, ρ, A and I can be found directly or indirectly, so E can be calculated inversely from this frequency formula. modal testing is carried out on a plate specimen and a rail specimen separately to obtain their natural frequencies. The Young's moduli of the rails and the plate are calculated to be around 86.6 GPa and 183.4 GPa, respectively. It can be determined from the densities and Young's moduli of the rails and plate that their materials could be copper alloy and cast iron, respectively (Brandes and Brook, 1998).

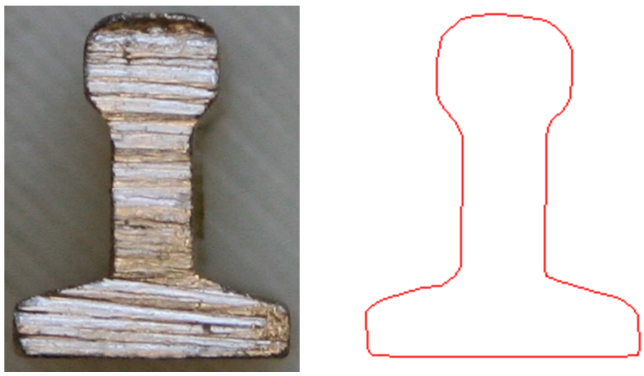

Figure 5.6. The picture of rail section and its CAD drawing

(b) Identification of shaker's properties

Impact testing for the actuator with and without an additional mass was done as in Figure 5.7. The Frequency Response Function (FRF) for this test is the ratio of the acceleration response of the actuator to the impact force by the hammer in the frequency domain and given in Figure 5.8. It can be seen in the figure that there is only one dominant frequency for the vertical vibration of the actuator, which indicates that it is reasonable to treat the actuator as a SDOF system in vertical vibration. The FRF curve is wide for the actuator without an additional mass, which reflects the damping of the actuator is large. The damping of a SDOF system can be estimated from its free vibration response.

If the vertical vibration of the shaker can be treated to be SDOF, identifying the mass and stiffness of the shaker in vertical vibration would not be hard. The idea is the assumption that the stiffness of the shaker remains the same after adding an additional mass on top of the shaker. Denoting k_s the vertical stiffness of the shaker, m_s the mass of the vibrating part of the shaker, m_a the additional mass which is 0.103 kg, the following equations regarding the frequencies of the two systems can be written as

$$\sqrt{\frac{k_s}{m_s}} = \omega_{n1} \tag{5.10}$$

$$\sqrt{\frac{k_s}{m_s+m_a}} = \omega_{n2} \tag{5.11}$$

where $\omega_{n1} = 2\pi f_1 = 2 \times \pi \times 107.7 \text{ rad/s} = 676.70 \text{ rad/s}$, $\omega_{n2} = 2 \times \pi \times 40.8 \text{ rad/s} = 256.35 \text{ rad/s}$. After calculating, one can get k_s to be 7903.1 N/m, and m_s to be 0.0173 kg.

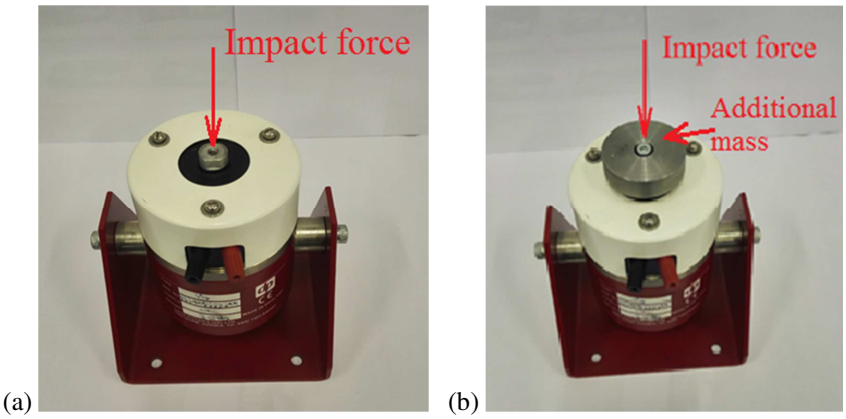

(a) (b)

Figure 5.7. Impact testing schematic for (a) shaker without additional mass, (b) shaker with additional mass

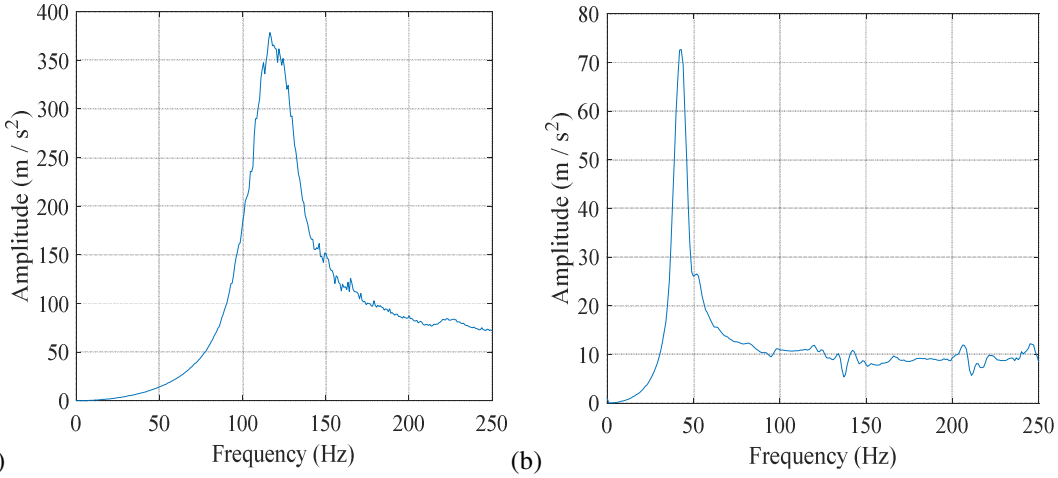

(a) (b)

Figure 5.8. The FRF of (a) an actuator without additional mass, (b) the shaker with additional mass

The damping ratio of the actuator can be identified by the logarithmic decrement as below (Inman, 2008)

$$\zeta = \frac{1}{\sqrt{1+\left(\frac{2\pi}{\delta}\right)^2}} \tag{5.12}$$

where $\delta = \frac{1}{n}\ln\frac{y(t)}{y(t+nT)}$, $y(t)$ is the amplitude of a peak at time t and $y(t+nT)$ is the amplitude of the peak n periods away.

Figure 5.9 is the acceleration signal of one shaker under impact loading. It can be seen from the figure that the acceleration drops down suddenly after impacting and goes up to a very high value, and then vibrates freely with amplitude decayed with

time. It is noticed that the amplitude takes a long time to finally recover to zero. As shown in the figure, $\mathrm{y}(t)$ is chosen to be 21.82 $\mathrm{m/s^2}$ and $\mathrm{y}(t+4T)$ 3.846 $\mathrm{m/s^2}$. In the calculation, $\mathrm{y}(t)$ and $\mathrm{y}(x+4T)$ subtract -0.7086 $\mathrm{m/s^2}$ which is taken as a temporary steady state to get their differences from the steady state. Substituting $\mathrm{y}(t)$ and $\mathrm{y}(t+4T)$ into Eq. (5.12), one can calculate out ζ as 6.35%, then the damping coefficient can be calculated to be 1.487 N s/m by following equation.

$$c = 2m_s\omega_{n1}\zeta \tag{5.13}$$

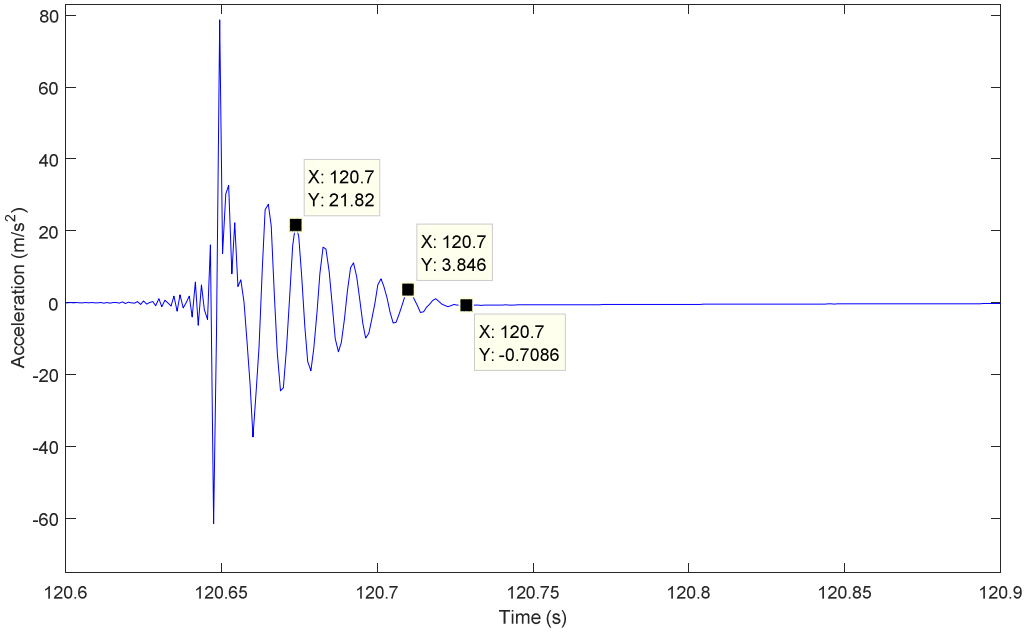

Figure 5.9. An acceleration signal of one shaker under impact loading

5.2.3. A Four-Span Continuous Beam Model

Assuming the rig could be modelled as a four-span Euler-Bernoulli beam, its *k*th natural frequency in Hz can be expressed as Eq. (5.9). The values of λ_k for a four-span continuous beam can be found in (Blevins, 1979), and the first four values are $\lambda_1 = 3.142, \lambda_2 = 3.393, \lambda_3 = 3.928, \lambda_4 = 4.463$. One way of obtaining those values is described as below.

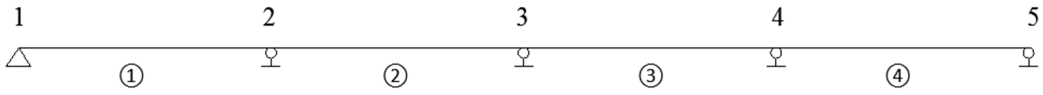

Figure 5.10. Four-span continuous beam model

According to the Euler-Bernoulli beam theory, the analytical mode shapes for each span can be expressed as

$$w_i(x) = A_i \sin\left(\frac{\lambda x}{l}\right) + B_i \cos\left(\frac{\lambda x}{l}\right) + C_i \sinh\left(\frac{\lambda x}{l}\right) + D_i \cosh\left(\frac{\lambda x}{l}\right) \tag{5.14}$$

where l is the length of each span, i is the number of spans ($i = 1, 2, 3, 4$) and x is the location of beam in local coordinates. For every span, $w_i(0) = 0$, so Eq. (5.14) can be reduced to

$$w_i(x) = A_i \sin\left(\frac{\lambda x}{l}\right) + C_i \sinh\left(\frac{\lambda x}{l}\right) + B_i\left(\cos\left(\frac{\lambda x}{l}\right) - \cosh\left(\frac{\lambda x}{l}\right)\right) \tag{5.15}$$

The first and second derivatives of Eq. (5.15) with respect to x can be derived as

$$w_i'(x) = A_i \frac{\lambda}{l} \cos\left(\frac{\lambda x}{l}\right) + C_i \frac{\lambda}{l} \cosh\left(\frac{\lambda x}{l}\right) - B_i \frac{\lambda}{l}\left(\sin\left(\frac{\lambda x}{l}\right) + \sinh\left(\frac{\lambda x}{l}\right)\right) \tag{5.16}$$

$$w_i''(x) = -A_i \frac{\lambda^2}{l^2} \sin\left(\frac{\lambda x}{l}\right) - C_i \frac{\lambda^2}{l^2} \sinh\left(\frac{\lambda x}{l}\right) - B_i \frac{\lambda^2}{l^2}\left(\cos\left(\frac{\lambda x}{l}\right) + \cosh\left(\frac{\lambda x}{l}\right)\right) \tag{5.17}$$

At support 1 in Figure 5.10, $w_1''(0) = 0$, so

$$B_1 = 0 \tag{5.18}$$

At support 2, $w_1(l) = 0$, $w_1'(l) = w_2'(0)$ and $w_1''(l) = w_2''(0)$ leading to

$$A_1 \sin(\lambda) + C_1 \sinh(\lambda) + B_1(\cos(\lambda) - \cosh(\lambda)) = 0 \tag{5.19}$$

$$A_1 \cos(\lambda) + C_1 \cosh(\lambda) - B_1(\sin(\lambda) + \sinh(\lambda)) - A_2 - C_2 = 0 \tag{5.20}$$

$$A_1 \sin(\lambda) + C_1 \sinh(\lambda) + B_1(\cos(\lambda) + \cosh(\lambda)) - 2B_2 = 0 \tag{5.21}$$

At support 3, $w_2(l) = 0, w_2'(l) = w_3'(0)$ and $w_2''(l) = w_3''(0)$ leading to

$$A_2 \sin(\lambda) + C_2 \sinh(\lambda) + B_2(\cos(\lambda) - \cosh(\lambda)) = 0 \tag{5.22}$$

$$A_2\cos(\lambda) + C_2\cosh(\lambda) - B_2(\sin(\lambda) + \sinh(\lambda)) - A_3 - C_3 = 0 \quad (5.23)$$

$$A_2\sin(\lambda) + C_2\sinh(\lambda) + B_2(\cos(\lambda) + \cosh(\lambda)) - 2B_3 = 0 \quad (5.24)$$

At support 4, $w_3(l) = 0, w_3'(l) = w_4'(0)$ and $w_3''(l) = w_4''(0)$ leading to

$$A_3\sin(\lambda) + C_3\sinh(\lambda) + B_3(\cos(\lambda) - \cosh(\lambda)) = 0 \quad (5.25)$$

$$A_3\cos(\lambda) + C_3\cosh(\lambda) - B_3(\sin(\lambda) + \sinh(\lambda)) - A_4 - C_4 = 0 \quad (5.26)$$

$$A_3\sin(\lambda) + C_3\sinh(\lambda) + B_3(\cos(\lambda) + \cosh(\lambda)) - 2B_4 = 0 \quad (5.27)$$

At support 5, $w_4(l) = 0$ and $w_4''(l) = 0$ leading to

$$A_4\sin(\lambda) + C_4\sinh(\lambda) + B_4(\cos(\lambda) - \cosh(\lambda)) = 0 \quad (5.28)$$

$$-A_4\sin(\lambda) + C_4\sinh(\lambda) - B_4(\cos(\lambda) + \cosh(\lambda)) = 0 \quad (5.29)$$

Eq. (5.18) to Eq. (5.29) form a matrix equation below

$$\mathbf{Ax} = \mathbf{0} \quad (5.30)$$

where $\mathbf{x} = [A_1; B_1; C_1; A_2; B_2; C_2; A_3; B_3; C_3; A_4; B_4; C_4]$ and $\mathbf{A}$ is a matrix with unknown λ.

As the solution $\mathbf{x}$ cannot be $\mathbf{0}$, $\det(\mathbf{A}) = 0$ from which λ_k can be solved by using Matlab as $\lambda_1 = 3.1416, \lambda_2 = 3.3932, \lambda_3 = 3.9266, \lambda_4 = 4.4633$. After λ_k is solved, $\mathbf{x}$ can be solved from Eq. (5.30) by assuming one element of $\mathbf{x}$ to be a constant. Thus the mode shapes of each span are known from Eq. (5.15). Figure 5.11 shows the first four normalized mode shapes of the four-span continuous beam.

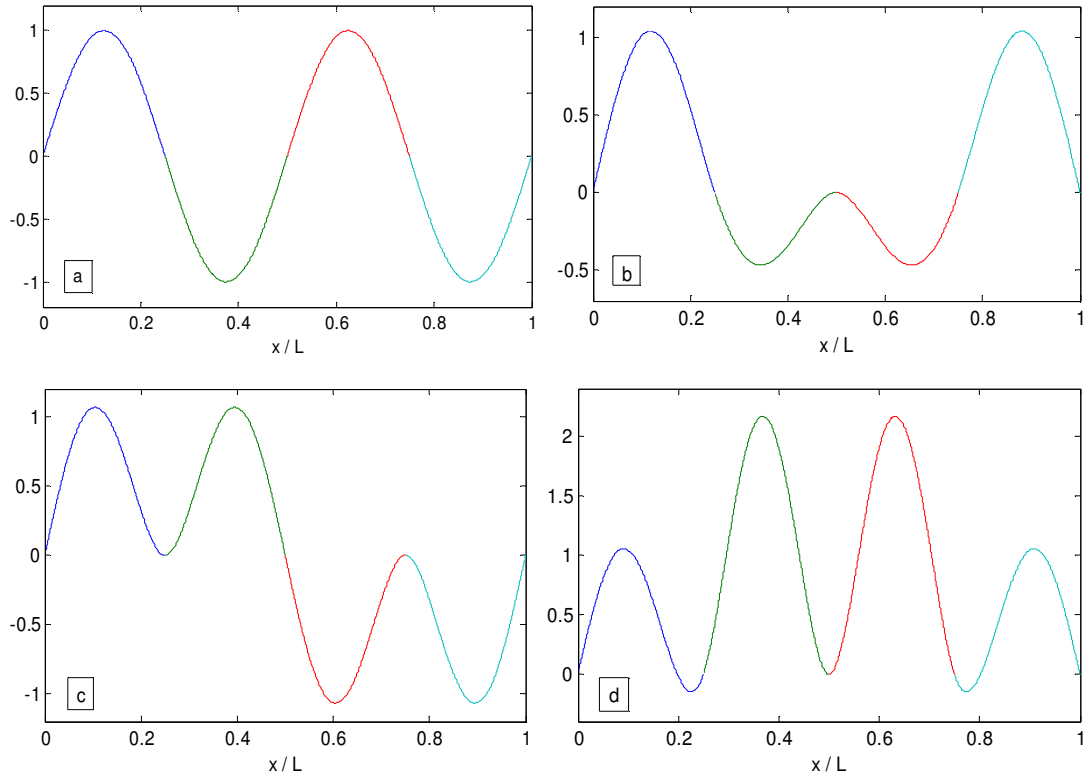

Figure 5.11. First four mode shapes of a four-span continuous beam

Modal testing was done on the four-span plate with rails (actuators not attached) using accelerometers. The first four frequencies of the rig can be obtained by an LMS System and the ratio of $\frac{EI}{\rho A}$ can be calculated inversely from Eq. (5.9). The length of each span is $l = 0.9$ m. It can be found from Table 5.1 that the ratio of $EI/\rho A$ varies much with the number of modes, which indicates that the four-span beam model may be not good. So an FE model of the plate structure is built below in section 5.2.5.

Table 5.1. Modal testing results for the plate structure and calculated ratio of $EI/\rho A$

Mode k	λ_k	Fre. by exp. (Hz)	$EI/\rho A$
1	3.1416	17.386	80.377
2	3.3932	19.779	76.434
3	3.9266	25.257	69.507
4	4.4633	31.436	64.499

5.2.4. Car Model

The model car is treated as a rigid body which consists of two DOFs (pitch θ_1 and heave q_{v1}) as shown in Figure 5.12. The centre of gravity of the car is assumed to be

at its geometric centre. The parameters of the car model are: $m_{v1} = 4.335$ kg (total mass of car body and an additional mass), second moment of area around the y axis $I_{v1} = 0.012$ kg m^2, its wheelbase $s = 0.126$ m and the car body length $L_c = 0.208$ m.

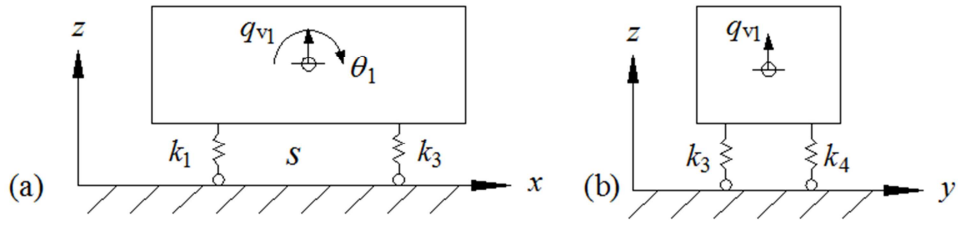

Figure 5.12. Idealization of the moving car: (a) elevation; (b) cross-sectional view at the front axle

The car moves from the end of the infrastructure to the starting point of the infrastructure. There are three stages representing different car locations on the infrastructure: stage 1 - the whole car at the rear extra span and its front wheel at end point of the plate; stage 2 - the whole car on the plate and its rear wheel at end point of the plate; stage 3 - the whole car on the plate and its front wheel at starting point of the plate. The dynamic response of the system during the time period of the car moving from stage 1 to stage 3 is simulated and compared with experimental measurement. As the extra spans are quite short and they are not connected with the plate, they can be taken to be rigid and undergo no vibration.

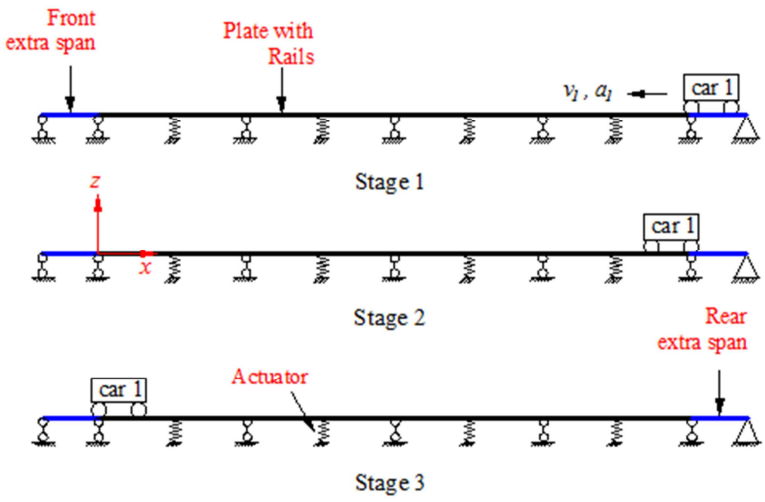

Figure 5.13. Different stages of the car moving process

The equations of motion of the moving car modelled as a rigid body in the vertical plane during stage 1 to stage 3 can be written as

$$m_{\mathrm{v1}}\ddot{q}_{\mathrm{v1}} = -m_{\mathrm{v1}}g - k_1\left[q_{\mathrm{v1}} + \theta_1\frac{s}{2} - w(x_1, y_1, t)\right] - k_2\left[q_{\mathrm{v1}} + \theta_1\frac{s}{2} - w(x_2, y_2, t)\right]$$

$$-k_3\left[q_{\mathrm{v1}} - \theta_1\frac{s}{2} - w(x_3, y_3, t)\right] - k_4\left[q_{\mathrm{v1}} - \theta_1\frac{s}{2} - w(x_4, y_4, t)\right] \quad (5.31)$$

$$I_{\mathrm{v1}}\ddot{\theta}_1 = -k_1\left[q_{\mathrm{v1}} + \theta_1\frac{s}{2} - w(x_1, y_1, t)\right]\frac{s}{2} - k_2\left[q_{\mathrm{v1}} + \theta_1\frac{s}{2} - w(x_2, y_2, t)\right]\frac{s}{2} +$$

$$k_3\left[q_{\mathrm{v1}} - \theta_1\frac{s}{2} - w(x_3, y_3, t)\right]\frac{s}{2} + k_4\left[q_{\mathrm{v1}} - \theta_1\frac{s}{2} - w(x_4, y_4, t)\right]\frac{s}{2} \quad (5.32)$$

where $w(x_i, y_i, t)$ ($i = 1, 2, 3, 4$) is the deflection of the rail at the contact point with ith spring; k_i is the stiffness of the ith spring and q_{v1} is the displacement of the gravity centre of the car body.

It should be noticed that the deflection of the extra spans is zero due to their rigid body and no-vibration assumptions. The car is given a push at the start and allowed to travel along the rails freely.

5.2.5. FE Model of the Plate Structure

A 3D FE model of the plate with supports and rails is built in ABAQUS. 480 shell elements (S4R) are used for the plate and 160 beam elements (B31) for each rail which is tied to the plate. Four spring elements and four mass elements are tied to the plate too, modelling the elastic springs and the vibrating mass provided by actuators. For the boundary conditions of the plate, only the rotational DOFs are allowed at the five pin supports. Modal analysis is done in ABAQUS to predict the frequencies of the structure which are compared with the experimental frequencies obtained by modal testing. An offset ratio for the shell elements defined as the fraction between the distance from the shell mid-surface to the reference surface and the shell thickness (Dassault-Systèmes, 2014) is needed to represent the connection between the rails to the plate since the neutral axis of the rails and the neutral plane of the plate are a short distance apart. As the structural FE model is an approximation of the actual structure, this value of the offset may not be the physical distance between the rails' neutral axis and the plate's neutral plane and it should be determined through

model updating, which turns out to be 1.87 and brings the numerical frequencies of the structure close to their experimental counterparts.

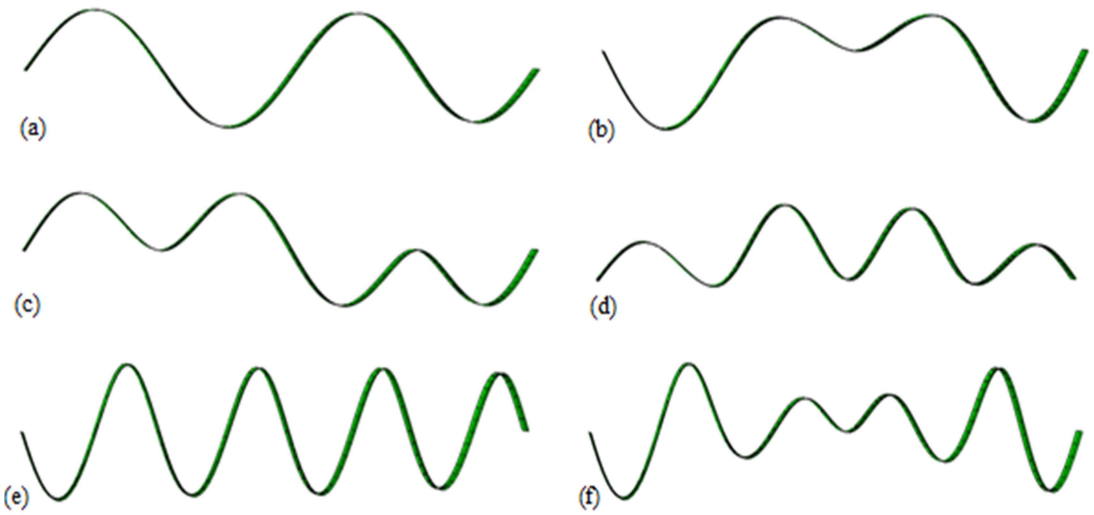

Figure 5.14. First six mode shapes of the structure from ABAQUS

Table 5.2 shows the differences between the first eight experimental frequencies and the corresponding numerical frequencies. It can be seen from the table that the differences are less than 5.0%, which indicates that the FE model of the structure is good enough for dynamic analysis. The first eight mode shapes of the structure obtained from ABAQUS are very similar to the mode shapes of the four-span continuous beam. The first torsional mode of the structure occurs as its 9th mode.

Table 5.2. Comparison between structural experimental and numerical frequencies

Mode	1	2	3	4	5	6	7	8
Experimental	21.242	23.381	28.632	36.374	68.541	73.564	83.080	93.560
Numerical	20.376	22.582	28.180	34.990	65.417	71.036	82.704	95.278
Difference	-4.1%	-3.4%	-1.6%	-3.8%	-4.6%	-3.4%	-0.5%	1.8%

The equation of motion of the FE model of the structure can be expressed as

$$\mathbf{M}\ddot{\mathbf{X}}(t) + \mathbf{K}\mathbf{X}(t) = \mathbf{F}(t) \tag{5.33}$$

where $\mathbf{M}$ and $\mathbf{K}$ are mass matrix and stiffness matrix of the structure model respectively; $\mathbf{F}(t)$ is the force vector which changes with the movement of the car. The concentrated forces F_i acting on the structure at the ith wheel location can be expressed as

$$F_i = k_i\left(q_{\mathrm{v1}} - w(x_i, y_i) + \frac{s}{2}\theta_1\right), i = 1, 2 \tag{5.34}$$

$$F_i = k_i\left(q_{\mathrm{v1}} - w(x_i, y_i) - \frac{s}{2}\theta_1\right), i = 3, 4 \tag{5.35}$$

What should be noticed is that the contact force f_i at the ith wheel is $-F_i$ as compression force is defined as positive force in contact mechanics.

$\mathbf{X}(t)$ is the nodal displacement vector of the structure which can be expressed as

$$\mathbf{X}(t) = \mathbf{\Phi}\mathbf{q}(t) \tag{5.36}$$

where $\mathbf{\Phi}$ is the mass-normalised modal matrix (numerical modes) of the structure model and $\mathbf{q}(t)$ is the vector of the modal coordinates.

Substituting Eq. (5.36) into Eq. (5.33) and multiplying $\mathbf{\Phi}^{\mathrm{T}}$ on both sides of Eq. (5.33) lead to

$$\ddot{\mathbf{q}}(t) + \mathrm{diag}(\omega_i^2)\mathbf{q}(t) = -\sum_{i=1}^{4} \boldsymbol{\varphi}(x_i, y_i) f_i(t) \tag{5.37}$$

where ω_i is the ith natural frequency of the structure. It is found that using 8 or more modes does not make a big difference on dynamic response of the system. Therefore, 8 modes are used. Modal analysis shows that the first torsional mode is the 9$^{\mathrm{th}}$ mode of the plate structure, which does not produce much influence on the structural dynamics. $\boldsymbol{\varphi}(x_i, y_i)$ is the modal vector at the contact point (x_i, y_i) which consists of 8 modes.

If the damping of four actuators which support the plate is considered, Eq. (5.33) and Eq. (5.37) become

$$\mathbf{M}\ddot{\mathbf{X}}(t) + \mathbf{K}\mathbf{X}(t) = \mathbf{F}(t) - \textstyle\sum_{j=1}^{4} c_j \dot{w}\left(x_j, y_j, t\right)\delta\left(x - x_j\right)\delta(y - y_j) \tag{5.38}$$

$$\ddot{\mathbf{q}}(t) + \mathrm{diag}\left[\omega_i^2\right]\mathbf{q}(t) = -\textstyle\sum_{i=1}^{4} \boldsymbol{\varphi}(x_i, y_i) f_{ci}(t) - \sum_{j=1}^{4} c_j \boldsymbol{\varphi}\left(x_j, y_j\right)\boldsymbol{\varphi}^{\mathbf{T}}\left(x_j, y_j\right)\dot{\mathbf{q}}(t) \tag{5.39}$$

where c_j is the damping of the jth actuator, (x_j, y_j) is the location of jth actuator (j=1, 2, 3, 4), and f_{ci} is the contact force at the ith contact point.

5.3. Experimental Verification of the Moving Car-Bridge Model

Test 1: one moving car with one additional mass (No. 1) without considering car acceleration and damping of actuator at low speed

An additional mass marked as No. 1 is put into the car body to enlarge the moving load. The total mass of the car body with the additional mass is 4.335 kg (mass ratio of 0.41). The structural model and the car model are combined and solved by the aforementioned iterative method in MATLAB. It is found from simulations that adopting 1×10^5 N/m or bigger values for the stiffness of springs k_1, k_2, k_3 and k_4 does not make much difference, so the stiffness of springs k_1, k_2, k_3 and k_4 is taken to be 1×10^5 N/m for modelling the rigid contact between the wheels and rails. The average velocity of the car is estimated to be around 1.05 m/s. The constant time step length is 0.0005 s. The dynamic responses of the plate at four measured points are predicted by the system model and compared with experimental measurements obtained by laser displacement transducers.

Figure 5.15 gives the displacements measured by four laser transducers shown in Figure 5.3 and the deflections of the four points on the plate predicted by the system model, respectively. It can be seen from the figure that the downward plate deflections from simulation and experiment are almost the same in magnitude, but numerical results of the upward deflections are slightly bigger than the experimental ones. In addition, all the numerical responses lag slightly behind the experimental ones. The difference between the two sets of results could be caused by the inevitable errors in the identified parameters and the assumption of constant car velocity used in the system model. Note that the car's travelling speed decreases slightly due to friction as it moves forward. Generally, the numerical results agree well with experimental ones.

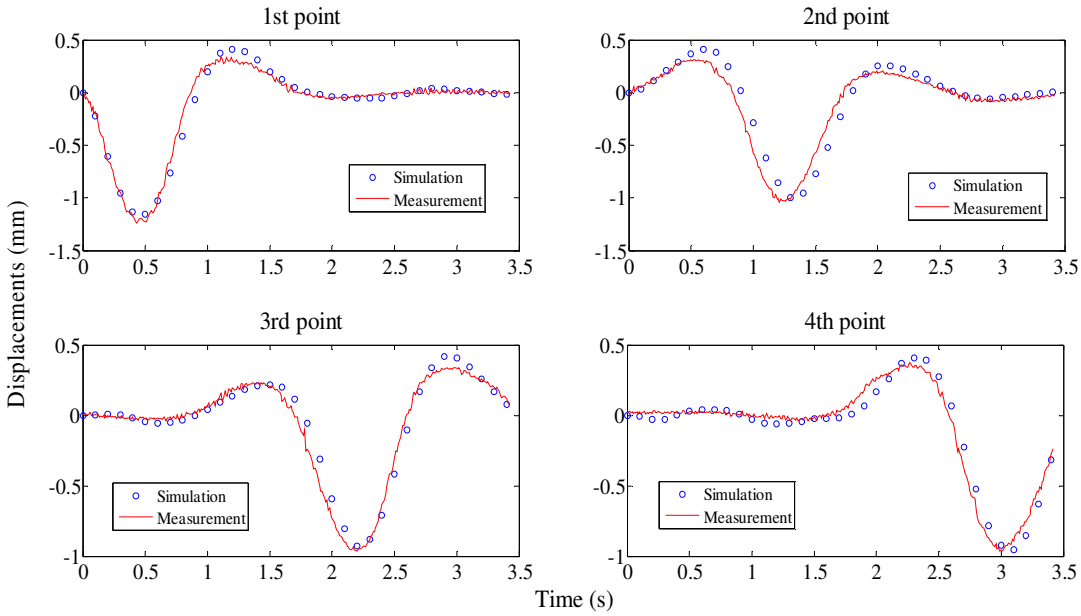

Figure 5.15. Comparison between displacements measured by laser transducers and numerical displacements of the plate at measurement points without considering car acceleration

Test 2: one moving car with one additional mass (No. 1) considering car acceleration and damping of actuator at low speed

The second test involves one car carrying the same mass block (No. 1) as in the first test and moving on the plate structure. The speed of the car is measured by the Laser Vibrometer PSV-500. Figure 5.16 (a) gives the measured car speed while the car stays on the plate structure, where it can be seen that large oscillations occur in the measured results especially when the car enters and leaves the plate structure. These large oscillations are suspected to come from three sources: (1) the oscillations at the start are due to a velocity jump caused by a sudden push of the car, (2) the oscillations at the end are due to the car falling off the track after exiting from the track, and (3) the oscillations during the car's travel on the plate structure are probably due to a larger change in rotation of the car when it approaches an intermediate support. Loss of the laser focus is thought to be another factor. Clearly those oscillations do not reflect true horizontal motion of the car and thus the associated data are not used. A number of data are selected from the raw data by hand, as the red points in Figure 5.16 (a) and plotted in Figure 5.16 (b) so as to remove the effect of the error data. It can be seen from Figure 5.16 (b) that the speed of the car varies at an almost constant deceleration (small local oscillation of the car

speed may be due to the deflection of the plate structure or measurement error), so it can be assumed that the car moves at a constant negative acceleration in the theoretical model. A straight line can be fitted to the picked speed data as $v = -0.07137t + 1.171$, so the acceleration of the car is $a = -0.07137\ m/s^2$ and the initial speed of the car is v_0=1.171 m/s. The travelled distance of the car after a time period of t can be described as $x_v = v_0 t + \frac{1}{2}at^2$.

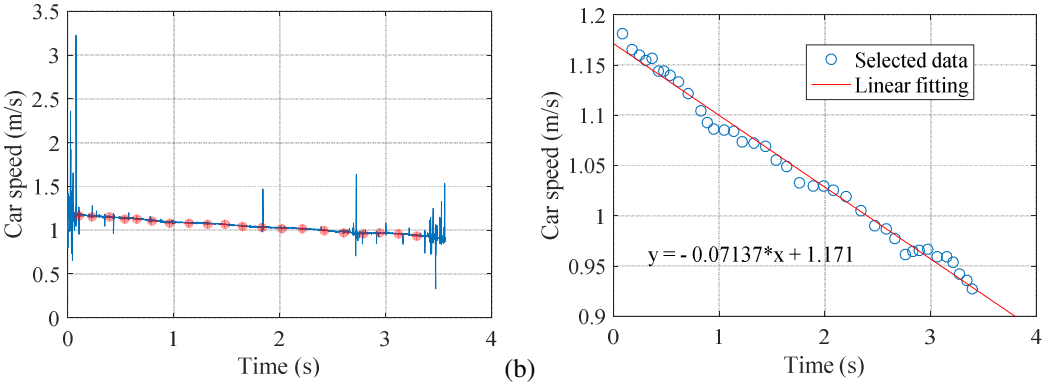

Figure 5.16. Measured car speed: (a) raw data and selected points, (b) selected data and linearly fitted line

Using the estimated initial car speed and acceleration as inputs in simulations, simulated displacements of the plate structure can be obtained and compared with experimental results, as in Figure 5.17. Good agreement between the two sets of results can be seen and small oscillations are found in experimental results, which are suspected of coming from the car-structure interaction and the measuring noise of the displacement laser transducers. The numerical results by using the averaged velocity of the car (1.0454 m/s) are also simulated and are found lagging behind the experimental results obviously, as shown in Figure 5.17. This indicates that the speed variation of the moving car should be considered in the theoretical model of the car-plate system. Please note that the damping of actuators is considered as well for both the blue curve and the black curve in Figure 5.17**.** A detailed discussion about damping of actuators can be seen in section 5.4.2.

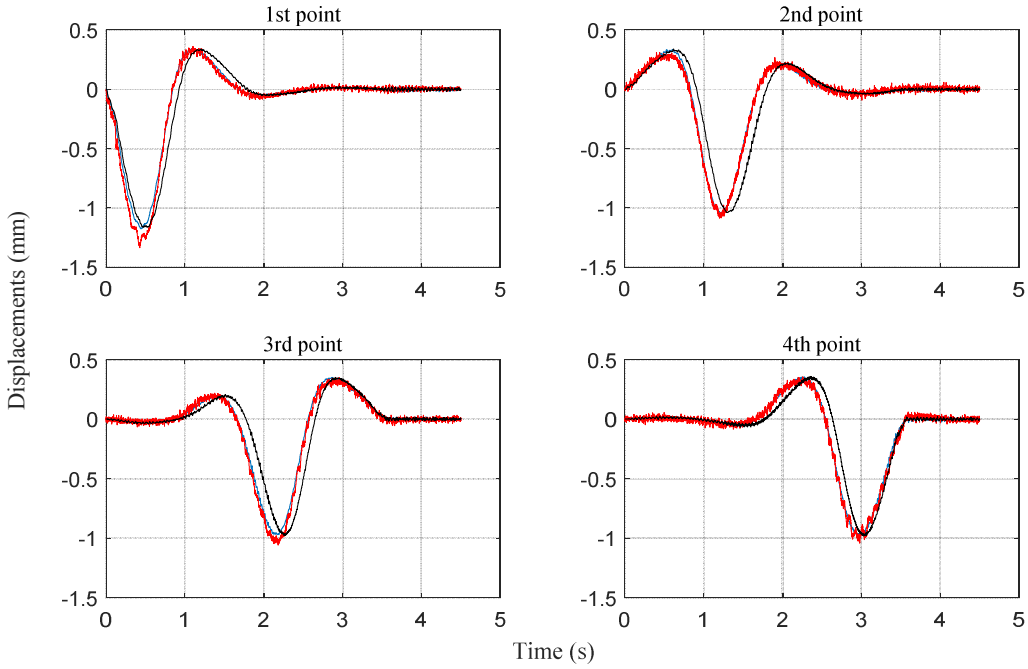

Figure 5.17. Displacements of plate at measured points by simulation considering acceleration of car (blue curve) and results by simulation using average velocity of car (black curve) compared with experimental results (red curve)

Transforming the measured car-excited response and the free response of the plate structure at the 1st measured point after the car leaves the structure from the time domain into the frequency domain, spectra for these two responses are obtained and shown in Figure 5.18 and Figure 5.19. The driving frequency can be calculated as $f_{\mathrm{d}} = \frac{1}{2\pi} \times \frac{\pi v}{l} = \frac{v}{2l}$ when the car moves at a constant speed v (Yau and Yang, 2006). The driving frequency can be estimated by using the averaged car speed to be around 0.58 Hz, which is very close to the frequency at the first peak (0.56 Hz) in Figure 5.18 (a). Clearly the 2nd bridge mode makes the greatest contribution in the free vibration response after the car exits the structure, shown in Figure 5.19.

It can be seen from Figure 5.18 (b) that the amplitudes of the bridge displacement subjected to a moving car within 30 Hz are basically large. These frequencies are actually the frequencies of the car-bridge system which is a time-varying system. The peak amplitudes above 20 Hz are at frequencies of 22.26 Hz, 25.32 Hz and 49.81 Hz and so on. The spectrum of the bridge displacement after the car leaves the bridge is shown in Figure 5.19. Only the second and the third bridge natural frequencies are excited to relatively large amplitudes. It is noticed that the frequency 22.26 Hz in Figure 5.18 (b) is a little bit smaller than the 2nd bridge natural frequency of 23.89 Hz

in Figure 5.19, and the amplitude at the former frequency (about 3×10^{-3} mm) is also smaller than the amplitude at the latter (about 4×10^{-3} mm).

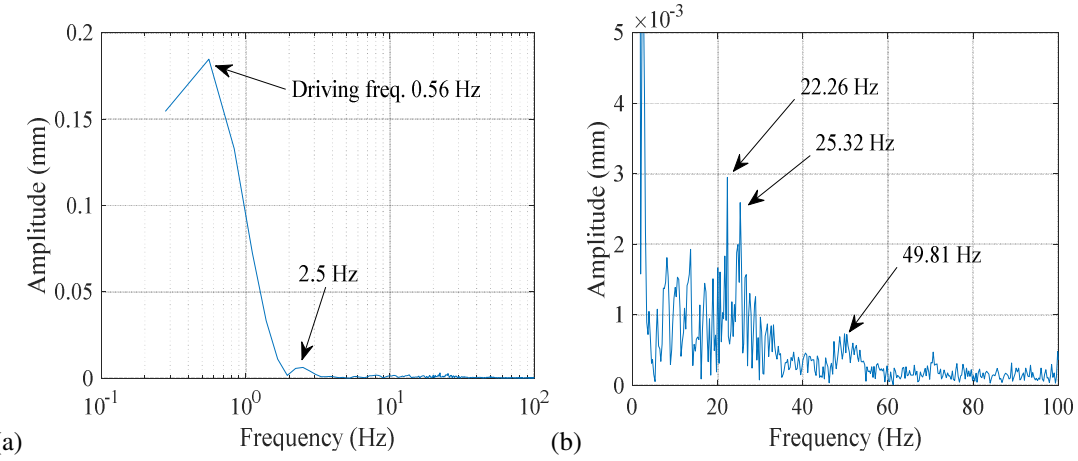

Figure 5.18. Spectrum of measured car-excited displacement of the plate structure at 1st measured point at initial car speed of 1.17 m/s: (a) whole amplitude view, (b) part amplitude view

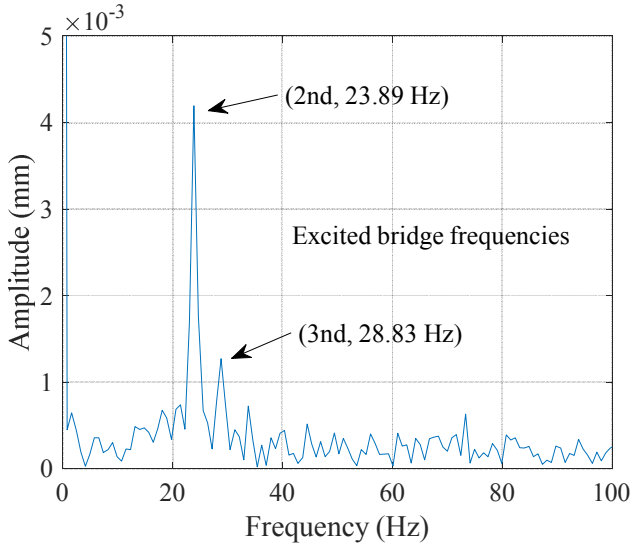

Figure 5.19. Spectrum of measured free vibration of the plate structure at 1st measured point at initial car speed of 1.17 m/s

Test 3: one moving car with one additional mass (No. 1) at high speed

Another test is done with the initial car speed increased to 2.44 m/s, as shown in Figure 5.20 and the displacement of the plate structure is shown in Figure 5.21, which basically does not increase compared with that for the lower car speed in Figure 5.17. However, the spectrum of the measured dynamic displacement of the

plate structure excited by the higher car speed shown in Figure 5.22 indicates some high frequencies with large amplitudes above the driving frequency 1.33 Hz, e.g. at 13.96Hz and 22.61 Hz. Only the first 3 bridge frequencies are found with high amplitudes in Figure 5.23 for the spectrum of the free response of the plate structure. It is noticed that the frequency of 22.61 Hz in Figure 5.22 (b) is close to the 1st bridge natural frequency of 21.5 Hz and the 2nd bridge natural frequency of 23.5 Hz in Figure 5.23, and the frequency of 28.59 Hz at the former figure is close to the 3rd bridge natural frequency of 28.5 Hz in the latter figure. The amplitudes of the frequencies in the former figure are almost the same as those of the corresponding close frequencies in the latter figure.

It is found that the amplitudes of the frequencies of the car-bridge system at a high car speed are basically larger than those at a low car speed by comparing Figure 5.22 with Figure 5.18. This indicates that the car-bridge interaction becomes stronger at a higher car speed (it should be noted that this trend would change at a high enough speed).

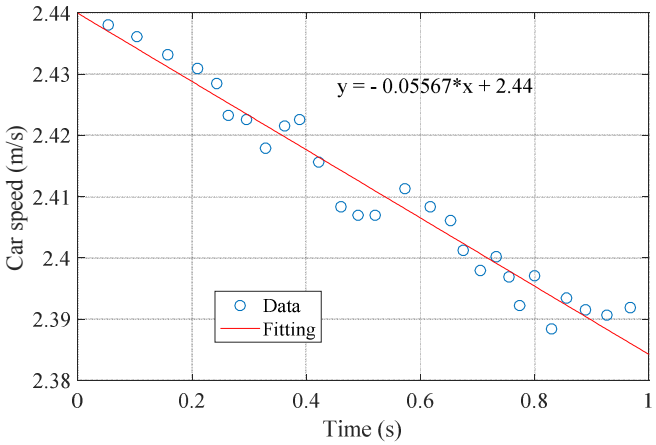

Figure 5.20. Measured speed of car 1 with linear fitting curve

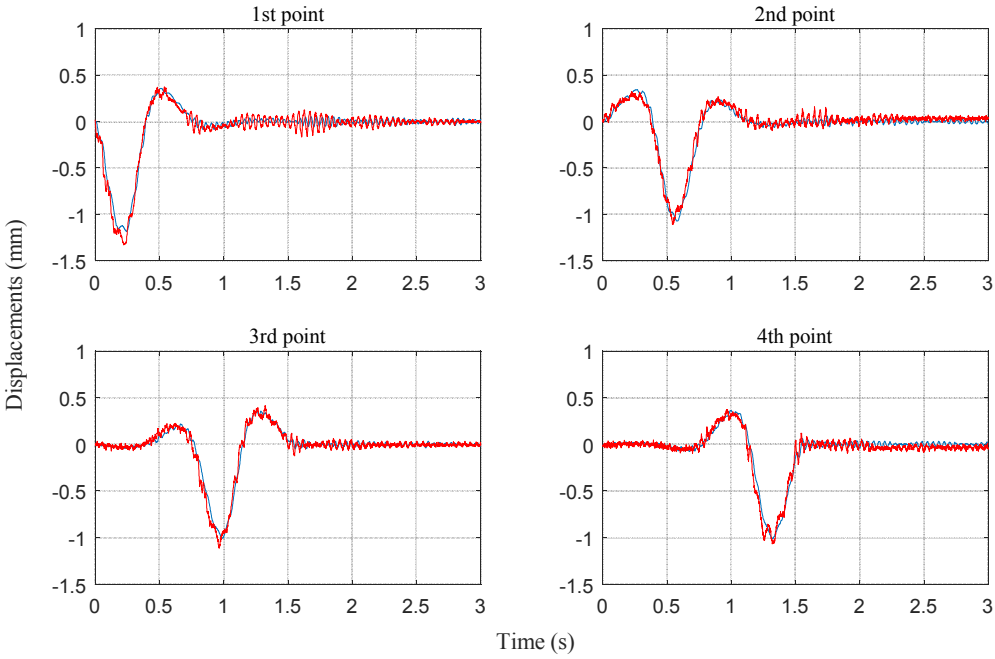

Figure 5.21. Displacements of plate at measured points by simulation considering acceleration of car (blue curve) compared with experimental results (red curve)

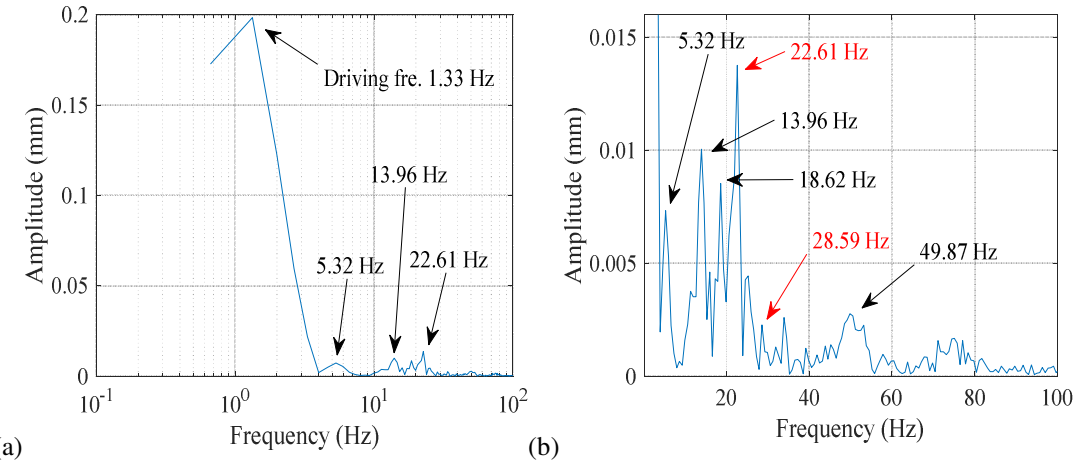

Figure 5.22. Spectrum of measured car-excited structural vibration at 1st measured point at initial car speed of 2.44 m/s: (a) whole amplitude view, (b) part amplitude view

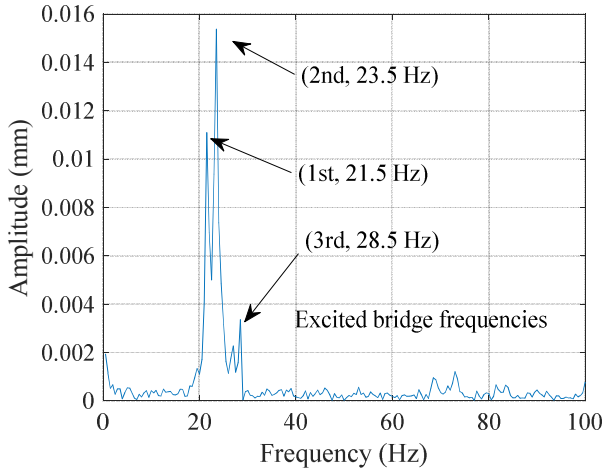

Figure 5.23. Spectrum of measured free vibration of the plate structure at 1st measured point at initial car speed of 2.44 m/s

5.4. Numerical Analysis

To begin with, the moving sprung mass model is compared with the moving car model (rigid-body). The effect of the damping of actuators is discussed next. Then, the influence of the speed ratio on the DAF of the plate structure is studied. The influence of the span ratio between wheelbase and plate span length and the effect of contact stiffness are analysed as well.

5.4.1. Influence of Car Model

To see the difference between the results by treating the car as a 2-DOF rigid body and the results by treating it as a moving sprung mass, a comparison is made below. The mass is the same as that of the car and the stiffness of the contact spring for the moving mass model is taken as the total stiffness between the car body and the plate: $k_{\mathrm{v}} = 4 \times 10^5$ N/m. The deflections of the plate at the four measured points from the two models are shown in Figure 5.24. It can be seen that there is little difference between the results from the two models: the time histories are almost the same, but the magnitude obtained by the moving mass model is slightly bigger. However, if a torsional mode of the plate is excited, a moving rigid-body model needs to be adopted to take account of the influence of this torsional mode. Please note that the above analysis is carried out for test 1 by using 5 structural modes.

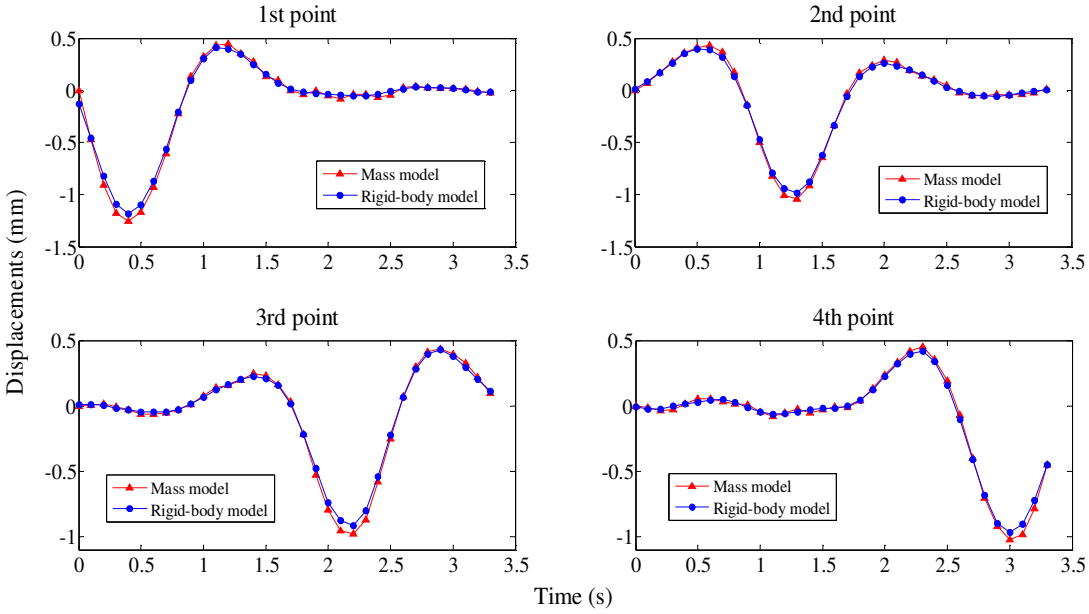

Figure 5.24. Comparison between numerical displacements of the plate at measurement points by moving rigid-body model and those by moving sprung mass model

The displacement of the centre of the car body and the displacement of the mass are shown in Figure 5.25. It can be found in the figure that the displacement of the car body is basically the same as, but slightly smaller than the displacement of the sprung mass.

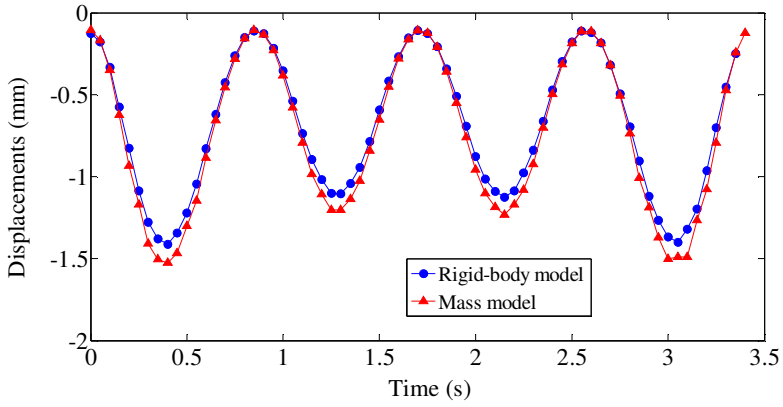

Figure 5.25. Comparison between displacement of rigid-body centre and that of moving mass

5.4.2. Influence of Damping of Actuators

Numerical simulations with different damping levels of shakers have been done to see the influence of shakers' damping on the dynamic response of the system. The

damping of the four actuators is taken to be the same. Three different damping levels of 1.487 Ns/m, 100 Ns/m and 1000 Ns/m are used in simulations. Comparisons between dynamic responses of the car-structure without considering damping of actuators and those with considering damping of actuators can be seen from Figure 5.26 to Figure 5.31. The influence of identified damping of actuators (1.487 Ns/m) on displacements of the plate structure is small. Still no obvious influence can be seen for the displacement of the plate structure when the damping of actuators increases to 100 Ns/m, which is shown in Figure 5.28, but the contact forces are clearly reduced and shown in Figure 5.29. When the damping of actuators increases to 1000 Ns/m, a clear lag for the displacements of the plate structure can be seen in Figure 5.30 and the contact forces decrease further in Figure 5.31. Overall, the point damping attached to the continuous plate structure does not make an obvious influence on the dynamic response of the structure unless the damping is very large.

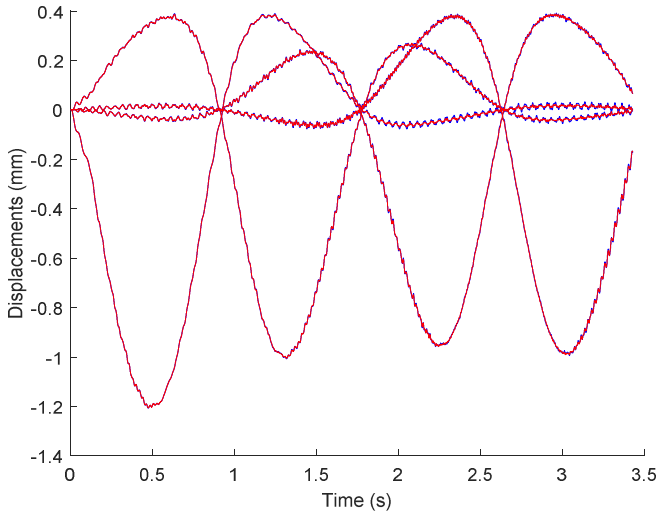

Figure 5.26. The numerical displacements of measured points without considering damping of actuators (blue curve) and with considering damping of actuators of 1.487 Ns/m (red curve)

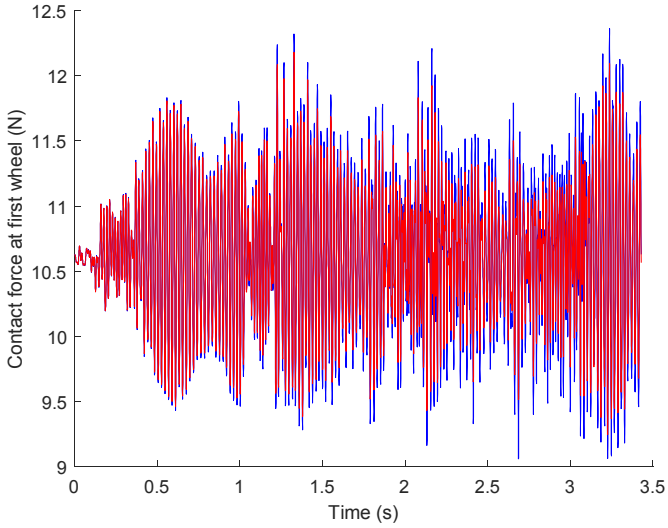

Figure 5.27. Contact force at first wheel without considering damping of actuators (blue curve) and with considering damping of actuators of 1.487 Ns/m (red curve)

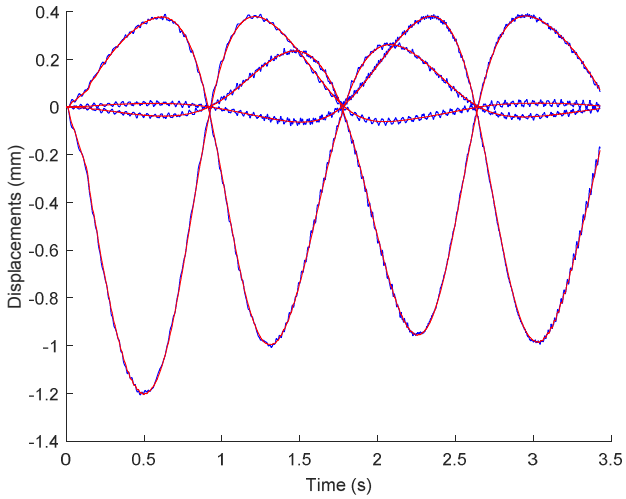

Figure 5.28. The numerical displacements of measured points without considering damping of actuators (blue curve) and with considering damping of actuators of 100 Ns/m (red curve)

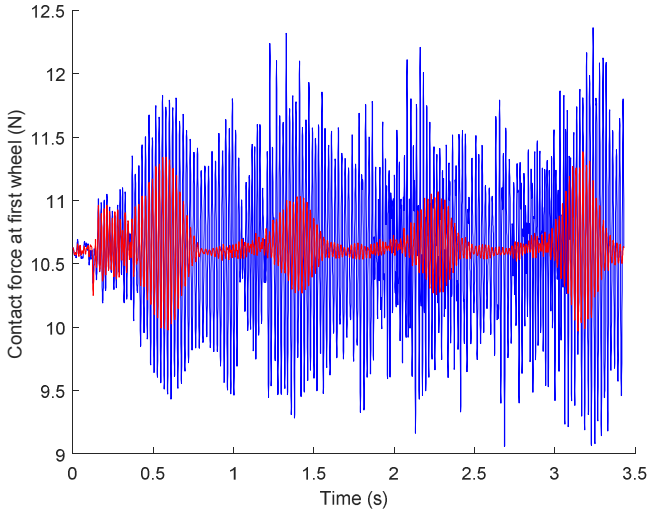

Figure 5.29. Contact force at first wheel without considering damping of actuators (blue curve) and with considering damping of actuators of 100 Ns/m (red curve)

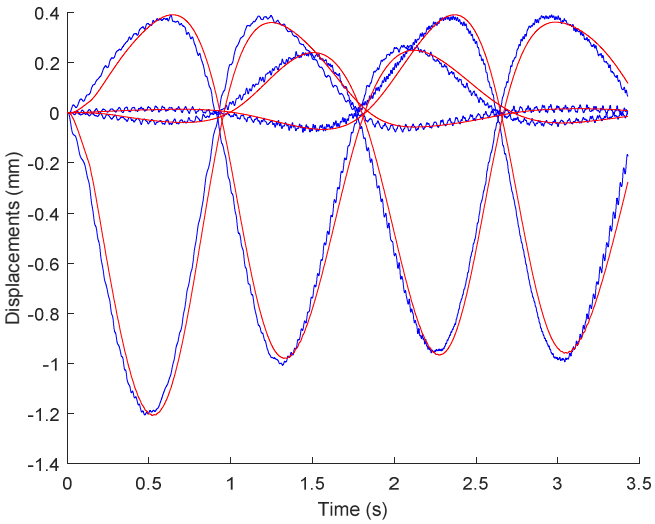

Figure 5.30. The numerical displacements of measured points without considering damping of actuators (blue curve) and with considering damping of actuators of 1000 Ns/m (red curve)

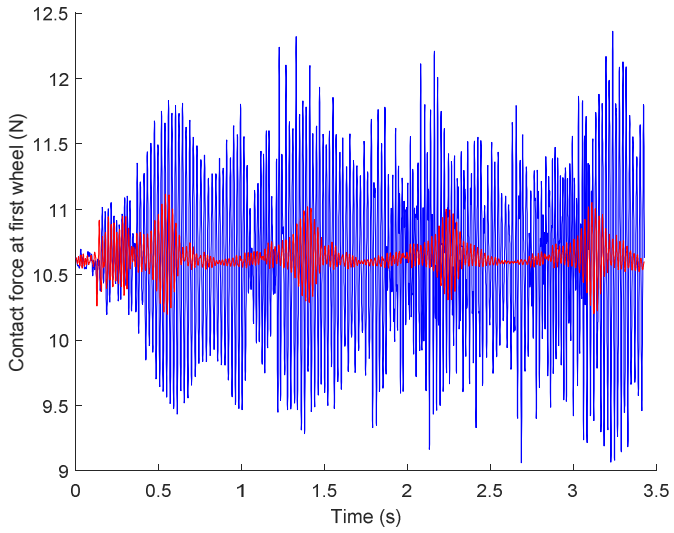

Figure 5.31. Contact force at first wheel without considering damping of actuators (blue curve) and with considering damping of actuators of 1000 Ns/m (red curve)

5.4.3. Influence of Car Speed

Figure 5.32 shows the influence of car speed on the dynamic response of the four mid-span points (not the same as the four measured points) of the structure. The critical speed of the structure is $v_{\mathrm{cr}} = 38.236$ m/s. The mass ratio between the car mass and the structure mass is 0.41 for test 1 to test 3.

The reference static deflections are obtained in ABAQUS by using four concentrated forces at the mid-spans of the plate to model the four axle loadings of the car. DAF is defined as the ratio between the maximum dynamic response of the mid-span point of one span and its static deflection with the car on the mid-span of this span. It can be seen from the figure that the maximum dynamic responses of the mid-span points basically increase with the ratio of the car speed to the critical speed in the range of 0.015 to 0.15. A small local peak occurs at the ratio of 0.075. The DAFs of the mid-span points in spans 2-4 fluctuate very much when the speed ratio is greater than 0.135. This is probably because that the influence of vibration of front spans on rear spans becomes strong under high car speeds. It is found that negative contact forces always occur when car speed ratio is greater than 0.2, which means that contact loss happens when the speed ratio is greater than 0.2. The dynamic responses with car speed ratio greater than 0.2 are not presented in this thesis. Fryba (Frýba, 1999) showed that the maximum dynamic response of a simply supported beam under a

moving constant force increases firstly and then decreases with the speed and the peak response happens at the speed ratio in the range of 0.5 to 0.7 for different damping of the beam. What should be paid attention to is that the car speed that leads to loss of contact changes with car mass as shown in Figure 5.33. For a heavier car, a lower car speed for loss of contact is found.

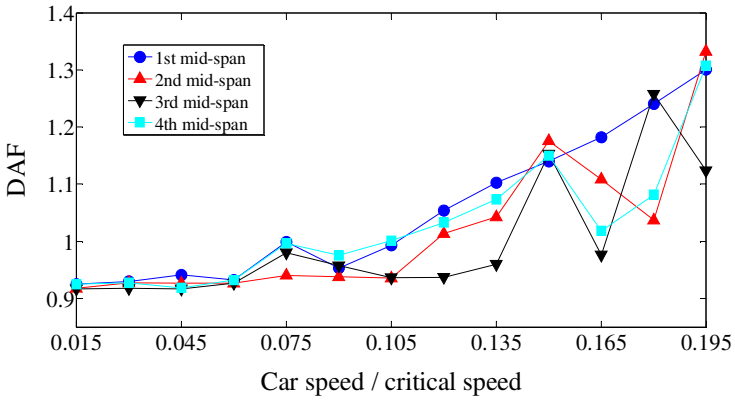

Figure 5.32. DAF of mid-span points against car speed ratio for mass ratio of 0.41

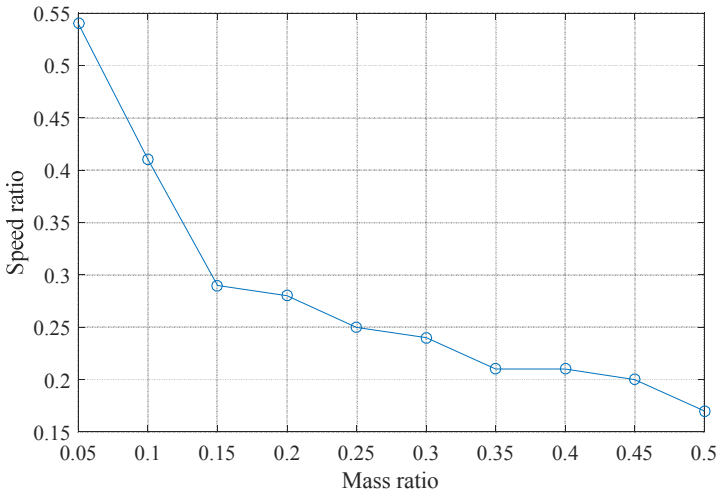

Figure 5.33. The speed ratio from which contact loss begins to happen

Figure 5.34 shows the dynamic effect changing with mass ratio and speed ratio. It can be seen from the figure that when the speed ratio is small, DAF basically does not vary with mass ratio. The dynamic effect fluctuates with mass ratio when the speed ratio is big. Basically, the dynamic effect is strongest at maximum mass ratio of 0.35 and maximum speed ratio of 0.2 for the experimental rig in the simulated range of mass ratio and speed ratio.

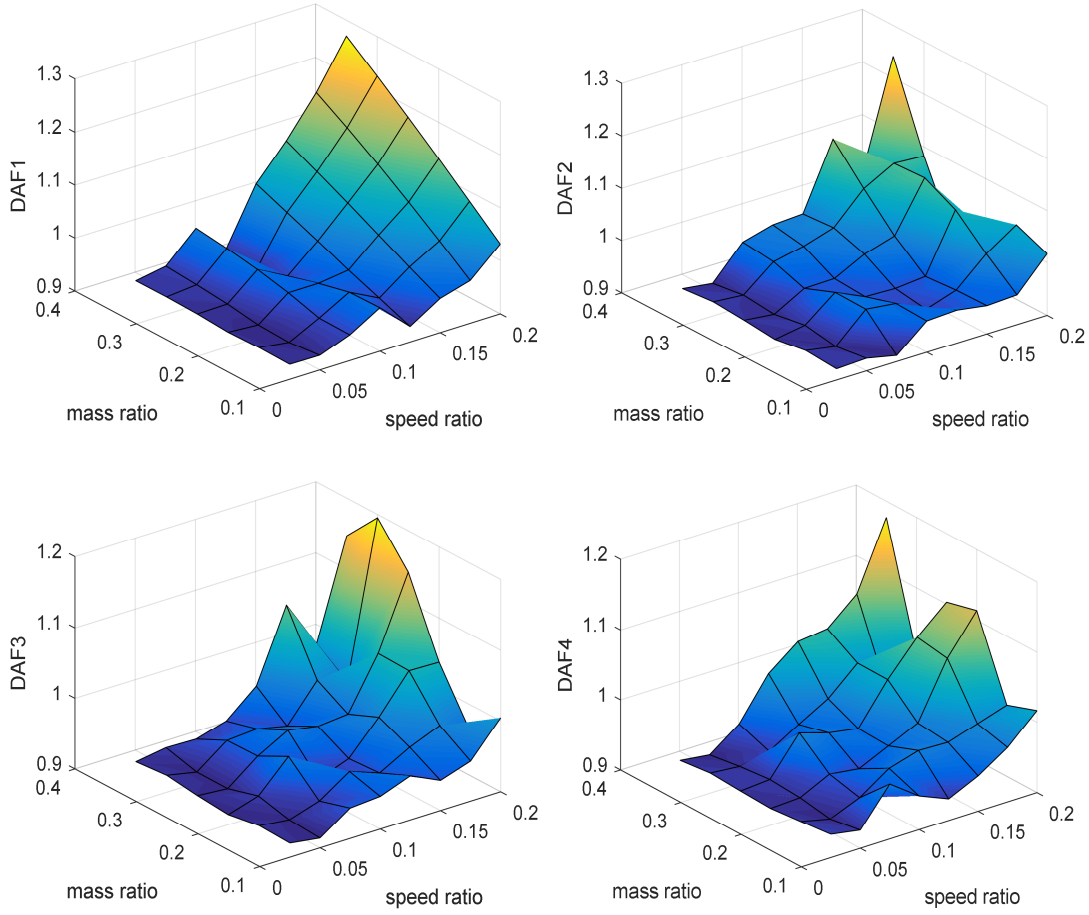

Figure 5.34. DAFs versus mass ratio and speed ratio (DAF*i* representing DAF at *i*th mid-span, *i*=1, 2, 3, 4)

5.4.4. Influence of Car mass

To study the influence of car mass on the dynamic response of the plate structure, simulations are carried out for different mass ratios and speed ratios by using a moving mass model to remove the effect of the complicated car model. It can be seen from Figure 5.35 that when the car speed is low, DAF does not vary much with the mass ratio. The dynamic effect fluctuates with the mass ratio when the speed of mass is high. Basically, the dynamic effect, represented by DAFs (*s*=1, 2, 3 ,4, which refers to the *s*th span), increases broadly with the speed ratio with fluctuations, which is in a similar trend to the results of a single-span beam excited by a moving oscillator by Frýba (1999). DAF1 has a simpler trend compared with those of the other DAFs. It is because the car moves on the first span firstly and there is no influence of other spans on this span.

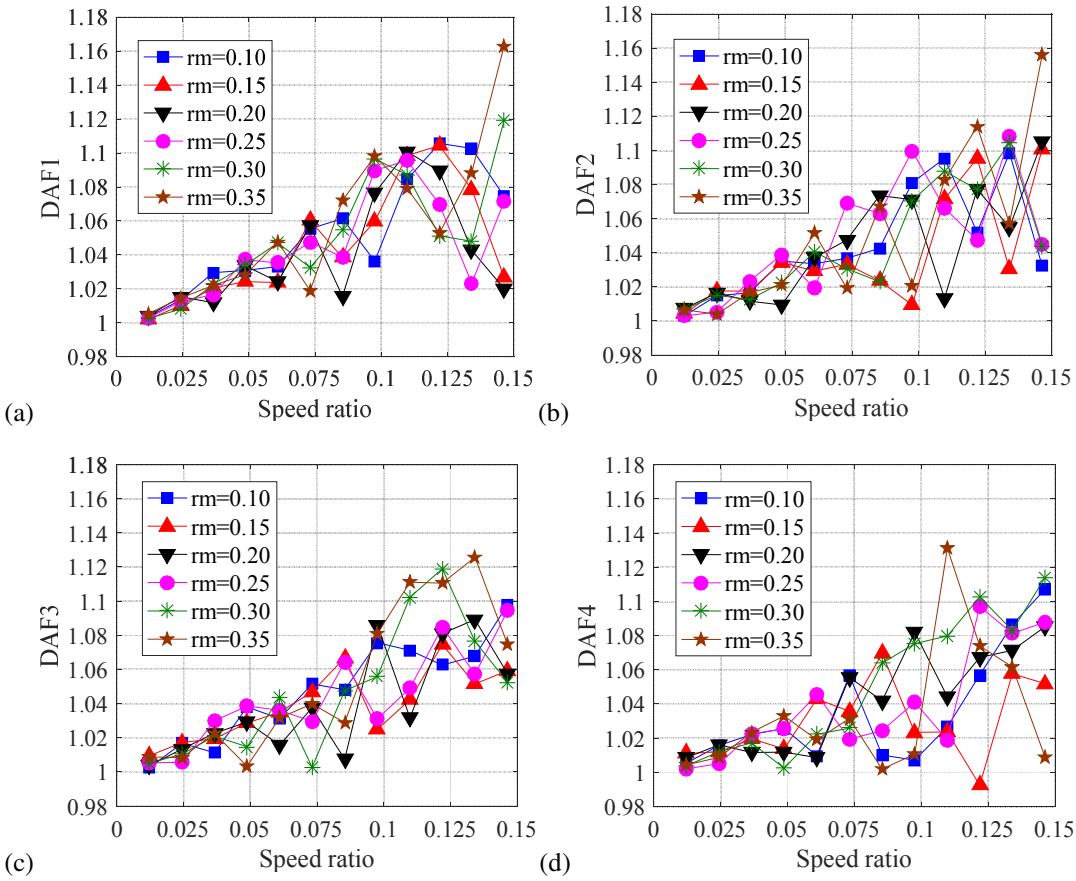

Figure 5.35. DAF versus speed ratio for different mass ratios by moving-mass model ('rm' representing mass ratio): (a) DAF at 1st mid-span, (b) DAF at 2nd mid-span, (c) DAF at 3rd mid-span, (d) DAF at 4th mid-span.

5.4.5. Influence of Span Ratio

The relationship between the displacement response of the structure and the span ratio of wheelbase to plate span length for the mass ratio of 0.41 and the speed ratio of 0.027 is shown in Figure 5.36. The span ratio is changed by changing the wheelbase only and keeping the span length of the structure to be the same. Increasing wheelbase can make the dynamic response of the structure decrease in the range of span ratio between 0 and 0.8, and increase to a steady state afterwards. That is to say that a shorter car can cause a greater structural dynamic response, which is verified by the previous fact that the displacements of the structure obtained from the moving mass model are bigger than that from the moving rigid-body model. It is interesting to find that the dynamic response of the first span reaches a steady state with shorter wheelbase than those of other spans as shown in the figure. The

minimum deflection of the first mid-span occurs at the span ratio of 0.7, whereas the minimum deflections of the other mid-spans take place at the span ratio of 0.8. It was found that the vibration of a simply supported beam excited by a series of moving axle loads is minimum at the span ratio 0.67, to which the first span has the similar trend. This phenomenon is largely due to that the cancellation condition for the simply supported beam is met at this span ratio (Yang et al., 2004).

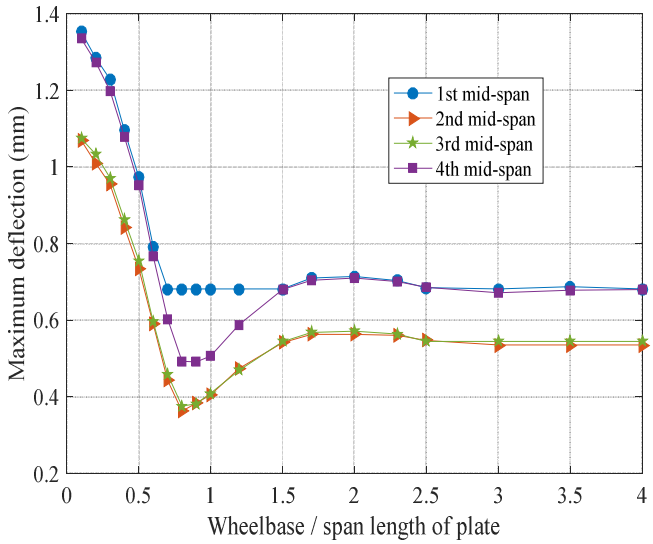

Figure 5.36. Maximum deflection of mid-span points against span ratio at speed ratio of 0.027 and mass ratios of 0.41

The dynamic responses for several wheelbases are shown in Figure 5.37. It can be seen that initially when the span ratio is 0.3 the dynamic response of one mid-span point only has one downward peak, but has two downward peaks for the span ratio of 0.8 or higher and the time difference between the two peaks increases with wheelbase. The two sets of wheel loads are like two separate loads at a certain distance apart, which may cause two peaks in the dynamic response of the structure. When the wheelbase increases, it seems that the distance between two mass loads increases. In consequence, the time interval between the two peaks becomes bigger. It is noticed that the span ratio for test 1 to test 3 is 0.23.

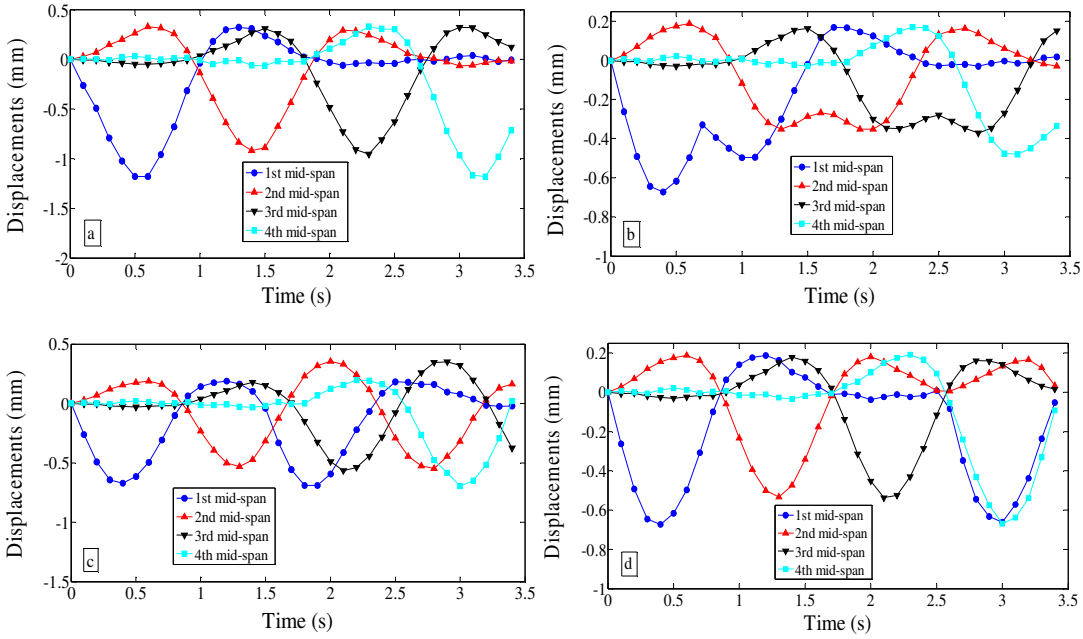

Figure 5.37. Dynamic responses of mid-span points for span ratios of (a) 0.3, (b) 0.8, (c) 1.7, (d) 3.0

5.4.6. Influence of Contact Spring Stiffness

The influence of contact spring stiffness on the dynamic response of the structure can be seen in Figure 5.38 (mass ratio of 0.41 and span ratio of 0.23). As can be seen in the figure, the contact spring stiffness does not influence the dynamic response of the structure much under car speed of a 1.05 m/s (speed ratio 0.027), but the influence becomes stronger at higher car speeds. It is interesting to find that the magnitude of the contact force between the first car wheel and the plate structure does not differ much with contact spring stiffness at v=1.05 m/s as shown in Figure 5.39. This is because when the car speed is low, the inertial force in the contact force is small and the main contribution to the contact force is the dead-weight of the car which is constant. However, higher frequencies of the contact force occur when the contact spring stiffness increases at the car speed of v=1.05 m/s, as found in Figure 5.40. This is also true for the car speed of v=5.74 m/s (speed ratio 0.15) shown in Figure 5.42. On the other hand, the magnitude of structural response differs significantly with changing contact spring stiffness at v=5.74 m/s as shown in Figure 5.38 and the magnitude of the contact force basically increases with contact spring stiffness at v=5.74 m/s as shown in Figure 5.41. Figure 5.43 and Figure 5.44 show that the dynamic response of the car body decreases much in magnitude with contact spring

stiffness for both car speeds (1.05 m/s and 5.74 m/s). It can be seen from Figure 5.45 that the car basically oscillates slightly faster with larger contact spring stiffness when the car moves at 5.74 m/s. However, this is not true when v=1.05 m/s. It can be estimated from Figure 5.43 that the car almost oscillates at the same frequency with different contact spring stiffness. Please note that the above phenomenon found for the contact force between the first car wheel and the rail is also true for the contact forces between other car wheels and the rails, although they are not presented in this thesis.

When the car speed is 1.05 m/s, the driving frequency of the moving car (different from the natural frequency of the car) is related to the car speed and equals $f_{\mathrm{v}} = \frac{v}{l} = \frac{1.05}{0.9} = 1.167$ Hz. This frequency and the natural frequency of the car in the vertical bouncing mode presented in Table 5.3 are the source of the frequencies of the contact force, which can be found in Figure 5.40. When the car speed is 5.74 m/s, the driving frequency of the moving car related to the car speed becomes $f_{\mathrm{v}} = \frac{v}{l} = 6.373$ Hz. This frequency and the natural frequency of the car shown in Table 5.3 are the source of the frequencies of the contact force and can be found in Figure 5.42. The higher frequencies of the contact force look like integer multiples of f_{v}, which seem quite obvious in Figure 5.42 (c).

Table 5.3. Natural frequencies (Hz) of the car in the vertical bouncing mode and rotation mode

Spring stiffness (N/m)	10^2	10^3	10^4	10^5
Frequency in bouncing	1.529	4.835	15.288	48.345
Frequency in rotation	2.648	8.374	26.479	83.734

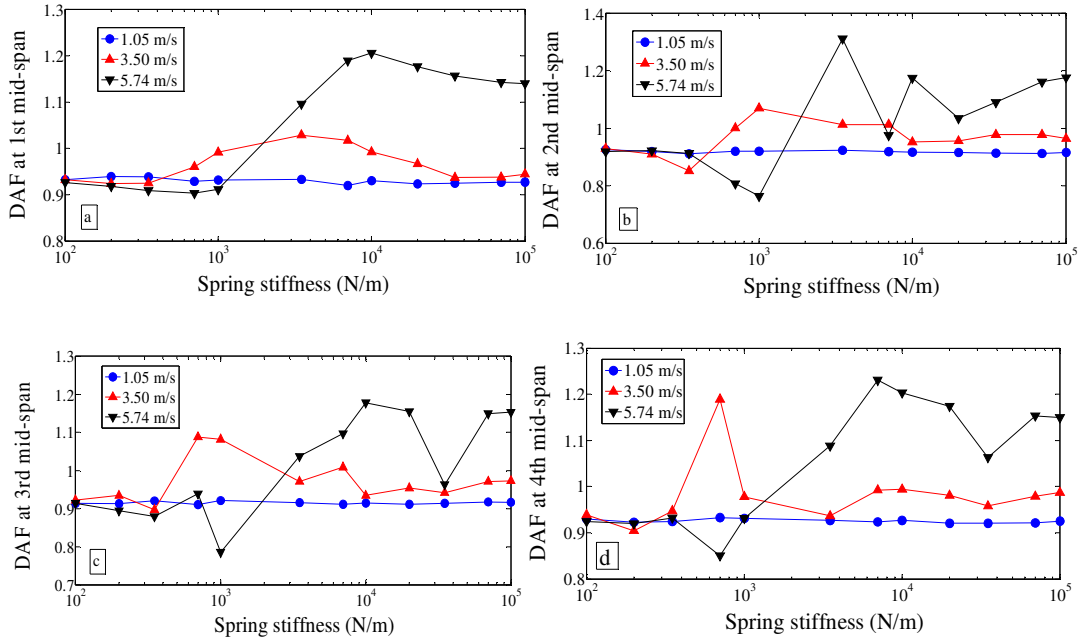

Figure 5.38. The influence of contact stiffness of one spring on DAF at (a) 1st, (b) 2nd, (c) 3rd, (d) 4th mid-span points under different car speeds

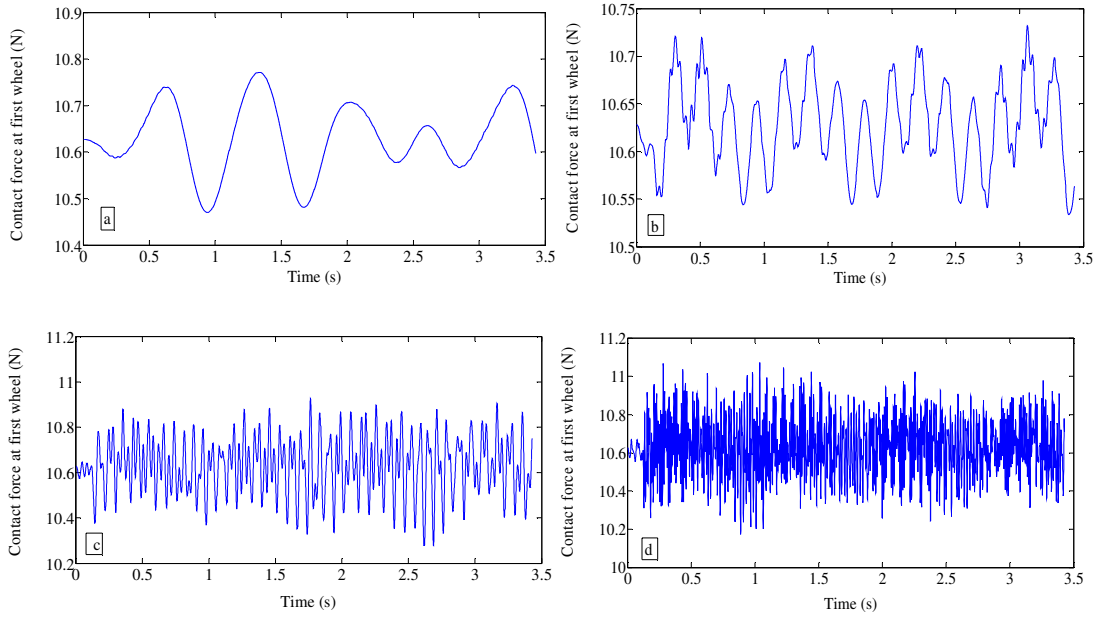

Figure 5.39. Contact force at first wheel for contact stiffness of one spring (a) 1.0×10^2, (b) 1.0×10^3, (c) 1.0×10^4, (d) 1.0×10^5 N/m at car speed of 1.05 m/s

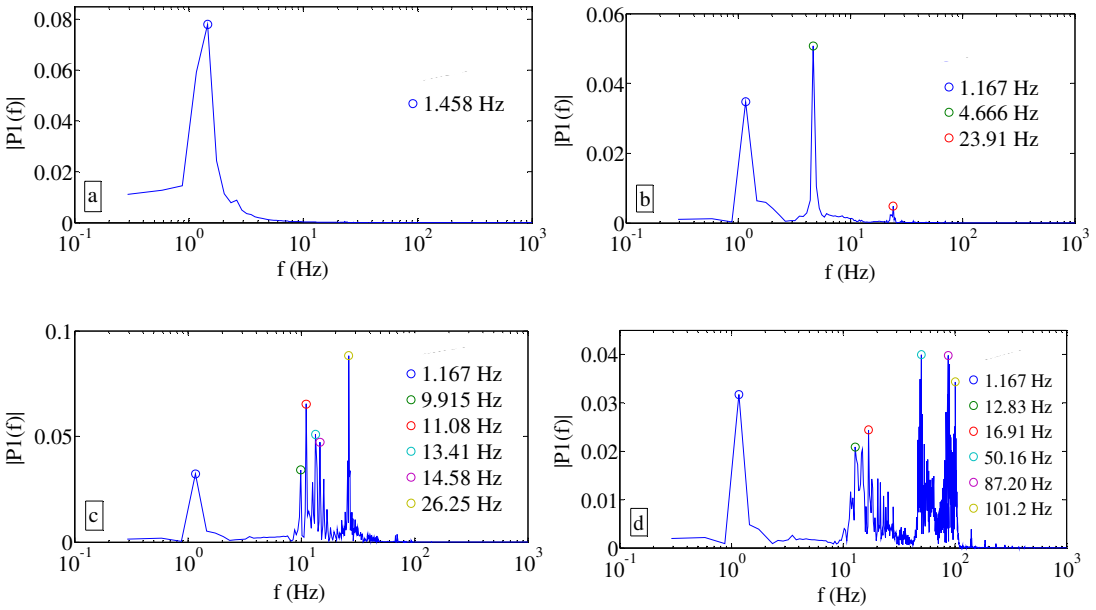

Figure 5.40. Single-sided amplitude spectrum of contact force at first wheel for contact stiffness of one spring (a) 1.0×10^2, (b) 1.0×10^3, (c) 1.0×10^4, (d) 1.0×10^5 N/m at car speed of 1.05 m/s

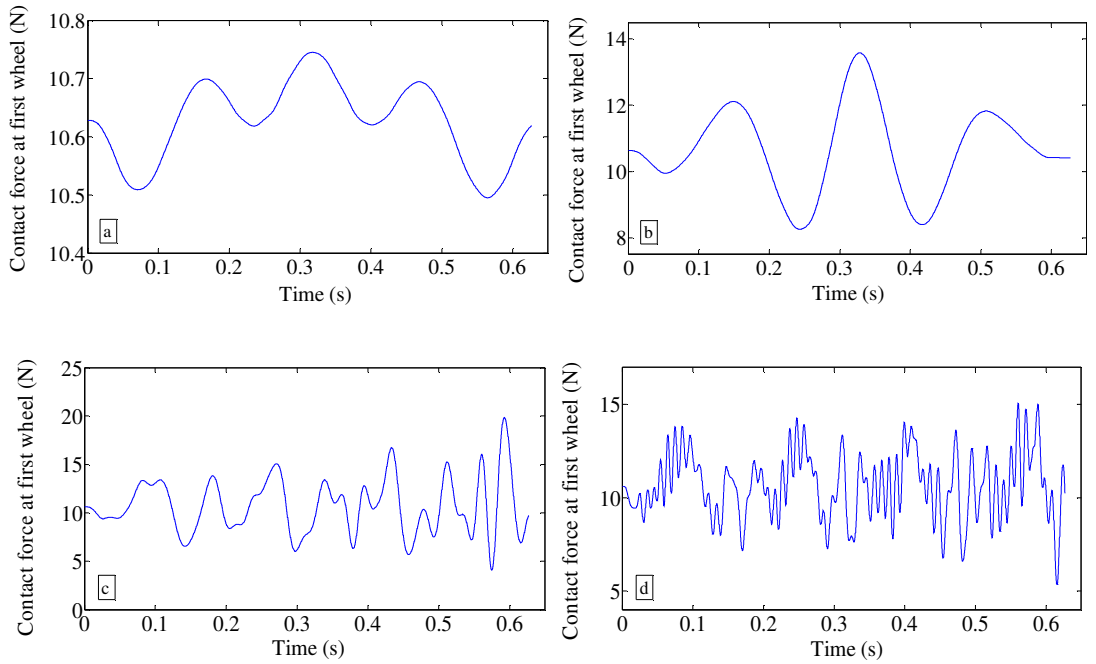

Figure 5.41. Contact force at first wheel for contact stiffness of one spring (a) 1.0×10^2, (b) 1.0×10^3, (c) 1.0×10^4, (d) 1.0×10^5 N/m at car speed of 5.74 m/s

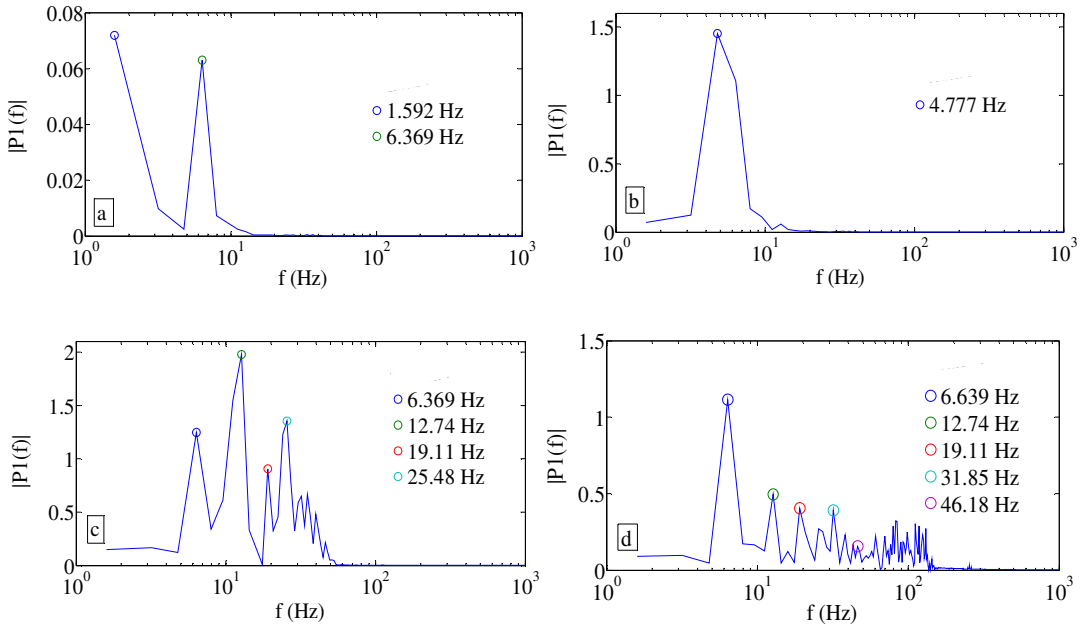

Figure 5.42. Single-sided amplitude spectrum of contact force at first wheel for contact stiffness of one spring (a) 1.0×10^2, (b) 1.0×10^3, (c) 1.0×10^4, (d) 1.0×10^5 N/m at car speed of 5.74 m/s

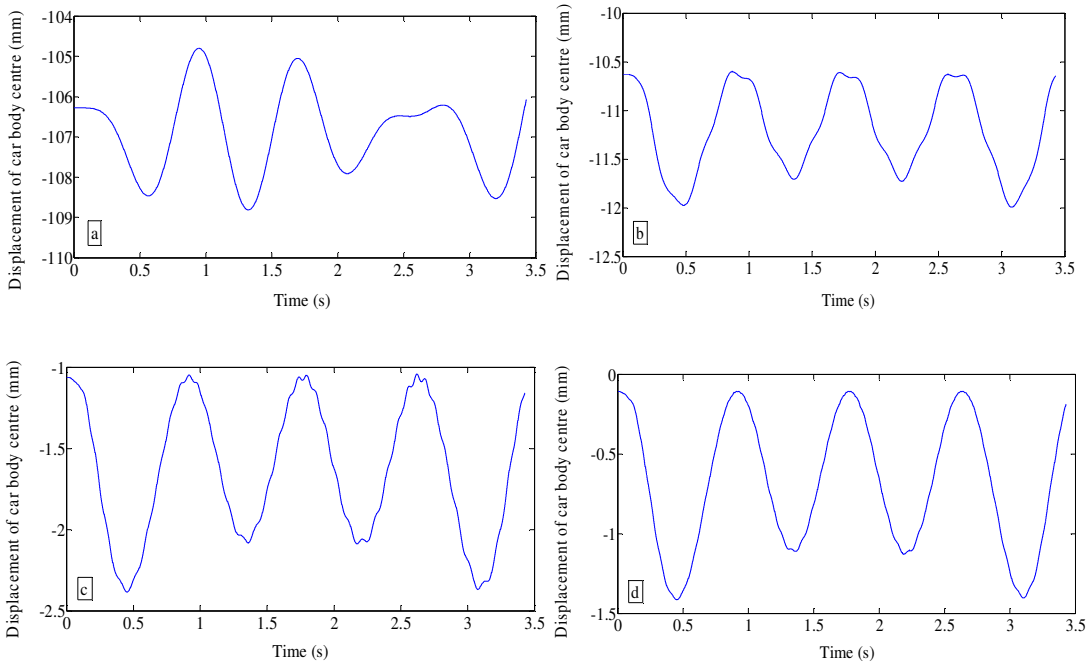

Figure 5.43. Displacement of car body centre for contact stiffness of one spring (a) 1.0×10^2, (b) 1.0×10^3, (c) 1.0×10^4, (d) 1.0×10^5 N/m with car speed of 1.05 m/s

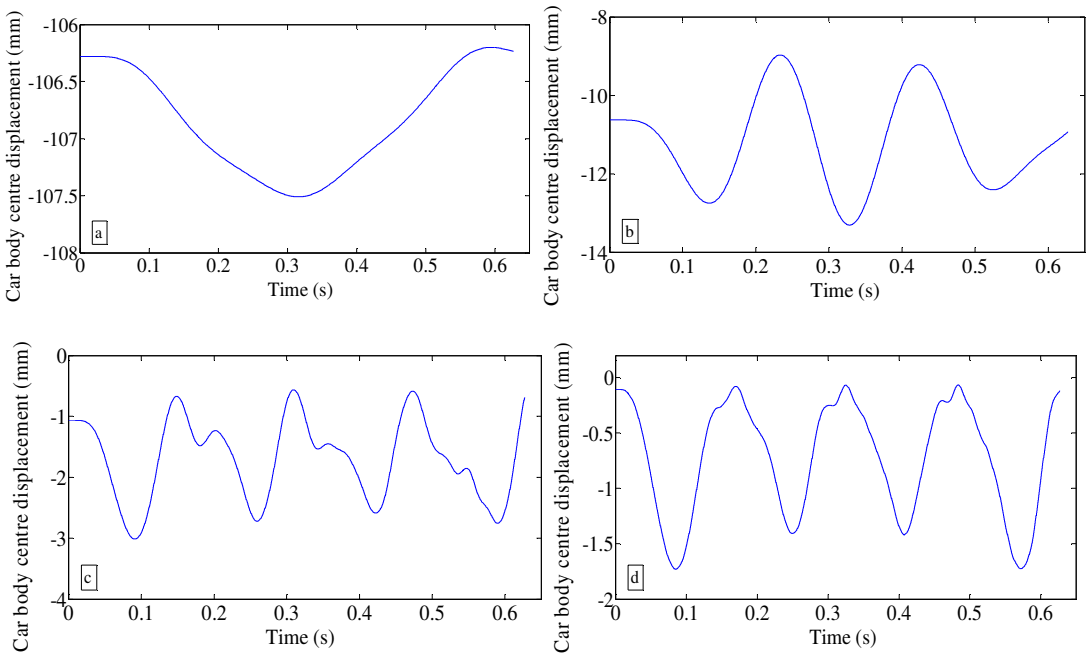

Figure 5.44. Displacements of car body centre for contact stiffness of one spring (a) 1.0×10^2, (b) 1.0×10^3, (c) 1.0×10^4, (d) 1.0×10^5 N/m at car speed of 5.74 m/s

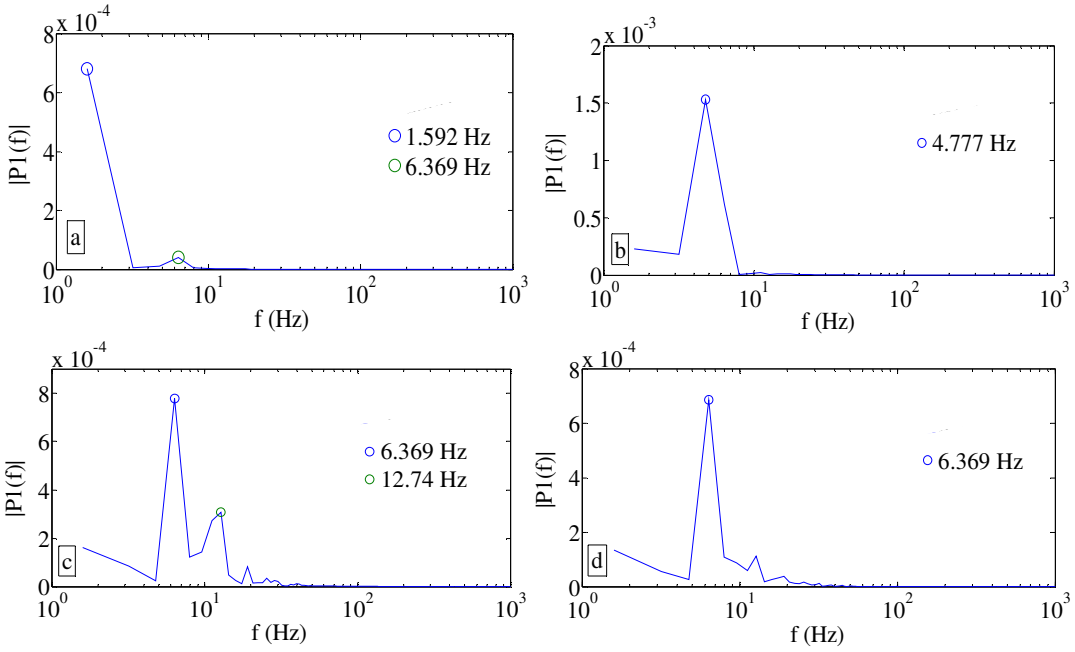

Figure 5.45. Single-sided amplitude spectrum of displacements of car body centre for contact spring of one spring (a) 1.0×10^2, (b) 1.0×10^3, (c) 1.0×10^4, (d) 1.0×10^5 N/m at car speed of 5.74 m/s

5.5. Concluding Remarks

Moving load problems are difficult to analyse and no commercial general-purpose structural analysis software packages can deal with them efficiently. A general and easy way to solve moving load problems is presented in this chapter by using ABAQUS and MATLAB. FE models of complicated structures are built in ABAQUS and their numerical modes are obtained and imported into MATLAB codes where the MS method and an iterative method are implemented. The moving sprung mass model is adopted to verify the proposed approach. The numerical results show that this approach works well with high efficiency.

A four-span continuous plate with two rails on top and four extra actuator supports excited by a moving model car is studied numerically and experimentally. The car is treated as a rigid body with two DOFs in contact with the rails via four springs. An FE model of the plate with rails is built in ABAQUS to obtain its numerical modes and the parameters used in the FE model of the structure are identified based on measured frequencies. It is found that the torsional modes of the structure do not have much influence on the structural dynamic response within the speed range studied. The numerical prediction of structural displacements at four measured points of the structure agrees well with the experimental measurements. Further numerical studies reveal some interesting results:

(1) It is found from measurements that the car speeds decrease with time at almost a constant deceleration of 0.04 ~ 0.08 $\mathrm{m/s^2}$. An obvious time delay is found between numerical results by using an average car velocity and experimental results and this car deceleration could produce non-negligible influence on the dynamic response of the plate structure at certain car speeds. These findings indicate that the deceleration of the car should be included in the theoretical model of the car-plate system.

(2) Spectrum analysis of the experimental results shows that a higher speed car below 2.5 m/s can excite the plate structure into the vibration with larger amplitudes at a wide range of frequencies, which indicates that the car-bridge interaction becomes stronger at a higher car speed. The wide range frequencies of the car-bridge system are due to the movement of the car which makes the system time-varying.

(3) The structural response and car displacement from the moving rigid-body model are slightly smaller than those from the moving sprung mass model.

(4) Damping of actuators does not make an obvious influence on the dynamic response of the plate structure and the contact force unless it is extremely high.

(5) Increasing car speed can increase structural dynamic response in a certain speed range and wheel/rail contact loss occurs at a lower car speed for a heavier car.

(6) The mass ratio has a significant influence on the structural response when the speed ratio is large.

(6) A longer car decreases structural dynamic displacement when the span ratio of the wheelbase to the span length is less than 0.8, and increases the structural displacement slightly to a stable value when the span ratio is bigger.

(7) When the car speed is low, the variation of contact spring stiffness does not make much difference on structural response, but at a high car speed, the influence becomes strong. Additionally, at high car speeds larger contact spring stiffness basically leads to bigger contact forces between the car wheels and the rails and slightly quicker oscillation of the car. Regardless of the car speed, the frequencies of the contact forces basically increase but the dynamic response of the moving car body decreases, with contact spring stiffness.

Noisy and local oscillations are found in displacement measurements. The noise may come from the measurement by laser displacement transducers and ambient vibration of the plate structure. Some local oscillations are suspected of coming from the lateral vibration of moving cars, which will be investigated in the future. Although only the dynamic response of the plate is measured in this chapter, the vibration of the moving cars is another interesting topic worth to be studied experimentally in the future.

6. Vibration of a Four-Span Continuous Plate Structure Subjected to Two Moving Cars

The free vibration of a bridge with high amplitude is very helpful for identifying more accurate modal properties of the bridge (Qin et al., 2014). Such high amplitude may be caused by the passage of a moving train or a heavy truck. The theoretical and experimental studies of two cars moving on a four-span continuous plate structure are conducted in this chapter to examine the influence of excitation scenario on the identified bridge frequencies from the free vibration of the bridge. Two cars are set to move on the plate structure separately with different time gaps or move together through a connector at various speeds. Predicted results for the car-plate vibration are compared with the experimental results. The bridge frequencies under moving cars and without cars (free vibration) are obtained by transforming measured structural displacements from the time domain to the frequency domain. It should be mentioned that laboratory experiments for two cars moving on a continuous structure with such a complexity as that in this thesis have not been reported in the literature. The nearest work is an experiment of 3 connected model cars travelling on a single-span simply-supported beam (Kim et al., 2016).

6.1. Experimental Setup

The plate structure remains basically the same as that in Figure 5.3 except that the location of actuators is slightly different. Figure 6.1 gives the schematic of the plate structure. Two cars are optionally connected by an aluminium stick which lets two cars travel at the same speed in time and allows the relative rotation between the two cars. The second span of the plate structure and two connected cars are shown in Figure 6.2. The travelling speeds of the moving cars in time are measured by using the Polytec Laser Vibrometer (PSV 500) based on the Doppler-effect as well.

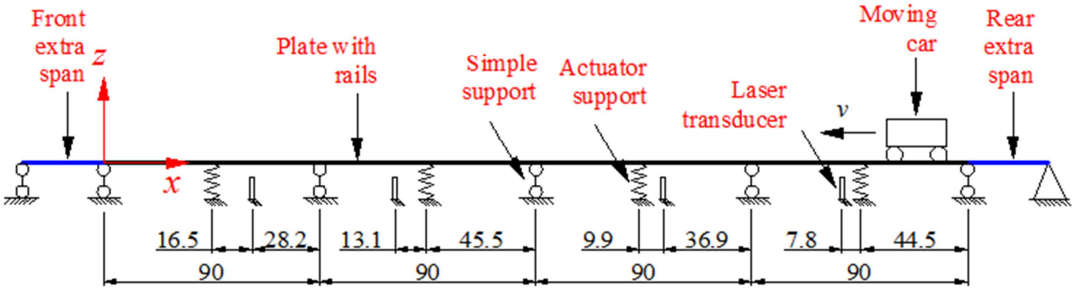

Figure 6.1. Schematic of the whole experimental setup from lateral view (unit: cm)

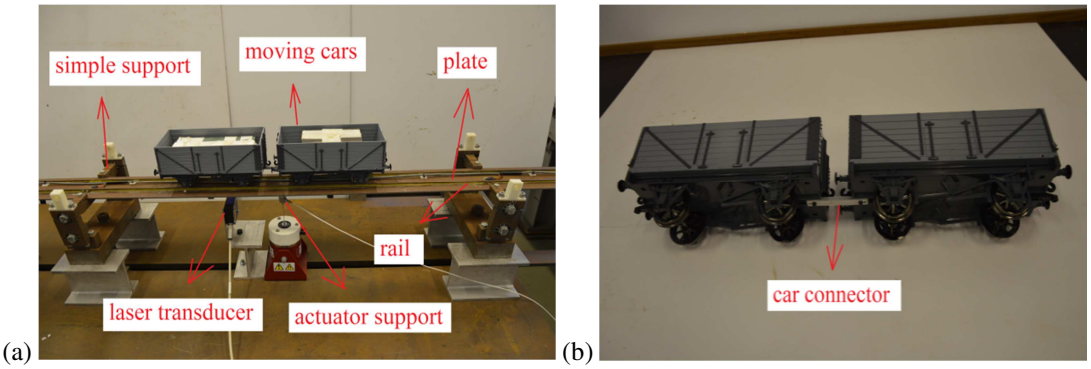

Figure 6.2. Pictures of experimental setup: (a) the second span of the four-span plate structure; (b) two connected cars

6.2. Theoretical Model of Two Cars-Bridge System

Similarly to the theoretical model of the one car-bridge model in chapter 5, an FE model of the plate structure is built in ABAQUS to obtain the numerical frequencies and mode shapes of the structure. Shell elements (S4R) and 3D beam elements (B31) are used to model the plate and the rails, respectively. Point mass and spring elements are used to model the additional masses and stiffness provided by the actuators. The material properties of the plate and the rails are identified from measured natural frequencies by modal testing and the stiffness of an actuator is measured by tension and compression tests using an INSTRON machine (Yang et al., 2017). The damping coefficients of actuators are assumed to be the same and identified from a free vibration test of one actuator to be around 1.487 Ns/m. The detailed identification of the damping of the actuator was given in section 5.2.2. The beam elements are tied to the shell elements. The offset between connected beam and shell elements is often taken as a model updating parameter to validate the model by

comparing theoretical frequencies with measured counterparts (Mottershead et al., 2011). In this chapter, the offset ratio defined in section 5.2.5 is updated. It is found that when the offset ratio is 1.885, the theoretical frequencies of the plate structure are closest to the measured counterparts. Table 6.1 shows the differences between the two sets of frequencies for the first eight modes of the plate structure.

Table 6.1 Comparison between theoretical frequencies and measured frequencies

Mode	1	2	3	4	5	6	7	8
Measured Fre. (Hz)	21.781	23.676	27.995	33.386	68.573	72.964	81.002	89.935
Theoretical Fre. (Hz)	20.218	22.465	28.069	34.919	65.921	71.591	83.429	96.343
Difference (%)	-7.2	-5.1	0.3	4.6	-3.9	-1.9	3.0	7.1

Applying the MS method to the equation of motion of the plate structure leads to (Baeza and Ouyang, 2008)

$$\ddot{\mathbf{q}}(t) + \text{diag}[\omega_i^2]\mathbf{q}(t) = -\sum_{j=1}^{8} \boldsymbol{\varphi}(x_j, y_j) f_{cj}(t) - \sum_{k=1}^{4} c_k \boldsymbol{\varphi}(x_k, y_k) \boldsymbol{\varphi}^{\mathrm{T}}(x_k, y_k) \dot{\mathbf{q}}(t) \quad (6.1)$$

where ω_i $(i = 1, 2 \ldots n)$ is the ith natural frequency of the plate structure (which includes the mass and stiffness of all actuators), with n being the number of modes used; x_j and y_j the coordinates of the jth wheel of the cars, x_k and y_k the coordinates of the kth actuator; $\boldsymbol{\varphi}(x, y)$ is the vector of the analytical modal functions of the plate structure, $\mathbf{q}$ the vector of the corresponding modal coordinates; f_{cj} the contact force at the jth wheel, c_k the viscous damping coefficient of the kth actuator; a dot over w denotes a derivative with respect to t. Please note that $\boldsymbol{\varphi}(x, y)$ is approximated by the products of the element shape functions and the numerical modes of the plate structure which are obtained from the modal analysis of its FE model in ABAQUS.

Each car is treated as a rigid-body with two DOFs and only heave q_{v} and pitch θ motions are considered, as shown in Figure 6.3.

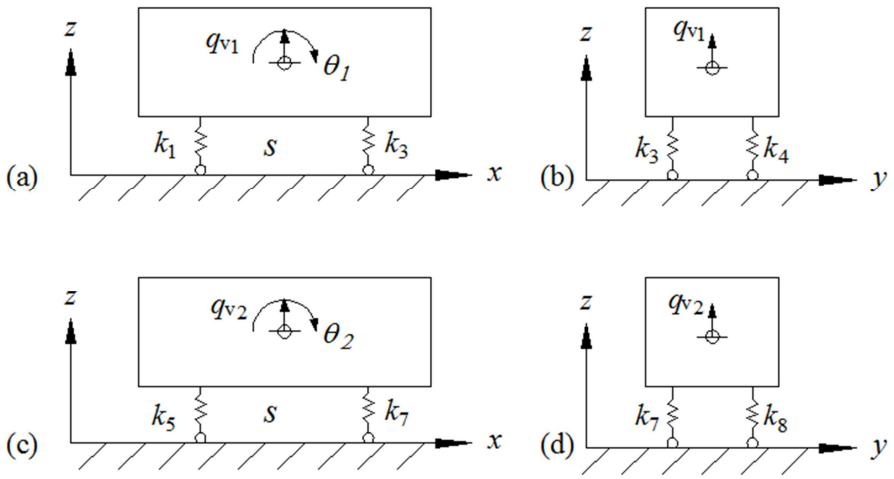

Figure 6.3. Theoretical model of two cars: (a) elevation view of the first car, (b) cross-section view of the first car, (c) elevation view of the second car, (d) cross-section view of the second car

The contact force $f_{cj}(t)$ between the jth wheel of the cars and the rails can be expressed as

$$f_{cj}(t) = k_j[-q_{v1}(t) + w(x_j, y_j, t) - \frac{s}{2}\theta_1(t)], j = 1, 2 \quad (6.2)$$

$$f_{cj}(t) = k_j[-q_{v1}(t) + w(x_j, y_j, t) + \frac{s}{2}\theta_1(t)], j = 3, 4 \quad (6.3)$$

$$f_{cj}(t) = k_j[-q_{v2}(t) + w(x_j, y_j, t) - \frac{s}{2}\theta_2(t)], j = 5, 6 \quad (6.4)$$

$$f_{cj}(t) = k_j[-q_{v2}(t) + w(x_j, y_j, t) + \frac{s}{2}\theta_2(t)], j = 7, 8 \quad (6.5)$$

where q_{v1} and q_{v2} are the vertical displacements of the first car and the second car, respectively and θ_1 and θ_2 are the rotations of the first car and second car, respectively, as shown in Figure 6.3. $w(x_j, y_j, t)$ is the displacement of the plate structure at the contact point between the ith wheel and the rails (x_j and y_j are the coordinates of the jth wheel).

The equation of motion of the first car can be described as

$$m_{v1}\ddot{q}_{v1} = -m_{v1}g - k_1[q_{v1} + \frac{s}{2}\theta_1 - w(x_1, y_1, t)] - k_2[q_{v1} + \frac{s}{2}\theta_1 - w(x_2, y_2, t)] -$$

$$k_3[q_{v1} - \frac{s}{2}\theta_1 - w(x_3, y_3, t)] - k_4[q_{v1} - \frac{s}{2}\theta_1 - w(x_4, y_4, t)] \quad (6.6)$$

$$I_{v1}\ddot{\theta}_1 = -k_1\left[q_{v1} + \frac{s}{2}\theta_1 - w(x_1, y_1, t)\right]\frac{s}{2} - k_2\left[q_{v1} + \frac{s}{2}\theta_1 - w(x_2, y_2, t)\right]\frac{s}{2} +$$

$$k_3\left[q_{v1} - \frac{s}{2}\theta_1 - w(x_3, y_3, t)\right]\frac{s}{2} + k_4\left[q_{v1} - \frac{s}{2}\theta_1 - w(x_4, y_4, t)\right]\frac{s}{2} \quad (6.7)$$

The equation of motion of the second car is similar as Eq. (6.6) and Eq. (6.7), but q_{v1}, θ_1, I_{v1} and k_1 to k_4 are changed to q_{v2}, θ_2, I_{v2} and k_5 to k_8, respectively. If the car connector is used to connect the two cars, the following relationships for the two cars can be obtained

$$x_5 = x_3 + \Delta s, \;\; x_6 = x_4 + \Delta s \quad (6.8)$$

where x_3 and x_4 are the coordinates of the rear wheels of the first car in x direction; x_5 and x_6 are the coordinates of the front wheels of the second car and Δs is the distance between the the rear wheel of the first car and the front wheel of the second car in x axis as shown in Figure 6.4. As only the heave and pitch motions of the cars are considered, the two wheels of one wheel-set can be taken at the same x coordinate, namely $x_3 = x_4$ and $x_5 = x_6$.

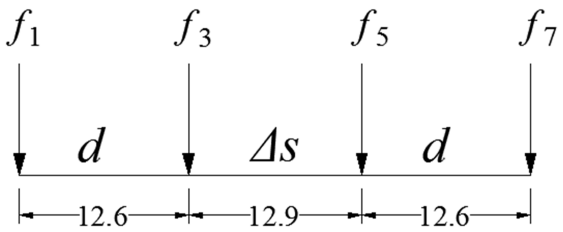

Figure 6.4. Lateral view of relative location of contact forces (unit: cm)

It should be noted that Eq. (6.1) to Eq. (6.7) are valid only when all the wheels of the two cars are on the plate structure. Actually, there are extra stretches of rails in front of and behind the plate structure, as shown in Figure 6.1. The stiffness of the extra rails or spans is taken to be infinitely large, which means $w(x_i, y_i, t) = 0$ when the ith wheel of the cars is on the extra rails. Eq. (6.1) to Eq. (6.7) should be changed according to the locations of wheels of the cars. The equations of motion of the plate structure and the cars can be solved by the iterative method presented in section 5.1.

6.3. Experimental Results

Two separate moving cars and two connected moving cars are used to excite the four-span plate structure in the tests. There are two different situations for two separate moving cars depending on the time gap between the time instants of two cars getting on the plate structure. If the time gap is long, the plate structure experiences a free vibration during the time period between the first car leaving the plate structure and the second car getting on the plate structure. However, this free vibration does not take place if the time gap is short. Two connected cars at a low speed and at a high speed are both tested.

6.3.1. Two Separate Cars

Supposing that the second car gets onto the plate structure at a time gap of Δt after the first car does. The time instants of two cars have a relationship of

$$t_2 = t_1 + \Delta t \tag{6.9}$$

where t_1 and t_2 are the time instants of the first car and the second car when they are arriving at the plate, respectively. If the time gap is short, eight wheels of the two cars can be acting on the plate structure at the same time for some time. However, when the time gap is long enough so that the second car arrives after the first car leaves the plate structure, the second car encounters a plate undergoing free vibration caused by the departure of the first car. Another special case is six wheels acting on the plate structure (rear wheel-set of the first car and two wheel-sets of the second car), which is not easy to achieve in experiments and not studied in this thesis.

(a) Situation one: two separate cars with short time gap

The first car carries a mass marked as *No*. 1 and they weigh 4.335 kg in total (mass ratio of 0.41), and the second car also carries a mass marked as *No*. 2 and they weigh 4.207 kg in total (mass ratio of 0.40). As the Laser Vibrometer can only measure the speed of one car at a time, the speed of the first car is measured first for a while. When the second car reaches the plate structure, its speed is measured until it leaves the plate structure. The measured speeds of the two cars are given in Figure 6.5. The initial speed of the first car is estimated to be 1.21 m/s and its acceleration is -0.0647 $\mathrm{m/s^2}$ from the fitted straight line. After the first car travels for $\Delta t = 2.385$ s

(estimated from Figure 6.6), the second car reaches the plate structure with an initial speed of 1.59 m/s and an acceleration of -0.0461 m/s^2.

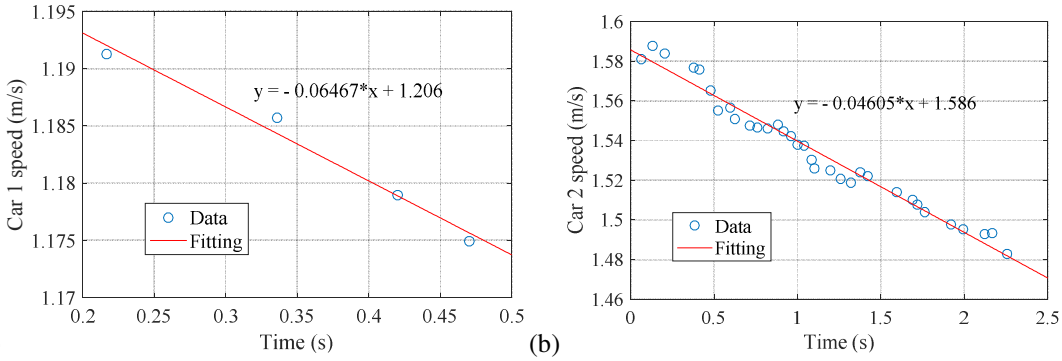

(a) (b)

Figure 6.5. Measured speeds of moving cars: (a) car 1, (b) car 2, with linear fitting curves

The simulated dynamic response of the plate structure agrees well with the measured response, as shown in Figure 6.6. There are high frequency oscillations in the measured results, especially during the period when the second car is travelling on the plate structure, which is mainly due to the second car travelling on a vibrating plate structure at a higher speed which causes a stronger car-plate interaction. The frequency of the high oscillation is around 14.01 Hz, seen from Figure 6.7 (b). A sudden change of the dynamic response of the plate structure can be seen at the grey points in Figure 6.6 when the second car gets onto the plate structure. The response of the plate structure subjected to two cars can be seen as the sum of the responses of the plate structure caused by two cars individually, as the vibration of the plate structure behaves linearly in the tests. The spectrum of the measured results in Figure 6.7 (a) shows two driving frequencies caused by two cars individually in the spectrum of the car-excited response of the plate structure and only the first two plate frequencies are excited largely in the free response of the plate structure shown in Figure 6.8. A new frequency of 1.25 Hz is found in the dynamic response of the plate structure, which is because the loading of the second car changes the original displacement trace of the plate structure.

The frequency of 21.95 Hz in Figure 6.7 (b) is close to the 1st structural frequency of 21.5 Hz in Figure 6.8, and the frequency of 23.0 Hz in the former figure is next to the 2nd structural frequency of 23.5 Hz in the latter figure. The amplitudes of the above frequencies in the former figure are increased in the latter figure.

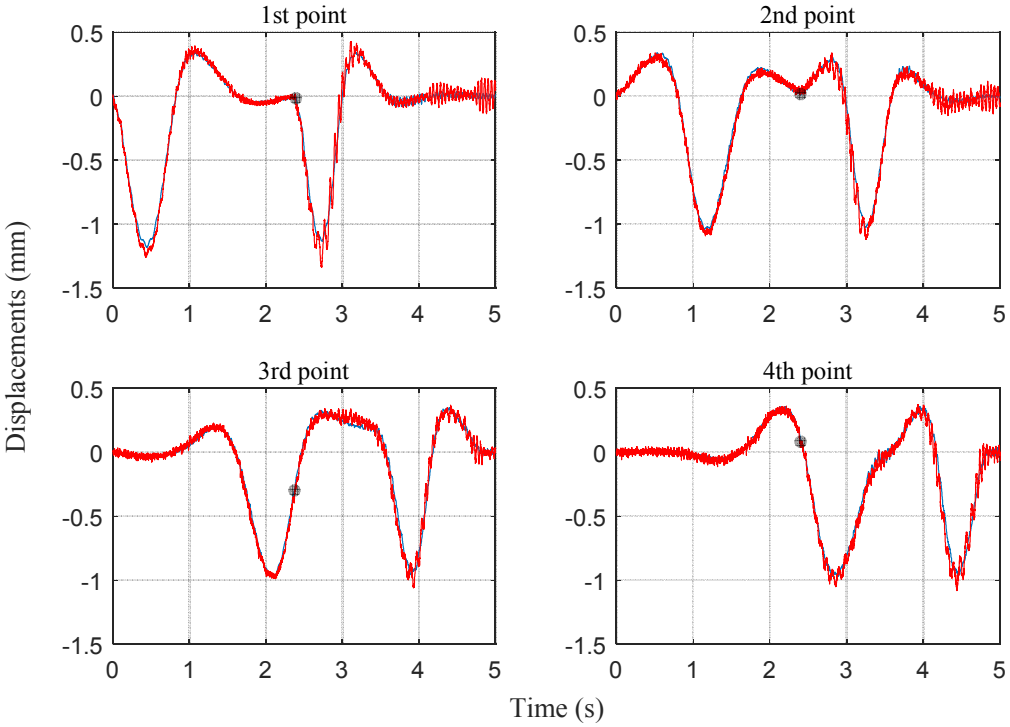

Figure 6.6. Displacements of the plate at measured points by simulation (blue curve) compared with experimental results (red curve) for two separate moving cars with short time gap

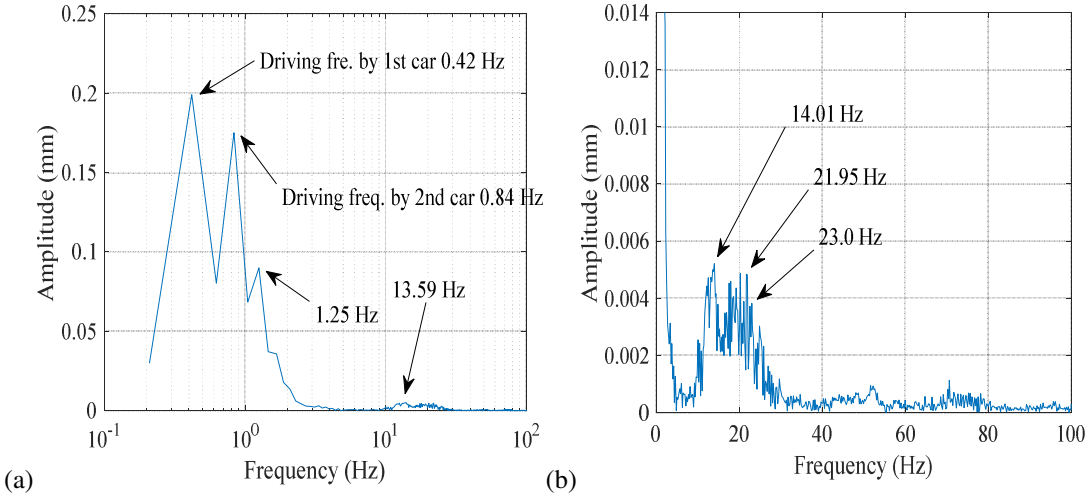

Figure 6.7. Spectrum of measured car-excited displacement of the plate structure at 1st measured point: (a) whole amplitude view, (b) part amplitude view at initial car speeds of 1.21 m/s and 1.59 m/s with short time gap

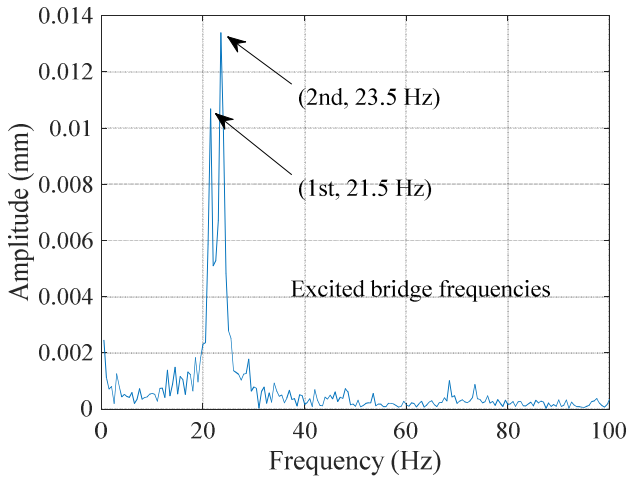

Figure 6.8. Spectrum of measured free vibration of the plate structure at 1st measured point at initial car speeds of 1.21 m/s and 1.59 m/s with short time gap

(b) Situation two: two separate cars with long time gap

The first car travels on the plate structure with an estimated initial speed of about 1.11 m/s and an acceleration of around -0.0628 $\mathrm{m/s^2}$, as shown in Figure 6.9 (a). After a time gap of $\Delta t = 4.298$ s, the second car starts to move on the plate structure with an estimated initial speed of about 1.79 m/s and an acceleration of around -0.0644 $\mathrm{m/s^2}$ as shown in Figure 6.9 (b). An obvious change occurs at the grey points when the second car arrives at the plate structure as seen in Figure 6.10. A time period of free vibration of the structure can be seen in the figure after the first car leaves the plate structure and before the second car arrives, but the free vibration is small and dies out quickly, which does not affect the vibration of the second car-plate system much. Larger high frequency oscillations can be seen in the car-excited response and free vibration response of the plate structure when the second car is travelling on the plate structure at a higher car speed, compared with those during the period before the arrival of the second car. The spectrum of the responses of the plate structure caused by two cars separately is similar to that by one car.

The spectrum of free vibration of the plate structure after the second car leaves the structure is depicted in Figure 6.11. It can be seen in the figure that the first two structural frequencies are excited into relatively high amplitudes.

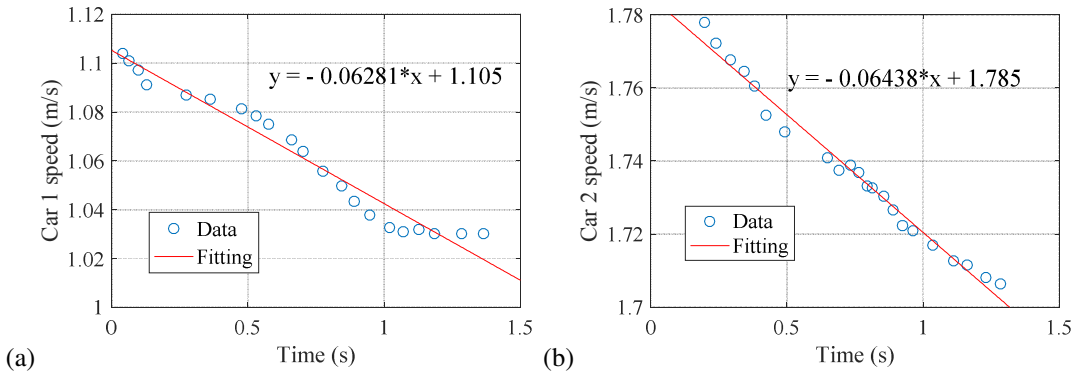

Figure 6.9. Measured speed of two cars: (a) car 1, (b) car 2, with linear fittings

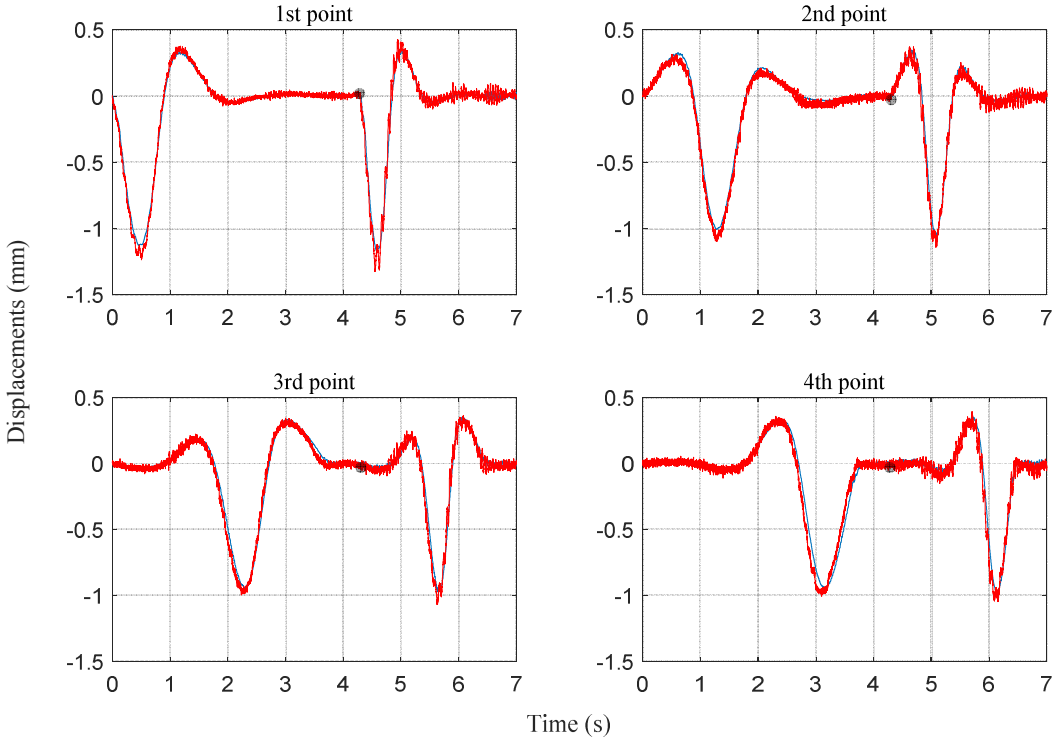

Figure 6.10. Displacements of the plate at measured points by simulation (blue curve) compared with experimental results (red curve) for two separate moving cars with long time gap

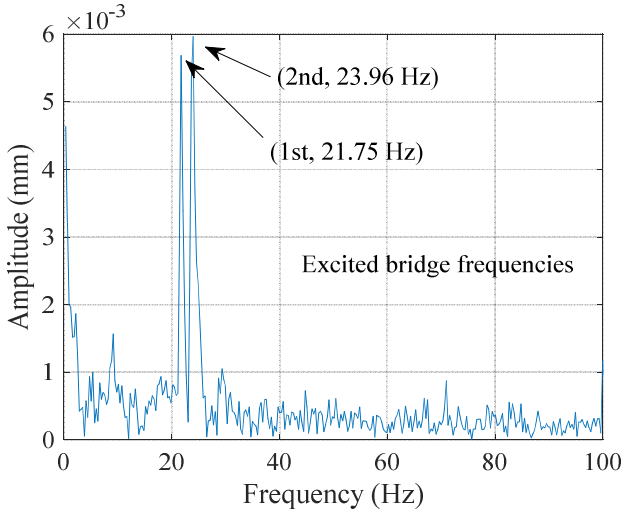

Figure 6.11. Spectrum of free vibration of the plate structure at 1st measured point at initial car speeds of 1.11 m/s and 1.79 m/s with long time gap

6.3.2. Two Connected Cars

(a) Plate structure subjected to two connected cars at low speed

The speed of two cars connected in series is measured and linearly fitted to a straight line for the selected data, as in Figure 6.12. The initial car speed is estimated to be about 1.03 m/s from the fitted line and the acceleration is around -0.0653 m/s^2. The responses of the plate structure from the simulation and the experiment are in good agreement, as shown in Figure 6.13. By comparing Figure 6.13 with Figure 5.17 (for one moving car), it is found that the dynamic response of the plate structure increases considerably with the moving load changing from one car to two connected cars and the shapes of the responses in the two figures look similar, but large high frequency oscillation is observed in the dynamic response of the plate structure in Figure 6.13 and the free vibration of the plate structure is larger in terms of amplitude in Figure 6.14 (b), compared with that in Figure 5.18 (b). The reason for the difference is that the car-plate interaction is stronger for two connected cars than that for one car, as the mass ratio for the two connected cars is bigger. The spectrum of the measured results in Figure 6.14 shows the high frequency of the dynamic response of the plate structure subjected to two connected cars is mainly 11.07 Hz.

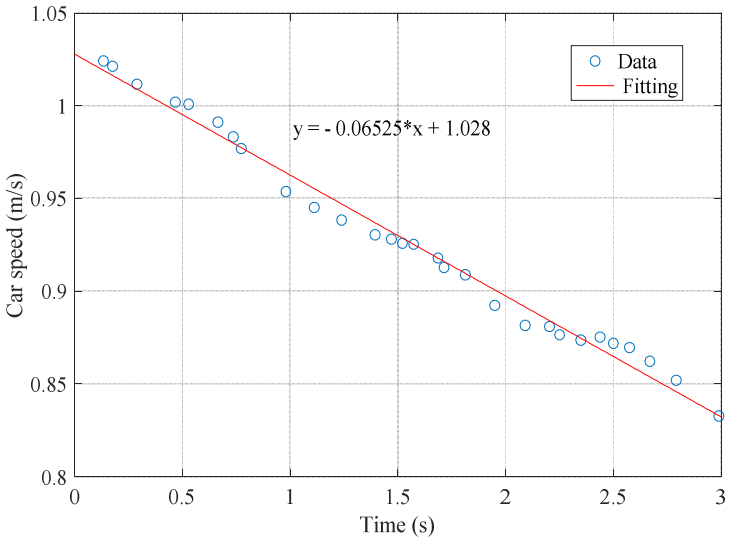

Figure 6.12. The speed of two connected cars measured by Laser Vibrometer and its linear fitting

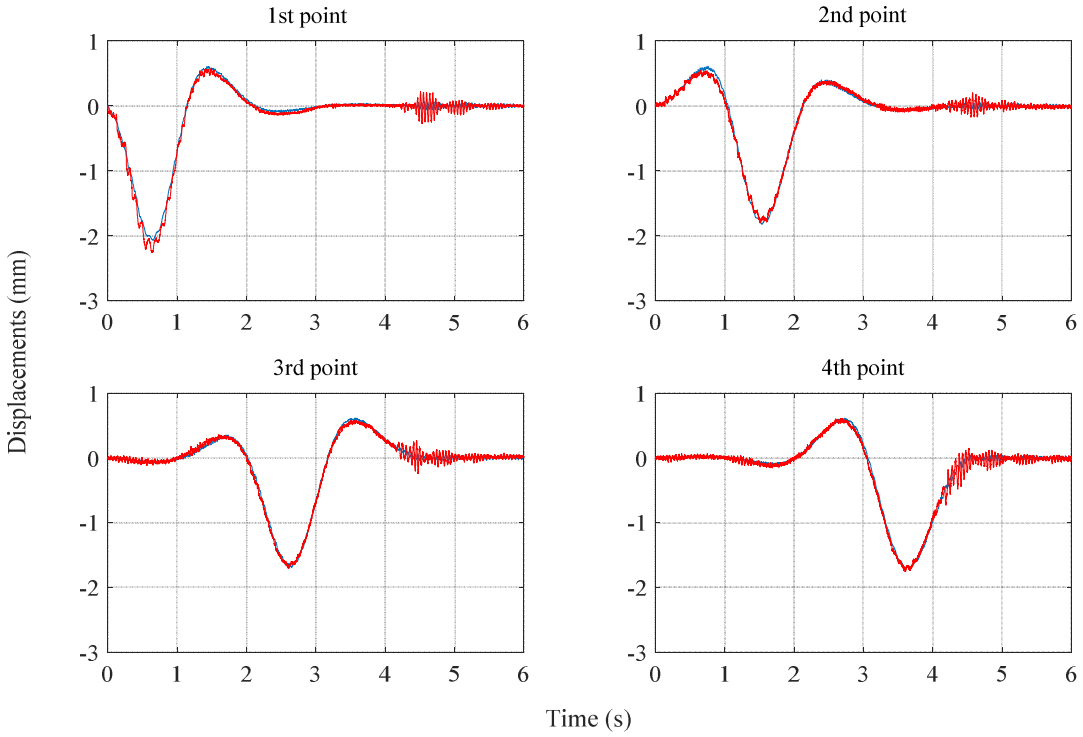

Figure 6.13. Displacements of the plate at measured points by simulation (blue curve) compared with experimental results (red curve) for two connected moving cars at initial car speed of 1.03 m/s

Comparing Figure 6.15 with Figure 6.14 (b), it can be found that the amplitude around the first bridge frequency increases from less than 0.005 mm to about 0.2 mm, and the amplitude around the second bridge frequency increases from about 0.005 mm to about 0.25 mm.

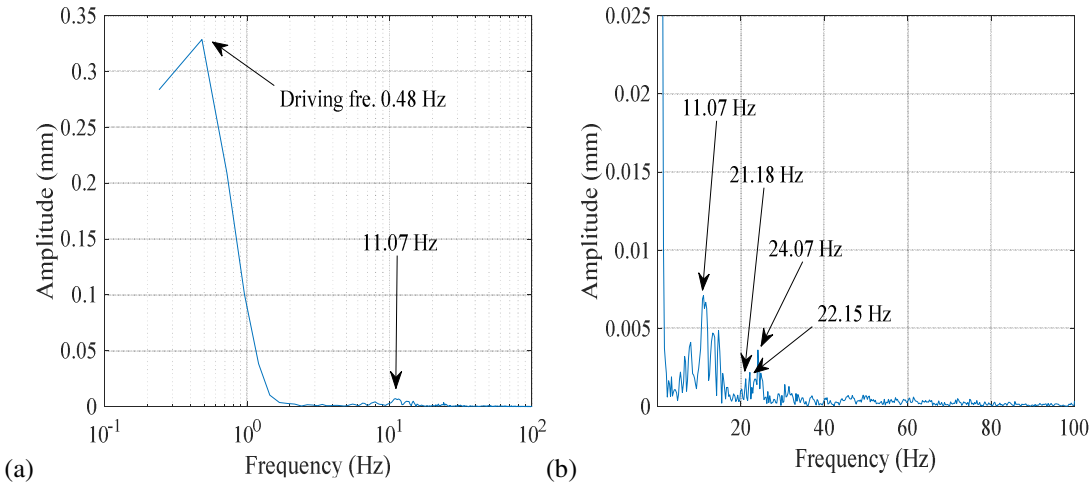

Figure 6.14. Spectrum of measured car-excited displacement of the plate structure at 1st measured point: (a) whole amplitude view, (b) part amplitude view at initial car speed of 1.03 m/s

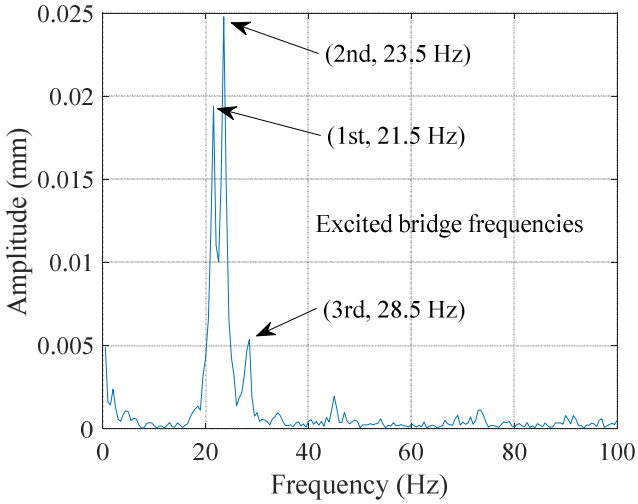

Figure 6.15. Spectrum of measured free vibration of the plate structure at 1st measured point at car speed of 1.03 m/s

(b) Plate structure subjected to two connected cars at high speed

Another test is conducted at a higher initial car speed of about 2.51 m/s and an acceleration of -0.051 m/s^2, shown in Figure 6.16. Large high frequency local oscillations are observed in measured plate responses, shown in Figure 6.17. The frequencies of the local oscillation are mainly around 12.61 Hz which is due to the car-plate interaction, shown as the highest peak after the driving frequency in Figure 6.18 and the third bridge frequency is excited into a higher level in the free response as in Figure 6.19, compared with that in Figure 6.14. It is noticed that the frequency band in Figure 6.18 is narrower than that in Figure 5.22.

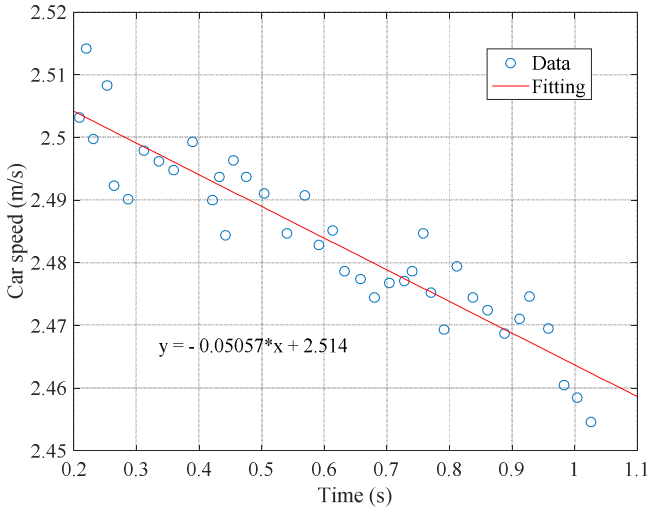

Figure 6.16. The speed of two connected cars measured by Laser Vibrometer and its linear fitting

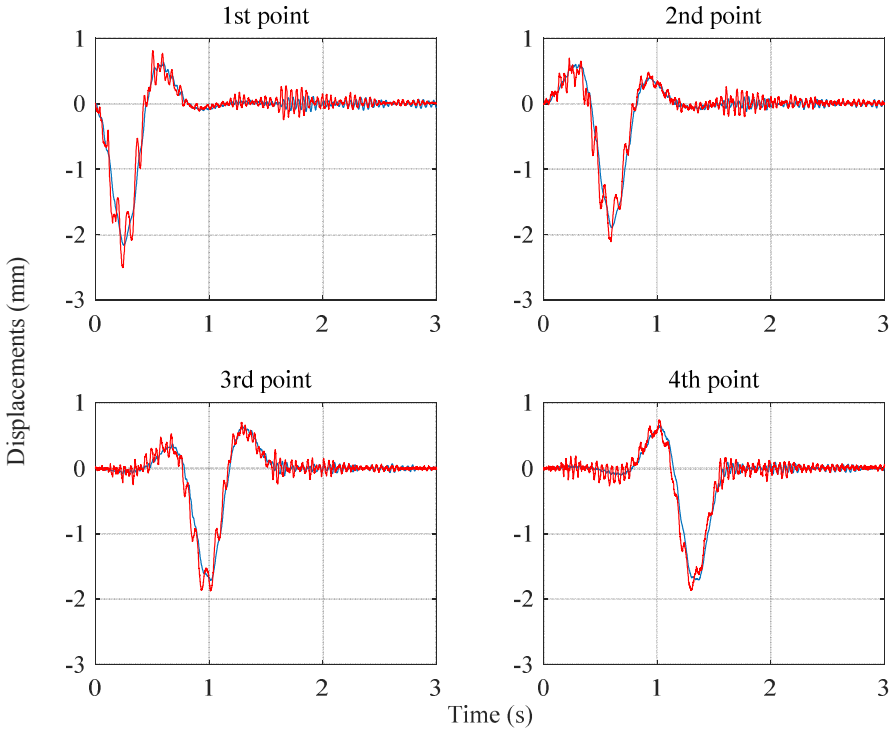

Figure 6.17. Displacements of measured points by simulation (blue curve) compared with experimental results (red curve) for two connected moving cars at initial car speed of 2.51 m/s

Comparing Figure 6.19 with Figure 6.18 (b), it can be found that the first two frequencies of the bridge are excited into noticeable amplitudes and there are not big changes for the amplitudes of these frequencies when the cars are on or not on the plate structure.

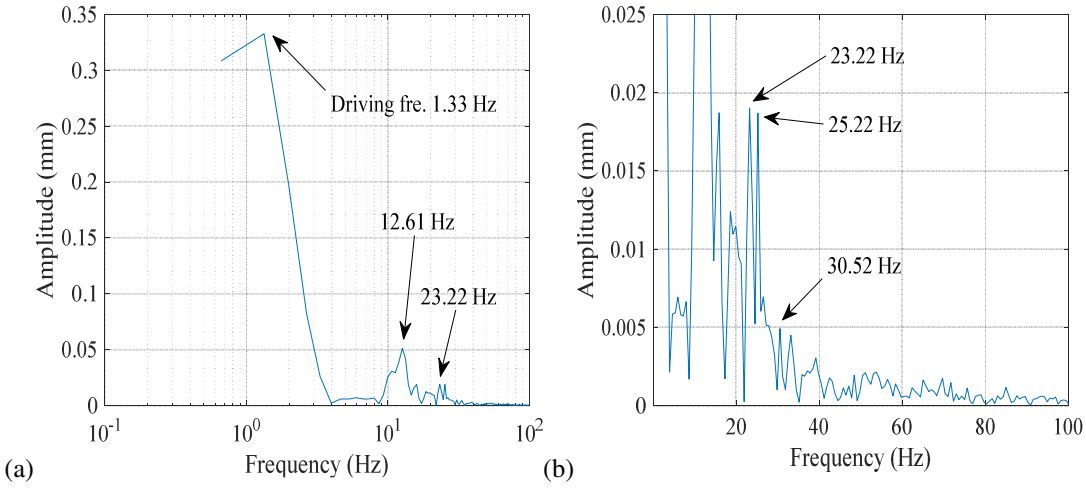

Figure 6.18. Spectrum of measured car-excited displacement of the plate structure at 1st measured point: (a) whole amplitude view, (b) part amplitude view at initial car speed of 2.51 m/s

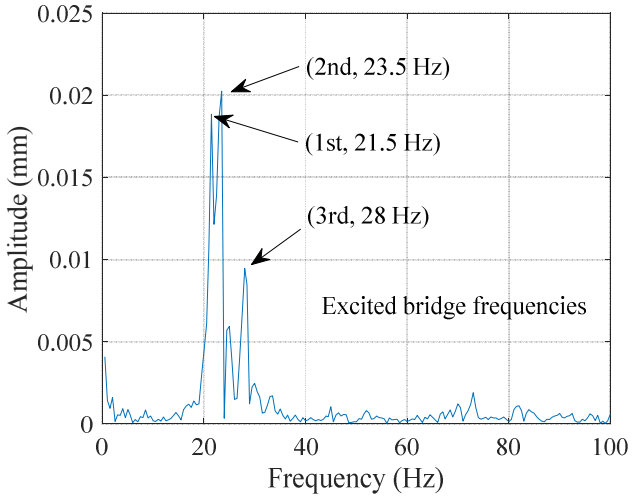

Figure 6.19. Spectrum of measured free vibration of the plate structure at 1st measured point at initial car speed of 2.51 m/s

6.4. Numerical Study

The simulation results agree well with the experimental results in section 6.3, which validates the theoretical model in this chapter. It is not easy to control the speed of the moving car accurately in experiments and high speeds of cars are hard to implement. Therefore, a numerical study based on the validated theoretical model is necessary to investigate the influence of different parameters of the moving car, like the number of cars, the loads of two-connected cars and the car acceleration on the dynamic response of the plate structure.

6.4.1. Influence of the Number of Cars on Separation

Dynamic Amplification Factor (DAF), mass ratio and speed ratio are used in this section to study the dynamic effect. For the plate structure, the critical speed is calculated to be $v_{\mathrm{cr}} = \frac{l\omega_1}{\pi} = 39.206\ \mathrm{m/s}$, where l and ω_1 are the length of one span and the first natural frequency of the plate structure respectively.

Assuming that the car moves on the plate structure at a constant speed, it is found by simulations that contact loss happens when the car speed is high enough and lower car speed leads to contact loss for a heavier car (Yang et al., 2017). Figure 6.20 gives the speed ratios where contact loss begins to happen for different mass ratios by using the one-car model and the two-connected-car model. The total car mass is distributed equally to each car in the two-connected-car model. It can be found from the table that two cars lead to contact loss at lower car speeds compared with one car at the same mass ratio. To avoid contact loss, ranges of the mass ratio and the speed ratio are selected for simulation (0.1~0.35 for mass ratio and 0.0122~0.1463 for speed ratio).

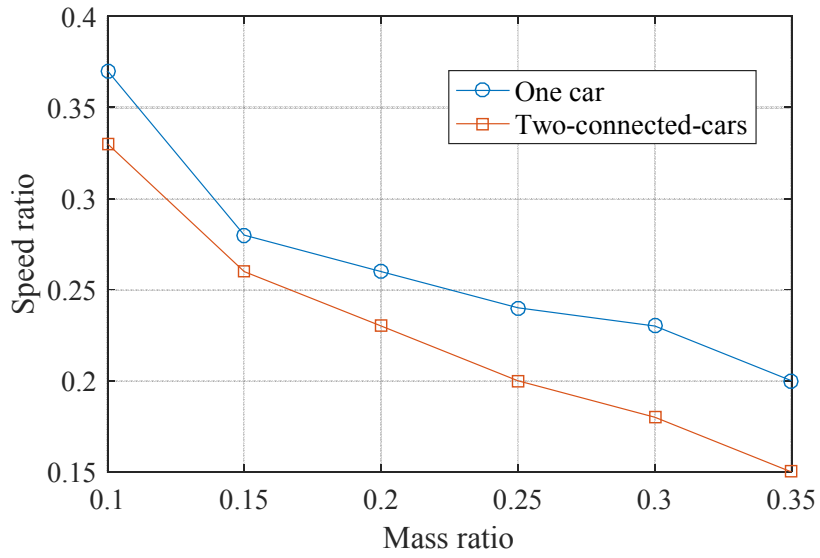

Figure 6.20. Speed ratios where contact loss begins for two car models

6.4.2. Influence of the Loads of Two-Connected-Cars

The relative location of four wheel-sets of two-connected-cars is illustrated in Figure 6.4. It can be found from the figure that different adjacent wheel-sets are at almost

the same distance ($d = 12.6$ cm) away. If the two-connected-cars travel on the plate structure at a constant speed v_c, the contact forces act like four sets of moving contact forces with a frequency of $f_t = \frac{v_c}{d}$ (defined as travelling frequency in this thesis). The travelling frequency of the contact forces may become close to the first natural frequency of the plate structure when the car speed changes. Yau and Yang (Yau and Yang, 2006) found analytically that successive moving forces with the same adjacent distance d could excite a simply supported beam into resonance at its first mode when $f_t = \frac{v_c}{d} = f_1$ where f_1 is the first natural frequency of the beam in Hz. Similarly, one may expect the resonance to occur for the car-plate system when the travelling frequency is close to the first natural frequency of the plate structure.

Figure 6.21 shows the relationship between DAF at mid-span points and the speed ratio for different mass ratios. A new peak emerges at the speed ratio of $r_s = 0.0731$(car speed of $v_{cr}r_s = 2.87$ m/s) in Figure 6.21 compared with Figure 5.35. The travelling frequency at this speed ratio is $f_t = \frac{v_{cr}r_s}{d} = 22.746$ Hz which is close to the first natural frequency (21.781 Hz) of the plate structure, so the new peak could be due to the resonance of the plate structure excited by the two moving connected cars. It is also noted in Figure 6.21 that the DAF at the speed ratio of 0.0731 varies depending on the mass ratio and the location of the DAF.

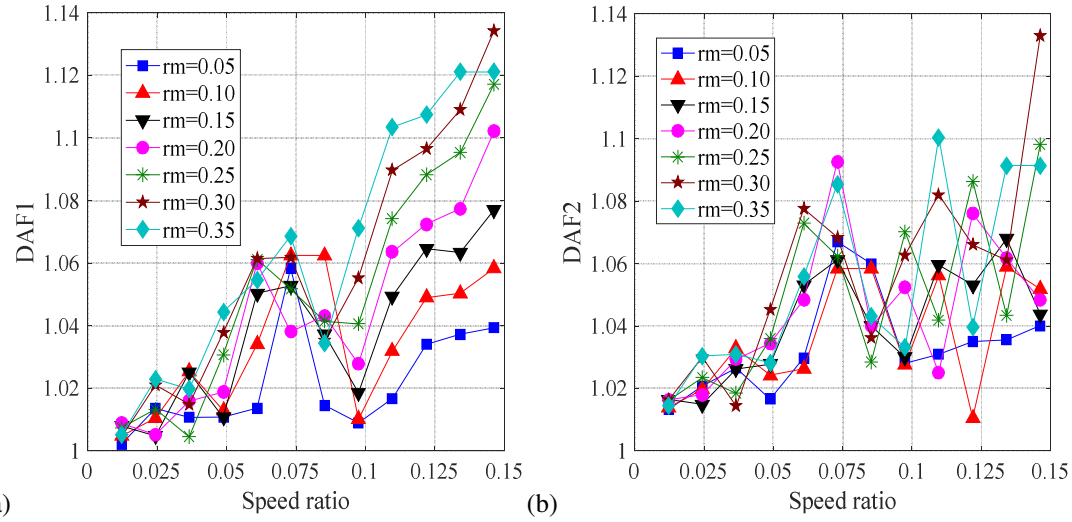

(a) (b)

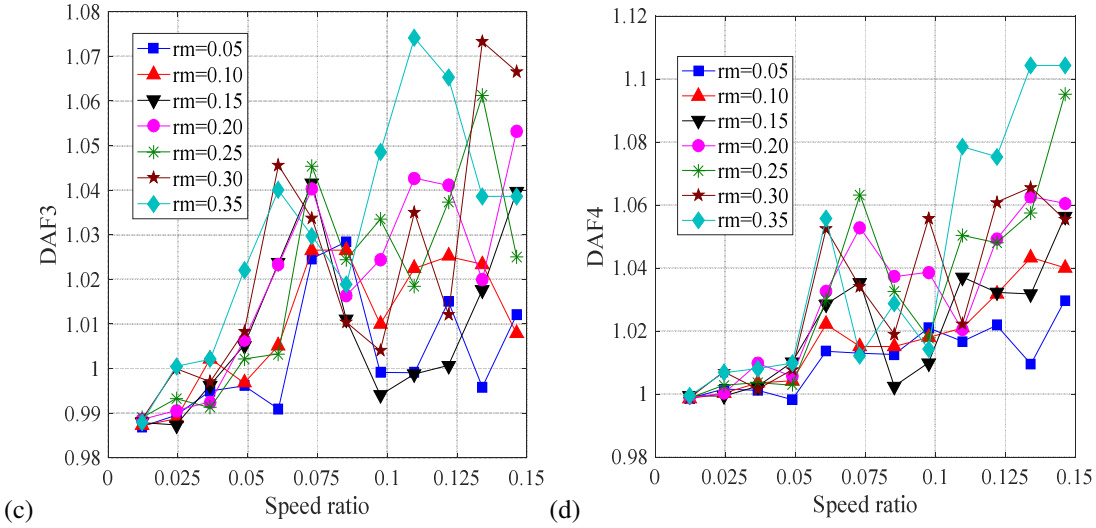

Figure 6.21. DAF versus speed ratio for different mass ratios by two-connected-car model ('rm' representing mass ratio): (a) DAF at 1st mid-span, (b) DAF at 2nd mid-span, (c) DAF at 3rd mid-span, (d) DAF at 4th mid-span

To verify the above explanation for the peak at the speed ratio of 0.0731, the spectrum of the dynamic response of the plate structure subjected to two connected cars with different masses is plotted as Figure 6.22. When the mass ratio is as small as 0.05, the interaction between the cars and the plate structure can be ignored. In this case, the moving two connected cars act as four sets of moving forces. Figure (a) shows only one peak at 20.79 Hz which is close to the first natural frequency of the plate structure (21.781 Hz) and well above the driving frequency 1.54 Hz. This explains the DAF peak at the speed ratio of 0.0731 for the mass ratio of 0.05 in Figure 6.21. However, more peaks appear above the driving frequency for larger mass ratios, due to the interaction between the cars and the plate structure, shown in figure (b) to figure (d). Those peaks expand towards both sides of 20.79 Hz along the *x* axis and the larger mass ratios, at smaller frequencies the peaks appear. It is noticed that among these peaks the second natural frequency of the plate structure (23.676 Hz) is excited for different mass ratios.

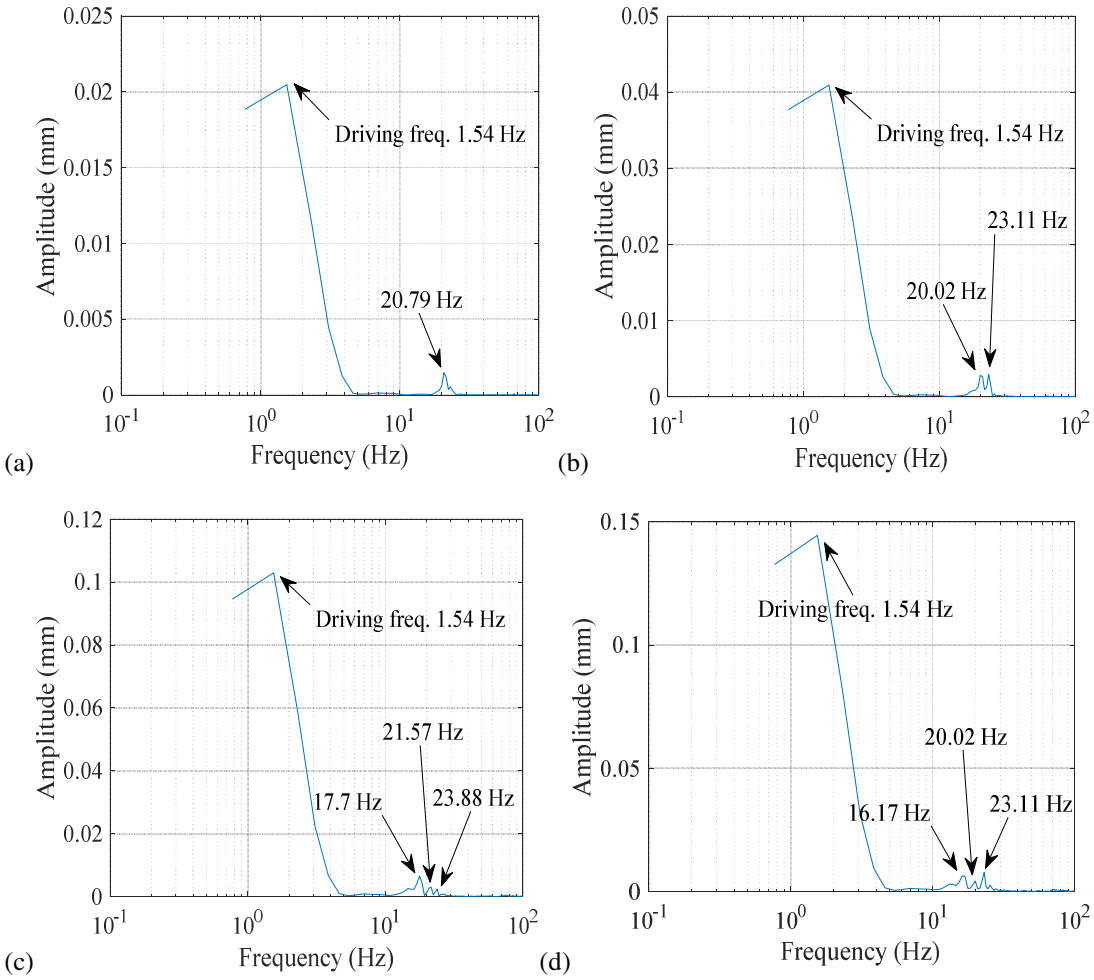

Figure 6.22. Spectrum of numerical displacement of the plate structure at 1st measured point for mass ratios of: (a) 0.05, (b) 0.1, (c) 0.25 and (d) 0.35 by two-connected-car model at speed ratio of 0.073

To look at the effect of these four sets of wheel loadings further, the spectrum of the dynamic response of the plate structure travelled by two connected cars (shown in Figure 6.22) is compared with that excited by an equivalent moving mass (shown in Figure 6.23). Compared with Figure 6.23, fewer and higher peaks near the travelling frequency (22.746 Hz) occur above the driving frequency in Figure 6.22, which indicates that the two moving connected cars at the speed ratio of 0.073 excite the plate structure into frequencies near the travelling frequency.

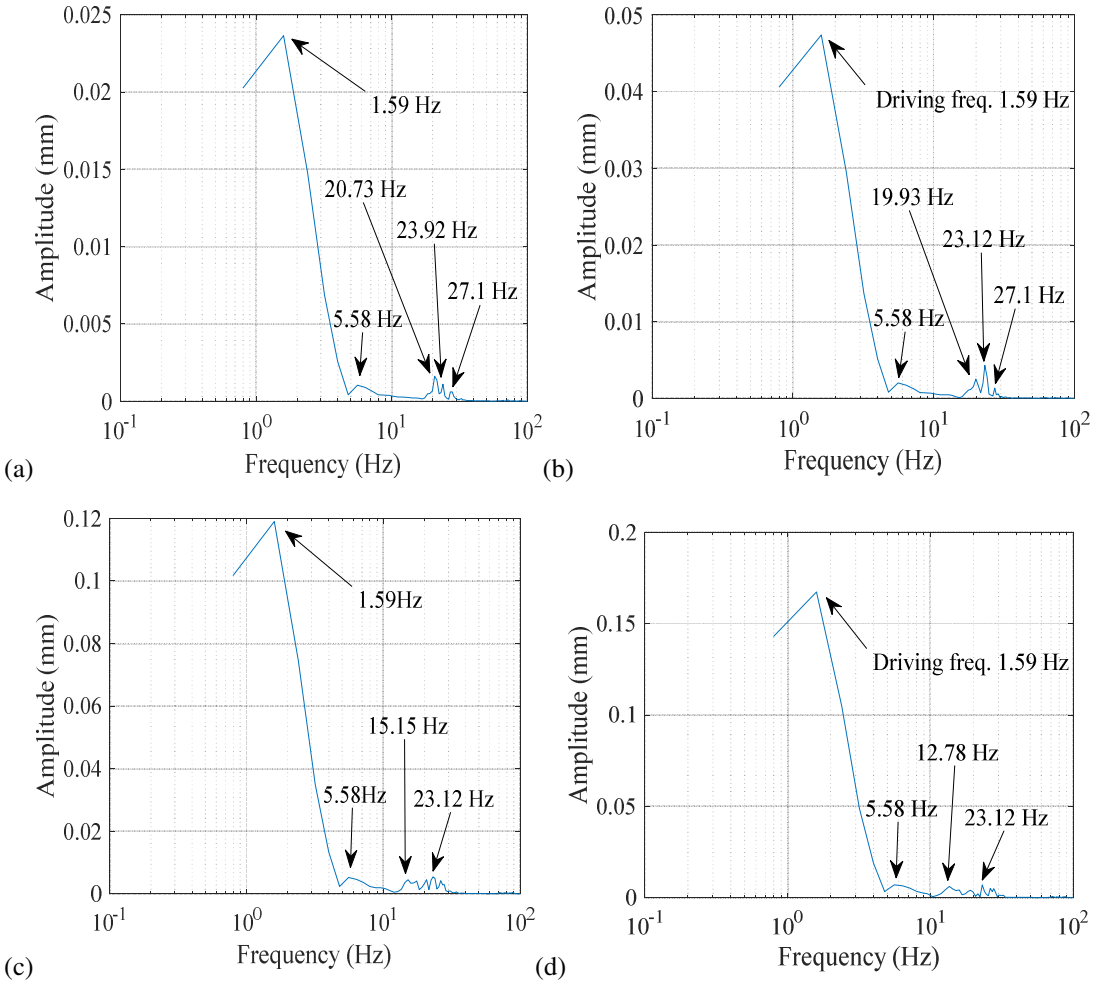

Figure 6.23. Spectrum of numerical displacement of the plate structure at 1st measured point for mass ratios of: (a) 0.05, (b) 0.1, (c) 0.25 and (d) 0.35 by moving mass model at speed ratio of 0.073

6.4.3. Influence of Car Acceleration

The influence of the two-connected-car acceleration on the DAF of four mid-span points of the plate structure can be seen in Figure 6.24. The speed ratio in the figure refers to the ratio of the initial speed of the moving car to the critical speed of the plate structure. It can be seen from the figure that DAF1 basically does not change with the car acceleration at different speed ratios except the speed ratio of 0.1463 where DAF1 is relatively large at car accelerations of -0.07 $\mathbf{m/s^2}$ and -0.14 $\mathbf{m/s^2}$. Basically the trend for DAF2 and DAF3 are the same as that for DAF1, but DAF2 and DAF3 vary more with the car acceleration. While it is found that DAF2 increases obviously with the car deceleration at speed ratios of 0.0610 and 0.0975, DAF3 basically decreases dramatically with the car deceleration at the speed ratios ranging

from 0.0488 to 0.1219. DAF4 changes significantly with the car accelerations at different speed ratios, but the trend is not clear, which is due to the influence of the vibration of other spans on the vibration of the fourth span. In the experiments, the car acceleration is measured between -0.04 ~ -0.08 $\mathbf{m/s^2}$ which can produce non-ignorable effect on the dynamic response of the plate structure at some speed ratios, as shown in Figure 6.24.

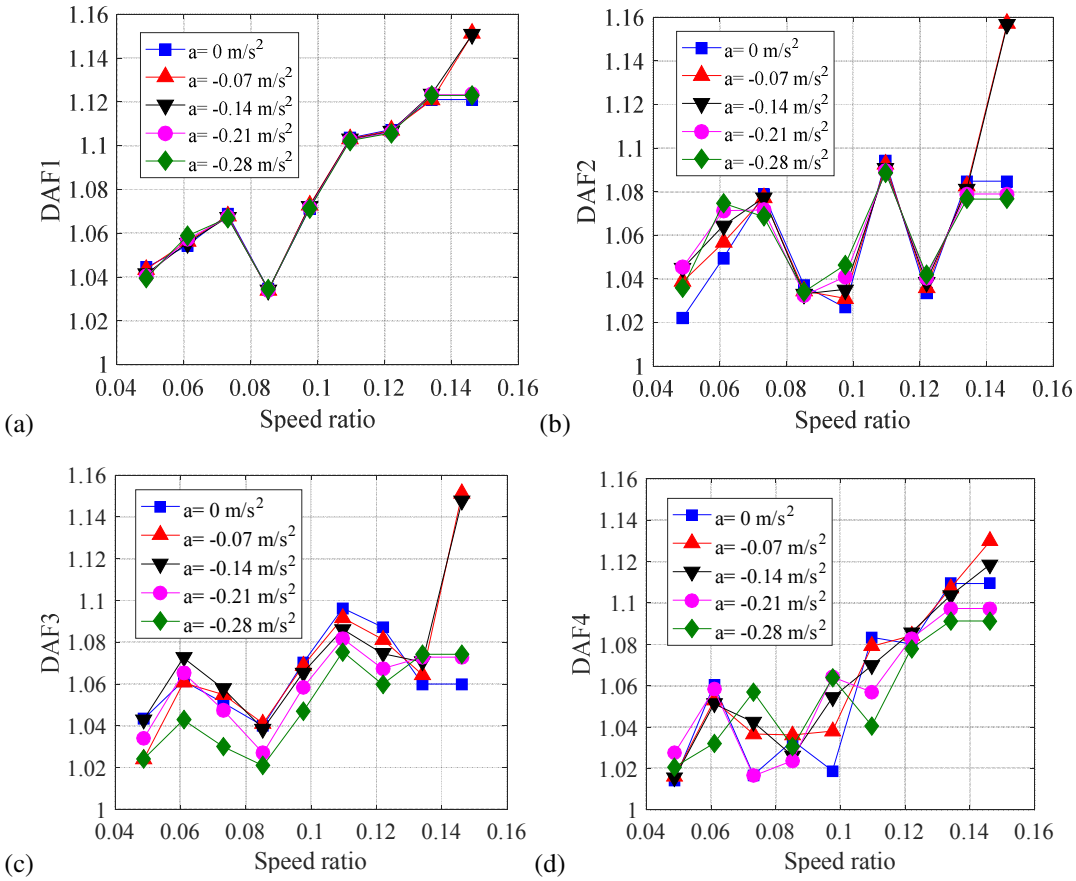

Figure 6.24. DAF versus initial speed ratio with mass ratio of 0.35 for different accelerations by two-connected-car model: (a) DAF at 1st mid-span, (b) DAF at 2nd mid-span, (c) DAF at 3rd mid-span, (d) DAF at 4th mid-span.

6.5. Concluding Remarks

An experimental and theoretical study of the vibration of a four-span continuous plate structure excited by two moving cars is carried out in this chapter. Two moving cars with different masses and initial speeds are tested. A novel situation in this chapter is two-connected-cars moving on the plate structure, which has not been reported in the literature. Some interesting findings are as follows:

(1) The vibration of the plate structure excited by two separate moving cars can be seen as the superposition of the vibrations of the structure subjected to each car individually. The initial speed of the first car and the time gap between the arriving time-instants of the two cars have a significant influence on the vibration of the second car by changing the initial condition of the structure when the second car arrives on the structure.

(2) Simulations show that separation between two-connected-cars and the plate structure is more likely to happen than for one car at the same speed and mass ratio.

(3) Spectrum analysis of the experimental results shows that higher car speeds can excite the plate structure into higher-frequency local oscillations, which is due to the stronger interaction between the cars and the plate structure.

(4) Two connected cars can also increase the car-plate interaction, compared with one car due to the larger mass ratio of two cars.

(5) The higher-frequency band of the dynamic response of the plate structure caused by two connected cars is narrower than that by one car, because of the loading of the four sets of wheels with almost the same adjacent distance.

(6) An interesting finding from numerical simulations for the two-connected-cars travelling on the plate structure is that the plate structure can be excited into narrow-band higher frequencies by the four sets of wheels travelling at the speed of 2.87 $\mathrm{m/s^2}$, and these higher frequencies are close to the first two natural frequencies of the plate structure, thus amplifying the amplitude of the dynamic response of the plate structure, like a resonance phenomenon. In addition, smaller car masses lead to narrower frequency bands of responses.

7. Conclusions and Future Work

This chapter gives a brief summary of the conclusions drawn in this thesis and elaborates the original contributions of this thesis. Future work is then discussed. Finally the publications by the author are listed.

7.1. Main Conclusions

The experimental studies of vehicle-bridge interactions are relatively much fewer than the theoretical studies of this problem in the literature. It is essential to combine the theoretical studies and experimental studies of this problem. Laboratory testing is a good way to study real vehicle-bridge interactions. Main conclusions of this thesis are presented below.

(a) Mid-supports of a continuous beam can be treated as elastic springs and the reaction forces at these supports can be taken as external forces acting on the beam during the vibration of the beam. Fourteen mode shapes of a simply supported beam are needed to approximate accurately the first eight mode shapes of a two-span continuous beam whose span length is half of the simple beam.

(b) Vehicle-bridge interaction can delay the bridge displacement and enlarge the structural maximum displacement which is at mid-span for a simple beam and at the second mid-span for a two-span continuous beam (please see section 4.2 for more details about this conclusion). The maximum Dynamic Amplification Factor (DAF) for a simple beam is about 1.75 when the speed ratio of the speed of a moving force to the critical speed of the beam is 0.6, whereas the DAF for a two-span continuous beam can be as large as 3.21 at the speed ratio of 0.85. Vehicle-bridge interaction is stronger at a larger speed ratio or the mass ratio of the vehicle mass to the bridge mass. It is found in section 6.4.2 that this interaction excites some high-frequency components in the dynamic response of the bridge subjected to travelling cars.

(c) Separation begins to happen at a vehicle speed higher than a threshold, and this threshold decreases with mass ratio. Vehicle-bridge separation is found unlikely to happen for a simply supported bridge with 30 m span length and zero initial conditions (no vibrations) under the current high-speed train speed if the track or

bridge irregularities can be ignored by using the moving sprung mass model. However, separation is likely to take place for a two-span continuous beam with a mass ratio bigger than 0.3. It is noted that contact stiffness has a significant influence on vehicle-bridge interaction and separation. The above conclusion for separation is drawn by using the contact stiffness of 1×10^{11} N/m and 2×10^{10} N/m for the simply supported beam and the two-span continuous beam, respectively.

(d) Frequency spectra show that a wide range of frequency components with relatively large amplitudes at frequencies less than 30 Hz appear for the car-plate time-varying system. The largest amplitude takes place at the driving frequency. The car speed needs to be large enough to excite high natural frequencies of the plate structure into noticeable amplitudes.

(e) The natural frequencies of the plate structure are more likely to be excited into large amplitudes by the two-connected-moving-cars which have the almost equal space between adjacent axle loads. The lowest speed of the two-connected-cars at which the plate structure is excited into resonance by the four sets of axle loads is about 2.75 m/s (speed ratio of 0.07). In addition, the frequency band of the plate structure excited by the two-connected-moving-cars is found to be narrower than that by one-moving-car. The four equidistant axle loads of the two cars produce a frequency which equals the ratio between the car velocity and the adjacent distance of the axle loads. This frequency is below 20 Hz under the current experimental car speed (maximum car speed about 2.5 m/s), which might narrow the frequency band of the car-plate system and amplify the amplitudes of the frequency components of the system around this frequency.

(f) A structural FE model and a rigid-body car model are adopted and an MS-iterative combined method is used for simulating the car-plate interaction. Simulated results agree well with experimental results for one or two cars at different speeds. Further numerical studies of the car-plate dynamic system reveal some interesting results: (1) the car deceleration (0.04 ~ 0.08 $\mathrm{m/s^2}$) can cause an obvious phase shift for the structural response and should be considered in the theoretical model of the system; (2) the sprung mass can be used to model the car simply, but brings slightly larger structural and vehicular displacements than those by the rigid-body model; (3) the point damping provided by four actuators at each span does not have any

influence on the structural response; (4) a longer car decreases the structural displacement when the span ratio of the car wheelbase to the plate span length is less than 0.8; (5) the structural displacement basically increases with the car speed under current maximum experimental car speed of about 2.5 m/s (speed ratio of 0.064); (6) the mass ratio has a significant influence on the response of the plate structure when the speed ratio is large; (7) car-rail separation happens for the plate structure subjected to one car travelling at a speed ratio bigger than 0.2 with a mass ratio of 0.35 and this speed ratio is found to be smaller (0.15) for the structure traversed by two-connected-cars with the same mass ratio; (8) when the car speed is low, say, 1 m/s, the structural displacement basically does not change with the wheel/rail contact stiffness, but the influence becomes strong when the car speed is high, say, higher than 3.5 m/s; (9) larger contact stiffness basically leads to bigger contact forces and slightly quicker car vibration when the car speed is high; (10) regardless of the car speed, the frequencies of the contact forces basically increase but the dynamic response of the car body decreases with the contact stiffness; (11) the frequency band of the car-plate system widens with the mass ratio of the car to the plate structure, which may be caused by the stronger car-plate interaction for a bigger mass ratio.

Overall, the aim and objectives mentioned in section 1.3 are all met.

7.2. Contributions to Knowledge

The main contributions of this thesis to knowledge are briefly summarized here. A list of publications by the author is presented later in section 7.4.

(1) The mode shapes of a two-span continuous beam are approximated by using a number of sinusoidal functions for the whole length of the beam, and the analytical solution of the continuous beam subjected to a moving force based on the approximated mode shapes is derived. The contributions of the natural frequencies of the continuous beam to the modal displacement or acceleration of the beam are clearly shown in the analytical solution.

(2) A simple elastic contact algorithm is developed to take vehicle-bridge separation into account by using the moving sprung mass model. The effect of impact between the vehicle and the bridge at the moment of reattachment

is assumed to be realized by the wheel/rail contact spring. No impact algorithm is needed and the vehicle-bridge interaction is applied to the system directly at the moment of reattachment.

(3) A general approach of simulating vehicle-bridge dynamics is presented and applied to an experimental rig in the lab (Yang et al., 2017). Firstly, the bridge FE model is built in an FE analysis software package to obtain its numerical modal properties. The bridge FE model is then updated with experimental frequencies of the bridge. The equation of motion of moving cars is established by treating them as rigid bodies, which are solved separately with that of the bridge by using an MS-iterative combined method and the numerical mode shapes of the bridge in MATLAB.

(4) The experimental studies of a four-span continuous plate structure subjected to one or two moving cars in the lab cannot be found in the literature. Chapter 5 and Chapter 6 are dedicated to the theoretical and experimental studies of this problem. A number of interesting results are found by experiments and simulations, which are shown in section 7.1.

7.3. Future Work and Discussion

Identifying the mode shapes of a bridge by using the responses of one or more vehicles moving on the bridge has attracted some recent research interest, as only a few sensors are needed to attach on the vehicles and the vehicular responses captured with the movement of the vehicles can reflect the mode shapes of the bridge along the trace of wheel movement. The identified mode shapes of a bridge can be used further to detect damages of the bridge (Zhang et al., 2012). However, to the student's best knowledge, this work has only been done for simply supported bridges theoretically and experimentally (Zhang et al., 2012; Yang et al., 2014; Malekjafarian and OBrien, 2017; Kong et al., 2017). Extending this idea to a continuous bridge is worth studying. The adjacent frequencies of a continuous bridge may be next to each other, which is because the wavenumber of a mode of the bridge may be close to each other for different modes. Removing the influence of neighbouring modes on the identified mode is an interesting research topic. To study

this problem experimentally in the lab, wireless sensors are needed to be attached on passing vehicles and the vehicles need to be controlled to move at a constant speed.

Moving loads can be used to excite bridges for identifying the bridge damages (Sun et al., 2016). Apart from using the mode shapes of a bridge to identify the bridge damages as mentioned above, model updating is another method widely utilized. Frequencies are often used to update structural models, but it is a global parameter of structures and not sensitive to local structural damages. It is an interesting research topic to identify bridge damages by using moving loads to excite the bridge.

Vibration control of a vehicle-bridge dynamic system which is time-varying has been done extensively by passive control methods. Using active control methods to tackle this problem has drawn much attention recently because of the smartness of this type of methods (Giraldo and Dyke, 2007; Stăncioiu and Ouyang, 2014; Nikkhoo, 2014). The Modal Superposition (MS) method is usually used for predicting the vibration of a bridge implemented with a control system subjected to moving vehicles due to the high computational efficiency of this method. However, the modal coordinates of a bridge cannot be directly measured in reality and they are usually estimated from the measured structural responses. The accuracy of the estimated modal coordinates depends largely on the number of sensors used in measurements. It is a problem to reduce the influence of the differences between the estimated modal coordinates and actual counterparts on the control effect by using reasonable amount of sensors.

The bridges studied in this thesis are uniform beams which are different from many real bridges with non-uniform cross sections, like continuous bridges, suspension bridges and cable-stayed bridges. In addition, a real bridge for a high-speed railway is normally made of pre-stressed concrete with a sophisticated track system. Another idea for future work is to make or obtain a more realistic bridge specimen and study it theoretically and experimentally in a lab. Field tests on a real bridge can be done in the future when there is such an opportunity.

7.4. Publications by Author

(a) Journal Papers

- YANG, J., OUYANG, H. & STĂNCIOIU, D. 2017. Numerical studies of vibration of four-span continuous plate with rails excited by moving car with experimental validation. *International Journal of Structural Stability and Dynamics,* 17**,** 1750119.

- YANG, J., OUYANG, H., STĂNCIOIU, D. & CAO S. C. 2017. Dynamic responses of a four-span continuous plate structure subjected to two moving cars with time-varying speeds. (under review)

(b) Conference Papers

- YANG, J., OUYANG, H. & STĂNCIOIU, D. Sep 2015. An approach of solving moving load problems by Abaqus and Matlab using numerical modes. *The 7th International Conference on Vibration Engineering*. Shanghai.

- YANG, J., OUYANG, H. & STĂNCIOIU, D. July 2016. An approach of solving moving load problems with application to an experimental case. *The 23th International Congress on Sound & Vibration.* Athens.

References

AKIN, J. E. & MOFID, M. 1989. Numerical solution for response of beams with moving mass. *Journal of Structural Engineering,* 115**,** 120.

AKTAN, E., CATBAS, N., TURER, A. & ZHANG, Z. 1998. Structural identification: Analytical aspects. *Journal of Structural Engineering,* 124**,** 817-829.

ANTOLÍN, P., ZHANG, N., GOICOLEA, J. M., XIA, H., ASTIZ, M. Á. & OLIVA, J. 2013. Consideration of nonlinear wheel–rail contact forces for dynamic vehicle–bridge interaction in high-speed railways. *Journal of Sound and Vibration,* 332**,** 1231-1251.

ARVIDSSON, T. & KAROUMI, R. 2014. Train–bridge interaction – a review and discussion of key model parameters. *International Journal of Rail Transportation,* 2**,** 147-186.

AU, F. T. K., CHENG, Y. S. & CHEUNG, Y. K. 2001. Vibration analysis of bridges under moving vehicles and trains: an overview. *Progress in Structural Engineering and Materials,* 3**,** 299-304.

AU, S.-K. 2011. Fast Bayesian FFT method for ambient modal identification with separated modes. *Journal of Engineering Mechanics***,** 214-226.

BAEZA, L. & OUYANG, H. 2008. Dynamics of a truss structure and its moving-oscillator exciter with separation and impact-reattachment. *Proceedings of the Royal Society A: Mathematical, Physical and Engineering Sciences,* 464**,** 2517-2533.

BAJER, C. I. & DYNIEWICZ, B. 2009. Virtual functions of the space–time finite element method in moving mass problems. *Computers & Structures,* 87**,** 444-455.

BELOTSERKOVSKIY, P. M. 1996. On the oscillations of infinite periodic beams subjected to a moving concentrated force. *Journal of Sound and Vibration,* 193**,** 705-712.

BIAN, X., JIANG, H., CHENG, C., CHEN, Y., CHEN, R. & JIANG, J. 2014. Full-scale model testing on a ballastless high-speed railway under simulated train moving loads. *Soil Dynamics and Earthquake Engineering,* 66**,** 368-384.

BILELLO, C., BERGMAN, L. A. & KUCHMA, D. 2004. Experimental investigation of a small-scale bridge model under a moving mass. *Journal of Structural Engineering,* 130**,** 799-804.

BIONDI, B., MUSCOLINO, G. & SOFI, A. 2005. A substructure approach for the dynamic analysis of train-track-bridge system. *Computers and Structures,* 83**,** 2271-2281.

BLEVINS, R. D. 1979. *Formulas for Natural Frequency and Mode Shape,* Malabar, Robert E. Krieger publishing company.

BOWE, C. J. & MULLARKEY, T. P. 2008. Unsprung wheel-beam interactions using modal and finite element models. *Advances in Engineering Software,* 39**,** 911-922.

BRANDES, E. A. & BROOK, G. B. 1998. *Smithells metals reference book,* Oxford, Butterworth-Heinemann.

BROWNJOHN, J. M. W., MOYO, P., OMENZETTER, P. & LU, Y. 2003. Assessment of highway bridge upgrading by dynamic testing and finite-element model updating. *Journal of Bridge Engineering,* 8**,** 162-172.

CAI, C. S., SHI, X. M., ARAUJO, M. & CHEN, S. R. 2007. Effect of approach span condition on vehicle-induced dynamic response of slab-on-girder road bridges. *Engineering Structures,* 29**,** 3210-3226.

CERDA, F., GARRETT, J. H., BIELAK, J., RIZZO, P. & BARRERA, J. Indirect structural health monitoring in bridges: scale experiments. *In:* BIONDINI, F. & FRANGOPOL, D. M., eds. Proceedings of the International IABMAS Conference, 2012 Italy. 346-353.

CHAN, T. H. T. & ASHEBO, D. B. 2006. Moving axle load from multi-span continuous bridge: laboratory study. *ASME Journal of Vibration and Acoustics,* 128**,** 521-526.

CHANG, K.-C., KIM, C.-W. & KAWATANI, M. 2013. Feasibility investigation for a bridge damage identification method through moving vehicle laboratory experiment. *Structure and Infrastructure Engineering***,** 1-18.

CHATTERJEE, P. K., DATTA, T. K. & SURANA, C. S. 1994a. Vibration of continuous bridges under moving vehicles. *Journal of Sound and Vibration,* 169**,** 619-632.

CHATTERJEE, P. K., DATTA, T. K. & SURANA, C. S. 1994b. Vibration of suspension bridges under vehicular movement. *Journal of Structural Engineering New York, N.Y.,* 120**,** 681-703.

CHEN, G., QIAN, L. & YIN, Q. 2014. Dynamic analysis of a Timoshenko beam subjected to an accelerating mass using spectral element method. *Shock and Vibration,* 2014**,** 1-12.

CHENG, Y. S., AU, F. T. K. & CHEUNG, Y. K. 2001. Vibration of railway bridges under a moving train by using bridge-track-vehicle element. *Engineering Structures,* 23**,** 1597-1606.

CHENG, Y. S., AU, F. T. K., CHEUNG, Y. K. & ZHENG, D. Y. 1999. On the separation between moving vehicles and bridge. *Journal of Sound and Vibration,* 222**,** 781-801.

CHEUNG, Y. K., AU, F. T. K., ZHENG, D. Y. & CHENG, Y. S. 1999. Vibration of multi-span non-uniform bridges under moving vehicles and trains by using modified beam vibration functions. *Journal of Sound and Vibration,* 228**,** 611-628.

CIFUENTES, A. O. 1989. Dynamic response of a beam excited by a moving mass. *Finite Elements in Analysis and Design,* 5**,** 237-246.

COJOCARU, E. C., IRSCHIK, H. & GATTRINGER, H. 2004. Dynamic response of an elastic bridge due to a moving elastic beam. *Computers & Structures,* 82**,** 931-943.

DASSAULT-SYSTÈMES 2014. *ABAQUS Documentation,* Providence, RI, USA.

DE SALVO, V., MUSCOLINO, G. & PALMERI, A. 2010. A substructure approach tailored to the dynamic analysis of multi-span continuous beams under moving loads. *Journal of Sound and Vibration,* 329**,** 3101-3120.

DEFARIA, A. R. & OGUAMANAM, D. C. D. 2004. Finite element analysis of the dynamic response of plates under traversing loads using adaptive meshes. *Thin-Walled Structures,* 42**,** 1481-1493.

DENG, L. & CAI, C. S. 2009. Identification of parameters of vehicles moving on bridges. *Engineering Structures,* 31**,** 2474-2485.

DENG, L. & CAI, C. S. 2010a. Identification of dynamic vehicular axle loads: demonstration by a field study. *Journal of Vibration and Control,* 17**,** 183-195.

DENG, L. & CAI, C. S. 2010b. Identification of Dynamic Vehicular Axle Loads: Theory and Simulations. *Journal of Vibration and Control,* 16**,** 2167-2194.

DIMITROVOVÁ, Z. & VARANDAS, J. N. 2009. Critical velocity of a load moving on a beam with a sudden change of foundation stiffness: Applications to high-speed trains. *Computers & Structures,* 87**,** 1224-1232.

DING, L., HAO, H. & ZHU, X. 2009. Evaluation of dynamic vehicle axle loads on bridges with different surface conditions. *Journal of Sound and Vibration,* 323**,** 826-848.

DINH, V. N., KIM, K. D. & WARNITCHAI, P. 2009. Dynamic analysis of three-dimensional bridge–high-speed train interactions using a wheel–rail contact model. *Engineering Structures,* 31**,** 3090-3106.

DOMÉNECH, A., MUSEROS, P. & MARTÍNEZ-RODRIGO, M. D. 2014. Influence of the vehicle model on the prediction of the maximum bending response of simply-supported bridges under high-speed railway traffic. *Engineering Structures,* 72**,** 123-139.

EBRAHIMI, M., GHOLAMPOUR, S., JAFARIAN KAFSHGARKOLAEI, H. & NIKBIN, I. M. 2015. Dynamic behavior of a multispan continuous beam traversed by a moving oscillator. *Acta Mechanica,* 226**,** 4247-4257.

EFTEKHARI, S. A. & KHANI, M. 2010. A coupled finite element-differential quadrature element method and its accuracy for moving load problem. *Applied Mathematical Modelling,* 34**,** 228-237.

EWINS, D. J. 2000. *Modal Testing: Theory, Practice and Application,* Baldock, Hertfordshire, England, Research Studies Press Ltd.

FENG, D. & FENG, M. Q. 2015. Model Updating of Railway Bridge Using In Situ Dynamic Displacement Measurement under Trainloads. *Journal of Bridge Engineering,* 20**,** 04015019.

FENG, D. & FENG, M. Q. 2016. Output-only damage detection using vehicle-induced displacement response and mode shape curvature index. *Structural Control and Health Monitoring,* 23**,** 1088-1107.

FERIANI, A., MULAS, M. G. & CANDIDO, L. 2010. Iterative procedures for the uncoupled analysis of vehicle-bridge dynamic interaction. *Proceedings of ISMA 2010 including USD2010.* Katoomba.

FRÝBA, L. 1968. Impacts of two-axle system traversing a beam. *International Journal of Solids and Structures,* 4**,** 1107-1123.

FRÝBA, L. 1999. *Vibration of Solids and Structures under Moving Loads,* Prague, Thomas Telford.

GARINEI, A. & RISITANO, G. 2008. Vibrations of railway bridges for high speed trains under moving loads varying in time. *Engineering Structures,* 30**,** 724-732.

GIRALDO, D. & DYKE, S. J. 2007. Control of an elastic continuum when traversed by a moving oscillator. *Structural Control and Health Monitoring,* 14**,** 197-217.

GONZALEZ, A., OBRIEN, E. J., CANTERO, D., LI, Y., DOWLING, J. & ZNIDARIC, A. 2010. Critical speed for the dynamics of truck events on bridges with a smooth road surface. *Journal of Sound and Vibration,* 329**,** 2127-2146.

GREEN, M. F. 1990. *Dynamic response of short-span highway bridges to heavy vehicle loads*. PhD, University of Cambridge.

GREEN, M. F. & CEBON, D. 1994. Dynamic response of highway bridges to heavy vehicle loads: theory and experimental validation. *Journal of Sound and Vibration,* 170**,** 51-78.

GUO, W. W., XIA, H., DE ROECK, G. & LIU, K. 2012. Integral model for train-track-bridge interaction on the Sesia viaduct: Dynamic simulation and critical assessment. *Computers and Structures,* 112-113**,** 205-216.

HAN, W., WU, J., CAI, C. S. & CHEN, S. 2015. Characteristics and Dynamic Impact of Overloaded Extra Heavy Trucks on Typical Highway Bridges. *Journal of Bridge Engineering,* 20**,** 05014011.

HE, X., WU, T., ZOU, Y., CHEN, Y. F., GUO, H. & YU, Z. 2017. Recent developments of high-speed railway bridges in China. *Structure and Infrastructure Engineering,* 13**,** 1-12.

HENCHI, K. & FAFARD, M. 1997. Dynamic behavior of multi-span beams under moving loads. *Journal of Sound and Vibration,* 199**,** 33-50.

HESTER, D. & GONZÁLEZ, A. 2017. A discussion on the merits and limitations of using drive-by monitoring to detect localised damage in a bridge. *Mechanical Systems and Signal Processing,* 90**,** 234-253.

HOANG, T., DUHAMEL, D., FORET, G., YIN, H. P., JOYEZ, P. & CABY, R. 2017. Calculation of force distribution for a periodically supported beam subjected to moving loads. *Journal of Sound and Vibration,* 388**,** 327-338.

HU, W., DENG, Z. & OUYANG, H. 2013. Generalized multi-symplectic method for dynamic response of continuous beam under moving load. *International Journal of Applied Mechanics,* 5**,** 1350033.

HUANG, C. S., YANG, Y. B., LU, L. Y. & CHEN, C. H. 1999. Dynamic testing and system identification of a multi-span highway bridge. *Earthquake engineering and structural dynamics,* 28**,** 857-878.

HUANG, D. & WANG, T.-L. 1998. Vibration of highway steel bridges with longitudinal grades. *Computers and Structures,* 69**,** 235-245.

HUMAR, J. L. & KASHIF, A. H. 1995. Dynamic response analysis of slab-type bridges. *Journal of Structural Engineering* 121**,** 48-62.

HWANG, E. S. & NOWAK, A. S. 1991. Simulation of dynamic load for bridges *Journal of Structural Engineering,* 117**,** 1413-1434.

INMAN, D. J. 2008. *Engineering Vibration*, Pearson.

IWNICKI, S. 2006. *Handbook of Railway Vehicle Dynamics* Boca Raton, CRC Press.

JIN, B. 2004. Dynamic displacements of an infinite beam on a poroelastic half space due to a moving oscillating load. *Archive of Applied Mechanics,* 74**,** 277-287.

JU, S. H. 2013. 3D analysis of high-speed trains moving on bridges with foundation settlements. *Archive of Applied Mechanics,* 83**,** 281-291.

JU, S. H. & LIAO, J. R. 2010. Error study of rail/wheel point contact method for moving trains with rail roughness. *Computers & Structures,* 88**,** 813-824.

KALKER, J. J. 1991. Wheel-rail rolling contact theory. *Wear,* 144**,** 243-261.

KARGARNOVIN, M. H. & YOUNESIAN, D. 2004. Dynamics of Timoshenko beams on Pasternak foundation under moving load. *Mechanics Research Communications,* 31**,** 713-723.

KAROUMI, R., WIBERG, J. & LILJENCRANTZ, A. 2005. Monitoring traffic loads and dynamic effects using an instrumented railway bridge. *Engineering Structures,* 27**,** 1813-1819.

KIM, C. W., INOUE, S., SUGIURA, K., MCGETRICK, P. & KAWATANI, M. Extracting bridge frequencies from dynamic responses of two passing vehicles. *In:* ZINGONI, A., ed. Insights and Innovations in Structural Engineering, Mechanics and Computation: Proceedngs of the Sixth International Conference on Structural Engineering, Mechanics and Computation, 2016 Cape Town, South Africa. CRC Press, 1858-1864.

KIM, S.-I. & KIM, N.-S. 2010. Dynamic performances of a railway bridge under moving train load using experimental modal parameters. *International Journal of Structural Stability and Dynamics,* 10**,** 91-109.

KLASZTORNY, M. & LANGER, J. 1990. Dynamic response of single-span beam bridges to a series of moving loads. *Earthquake engineering and structural dynamics,* 19**,** 1107-1124.

KONG, X., CAI, C. S., DENG, L. & ZHANG, W. 2017. Using dynamic response of moving vehicles to extract bridge modal properties of a field bridge. *Journal of Bridge Engineering,* 22.

KOU, J. W. & DEWOLF, J. T. 1997. Vibrational behavior of continuous span highway bridge-influencing variables. *Journal of Structural Engineering,* 123**,** 333-344.

KOZIOL, P. 2016. Experimental validation of wavelet based solution for dynamic response of railway track subjected to a moving train. *Mechanical Systems and Signal Processing,* 79**,** 174-181.

KOZIOL, P., MARES, C. & ESAT, I. 2008. Wavelet approach to vibratory analysis of surface due to a load moving in the layer. *International Journal of Solids and Structures,* 45**,** 2140-2159.

KUMAR, A. & SALEEB, A. F. 2009. Computer modeling for the complex response analysis of nonstandard structural dynamics problems. *Journal of Aerospace Engineering,* 22**,** 324-330.

KWARK, J. W., CHOI, E. S., KIM, Y. J., KIM, B. S. & KIM, S. I. 2004. Dynamic behavior of two-span continuous concrete bridges under moving high-speed train. *Computers & Structures,* 82**,** 463-474.

LEE, E.-T., EUN, H.-C., CHOI, Y.-J., AHN, Y.-J., LEE, S.-G. & PARK, S.-W. 2016. Structural performance experiment by moving cart to mount measurement sensors. *Journal of Vibroengineering,* 18**,** 1157-1166.

LEE, H. P. 1995. On the separation of a mass travelling on a beam with axial forces. *Mechanics Research Communications,* 22**,** 371-376.

LEE, S.-Y. & YHIM, S.-S. 2005. Dynamic behavior of long-span box girder bridges subjected to moving loads: Numerical analysis and experimental verification. *International Journal of Solids and Structures,* 42**,** 5021-5035.

LEE, U. 1996. Revisiting the moving mass problem: onset of separation between the mass and beam. *ASME Journal of Vibration and Acoustics,* 118**,** 516-521.

LEE, U. 1998. Separation between the flexible structure and the moving mass sliding on it. *Journal of Sound and Vibration,* 209**,** 867-877.

LEI, X. & NODA, M.-A. 2002. Analyses of dynamic response of vehicle and track coupling system with random irregularity of track vertical profile. *Journal of Sound and Vibration,* 258**,** 147-165.

LI, J., HAO, H., FAN, K. & BROWNJOHN, J. 2015. Development and application of a relative displacement sensor for structural health monitoring of composite bridges. *Structural Control and Health Monitoring,* 22**,** 726-742.

LI, J. & SU, M. 1999. The resonant vibration for a simply supported girder bridge under high-speed trains. *Journal of Sound and Vibration,* 224**,** 897-915.

LI, Q., XU, Y. L., WU, D. J. & CHEN, Z. W. 2010. Computer aided nonlinear vehicle-bridge interaction analysis. *Journal of Vibration and Control,* 16**,** 1791-1816.

LIU, K., REYNDERS, E., DE ROECK, G. & LOMBAERT, G. 2009. Experimental and numerical analysis of a composite bridge for high-speed trains. *Journal of Sound and Vibration,* 320**,** 201-220.

LIU, K., ZHANG, N., XIA, H. & DE ROECK, G. 2014. A comparison of different solution algorithms for the numerical analysis of vehicle–bridge interaction. *International Journal of Structural Stability and Dynamics,* 14**,** 1350065.

LIU, X.-W., XIE, J., WU, C. & HUANG, X.-C. 2008. Semi-analytical solution of vehicle–bridge interaction on transient jump of wheel. *Engineering Structures,* 30**,** 2401-2412.

LOU, P. 2005. A vehicle-track-bridge interaction element considering vehicle's pitching effect. *Finite Elements in Analysis and Design,* 41**,** 397-427.

LOU, P. 2007. Finite element analysis for train–track–bridge interaction system. *Archive of Applied Mechanics,* 77**,** 707-728.

LOU, P. & AU, F. T. K. 2013. Finite element formulae for internal forces of Bernoulli–Euler beams under moving vehicles. *Journal of Sound and Vibration,* 332**,** 1533-1552.

LOU, P., YU, Z.-W. & AU, F. T. K. 2012. Rail-bridge coupling element of unequal lengths for analysing train-track-bridge interaction systems. *Applied Mathematical Modelling,* 36**,** 1395-1414.

LOU, P. & ZENG, Q. Y. 2005. Formulation of equations of motion of finite element form for vehicle-track-bridge interaction system with two types of vehicle model. *International Journal for Numerical Methods in Engineering,* 62**,** 435-474.

MA, L. & LIU, W. 2016. A numerical train-floating slab track coupling model based on the periodic-Fourier-modal method. *Proceedings of the Institution of Mechanical Engineers, Part F: Journal of Rail and Rapid Transit*.

MALEKJAFARIAN, A., MCGETRICK, P. J. & OBRIEN, E. J. 2015. A Review of Indirect Bridge Monitoring Using Passing Vehicles. *Shock and Vibration,* 2015**,** 1-16.

MALEKJAFARIAN, A. & OBRIEN, E. J. 2014. Identification of bridge mode shapes using Short Time Frequency Domain Decomposition of the responses measured in a passing vehicle. *Engineering Structures,* 81**,** 386-397.

MALEKJAFARIAN, A. & OBRIEN, E. J. 2017. On the use of a passing vehicle for the estimation of bridge mode shapes. *Journal of Sound and Vibration,* 397**,** 77-91.

MAMANDI, A. & KARGARNOVIN, M. H. 2010. Dynamic analysis of an inclined Timoshenko beam traveled by successive moving masses/forces with inclusion of geometric nonlinearities. *Acta Mechanica,* 218**,** 9-29.

MARCHESIELLO, S., FASANA, A., GARIBALDI, L. & PIOMBO, B. A. D. 1999. Dynamics of multi-span continuous straight bridges subject to multi-degrees of freedom moving vehicle excitation. *Journal of Sound and Vibration,* 224**,** 541-561.

MARTINEZ-CASTRO, A. E., MUSEROS, P. & CASTILLO-LINARES, A. 2006. Semi-analytic solution in the time domain for non-uniform multi-span Bernoulli-Euler beams traversed by moving loads. *Journal of Sound and Vibration,* 294**,** 278-297.

MCGETRICK, P. J., KIM, C. W., GONZALEZ, A. & BRIEN, E. J. O. 2015. Experimental validation of a drive-by stiffness identification method for bridge monitoring. *Structural Health Monitoring,* 14**,** 317-331.

MICHALTSOS, G. T. 2010. Bouncing of a vehicle on an irregularity: A mathematical model. *Journal of Vibration and Control,* 16**,** 181-206.

MOREU, F., KIM, R. E. & SPENCER, B. F. 2017. Railroad bridge monitoring using wireless smart sensors. *Structural Control and Health Monitoring,* 24**,** e1863.

MOTTERSHEAD, J. E. & FRISWELL, M. I. 1993. Model updating in structural dynamics: A survey. *Journal of Sound and Vibration,* 167**,** 347-375.

MOTTERSHEAD, J. E., LINK, M. & FRISWELL, M. I. 2011. The sensitivity method in finite element model updating: A tutorial. *Mechanical Systems and Signal Processing,* 25**,** 2275-2296.

MUSCOLINO, G., PALMERI, A. & SOFI, A. 2009. Absolute versus relative formulations of the moving oscillator problem. *International Journal of Solids and Structures,* 46**,** 1085-1094.

MUSEROS, P., MOLINER, E. & MARTÍNEZ-RODRIGO, M. D. 2013. Free vibrations of simply-supported beam bridges under moving loads: Maximum resonance, cancellation and resonant vertical acceleration. *Journal of Sound and Vibration,* 332**,** 326-345.

NAGAYAMA, T., REKSOWARDOJO, A. P., SU, D., MIZUTANI, T. & ZHANG, C. 2015. Bridge natural frequency estimation by extracting the common vibration component from the responses of two vehicles. *6th International Conference on Advances in*

Experimental Structural Engineering & 11th International Workshop on Advanced Smart Materials and Smart Structures Technology University of Illinois.

NEVES, S. G. M., AZEVEDO, A. F. M. & CALÇADA, R. 2012. A direct method for analyzing the vertical vehicle–structure interaction. *Engineering Structures,* 34**,** 414-420.

NEVES, S. G. M., MONTENEGRO, P. A., AZEVEDO, A. F. M. & CALÇADA, R. 2014. A direct method for analyzing the nonlinear vehicle–structure interaction. *Engineering Structures,* 69**,** 83-89.

NGUYEN, D. V., KIM, K. D. & WARNITCHAI, P. 2009. Simulation procedure for vehicle-substructure dynamic interactions and wheel movements using linearized wheel-rail interfaces. *Finite Elements in Analysis and Design,* 45**,** 341-356.

NIKKHOO, A. 2014. Investigating the behavior of smart thin beams with piezoelectric actuators under dynamic loads. *Mechanical Systems and Signal Processing,* 45**,** 513-530.

NIKKHOO, A., EBRAHIMZADEH HASSANABADI, M., EFTEKHAR AZAM, S. & VASEGHI AMIRI, J. 2014. Vibration of a thin rectangular plate subjected to series of moving inertial loads. *Mechanics Research Communications,* 55**,** 105-113.

NIKKHOO, A., ROFOOEI, F. R. & SHADNAM, M. R. 2007. Dynamic behavior and modal control of beams under moving mass. *Journal of Sound and Vibration,* 306**,** 712-724.

OBRIEN, E. J. & MALEKJAFARIAN, A. 2016. A mode shape-based damage detection approach using laser measurement from a vehicle crossing a simply supported bridge. *Structural Control and Health Monitoring,* 23**,** 1273-1286.

OBRIEN, E. J., MCGETRICK, P. J. & GONZALEZ, A. 2014. A drive-by inspection system via vehicle moving force identification. *Smart Structures and Systems,* 13**,** 821-848.

OLSSON, M. 1985. Finite element, modal co-ordinate analysis of structures subjected to moving loads. *Journal of Sound and Vibration,* 99**,** 1-12.

OLSSON, M. 1991. On the fundamental moving load problem. *Journal of Sound and Vibration,* 145**,** 299-307.

OUYANG, H. 2011. Moving-load dynamic problems: A tutorial (with a brief overview). *Mechanical Systems and Signal Processing,* 25**,** 2039-2060.

OUYANG, H. & MOTTERSHEAD, J. E. 2007. A numerical-analytical combined method for vibration of a beam excited by a moving flexible body. *International Journal for Numerical Methods in Engineering,* 72**,** 1181-1191.

PAPADIMITRIOU, C., KATAFYGIOTIS, L. S. & AU, S. K. 1997. Effects of structural uncertainties on TMD design: A reliability-based approach. *Journal of Structural Control,* 65-88.

PATTEN, W. N., SUN, J., LI, G., KUEHN, J. & SONG, G. 1999. Field test of an intelligent stiffener for bridges at the I-35 walnut creek bridge. *Earthquake engineering and structural dynamics,* 28**,** 109-126.

PAULTRE, P., PROULX, J. & TALBOT, M. 1995. Dynamic testing procedures for highway bridges using traffic loads. *Journal of Structural Engineering,* 121**,** 362-376.

PESTEREV, A. V. & BERGMAN, L. A. 1998. A contribution to the moving mass problem. *Journal of Vibration and Acoustics,* 120**,** 824-826.

PESTEREV, A. V. & BERGMAN, L. A. 2000. An improved series expansion of the solution to the moving oscillator problem. *ASME Journal of Vibration and Acoustics,* 122**,** 54-61.

PESTEREV, A. V., BERGMAN, L. A. & TAN, C. A. 2004. A novel approach to the calculation of pothole-induced contact forces in MDOF vehicle models. *Journal of Sound and Vibration,* 275**,** 127-149.

PESTEREV, A. V., BERGMAN, L. A., TAN, C. A., TSAO, T. C. & YANG, B. 2003a. On asymptotics of the solution of the moving oscillator problem. *Journal of Sound and Vibration,* 260**,** 519-536.

PESTEREV, A. V., YANG, B., BERGMAN, L. A. & TAN, C. A. 2003b. Revisiting the moving force problem. *Journal of Sound and Vibration,* 261**,** 75-91.

PISAL, A. Y. & JANGID, R. S. 2016. Vibration control of bridge subjected to multi-axle vehicle using multiple tuned mass friction dampers. *International Journal of Advanced Structural Engineering (IJASE),* 8**,** 213-227.

PU, J. & LIU, P. 2010. Numerical calculation of dynamic response for multi-span non-uniform beam subjected to moving mass with friction. *Engineering,* 02**,** 367-377.

QIN, S., REYNDERS, E., HE, L., BUI, T. & DE ROECK, G. 2014. Effects of initial conditions in operational modal analysis. *Structural Control and Health Monitoring,* 21**,** 557-573.

RAO, G. V. 2000. Linear Dynamics of an Elastic Beam Under Moving Loads. *ASME Journal of Vibration and Acoustics,* 122**,** 281-289.

RAO, S. S. 2007. *Vibration of Continuous Systems,* Hoboken, New Jersey, John Wiley and Sons Inc.

SALCHER, P. & ADAM, C. 2015. Modeling of dynamic train–bridge interaction in high-speed railways. *Acta Mechanica,* 226**,** 2473-2495.

SAMANI, F. S. & PELLICANO, F. 2012. Vibration reduction of beams under successive traveling loads by means of linear and nonlinear dynamic absorbers. *Journal of Sound and Vibration,* 331**,** 2272-2290.

SAVIN, E. 2001. Dynamic Amplification Factor and Response Spectrum for the Evaluation of Vibrations of Beams under Successive Moving Loads. *Journal of Sound and Vibration,* 248**,** 267-288.

SEHGAL, S. & KUMAR, H. 2016. Structural dynamic model updating techniques: a state of the art review. *Archives of Computational Methods in Engineering,* 23**,** 551-533.

SEKIYA, H., KIMURA, K. & MIKI, C. 2016. Technique for Determining Bridge Displacement Response Using MEMS Accelerometers. *Sensors (Basel),* 16**,** 257.

SHA, X., LU, J. F. & ZHANG, R. 2016. Resonance and cancelation phenomena in a periodic viaduct under a series of equidistant moving loadings. *Archive of Applied Mechanics,* 86**,** 1431-1447.

SHENG, X. 2015. Generalization of the Fourier transform-based method for calculating the response of a periodic railway track subject to a moving harmonic load. *Journal of Modern Transportation,* 23**,** 12-29.

SHENG, X., JONES, C. J. C. & THOMPSON, D. J. 2004. A theoretical model for ground vibration from trains generated by vertical track irregularities. *Journal of Sound and Vibration,* 272**,** 937-965.

SONG, M. K., NOH, H. C. & CHOI, C. K. 2003. A new three-dimensional finite element analysis model of high-speed train–bridge interactions. *Engineering Structures,* 25**,** 1611-1626.

STĂNCIOIU, D. & OUYANG, H. 2014. Optimal vibration control of beams subjected to a mass moving at constant speed. *Journal of Vibration and Control*.

STĂNCIOIU, D., OUYANG, H. & MOTTERSHEAD, J. E. 2008a. Dynamics of a beam and a moving two-axle system with separation. *Proceedings of the Institution of Mechanical Engineers, Part C: Journal of Mechanical Engineering Science,* 222**,** 1947-1956.

STĂNCIOIU, D., OUYANG, H. & MOTTERSHEAD, J. E. 2008b. Vibration of a beam excited by a moving oscillator considering separation and reattachment. *Journal of Sound and Vibration,* 310**,** 1128-1140.

STĂNCIOIU, D., OUYANG, H. & MOTTERSHEAD, J. E. 2009. Vibration of a continuous beam with multiple elastic supports excited by a moving two-axle system with separation. *Meccanica,* 44**,** 293-303.

STĂNCIOIU, D., OUYANG, H., MOTTERSHEAD, J. E. & JAMES, S. 2011. Experimental investigations of a multi-span flexible structure subjected to moving masses. *Journal of Sound and Vibration,* 330**,** 2004-2016.

STEENBERGEN, M. J. M. M. & METRIKINE, A. V. 2007. The effect of the interface conditions on the dynamic response of a beam on a half-space to a moving load. *European Journal of Mechanics - A/Solids,* 26**,** 33-54.

SUN, S., SUN, L. & CHEN, L. 2016. Damage Detection Based on Structural Responses Induced by Traffic Load: Methodology and Application. *International Journal of Structural Stability and Dynamics,* 16**,** 1640026.

SUN, S. L. 2011. *High speed railway bridge design and practice,* Beijing, China Railway Publishing House. [In Chinese]

SUN, Y. Q. & DHANASEKAR, M. 2002. A dynamic model for the vertical interaction of the rail track and wagon system. *International Journal of Solids and Structures,* 39**,** 1337-1359.

THOMPSON, D. 2008. *Railway noise and vibration: mechanisms, modelling and means of control,* Oxford, UK, Elsevier Science.

TIMOSHENKO, S. P. 1953. *History of Strength of Materials: With a Brief Account of the History of Theory of Elasticity and Theory of Structures,* New York, McGraw-Hill.

TING, E. C., GENIN, J. & GINSBERG, J. H. 1974. A general algorithm for moving mass problems. *Journal of Sound and Vibration,* 33**,** 49-58.

TOMÁS-RODRÍGUEZ, M. & P.BANKS, S. 2010. *Linear, Time-varying Approximations to Nonlinear Dynamical Systems: With Applications in Control and Optimization*, Springer.

UIC. 2017a. *High speed* [Online]. http://www.uic.org/highspeed. [Accessed 04/04/2017].

UIC. 2017b. *High speed lines in the world* [Online]. http://www.uic.org/high-speed-database-maps. [Accessed 04/04/2017].

VERICHEV, S. N. & METRIKINE, A. V. 2000. Dynamic rigidity of a beam in a moving contact. *Journal of Applied Mechanics and Technical Physics,* 41**,** 1111-1117.

WANG, R. T. & LIN, J. S. 1998. Vibration of multi-span Timoshenko frames due to moving loads. *Journal of Sound and Vibration,* 212**,** 417-434.

WANG, Y., WEI, Q., SHI, J. & LONG, X. 2010. Resonance characteristics of two-span continuous beam under moving high speed trains. *Latin American Journal of Solids and Structures,* 7**,** 185-199.

WANG, Y. J., WEI, Q. C. & YAU, J. D. 2013. Interaction response of train loads over a two-span continuous beam. *International Journal of Structural Stability and Dynamics,* 13**,** 1350002 (18 pages).

WHELAN, M. J., GANGONE, M. V., JANOYAN, K. D., HOULT, N. A., MIDDLETON, C. R. & SOGA, K. 2010. Wireless operational modal analysis of a multi-span prestressed concrete bridge for structural identification. *Smart Structures and Systems,* 6**,** 579-593.

WU, J. S., LEE, M. L. & LAI, T. S. 1987. The dynamic analysis of a flat plate under a moving load by the finite element method. *International Journal for Numerical Methods in Engineering,* 24**,** 743-762.

WU, J. S. & LIN, T. L. 1990. Free vibration analysis of a uniform cantilever beam with point masses by an analytical-and-numerical-combined method. *Journal of Sound and Vibration,* 136**,** 201-213.

XIA, H., DE ROECK, G., ZHANG, N. & MAECK, J. 2003a. Experimental analysis of a high-speed railway bridge under Thalys trains. *Journal of Sound and Vibration,* 268**,** 103-113.

XIA, H., LI, H. L., GUO, W. W. & DE ROECK, G. 2014. Vibration Resonance and Cancellation of Simply Supported Bridges under Moving Train Loads. *Journal of Engineering Mechanics,* 140**,** 04014015.

XIA, H. & ZHANG, N. 2005. Dynamic analysis of railway bridge under high-speed trains. *Computers & Structures,* 83**,** 1891-1901.

XIA, H., ZHANG, N. & DE ROECK, G. 2003b. Dynamic analysis of high speed railway bridge under articulated trains. *Computers and Structures,* 81**,** 2467-2478.

XIAO, X., JIN, X., WEN, Z., ZHU, M. & ZHANG, W. 2010. Effect of tangent track buckle on vehicle derailment. *Multibody System Dynamics,* 25**,** 1-41.

XU, W. T., LIN, J. H., ZHANG, Y. H., KENNEDY, D. & WILLIAMS, F. W. 2009. 2D moving element method for random vibration analysis of vehicles on Kirchhoff plate with Kelvin foundation. *Latin American Journal of Solids and Structures,* 6**,** 169-183.

XU, W. T., ZHANG, Y. H., LIN, J. H., KENNEDY, D. & WILLIAMS, F. W. 2011. Sensitivity analysis and optimization of vehicle–bridge systems based on combined PEM–PIM strategy. *Computers & Structures,* 89**,** 339-345.

YAMCHELOU, M. T. & NOURI, G. 2016. Spectral analysis of dynamic response of a thin beam subjected to a varying speed moving mass. *Journal of Mechanical Science and Technology,* 30**,** 3009-3017.

YAN, B., DAI, G.-L. & HU, N. 2015. Recent development of design and construction of short span high-speed railway bridges in China. *Engineering Structures,* 100**,** 707-717.

YANG, B., TAN, C. A. & BERGMAN, L. A. 2000. Direct numerical procedure for solution of moving oscillator problems. *Journal of Engineering Mechanics,* 126**,** 462-469.

YANG, F. & FONDER, G. A. 1996. An iterative solution method for dynamic response of bridge–vehicles systems. *Earthquake Engineering and Structural Dynamics,* 25**,** 195-215.

YANG, J., OUYANG, H. & STĂNCIOIU, D. 2017. Numerical studies of vibration of four-span continuous plate with rails excited by moving car with experimental validation. *International Journal of Structural Stability and Dynamics,* 17**,** 1750119.

YANG, Y.-B., CHEN, W.-F., YU, H.-W. & CHAN, C. S. 2013a. Experimental study of a hand-drawn cart for measuring the bridge frequencies. *Engineering Structures,* 57**,** 222-231.

YANG, Y.-B., LIAO, S.-S. & LIN, B.-H. 1995. Impact formulas for vehicles moving over simple and continuous beams. *Journal of Structural Engineering,* 121**,** 1644-1650.

YANG, Y.-B. & LIN, B.-H. 1995. Vehicle-bridge interaction analysis by dynamic condensation method. *Journal of Structural Engineering,* 121**,** 1636-1643.

YANG, Y.-B. & WU, Y.-S. 2001. A versatile element for analyzing vehicle–bridge interaction response. *Engineering Structures,* 23**,** 452-469.

YANG, Y.-B. & YAU, J.-D. 1997. Vehicle-bridge interaction element for dynamic analysis. *Journal of Structural Engineering,* 123**,** 1512-1518.

YANG, Y. B. & CHANG, K. C. 2009a. Extracting the bridge frequencies indirectly from a passing vehicle: Parametric study. *Engineering Structures,* 31**,** 2448-2459.

YANG, Y. B. & CHANG, K. C. 2009b. Extraction of bridge frequencies from the dynamic response of a passing vehicle enhanced by the EMD technique. *Journal of Sound and Vibration,* 322**,** 718-739.

YANG, Y. B., CHANG, K. C. & LI, Y. C. 2013b. Filtering techniques for extracting bridge frequencies from a test vehicle moving over the bridge. *Engineering Structures,* 48**,** 353-362.

YANG, Y. B., LI, Y. C. & CHANG, K. C. 2012. Using two connected vehicles to measure the frequencies of bridges with rough surface: A theoretical study. *Acta Mechanica,* 223**,** 1851-1861.

YANG, Y. B., LI, Y. C. & CHANG, K. C. 2014. Constructing the mode shapes of a bridge from a passing vehicle: a theoretical study. *Smart Structures and Systems,* 13**,** 797-819.

YANG, Y. B. & LIN, C. W. 2005. Vehicle–bridge interaction dynamics and potential applications. *Journal of Sound and Vibration,* 284**,** 205-226.

YANG, Y. B. & YAU, J. D. 2015. Vertical and pitching resonance of train cars moving over a series of simple beams. *Journal of Sound and Vibration,* 337**,** 135-149.

YANG, Y. B., YAU, J. D. & WU, Y. S. 2004. *Vehicle-Bridge Interaction Dynamics with Applications to High-Speed Railways,* Singapore, World Scientific.

YAU, J. D. 2001. Resonance of continuous bridges due to high speed trains. *Journal of Marine Science and Technology,* 9**,** 14-20.

YAU, J. D. & YANG, Y. B. 2004. Vibration reduction for cable-stayed bridges traveled by high-speed trains. *Finite Elements in Analysis and Design,* 40**,** 341-359.

YAU, J. D. & YANG, Y. B. 2006. Vertical accelerations of simple beams due to successive loads traveling at resonant speeds. *Journal of Sound and Vibration,* 289**,** 210-228.

YU, L. & CHAN, T. H. T. 2007. Recent research on identification of moving loads on bridges. *Journal of Sound and Vibration,* 305**,** 3-21.

ZHAI, W., WANG, K. & CAI, C. 2009. Fundamentals of vehicle-track coupled dynamics. *Vehicle System Dynamics,* 47**,** 1349-1376.

ZHAI, W., XIA, H., CAI, C., GAO, M., LI, X., GUO, X., ZHANG, N. & WANG, K. 2013. High-speed train–track–bridge dynamic interactions – Part I: theoretical model and numerical simulation. *International Journal of Rail Transportation,* 1**,** 3-24.

ZHAI, W. M. 1996. Two simple fast integration methods for large-scale dynamic problems in engineering. *International Journal for Numerical Methods in Engineering,* 39**,** 4199-4214.

ZHANG, N. & XIA, H. 2013. Dynamic analysis of coupled vehicle–bridge system based on inter-system iteration method. *Computers and Structures,* 114-115**,** 26-34.

ZHANG, N., XIA, H. & GUO, W. 2008. Vehicle-bridge interaction analysis under high-speed trains. *Journal of Sound and Vibration,* 309**,** 407-425.

ZHANG, Y., WANG, L. & XIANG, Z. 2012. Damage detection by mode shape squares extracted from a passing vehicle. *Journal of Sound and Vibration,* 331**,** 291-307.

ZHAO, Y., SI, L. T. & OUYANG, H. 2017. Dynamic Analysis of an Infinitely Long Beam Resting on a Kelvin Foundation under Moving Random Loads. *Shock and Vibration,* 2017**,** 1-13.

ZHU, D. Y., ZHANG, Y. H. & OUYANG, H. 2015. A linear complementarity method for dynamic analysis of bridges under moving vehicles considering separation and surface roughness. *Computers & Structures,* 154**,** 135-144.

ZHU, X. Q. & LAW, S. S. 1999. Moving forces identification on a multi-span continuous bridge. *Journal of Sound and Vibration,* 228**,** 377-396.

ZHU, X. Q. & LAW, S. S. 2002. Dynamic load on continuous multi-lane bridge deck from moving vehicles. *Journal of Sound and Vibration,* 251**,** 697-716.

ZHU, X. Q. & LAW, S. S. 2015. Structural health monitoring based on vehicle-bridge interaction: accomplishments and challenges. *Advances in Structural Engineering,* 18**,** 1999-2015.